NASA CR-137537
ASRL TR 174-1

A STUDY OF GUST RESPONSE FOR A ROTOR-PROPELLER IN CRUISING FLIGHT

Masahiro Yasue

August 1974

Prepared under Contract No. NAS2-7262 by

Aeroelastic and Structures Research Laboratory
Department of Aeronautics and Astronautics
Massachusetts Institute of Technology
Cambridge, Massachusetts 02139

for

AMES RESEARCH CENTER
NATIONAL AERONAUTICS AND SPACE ADMINISTRATION
MOFFETT FIELD, CALIFORNIA 94035

NASA CR-137537
ASRL TR 174-1

A STUDY OF GUST RESPONSE FOR A ROTOR-PROPELLER IN CRUISING FLIGHT

Masahiro Yasue

August 1974

Prepared under Contract No. NAS2-7262 by

Aeroelastic and Structures Research Laboratory
Department of Aeronautics and Astronautics
Massachusetts Institute of Technology
Cambridge, Massachusetts 02139

for

AMES RESEARCH CENTER
NATIONAL AERONAUTICS AND SPACE ADMINISTRATION
MOFFETT FIELD, CALIFORNIA 94035

1. Report No.	2. Government Accession No.	3. Recipient's Catalog No.
NASA CR-137537		

4. Title and Subtitle	5. Report Date
A STUDY OF GUST RESPONSE FOR A ROTOR-PROPELLER IN CRUISING FLIGHT	August 1974
	6. Performing Organization Code
7. Author(s)	8. Performing Organization Report No.
Masahiro Yasue	ASRL TR 174-1
	10. Work Unit No.
9. Performing Organization Name and Address	11. Contract or Grant No.
Massachusetts Institute of Technology Aeroelastic and Structures Research Laboratory Cambridge, Massachusetts 02139	NAS2-7262
	13. Type of Report and Period Covered
12. Sponsoring Agency Name and Address	Contractor Report
National Aeronautics and Space Administration Moffett Field, California 94035	14. Sponsoring Agency Code

15. Supplementary Notes

NASA Technical Monitors: J.P. Rabbott, Jr., and Wayne R. Johnson

16. Abstract

Equations of motion for a rotor-propeller aircraft in cruising flight have been developed and implemented in a computer program. The formulation is based on Galerkin's method using coupled mode shapes for the blade and wing. This procedure is applied to the analysis of two types of rotors, gimballed rotor and hingeless. The results are evaluated by means of eigenvalue analysis of the stability of the system and frequency response analysis of the gust and control response. In general, the results show that:

(a) The choice of mode shape (rigid-body mode with spring restraint at the root, or elastic coupled mode) to construct the equations of motion affects the damping of the system significantly. The dependency of the damping on the mode shape is estimated for the first beam bending mode. The frequencies of the system have little dependence on the mode-shape type.

(b) The results of the frequency response are quite similar to those of Johnson, in spite of the use of different models. However, the amplitude of the response is slightly different.

(c) Addition of higher mode degrees-of-freedom has little influence on the stability of the rotor and wing.

17. Key Words (Suggested by Author(s))	18. Distribution Statement
Rotary Wing Dynamics Gust Response Proprotor Tilt-Rotor	Unclassified, Unlimited

19. Security Classif. (of this report)	20. Security Classif. (of this page)	21. No. of Pages	22. Price*
Unclassified	Unclassified	235	

* For sale by the National Technical Information Service, Springfield, Virginia 22151

FOREWORD

This report has been prepared by the Aeroelastic and Structures Research Laboratory (ASRL), Department of Aeronautics and Astronautics, Massachusetts Institute of Technology, Cambridge, Massachusetts, under NASA Contract No. NAS 2-7262 from the Ames Research Center, National Aeronautics and Space Administration, Moffett Field, California 94035. Mr. John Rabbott and Dr. Wayne Johnson of the Ames Research Center served as technical monitors. The valuable assistance and advice received from these individuals is gratefully acknowledged.

The research described in this report was supervised by Professor Norman D. Ham and Associate Professor Pin Tong. The author would like to express his deep appreciation and gratitude for their invaluable advice and guidance throughout this study. The author is also deeply indebted to Professor John Dugundji and to Dr. Wayne Johnson, who contributed various useful suggestions. Professor E. A. Witmer's advice and assistance in various phases of the work is acknowledged gratefully.

SUMMARY

This study has been devoted to the development and evaluation of a theoretical model of the proprotor on a cantilevered wing, operating in normal cruising flight. This theory expresses the wing and blade motion in coupled form, and can include any number of mode shapes required to describe the motion accurately. It has been applied to the investigation of the dynamic characteristics of the Bell and of the Boeing design. The Bell rotors are gimballed and the Boeing rotors are hingeless. The analysis includes the frequency response to gusts and cyclic pitch, and an eigenvalue analysis of the dynamic system.

Based on the theoretical results included in this study, the following conclusions may be stated:

(a) The choice of mode shape (rigid-body mode or elastic-coupled mode) affects the damping significantly. The dependency of the damping on the mode shape can be estimated for the first beam bending mode. The blade inplane deflection opposing the rotor direction of rotation, accompanied by the forward out-of-plane deflection, increases the damping, comparing it with the rigid-body calculation. The inplane deflection proceeding in the rotor direction of rotation decreases the damping. The mode shape has little influence on the frequencies of the system.

(b) The results of the frequency response are quite similar to those of Johnson, in spite of the difference in the mode shapes. The amplitude of the response is slightly different, since structural damping was not included in the present calculation, and the mode shapes used were different.

(c) The analysis of the eighteen degree-of-freedom system showed that the higher-frequency degrees of freedom have small influence on the basic degrees of freedom.

Stresses or bending moments of the wing or blade can be predicted from the motions of the wing and blade obtained from this analysis. In addition, this analysis may be applied to the development of an automatic control device to alleviate the gust response of the vehicle.

CONTENTS

CONTENTS CONCLUDED

LIST OF ILLUSTRATIONS

LIST OF ILLUSTRATIONS CONTINUED

LIST OF ILLUSTRATIONS CONCLUDED

LIST OF SYMBOLS

a	Blade sectional lift-curve slope
a_j	Time function of the wing motion corresponding to the jth mode
a_w	Wing sectional lift-curve slope
C_{Do}	Blade-sectional drag coefficient
C_{Dow}	Wing-sectional drag coefficient
C_{mo}	Wing-sectional pitching moment coefficient
$C_{m\alpha}$	Wing-sectional pitching moment curve slope
dD	Sectional aerodynamic drag
dL	Sectional aerodynamic lift
$dM_{\bar{c}/4}$	Wing-sectional pitching moment at the quarter chord
$(EI)_B$	Blade bending stiffness perpendicular to the chordline
$(EI)_C$	Blade bending stiffness along the chordline
$(EI_w)_B$	Wing bending stiffness perpendicular to the chordline
$(EI_w)_C$	Wing bending stiffness along the chordline
e	Exciting force defined in Eq. 4.53
$\bar{e}$	Distance between the elastic axis and the aerodynamic center of the wing
F_x, F_z	Wing resultant forces per unit length in the x and z directions
f_i	Aerodynamic loading of the wing due to the rotor aerodynamic forces, corresponding to the ith wing mode shape

(GJ_w)	Wing torsional rigidity
g_i	Aerodynamic loading of the wing due to the wing aerodynamics, corresponding to the ith wing mode shape
h	Mast height
$\bar{h}$	Nondimensional mast height: h/R
I	Unit matrix
I_B	Blade mass moment of inertia about the virtual flapping hinge
I_{P_p}	Pylon pitching mass moment of inertia
I_{P_r}	Pylon rolling mass moment of inertia
I_{P_y}	Pylon yawing mass moment of inertia
I_w	Wing mass moment of inertia about the elastic axis per unit length
K_{pi}	Pitch-flap coupling coefficients corresponding to the ith blade mode shape defined in Eq. 4.26
L	Wing length (semispan)
M_B	Mass of one blade
M_P	Pylon mass
M_y	Wing resultant pitching moment about the elastic axis per unit length
m	Spanwise mass of the blade per unit length
m_w	Spanwise mass of the wing per unit length
N	Number of blades
n	Blade index

P_z	Resultant force per unit length in the z direction on the blade
P_θ	Resultant force per unit length in the circumferential direction of the rotating blade
$P_{\theta j}$, P_{zj}	Defined in Eq. 4.17
p_w	Wing torsion (positive nose up)
p	Time function corresponding to the wing torsion mode
Q_{jo}	jth blade collective motion degree of freedom
Q_{jc}	jth blade cosine cyclic motion degree of freedom
Q_{js}	jth blade sine cyclic motion degree of freedom
q_{nj}	Time function corresponding to the jth mode of the nth blade
q_1	Time function corresponding to the wing vertical bending
q_2	Time function corresponding to the wing chordwise bending
R	Blade radius
r	Blade running-spanwise coordinate
r_x	Pylon vertical displacement (positive upward)
r_z	Pylon longitudinal displacement (positive forward)
S_α	Static mass moment of the wing segment about the elastic axis
s	Distance between the elastic axis and local center of gravity of the wing

T	Matrix defined in Eq. 4.11
T	Centrifugal force of the blade
t	Time
U	Blade sectional resultant velocity
U_P	Blade sectional inplane velocity
U_T	Blade sectional out-of-plane velocity
U_w	Wing sectional resultant velocity
U_{xB}	Blade inplane velocity component in the x_B direction
U_{yB}	Blade inplane velocity component in the y_B direction
u_G	Vertical gust velocity
u_w	Vertical bending deflection of the wing (positive upward)
V	Aircraft forward velocity
V_{ij}	Defined in Eq. 4.16
V_j	Blade jth inplane bending mode shape
V_j^o	jth collective mode shape of the inplane bending of the blade
V_j^c	jth cyclic mode shape of the inplane bending of the blade
v	Rotor induced flow
v_G	Lateral gust velocity
v_n	Inplane deflection of the nth blade (positive clockwise)

W_B	Pylon vertical translation
W'_B	Pylon rolling angle
W_C	Pylon longitudinal translation
W'_C	Pylon yawing angle
W_{ij}	Defined in Eq. 4.16
W_j	Blade jth out-of-plane bending mode shape
W_j^o	jth collective mode shape of the out-of-plane bending of the blade
W_j^c	jth cyclic mode shape of the out-of-plane bending of the blade
W_{WB}	Work done on the wing by the blade aerodynamic forces
W_{ww}	Work done on the wing by the wing aerodynamic forces
w_G	Longitudinal gust velocity
w_n	Out-of-plane deflection of the nth blade (positive forward)
w_w	Chordwise bending of the wing (positive forward)
x	Blade nondimensional running spanwise coordinate r/R
x,y,z	Coordinates fixed to the wing root (see Fig. 2)
x_B,y_B	Coordinates fixed to the rotor (see Fig. 6)

α	Blade sectional angle of attack
α_o	Blade sectional angle of attack in the equilibrium state
α_w	Wing sectional angle of attack
β	Blade flapping degree of freedom
γ	Lock number $\frac{\rho a C_B R^4}{I_B}$
γ_j	Wing jth vertical bending mode shape
$\Delta\psi_n$	Phase angle between blades
δ	Variation
δ_3	Rotor blade pitch-flap coupling
ζ	Blade lagging degree of freedom
ζ_j	Wing jth chordwise bending mode shape
θ_{AT}	Built-in angle of twist of the blade
θ_B	Angle of twist of the blade
θ_c	Blade pitch angle due to pitch control
θ_D	Blade pitch angle defined according to the performance analysis
θ_{PF}	Blade pitch angle due to pitch-flap coupling
θ_w	Angle of twist of the wing
θ_o	Blade collective pitch control
θ_{lc}	Blade cyclic pitch control

θ_{ls}	Blade cyclic pitch control
$\theta_{.75}$	Blade pitch angle at 75% span
κ	Integral operator defined in Eq. 4.37
Λ_j	Wing jth natural frequency
λ	Inflow ratio $V/(\Omega R)$
$\bar{\lambda}$	Absolute value of the inflow ratio $\lvert\lambda\rvert$
λ_j	jth natural frequency of the rotating blade
ν_p	Pylon pitching motion (positive nose up)
ν_R	Blade rigid-body mode rotations in autorotation case (positive for clockwise rotation, when looking forward)
ν_r	Pylon rolling motion (positive for clockwise)
ν_y	Pylon yawing motion (positive for counterclockwise)
π	Variational functional
ρ	Air density
τ_i	Defined in Eq. 3.15
Φ	Pylon pitching angle
ϕ_i	Blade sectional inflow angle
ϕ_j	Wing jth torsional mode shape
ϕ_w	Wing sectional angle formed by the horizontal and vertical velocity components (see Fig. 7)

Ψ_n	Azimuth position of the nth blade
ψ_n	Azimuth position of the nth blade excluding the pylon roll motion
Ω	Rotational speed of the rotor
$\overline{\Omega}$	Direction of rotation $\Omega/\lvert\Omega\rvert$
$(\ )_o$	Value is evaluated in the equilibrium state
$(\dot{\ }), (\ddot{\ })$	Time derivative $\partial/\partial t$, $\partial^2/\partial t^2$
$(\overset{o}{\ }), (\overset{oo}{\ })$	Nondimensional time derivatives, $\frac{\partial}{\partial(\lvert\Omega\rvert t)}$, $\frac{\partial^2}{\partial(\lvert\Omega\rvert t)^2}$
$(\ )_n$	nth blade

Superscript

o	Collective mode of the rotor
c	Cyclic mode of the rotor

Subscript

o	Collective mode of the rotor
c	Cyclic mode of the rotor
s	Cyclic mode of the rotor
i,j,k	Indices

SECTION 1

INTRODUCTION

1.1 General

It has been recognized that the tilting proprotor aircraft, one of the composite aircraft family, is a very promising concept that combines into one aircraft the hover efficiency of the helicopter and the high-speed efficiency of the fixed-wing aircraft (Refs. 1-3).

The typical tilting proprotor aircraft is a twin-engine aircraft with tilting rotors mounted on each wing tip. Its configuration consists of a fuselage, a high swept-forward wing, and an empennage. The empennage has a vertical stabilizer and rudder, and a horizontal stabilizer and elevator. The large diameter rotors are three bladed. hingeless or gimbal-type rotors which are mounted on the rotor shaft. The rotor shaft is connected through the gearbox to each engine in the pylon attached at the wing tip. The conversion system provides the rotation of the rotor pylon from the vertical position to the horizontal position and return, in order to obtain the helicopter mode or airplane mode corresponding to the desired flight regime.

When the aircraft takes off or lands, the rotor pylon is rotated to the vertical position to achieve vertical takeoff or landing similar to the helicopter. The flight controls apply pitch changes to the rotor to provide the longitudinal and directional control corresponding to helicpoter rotor cyclic pitch, while the collective pitch controls vertical flight and roll motion.

In high-speed flight, the rotor pylon is rotated to a horizontal position similar to that of the conventional propeller type aircraft. The thrust is produced by the rotor, and the lift by the wing. The flight controls are provided by the conventional aircraft

control surfaces such as the elevator, rudder and aileron.

In addition to the above modes, various conversion modes can be obtained. At that time the rotor pylon tilts to some position between the vertical and horizontal, where it can be safely locked. This makes STOL-type operations possible.

The tilting proprotor is exposed to a severe aerodynamic environment including gusts, the wake of preceding blades, and harmonic airloading like a helicopter. But its dynamic and aeroelastic characteristics are in many ways unique; for example, the large flexible blades with a large amount of twist experience significant coupled out-of-plane (flapping) and inplane (lagging) motion.

As described later in Subsection 1.2, several years of experimental and theoretical analyses have been conducted to establish a fundamental understanding of the dynamic and aeroelastic behavior. However, it is necessary to understand the aeroelastic response of this aircraft to atmospheric turbulence more adequately and to predict it more accurately, since during the preliminary design phase, vibration level prediction is required in order: (a) to evaluate the fatigue life of the blade and wing, (b) to estimate the ride qualities of the vehicle, and, if necessary, (c) to develop suitable gust alleviation devices.

Several design compromise concepts, which make the present analysis distinct from helicopter aeroelastic analysis, are now stated briefly.

In order to obtain high hover efficiency from the rotor, it is desirable to achieve low disc loading, in other words to use large-diameter rotors whose swept discs reach nearly to the fuselage. When the aircraft is operated in high forward speed axial flight in the airplane mode, the rotor is operating at a high inflow ratio (the ratio of axial velocity to blade tip speed). This phenomenon is very different from the helicopter rotor operation which

involves low inflow. High inflow operation requires a large built-in angle of twist for efficient cruising. Therefore, significant coupled out-of-plane (flapping) and inplane (lagging) motion occurs in the large, flexible and twisted blade. This phenomenon makes analysis more complicated.

The engines and gearboxes are usually located at the wing tip to avoid transmitting high power through a long drive shaft. This leads to low wing natural frequencies and possible resonances in the low frequency range. Also, the center of gravity of the pylon and rotor does not usually coincide with the elastic axis of the wing. Hence, this results in coupled bending and torsion.

1.2 Brief Survey of Past Work

A good review and an elementary description of the dynamic and aeroelastic problems associated with the tilting proprotor aircraft were given by Reed in Ref. 4 and Loewy in Ref. 5. In this report no attempt will be made to repeat the reviews given in Refs. 4 and 5. The only references cited here will be those pertinent to the problem being treated.

The possibility of propeller whirl flutter -- a dynamic instability that can occur in a flexibly mounted aircraft engine-propeller combination -- was first recognized in the late 1930's by Taylor and Browne (Ref. 6). It was not until 1960 that it became a problem of practical concern -- with the appearance of the turboprop aircraft.

Following the two fatal turboprop aircraft accidents, it was established that propeller whirl flutter could have occurred if the nacelle stiffness was severely reduced, for example by a structural failure. Several generalized studies were conducted at NASA-Langley. One of them was carried out by Houbolt and Reed in Ref. 7; it gives an elementary and basic treatment of the equations of motion and propeller aerodynamics for propeller-nacelle whirl flutter.

Because VTOL configurations have unconventional propeller-rotor systems, whirl flutter was a major design consideration on present proprotor aircraft.

The analysis presented in Ref. 8 is for a two-bladed rotor free to tilt on a shaft with two nacelle degrees of freedom (pitch and yaw). No lag or coning degrees of freedom are considered. The analytical method was compared with test results for an existing tilting proprotor aircraft (the Bell XV-3) and of subsequently-tested scale models. They showed good agreement.

Young and Lytwyn in Ref. 9 present a very precise analysis for the whirl stability of a multi-bladed rotor mounted on a nacelle which has pitch and yaw degrees of freedom. Each blade has one flapwise degree of freedom. The blade mode shape is assumed to be a rigid body mode shape. It was concluded that whirl stability is poorest when the nacelle pitch frequency equals the nacelle yaw frequency, but in this situation nacelle damping is quite effective. There is an optimum value of flap bending frequency somewhere between 1.1 and 1.35 for highly stabilized whirl motion.

This analysis neglects (as do Refs. 4 and 8) the effect of coning on proprotor aerodynamics, and flap bending mode shapes other than the rigid blade mode used. Also, autorotation flight must be considered as well as powered flight.

In Ref. 10, Gaffey points out that a highly coupled blade mode has substantial flap bending even if the primary mode involves in-plane motion. This occurs in the case of a highly twisted blade or a blade operating at high geometric pitch angles such as a proprotor blade. The analysis shows that a moderate amount of negative δ_3 (flapping angle at the blade root gives the pitch angle reduction of the amount $\beta \cdot \tan \beta_3$ if δ_3 is positive) has a stabilizing influence on proprotors subject to flap-lag instability at high inflows.

Preliminary design studies of prototype vehicles (Refs. 11 and 12) as a part of the current NASA/ARMY sponsored tilting proprotor

research aircraft program give some results from dynamic and aeroelastic analyses done by Bell and Vertol.

Johnson (in Refs. 13 and 14) derived the equations of motion for a cantilever wing with the rotor at the wing tip. He develops a nine degree-of-freedom model which involves blade flapping motion and lagging motion (each has one collective and two cyclic motions, respectively), wing vertical bending, chordwise bending, and torsion. This model is applied to two proprotor designs and compared with the results of some full-scale wind tunnel tests. It shows reasonable correlation between theory and experiment.

In conclusion, it appears that most of the investigative work has been concerned with whirl flutter. The above review shows that more knowledge is needed for the solution of tilting proprotor aircraft dynamic and aeroelastic problems.

1.3 Objectives of the Present Study

The objective of this study is to establish a verified method of predicting the dynamic and aeroelastic behavior of the tilting proprotor aircraft in order to evaluate the fatigue life of the blades and wings and also to estimate the ride quality.

The equations of motion for a cantilever wing with a rotating rotor at the wing tip will be derived as consistently as possible. The great complexity of rotor blade motion will be included by accounting for blade rotation (i.e., centrifugal and Coriolis forces), significant inplane motion, and the large twist and high pitch angles at high inflows.

The resulting system of equations, obtained using modal analysis, will be applied to the analysis of the two proprotor designs (one is a rigid, soft-inplane type rotor and the other is a gimballed, stiff-inplane rotor).

Finally, the eigenvalues and frequency response of each proprotor design will be determined to establish their dynamic charac-

teristics; the results of the analyses will be compared in terms of eigenvalues for normal modes (coupled elastic modes), assumed modes (uncoupled elastic modes), and rigid body modes, using Galerkin's method.

SECTION 2

THE EQUATIONS OF MOTION

2.1 Model and Coordinate System for the Analysis

The primary interest of this study is in the dynamic and aeroelastic phenomena of the wing, pylon, and rotor of the tilting proprotor aircraft in cruising flight. Hence, the dynamical system considered here consists of a cantilever right wing with a pylon at the wing tip, and an N-bladed rotor mounted on the pylon, as shown in Fig. 1. The model will be restricted to the cantilever wing, since it is sufficient to obtain a basic understanding of the proprotor motion, and many such proprotor models have been tested in wind tunnels.

Therefore, the aircraft rigid body motions are neglected and the wing antisymmetrical modes are also dropped. The left wing motions including the pylon and rotor are given by the mirror image of the right wing.

The wing is assumed to have a high aspect ratio, so that strip theory is used for the wing aerodynamics and beam theory for elastic bending and torsion. Wing sweep and dihedral will not be considered, but angle of attack and angle of twist (built-in twist) will be considered. The elastic axis is assumed to be a straight line. The elastic axis coincides with the y-axis as shown in Fig. 2. The free stream vector coincides with the z-axis. Therefore, the angle between the z-axis and the chordline of the wing results in a wing angle of attack (positive nose up). The wing motion (Fig. 2) consists of elastic bending and elastic torsion. The deflection u_w of the wing elastic elastic axis perpendicular to the y-z plane is called vertical or beamwise bending (positive upward). The deflection w_w parallel to y-z plane is termed chordwise bending (positive forward). Torsion p_w is

defined as pitch angle change (positive nose-up).

A pylon of large mass and moment of inertia is assumed to be rigidly attached to the wing tip. Therefore, the pylon motions (Fig. 2) corresponding to the wing motions are defined as vertical displacement r_x along the x-axis (positive upward), longitudinal displacement r_z along the z-axis (positive forward), pylon yaw ν_y about the x-axis (positive counterclockwise), pylon pitch ν_p about y-axis (positive nose-up), and pylon roll ν_r about the z-axis (positive for clockwise rotation, when looking forward). The above pylon motions are accounted for at the point where the wing elastic axis crosses the plane, parallel to x-Z plane, which includes the rotor shaft. The pylon lateral displacement along the y-axis is neglected as a higher order effect.

The pylon and the rotor shaft are assumed to be parallel to the free stream in equilibrium flight (r_x, r_z, ν_y, ν_p, and ν_r are all zero), regardless of the wing angle of attack.

The rotor is located at the distance h (Fig. 2) from the wing tip elastic axis to the rotor-hub (positive forward from the elastic axis). The distance h is termed the mast height. The rotor consists of N blades, whose rotational speed Ω is defined as positive if clockwise looking foward. The blade (Fig. 2) has out-of-plane (flapping) deflection w_n, defined positive for forward displacement from the disc plane (upward in helicopter mode, while the rotor shaft is vertical), and inplane (lagging) deflection v_n, defined positive for clockwise deflection regardless of rotor direction of rotation. The lower case letter n means the nth blade, n=1,2,...N. Blade torsion is neglected here.

The azimuth position Ψ_n (Fig. 3) of the nth blade is defined as:

$$\Psi_n = \Omega t + \nu_r + \Delta\psi_n \tag{2.1}$$

where Ψ_n is measured from the vertical and t is time. The phase angle between blades, $\Delta\psi_n$ is defined as

$$\Delta\psi_n = (n-1)\frac{2\pi}{N} \tag{2.2}$$

The azimuth position of the nth blade excluding the pylon roll motion is denoted as

$$\psi_n = \Omega t + \Delta\psi_n \tag{2.3}$$

2.2 Basic Formulation for Powered Flight

The governing linear equations of motion are derived in this subsection. A more complete and detailed derivation is given in Appendix A.

The equations involve ten unknowns: v_n, w_n, r_x, r_z, ν_y, ν_p, ν_r, u_w, v_w, and r_w (actually v_n and w_n represent N unknowns, respectively, but for convenience they may be treated as one unknown without inconsistency). The equations consist of three categories: the blade equations, the wing equations, and matching conditions between rotor and pylon.

The blade equations are complicated by the pylon motions which produce the centrifugal forces and Coriolis forces. The wing equations are derived from beam theory. The rotor is rigidly attached to the pylon for the powered flight case and, therefore, rotor motion is related to pylon motion; this gives the matching conditions between the rotor and the pylon.

(a) Blade Equations

$$\frac{\partial^2}{\partial r^2}\left[\left\{(EI)_c \sin^2\theta_B + (EI)_B \cos^2\theta_B\right\}\frac{\partial^2 w_n}{\partial r^2}\right]$$

$$+\frac{\partial^2}{\partial r^2}\left[\left\{(EI)_c - (EI)_B\right\}\sin\theta_B\cos\theta_B\frac{\partial^2 v_n}{\partial r^2}\right]$$

$$-\frac{\partial}{\partial r}\left(T\frac{\partial w_n}{\partial r}\right) + m\left\{\ddot{w}_n + \ddot{r}_z + 2\Omega r \dot{\iota}_p \sin\Phi_n - r\ddot{\iota}_p \cos\Phi_n + 2\Omega r \dot{\iota}_y \cos\Phi_n + r\ddot{\iota}_y \sin\Phi_n\right\} = (P_z)_n \tag{2.4}$$

$$\frac{\partial^2}{\partial r^2}\left[\left\{(EI)_c \cos^2\theta_B + (EI)_B \sin^2\theta_B\right\}\frac{\partial^2 v_n}{\partial r^2}\right] + \frac{\partial^2}{\partial r^2}\left[\left\{(EI)_c - (EI)_B\right\}\sin\theta_B \cos\theta_B \frac{\partial^2 w_n}{\partial r^2}\right] - \frac{\partial}{\partial r}\left(T\frac{\partial v_n}{\partial r}\right) + m\left\{\ddot{v}_n - \Omega^2 v_n - \ddot{r}_x \sin\Phi_n + r\ddot{\iota}_r - h\ddot{\iota}_p \sin\Phi_n - h\ddot{\iota}_y \cos\Phi_n\right\} = (P_\theta)_n \tag{2.5}$$

wnere

r	running spanwise coordinate for the blade from the axis of rotation.
θ_B	angle formed by the rotor disc plane and the blade sectional chordline, usually including built-in angle of twist and collective pitch.
$(EI)_C$	bending stiffness in the blade sectional chordline direction.
$(EI)_B$	bending stiffness in the direction perpendicular to the chordline.
m	spanwise mass of the blade per unit length.

T	centrifugal force at r expressed as: $$T = \Omega^2 \int_r^R m\, r\, dr$$
P_z	resultant force per unit length in the z direction on the blade (positive forward).
P_θ	resultant force per unit length in the circumferential direction on the blades (positive clockwise when looking foward).
$(\ )_n$	about nth blade.

The blade geometry is shown in Fig. 3.

(b) Wing Equations

$$\frac{\partial^2}{\partial y^2}\left[\left\{(EI_w)_c \sin^2\theta_w + (EI_w)_B \cos^2\theta_w\right\}\frac{\partial^2 u_w}{\partial y^2}\right]$$

$$+ \frac{\partial^2}{\partial y^2}\left[\left\{(EI_w)_c - (EI_w)_B\right\}\sin\theta_w \cos\theta_w \frac{\partial^2 w_w}{\partial y^2}\right]$$

$$+ m_w \ddot{u}_w + S_a \ddot{p}_w = F_x \qquad (2.6)$$

$$\frac{\partial^2}{\partial y^2}\left[\left\{(EI_w)_c \cos^2\theta_w + (EI_w)_B \sin^2\theta_w\right\}\frac{\partial^2 w_w}{\partial y^2}\right]$$

$$+ \frac{\partial^2}{\partial y^2}\left[\left\{(EI_w)_c - (EI_w)_B\right\}\sin\theta_w \cos\theta_w \frac{\partial^2 u_w}{\partial y^2}\right]$$

$$+ m_w \ddot{w}_w = F_z \qquad (2.7)$$

$$\frac{\partial}{\partial y}\left\{(GJ_w)\frac{\partial P_w}{\partial y}\right\} + I_w \ddot{P}_w + S_\alpha \ddot{u}_w = M_y \qquad (2.8)$$

where

θ_w angle between the wing sectional chordline and free-stream direction.

$(EI_w)_C, (EI_w)_B$ wing bending stiffness defined similarly as for the blade.

(GJ_w) wing torsional rigidity.

m_w spanwise wing mass per unit length.

I_w wing mass moment of inertia about the elastic axis per unit length.

s_α static mass moment of wing segment about the elastic axis defined as

$$s_\alpha = ms$$

where s is a distance between the center of gravity and the elastic axis of the wing and positive if center of gravity is ahead of the elastic axis.

F_x, F_z resultant wing force per unit length in the x and z directions, respectively.

M_y resultant wing pitching moment per unit length.

The wing cross-sectional geometry is shown in Fig. 4, and pylon motions are expressed with wing deflections as

$$\begin{Bmatrix} \nu_x \\ \nu_z \\ \nu_y \\ \nu_p \\ \nu_r \end{Bmatrix} = \begin{Bmatrix} u_w \\ w_w \\ \frac{\partial w_w}{\partial y} \\ P_w \\ -\frac{\partial u_w}{\partial y} \end{Bmatrix}_{y=L} \qquad (2.9)$$

(c) Matching Conditions between the Blade and Pylon

$$M_p \ddot{r}_x - \frac{\partial}{\partial y}\left[\left\{(EI_w)_c \sin^2\theta_w + (EI_w)_B \cos^2\theta_w\right\}\frac{\partial^2 u_w}{\partial y^2}\right]_{y=L}$$
$$- \frac{\partial}{\partial y}\left[\left\{(EI_w)_c - (EI_w)_B\right\}\sin\theta_w \cos\theta_w \frac{\partial^2 w_w}{\partial y^2}\right]_{y=L}$$
$$+ \sum_{n=1}^{N}\left[\int_0^R m\left\{\ddot{r}_x + h\ddot{\nu}_p - (v_n \ddot{\sin}\,\Phi_n)\right\}dr\right]_n$$
$$= \sum_{n=1}^{N}\left[\int_0^R (-P_\theta \sin\Phi_n + \nu_p P_z)\,dr\right]_n \qquad (2.10)$$

$$M_p \ddot{r}_z - \frac{\partial}{\partial y}\left[\left\{(EI_w)_c \cos^2\theta_w + (EI_w)_B \sin^2\theta_w\right\}\frac{\partial^2 w_w}{\partial y^2}\right]_{y=L}$$
$$- \frac{\partial}{\partial y}\left[\left\{(EI_w)_c - (EI_w)_B\right\}\sin\theta_w \cos\theta_w \frac{\partial^2 u_w}{\partial y^2}\right]_{y=L}$$
$$+ \sum_{n=1}^{N}\left[\int_0^R m(\ddot{r}_z + \ddot{w}_n)\,dr\right]_n$$
$$= \sum_{n=1}^{N}\left[\int_0^R (\nu_p P_\theta \sin\Phi_n + \nu_y P_\theta \cos\Phi_n + P_z)\,dr\right]_n \qquad (2.11)$$

$$I_{p_y}\ddot{\nu}_y + \left[\left\{(EI_w)_c \cos^2\theta_w + (EI_w)_B \sin^2\theta_w\right\}\frac{\partial^2 w_w}{\partial y^2}\right]_{y=L}$$
$$+ \left[\left\{(EI_w)_c - (EI_w)_B\right\}\sin\theta_w \cos\theta_w \frac{\partial^2 u_w}{\partial y^2}\right]_{y=L}$$
$$+ \sum_{n=1}^{N}\left[\int_0^R m\left\{(h^2 + \frac{r^2}{2})\ddot{\nu}_y + \Omega r^2 \dot{\nu}_p + r(w_n \ddot{\sin}\,\Phi_n)\right.\right.$$
$$\left.\left. - 2\Omega r(w_n \dot{\cos}\,\Phi_n) - h(v_n \ddot{\cos}\,\Phi_n)\right\}dr\right]_n$$
$$= \sum_{n=1}^{N}\left[\int_0^R \left\{-h(P_\theta \cos\Phi_n - \nu_y P_z) + r\nu_p P_\theta + r P_z \sin\Phi_n\right.\right.$$

$$+ P_z v_n \cos\Phi_n - w_n P_\theta \cos\Phi_n \Big\} dr \Big]_n \qquad (2.12)$$

$$I_{P_p} \ddot{v}_p + \left[(GJ_w)\frac{\partial P_w}{\partial y}\right]_{y=L} + \sum_{n=1}^{N}\Big[\int_0^R m\Big\{-h(v_n \ddot{\sin}\Phi_n) + h(\ddot{r}_x + h\ddot{v}_p) - 2\Omega r(w_n \dot{\sin}\Phi_n) - r(w_n \ddot{\cos}\Phi_n) + \frac{1}{2}r^2\ddot{v}_p - \Omega r^2 \dot{v}_y \Big\} dr\Big]_n = \sum_{n=1}^{N}\Big[\int_0^R \Big\{ h(-P_\theta \sin\Phi_n + v_p P_z) - w_n P_\theta \sin\Phi_n + v_n P_z \sin\Phi_n - r P_z \cos\Phi_n \Big\} dr\Big]_n \qquad (2.13)$$

$$I_{P_r}\ddot{v}_r - \left[\left\{(EI_w)_c \sin^2\theta_w + (EI_w)_B \cos^2\theta_w\right\}\frac{\partial^2 u_w}{\partial y^2}\right]_{y=L} - \left[\left\{(EI_w)_c - (EI_w)_B\right\}\sin\theta_w \cos\theta_w \frac{\partial^2 w_n}{\partial y^2}\right]_{y=L} + \sum_{n=1}^{N}\Big[\int_0^R m(r^2\ddot{v}_r + r\ddot{v}_n)\,dr\Big]_n = \sum_{n=1}^{N}\Big[\int_0^R (rP_\theta)\,dr\Big]_n \qquad (2.14)$$

where

M_p Pylon mass

I_{p_y} Pylon yawing mass moment of inertia

I_{p_p} Pylon pitching mass moment of inertia

I_{p_r} Pylon rolling mass moment of inertia

$(\ddot{}),(\dot{})$ Time derivative applied to entire formula in the parentheses

The above equations are derived independently of Refs. 7, 9, and 13. However, if the wing motions are eliminated, the equations are similar to the basic whirl flutter equations derived in Ref. 7 or Ref. 9.

2.3 Supplement for Autorotational Flight

Autorotation may be defined as the condition of flight where there is no restraint of the rotor rotation about the rotor shaft. Therefore, no rotor torque is transmitted to the shaft, and no pylon roll motion is transmitted to the rotor. This means that rigid body rotation of the entire rotor about the shaft will be produced. This rigid body rotation is designated as ν_R (positive clockwise).

The equations of motion for autorotational flight are almost the same as those for powered flight. The equations: 2.4, 2.6, 2.7, 2.8, 2.10, 2.11, 2.12 and 2.13 are the same. In Eq. 2.5 ν_r must be replaced by ν_R. In lieu of Eq. 2.14 the fact that the rotor inplane motion is independent of the pylon roll motion in autorotation flight results in Eq. 2.15 as follows:

$$\sum_{n=1}^{N}\left[\int_0^R m\left(r^2\ddot{\nu}_R + r\ddot{v}_n\right)dr\right]_n = \sum_{n=1}^{N}\left[\int_0^R (rP_\Theta)\,dr\right]_n \tag{2.15}$$

This yields a new degree of freedom.

The angle in Eq. 2.1 is also expressed as

$$\Psi_n = \Omega t + \nu_R + \Delta\psi_n \tag{2.16}$$

in this case.

SECTION 3

AERODYNAMIC FORCES

3.1 Rotor Aerodynamic Forces

The rotor aerodynamic forces will be evaluated next. The analysis is almost the same as in the helicopter blade element theory. The significant difference is that it is impossible to assume small angles for the angle of twist, the collective pitch and the angle of attack of the blade operating in the high inflow. The basic idea is presented by Young and Lytwyn (Ref. 9).

The section aerodynamic lift and drag forces dL, dD yield the resultant forces P_z and P_θ as follows (in Fig. 5),

$$\begin{aligned} P_z &= dL \cos \phi_i - dD \sin \phi_i \\ P_\theta &= -dD \cos \phi_i - dL \sin \phi_i \end{aligned} \tag{3.1}$$

where

$$\begin{aligned} dL &= 1/2\ \rho a c_B U^2 \alpha \\ dD &= 1/2\ \rho\ c_B U^2 C_{DO} \end{aligned} \tag{3.2}$$

and the angle ϕ_i is defined as,

$$\begin{aligned} \sin\phi_i &= \frac{U_p}{U} \\ \cos\phi_i &= \frac{|U_T|}{U} \end{aligned} \tag{3.3}$$

The blade section inplane velocity (positive counterclockwise direction) is U_T and U_p is the blade section out-of-plane velocity (positive for negative z direction). Therefore, the resultant air velocity is expressed as,

$$U = \sqrt{U_p^2 + U_T^2} \tag{3.4}$$

In cruise flight,

$$\begin{aligned} U_T &= \Omega r \\ U_p &= V + v \end{aligned} \tag{3.5}$$

where V is the forward aircraft speed (axial velocity) and v is the induced inflow velocity. The induced velocity is very small compared with the forward velocity V in the high inflow operation. Therefore the induced velocity is neglected in this entire study.

The inflow ratio λ is defined as the ratio of the axial velocity to tip speed of the blade:

$$\lambda = \frac{V}{\Omega R} \tag{3.6}$$

The section effective angle of attack is

$$\alpha = \theta_B + \theta_{PF} - \tan^{-1}\frac{U_P}{|U_T|} + \theta_C \tag{3.7}$$

the angle θ_B formed by the disc plane and the blade chordline includes the angle of twist and collective pitch. Therefore

$$\theta_B = \theta_{AT} + \theta_{.75} \tag{3.8}$$

where θ_{AT} is the built-in section angle of twist of the blade, which is zero at 75% span of the blade, and $\theta_{.75}$ is the collective pitch to be obtained from the performance calculation. Usually $\theta_{.75}$ is:

$$\theta_{.75} = \tan^{-1}\left(\frac{V}{\frac{3}{4}R\Omega}\right) + \theta_D \tag{3.9}$$

The first term express the inflow at 75% span and θ_D depends on the proprotor design to obtain the optimum cruising performance. Pitch-flap coupling θ_{PF}, and blade pitch control θ_C will be discussed later. Finally:

$$\alpha = \theta_{AT} + \theta_{.75} + \theta_{PF} - \tan^{-1}\frac{U_P}{|U_T|} + \theta_C \tag{3.10}$$

Substituting Eqs. 3.2 and 3.3 into Eq. 3.1 yields

$$P_x = \frac{1}{2}\rho c_B a\, U|U_T|\alpha - \frac{1}{2}\rho c_B C_{D_0} U U_P$$

$$P_\theta = \bar{\Omega}\left[-\frac{1}{2}\rho c_B C_{D_0} U|U_T| - \frac{1}{2}\rho c_B a\, U U_P \alpha\right] \qquad (3.11)$$

where

$$\text{sign}\ (\Omega) = \frac{\Omega}{|\Omega|} = \bar{\Omega} \qquad (3.12)$$

Next the perturbation method is applied to Eq. 3.11 to derive the aerodynamic forces of the rotor in disturbed motion:

$$P_x = (P_x)_0 + \left(\frac{\partial P_x}{\partial U_T}\right)_0 \delta U_T + \left(\frac{\partial P_x}{\partial U_P}\right)_0 \delta U_P + \left(\frac{\partial P_x}{\partial \alpha}\right)_0 \delta\alpha$$

$$P_\theta = (P_\theta)_0 + \left(\frac{\partial P_\theta}{\partial U_T}\right)_0 \delta U_T + \left(\frac{\partial P_\theta}{\partial U_P}\right)_0 \delta U_P + \left(\frac{\partial P_\theta}{\partial \alpha}\right)_0 \delta\alpha \qquad (3.13)$$

In these equations, $(\ )_0$ means those values are evaluated in the equilibrium state, given by the following expressions:

$$(P_x)_0 = \frac{1}{2}\rho c_B a\,(\Omega R)^2\left[\alpha_0\tau_3 - \frac{C_{D_0}}{a}\bar{\lambda}\tau_2 + \bar{\lambda}^2\alpha_0\tau_1 - \frac{C_{D_0}}{a}\bar{\lambda}^3\tau_0\right]$$

$$\left(\frac{\partial P_x}{\partial U_T}\right)_0 = \frac{1}{2}\rho c_B a|\Omega|R\left[2\alpha_0\tau_2 + \bar{\lambda}\left(1 - \frac{C_{D_0}}{a}\right)\tau_1 + \bar{\lambda}^2\alpha_0\tau_0\right]\bar{\Omega}$$

$$\left(\frac{\partial P_x}{\partial U_P}\right)_0 = \frac{1}{2}\rho c_B a|\Omega|R\left[-\left(1 + \frac{C_{D_0}}{a}\right)\tau_2 + \bar{\lambda}\alpha_0\tau_1 - 2\bar{\lambda}^2\frac{C_{D_0}}{a}\tau_0\right]$$

$$\left(\frac{\partial P_x}{\partial \alpha}\right)_0 = \frac{1}{2}\rho c_B a\,(\Omega R)^2\left[\tau_3 + \bar{\lambda}^2\tau_1\right] \qquad (3.14a)$$

$$(P_\theta)_0 = \frac{1}{2}\rho c_\theta a (\Omega R)^2 \left[-\frac{C_{D_0}}{a}\tau_3 - \bar{\lambda}\alpha_0\tau_2 - \bar{\lambda}^2\frac{C_{D_0}}{a}\tau_1 - \bar{\lambda}^3\alpha_0\tau_0 \right]\bar{\Omega}$$

$$\left(\frac{\partial P_\theta}{\partial U_T}\right)_0 = \frac{1}{2}\rho c_\theta a |\Omega| R \left[-2\frac{C_{D_0}}{a}\tau_2 - \bar{\lambda}\alpha_0\tau_1 - \bar{\lambda}^2\left(1+\frac{C_{D_0}}{a}\right)\tau_0 \right]$$

$$\left(\frac{\partial P_\theta}{\partial U_P}\right)_0 = \frac{1}{2}\rho c_\theta a |\Omega| R \left[-\alpha_0\tau_2 + \bar{\lambda}\left(1-\frac{C_{D_0}}{a}\right)\tau_1 - 2\alpha_0\tau_0 \right]\bar{\Omega}$$

$$\left(\frac{\partial P_\theta}{\partial \alpha}\right)_0 = \frac{1}{2}\rho c_\theta a (\Omega R)^2 \left[-\bar{\lambda}\tau_2 - \bar{\lambda}^3\tau_0 \right]\bar{\Omega} \qquad (3.14b)$$

where

$$\tau_k = \frac{x^k}{\sqrt{x^2+\bar{\lambda}^2}} \qquad (k = 0, 1, 2, 3) \qquad (3.15)$$

$$x = r/R \qquad (3.16)$$

$$\bar{\lambda} = |\lambda| \qquad (3.17)$$

$$\alpha_0 = \theta_{AT} + \theta_{.75} - \tan^{-1}\frac{U_P}{|U_T|} \qquad (3.18)$$

The perturbation quantities δU_T, δU_p and $\delta\alpha$ will be considered next. The perturbation velocities δU_T and δU_p consist of rotor and pylon motion and gust velocities.

The velocity at the position of the blade axis in x,y,z coordinate (Fig. 2, see details in Appendix A) can be written as

$$\dot{x} = -\Omega r \sin\psi_n - \Omega v_n \sin\psi_n - \dot{v}_n \sin\psi_n + \dot{r}_x + h\dot{v}_p - \dot{v}_r r \sin\psi_n - \Omega r v_r \cos\psi_n$$

$$\dot{y} = \Omega r \cos\psi_n - h\dot{v}_y + r\dot{v}_r \cos\psi_n - \Omega r v_r \sin\psi_n + \dot{v}_n \cos\psi_n - \Omega v_n \sin\psi_n$$

$$\dot{z} = \dot{w}_n + \dot{r}_z - r\dot{v}_p \cos\psi_n + \Omega r v_p \sin\psi_n + r\dot{v}_y \sin\psi_n + \Omega r v_y \cos\psi_n \qquad (3.19)$$

Wind velocities at the blade element in the disc plane U_T are then obtained by applying the transformation matrix due to pylon motion to change the x,y,z coordinate system to blade disc coordinate system. Wind velocities U_{xB} and U_{yB} are x_B, y_B components of the inplane velocity of the blade in the x_B-y_B coordinate system fixed to the rotor hub (Fig. 6). Gust velocity as well as the aircraft forward velocity is included.

$$\begin{Bmatrix} U_{xB} \\ U_{yB} \\ U_p \end{Bmatrix} = \begin{bmatrix} 1 & v_r & -v_p \\ -v_r & 1 & v_y \\ v_p & -v_y & 1 \end{bmatrix} \begin{Bmatrix} \dot{x} + u_G \\ \dot{y} + v_G \\ V + \dot{z} + w_G \end{Bmatrix} \qquad (3.20)$$

Tangential velocity U_T is expressed as

$$U_T = -U_{xB} \sin\psi_n + U_{yB} \cos\psi_n \qquad (3.21)$$

After higher order terms are neglected,

$$U_T = r\Omega - u_G \sin\psi_n + v_G \cos\psi_n + \dot{v}_n - \dot{r}_x \sin\psi_n - h(\dot{v}_p \sin\psi_n + \dot{v}_y \cos\psi_n)$$

$$U_p = V + w_g + \dot{w}_n + \dot{r}_z - r\dot{\nu}_p \cos\psi_n + r\dot{\nu}_y \sin\psi_n \tag{3.22}$$

Finally the perturbation velocities δU_T and δU_p are given as

$$\begin{aligned}\delta U_T = |\Omega| R\Big[& -\bar{\lambda}\frac{u_g}{V}\sin\psi_n + \bar{\lambda}\frac{v_g}{V}\cos\psi_n + \frac{\dot{v}_n}{R} \\ & - \frac{\dot{r}_z}{R}\sin\psi_n + x\dot{\nu}_r - \bar{h}\,(\dot{\nu}_p \sin\psi_n \\ & + \dot{\nu}_y \cos\psi_n) + \bar{\lambda}(\nu_p \sin\psi_n + \nu_y \cos\psi_n)\Big] \\ \delta U_p = |\Omega| R\Big[& \bar{\lambda}\frac{w_g}{V} + \frac{\dot{w}_n}{R} + \frac{\dot{r}_z}{R} - x\dot{\nu}_p \cos\psi_n \\ & + x\dot{\nu}_y \sin\psi_n\Big]\end{aligned} \tag{3.23}$$

where

$$(\dot{}) = \frac{\partial}{\partial(|\Omega| t)}$$

$$\bar{h} = h/R \tag{3.24}$$

Pitch-flap coupling gives a change in blade pitch angle proportional to the flapping angle at the root. It is defined as

$$(\theta_{pF})_n = -\left.\frac{\partial w_n}{\partial r}\right|_{r=0} \tan\delta_3 \tag{3.25}$$

The angle δ_3 is a design factor to yield the optimum pitch angle gain to prevent blade motion instability. Blade pitch control consists of collective pitch control and cyclic pitch control.

$$(\theta_c)_n = \theta_0(t) + \theta_{1c}(t)\cos\psi_n + \theta_{1s}(t)\sin\psi_n \tag{3.26}$$

Therefore, the perturbation quantity associated with the angle of attack of the blade is simply derived from Eq. 3.7 as

$$\delta\alpha = \theta_{pF} + \theta_c \tag{3.27}$$

3.2 Wing Aerodynamic Forces

Wing aerodynamic forces are derived by the blade aerodynamic perturbation method. Aerodynamic coefficients are obtained from strip theory (Ref. 15).

The wing element lift, drag and pitching moment (Fig. 7) per unit span length can be written as

$$dL = \frac{1}{2}\rho U_w^2 a_w \alpha_w c_w$$

$$dD = \frac{1}{2}\rho U_w^2 C_{D_0 w} c_w$$

$$dM_{\frac{1}{4}\bar{c}} = \frac{1}{2}\rho U_w^2 (C_{m_0} + C_{m_\alpha}\alpha_w) c_w^2 \qquad (3.28)$$

These values are transformed to the x,y,z coordinate system:

$$F_x = dL\cos\phi_w - dD\sin\phi_w$$
$$= \frac{1}{2}\rho c_w a_w U_w^2 \alpha_w \cos\phi_w - \frac{1}{2}\rho c_w C_{D_0 w} U_w^2 \sin\phi_w$$

$$F_z = -dD\cos\phi_w - dL\sin\phi_w$$
$$= -\frac{1}{2}\rho c_w C_{D_0 w} U_w^2 \cos\phi_w - \frac{1}{2}\rho c_w a_w U_w^2 \alpha_w \sin\phi_w$$

$$M_y = dM_{\frac{1}{4}\bar{c}} + dL\cdot\bar{e}\,c_w$$
$$= \frac{1}{2}\rho c_w^2 (C_{m_0} + C_{m_\alpha}\alpha_w) U_w^2$$
$$+ \frac{1}{2}\rho c_w^2 \bar{e}\, a_w U_w^2 \alpha_w \qquad (3.29)$$

where

$$U_w^2 = (V + \dot{w}_w + w_q)^2 + (\dot{u}_w + u_q)^2$$

$$\alpha_w = \theta_w + p_w - \phi_w$$

$$\tan\phi_w = \frac{\dot{u}_w + u_q}{V + \dot{w}_w + w_q} \qquad (3.30)$$

and $\bar{e}$ is the distance (nondimensionalized by wing chord) between the elastic axis and the quarter-chord line (positive if the quarter-chord line is ahead of the elastic axis).

Hereafter the small angle assumption may be used for the wing aerodynamic forces because of the small angle of attack and angle of twist. Then it is approximated that $\sin \phi_w = \phi_w$, $\cos \phi_w = 1$, etc.

Perturbation velocities $\dot{u}_w$, $\dot{w}_w$, p_w, u_G and w_G are chosen to express the aerodynamic forces. The perturbation equations are then given by

$$F_x = (F_x)_o + \left(\frac{\partial F_x}{\partial \dot{u}_w}\right)_o \dot{u}_w + \left(\frac{\partial F_x}{\partial \dot{w}_w}\right)_o \dot{w}_w + \left(\frac{\partial F_x}{\partial p_w}\right)_o p_w + \left(\frac{\partial F_x}{\partial u_G}\right)_o u_G + \left(\frac{\partial F_x}{\partial w_G}\right)_o w_G$$

$$F_z = (F_z)_o + \left(\frac{\partial F_z}{\partial \dot{u}_w}\right)_o \dot{u}_w + \left(\frac{\partial F_z}{\partial \dot{w}_w}\right)_o \dot{w}_w + \left(\frac{\partial F_z}{\partial p_w}\right)_o p_w + \left(\frac{\partial F_z}{\partial u_G}\right)_o u_G + \left(\frac{\partial F_z}{\partial w_G}\right)_o w_G$$

$$M_y = (M_y)_o + \left(\frac{\partial M_y}{\partial \dot{u}_w}\right)_o \dot{u}_w + \left(\frac{\partial M_y}{\partial \dot{w}_w}\right)_o \dot{w}_w + \left(\frac{\partial M_y}{\partial p_w}\right)_o p_w + \left(\frac{\partial M_y}{\partial u_G}\right)_o u_G + \left(\frac{\partial M_y}{\partial w_G}\right) w_G \qquad (3.31)$$

This study is concerned only with deviation from the equilibrium state. Then the steady state aerodynamic forces $(F_x)_o$, $(F_z)_o$ and $(M_y)_o$ may be dropped from the equations without inconsistency although the blade steady state aerodynamic forces $(P_z)_o$ and $(P_\theta)_o$ cannot be neglected since they influence the pylon motion.

Applying Eq. 3.31 to Eq. 3.29, the following expressions for the wing aerodynamic forces due to wing motion are obtained

$$F_x = \begin{bmatrix} -\frac{1}{2}\rho C_w V a_w \left(1 + \frac{C_{Dow}}{a_w}\right) \\ \rho C_w V a_w \alpha_{wo} \\ 0 \end{bmatrix}^T \begin{Bmatrix} \dot{u}_w \\ \dot{w}_w \\ \dot{p}_w \end{Bmatrix} + \begin{bmatrix} 0 \\ 0 \\ \frac{1}{2}\rho C_w V^2 a_w \end{bmatrix}^T \begin{Bmatrix} u_w \\ w_w \\ p_w \end{Bmatrix} + \begin{bmatrix} -\frac{1}{2}\rho C_w V a_w \left(1 + \frac{C_{Dow}}{a_w}\right) \\ 0 \\ \rho C_w V a_w \alpha_w \end{bmatrix}^T \begin{Bmatrix} u_g \\ v_g \\ w_g \end{Bmatrix} \qquad (3.32a)$$

$$F_z = \begin{bmatrix} -\frac{1}{2}\rho C_w V a_w \alpha_{wo} \\ -\rho C_w V C_{Dow} \\ 0 \end{bmatrix}^T \begin{Bmatrix} \dot{u}_w \\ \dot{w}_w \\ \dot{p}_w \end{Bmatrix} + \begin{bmatrix} -\frac{1}{2}\rho C_w V a_w \alpha_{wo} \\ 0 \\ -\rho C_w V C_{Dow} \end{bmatrix}^T \begin{Bmatrix} u_g \\ v_g \\ w_g \end{Bmatrix} \qquad (3.32b)$$

$$M_y = \begin{bmatrix} -\frac{1}{2}\rho C_w^2 V(C_{m_\alpha} + a_w \bar{e}) \\ \rho C_w^2 V(C_{m_0} + C_{m_\alpha}\alpha_{w_0} + a_w \alpha_{w_0} \bar{e}) \\ 0 \end{bmatrix}^T \begin{Bmatrix} \dot{u}_w \\ \dot{w}_w \\ \dot{p}_w \end{Bmatrix}$$

$$+ \begin{bmatrix} 0 \\ 0 \\ \frac{1}{2}\rho C_w^2 V^2 (C_{m_\alpha} + a_w \bar{e}) \end{bmatrix}^T \begin{Bmatrix} u_w \\ w_w \\ p_w \end{Bmatrix}$$

$$+ \begin{bmatrix} -\frac{1}{2}\rho C_w^2 V (C_{m_\alpha} + a_w \bar{e}) \\ 0 \\ \rho C_w^2 V(C_{m_0} + C_{m_\alpha}\alpha_{w_0} + a_w \alpha_{w_0} \bar{e}) \end{bmatrix}^T \begin{Bmatrix} u_g \\ v_g \\ w_g \end{Bmatrix} \tag{3.32c}$$

where the angle of attack in equilibrium state is given as

$$\alpha_{w_0} = \theta_w \tag{3.33}$$

SECTION 4

MODAL ANALYSES

4.1 Variational Functional

In order to apply Galerkin's method the variational functional is derived from Eqs. 2.4, 2.5, 2.6, 2.7, 2.8, 2.10, 2.11, 2.12, 2.13, and 2.14.

$$
\begin{aligned}
\Pi = &- \sum_{n=1}^{N}\left[\frac{1}{2}\int_0^R \left\{(EI)_C \sin^2\theta_B + (EI)_B \cos^2\theta_B\right\}\left(\frac{\partial^2 w_n}{\partial r^2}\right)^2 dr\right]_n \\
&- \sum_{n=1}^{N}\left[\frac{1}{2}\int_0^R \left\{(EI)_C \cos^2\theta_B + (EI)_B \sin^2\theta_B\right\}\left(\frac{\partial^2 v_n}{\partial r^2}\right)^2 dr\right]_n \\
&- \sum_{n=1}^{N}\left[\frac{1}{2}\int_0^R \left\{(EI)_C - (EI)_B\right\}\sin\theta_B\cos\theta_B \frac{\partial^2 w_n}{\partial r^2}\frac{\partial^2 v_n}{\partial r^2} dr\right]_n \\
&- \sum_{n=1}^{N}\left[\frac{1}{2}\int_0^R \left\{T\left(\frac{\partial w_n}{\partial r}\right)^2 + T\left(\frac{\partial v_n}{\partial r}\right)^2\right\} dr\right]_n \\
&+ \sum_{n=1}^{N}\left[\frac{1}{2}\int_0^R m\left(\dot{w}_n^2 + \dot{v}_n + \Omega^2 v_n^2\right) dr\right] \\
&+ \sum_{n=1}^{N}\left[\frac{1}{2}\int_0^R m\left(r\dot{v}_n\dot{\nu}_r - (v_n \dot{\sin\psi_n})(\dot{r}_x + h\dot{\nu}_p)\right.\right. \\
&\quad + \dot{w}_n \dot{r}_E - h(v_n \dot{\cos\psi_n})\dot{\nu}_y + r\left\{(w_n \dot{\sin\psi_n})\dot{\nu}_y\right. \\
&\quad - (w_n \dot{\cos\psi_n})\dot{\nu}_p - 2\Omega w_n \dot{\nu}_y \cos\psi_n \\
&\quad \left.\left.\left. - 2\Omega w_n \dot{\nu}_p \sin\psi_n\right\}\right) dr\right]_n \\
&+ \frac{M_B N}{2}\left\{(\dot{r}_x + h\dot{\nu}_p)^2 + \dot{r}_E^2 + h^2\dot{\nu}_y^2\right\} \\
&+ \frac{I_B N}{2}\left\{\frac{\dot{\nu}_R^2}{2} + \frac{\dot{\nu}_P^2}{2} + \dot{\nu}_r^2 + 2\Omega\nu_p\dot{\nu}_y\right\}
\end{aligned}
$$

$$-\frac{1}{2}\int_0^L \left\{(EI_w)_c \sin^2\theta_w + (EI_w)_s \cos^2\theta_w\right\}\left(\frac{\partial^2 u_w}{\partial y^2}\right)^2 dy$$

$$-\frac{1}{2}\int_0^L \left\{(EI_w)_c \cos^2\theta_w + (EI_w)_s \sin^2\theta_w\right\}\left(\frac{\partial^2 v_w}{\partial y^2}\right)^2 dy$$

$$-\frac{1}{2}\int_0^L \left\{(EI_w)_c - (EI_w)_s \sin\theta_w \cos\theta_w\right\}\frac{\partial^2 u_w}{\partial y^2}\frac{\partial^2 v_w}{\partial y^2} dy$$

$$-\frac{1}{2}\int_0^L (GJ)\left(\frac{\partial \beta_w}{\partial y}\right)^2 dy$$

$$+\frac{1}{2}\int_0^L m_w \dot{u}_w^2 dy + \frac{1}{2}\int_0^L m_w \dot{v}_w^2 dy$$

$$+\frac{1}{2}\int_0^L I_w \dot{\beta}_w^2 dy + \int_0^L S_x \dot{u}_w \dot{\beta}_w dy$$

$$+\frac{1}{2} M_p \dot{r}_x^2 + \frac{1}{2} M_p \dot{r}_z^2 + \frac{1}{2} I_{p_y} \dot{\nu}_y^2$$

$$+\frac{1}{2} I_{p_p} \dot{\nu}_p^2 + \frac{1}{2} I_{p_r} \dot{\nu}_r^2$$

$$+\frac{1}{2}\sum_{n=1}^{N}\left[\int_0^R (P_z\ w_n) dr\right]_n$$

$$+\frac{1}{2}\sum_{n=1}^{N}\left[\int_0^R (P_\theta\ v_n) dr\right]_n$$

$$+\sum_{n=1}^{N}\left[\int_0^R (-P_\theta \sin\Phi_n + \nu_p P_z) dr\right]_n r_x$$

$$+\sum_{n=1}^{N}\left[\int_0^R (-\nu_p P_\theta \sin\Phi_n + \nu_y P_\theta \cos\Phi_n + P_z) dr\right]_n r_z$$

$$+\sum_{n=1}^{N}\left[\int_0^R \left\{-h(P_\theta \cos\Phi_n - \nu_y P_z) + r\nu_p P_\theta\right.\right.$$

$$\left. + r P_z \sin\Phi_n + P_z v_n \cos\Phi_n\right.$$

$$\left.\left. - P_\theta w_n \cos\Phi_n\right\} dr\right]_n \nu_y$$

$$+\sum_{n=1}^{N}\left[\int_0^R\left\{\rho\left(-P_\theta \sin\Phi_n + v_p P_z - w_n P_\theta \sin\Phi_n\right.\right.\right.$$

$$\left.\left.\left. + v_n P_z \sin\Phi_n - r P_z \cos\Phi_n\right\} dr\right]_n v_p$$

$$+\sum_{n=1}^{N}\left[\int_0^R (r P_\theta)\, dr\right]_n v_r$$

$$+\int_0^L F_x u_w\, dy$$

$$+\int_0^L F_z w_w\, dy$$

$$+\int_0^L M_y p_w\, dy \qquad (4.1)$$

4.2 Free Vibration of the Blade and Wing

In preparation for modal analysis of the basic equations, the free vibration of the rotating blade and the cantilever wing will be considered. It is very advantageous to use the natural frequency of the free vibrating beam to represent the quite complicated stiffness terms of the beam.

The variational functional for free vibration of the rotating blade is derived from Eqs. 4.1, neglecting aerodynamic forces, pylon and wing motion.

$$\pi_\theta = -\sum_{n=1}^{N}\left[\frac{1}{2}\int_0^R\left\{(EI)_c \sin^2\theta_s + (EI)_s \cos^2\theta_s\right\}\left(\frac{\partial^2 w_n}{\partial r^2}\right)^2 dr\right]_n$$

$$- \sum_{n=1}^{N} \left[\frac{1}{2} \int_0^R \left\{ (EI)_c \cos^2\theta_B + (EI)_B \sin^2\theta_B \right\} \left(\frac{\partial^2 U_n}{\partial r^2} \right)^2 dr \right]_n$$

$$- \sum_{n=1}^{N} \left[\frac{1}{2} \int_0^R \left\{ (EI)_c - (EI)_B \right\} \sin\theta_B \cos\theta_B \right\} \frac{\partial^2 W_n}{\partial r^2} \frac{\partial^2 U_n}{\partial r^2} \Big]_n$$

$$- \sum_{n=1}^{N} \left[\frac{1}{2} \int_0^R \left\{ T \left(\frac{\partial W_n}{\partial r} \right)^2 + T \left(\frac{\partial U_n}{\partial r} \right)^2 \right\} dr \right]_n$$

$$+ \sum_{n=1}^{N} \left[\frac{1}{2} \int_0^R m \left(\dot{W}_n^2 + \dot{U}_n^2 + \Omega^2 U_n^2 \right) dr \right]_n \qquad (4.2)$$

Assume a series solution in terms of normal modes which express the coupled motion of inplane and out-of-plane motion

$$\begin{Bmatrix} W_n \\ U_n \end{Bmatrix} = \sum_j \begin{Bmatrix} W_j(r) \\ V_j(r) \end{Bmatrix} q_{nj}(t) \qquad (4.3)$$

Substituting Eq. 4.3 into Eq. 4.2 and applying Lagrange's equations as follows:

$$\frac{d}{dt} \left(\frac{\partial \pi_B}{\partial \dot{q}_{ni}} \right) - \frac{\partial \pi_B}{\partial q_{ni}} = 0 \qquad (4.4)$$

yields

$$\int_0^R \Big[\left\{ (EI)_c \sin^2\theta_B + (EI)_B \cos^2\theta_B \right\} \left(\frac{d^2 W_i}{dr^2} \right) \left(\frac{d^2 W_j}{dr^2} \right)$$

$$+ \left\{ (EI)_c \cos^2\theta_B + (EI)_B \sin^2\theta_B \right\} \left(\frac{d^2 V_i}{dr^2} \right) \left(\frac{d^2 V_j}{dr^2} \right)$$

$$+\frac{1}{2}\left\{(EI)_c-(EI)_B\right\}\sin\theta_B\cos\theta_B\left(\frac{d^2W_i}{dr^2}\frac{d^2V_j}{dr^2}+\frac{d^2W_j}{dr^2}\frac{d^2V_i}{dr^2}\right)$$

$$+T\frac{dW_i}{dr}\frac{dW_j}{dr}+T\frac{dV_i}{dr}\frac{dV_j}{dr}+\Omega^2 m V_i V_j\Big]dr$$

$$=\lambda_j^2\int_0^R m\left(W_i W_j+V_i V_j\right)dr \qquad (4.5)$$

where λ_j denotes the jth rotating undamped natural frequency of the blade. Simplification of Eq. 4.5 will result from use of the orthogonality condition (Ref. 15) of the normal modes which is expressed as

$$\int_0^R m(W_i W_j+V_i V_j)dr=\begin{cases}\int_0^R m(W_i^2+V_i^2)dr & j=i\\ 0 & j\neq i\end{cases} \qquad (4.6)$$

The amplitude of the mode shape is normalized to unity as

$$\int_0^R m\left(W_i^2+V_i^2\right)dr=1 \qquad (4.7)$$

Hence, Eq. 4.4 results in

$$\int_0^R\Big[\left\{(EI)_c\sin^2\theta_B+(EI)_B\cos^2\theta_B\right\}\left(\frac{d^2W_i}{dr^2}\right)\left(\frac{d^2W_j}{dr^2}\right)$$

$$+\left\{(EI)_c\cos^2\theta_B+(EI)_B\sin^2\theta_B\right\}\left(\frac{d^2V_i}{dr^2}\right)\left(\frac{d^2V_j}{dr^2}\right)$$

$$+\frac{1}{2}\left\{(EI)_c-(EI)_B\right\}\sin\theta_B\cos\theta_B\left(\frac{d^2W_i}{dr^2}\frac{d^2V_j}{dr^2}+\frac{d^2W_j}{dr^2}\frac{d^2V_i}{dr^2}\right)$$

$$+ T \frac{dW_i}{dr} \frac{dW_j}{dr} + T \frac{dV_i}{dr} \frac{dV_j}{dr} + \Omega^2 m V_i V_j \Big] dr$$

$$= \begin{cases} \lambda_i^2 & j = i \\ 0 & j \neq i \end{cases} \qquad (4.8)$$

In the similar way the free vibration of the wing will be analyzed, treating the rotor and pylon as lumped masses at the wing tip. The wing deflection can be expressed as

$$\begin{Bmatrix} u_w \\ w_w \\ \phi_w \end{Bmatrix} = \sum_j \begin{Bmatrix} \gamma_j(y) \\ \zeta_j(y) \\ \phi_j(y) \end{Bmatrix} q_j(t) \qquad (4.9)$$

Then, pylon motion is described by

$$\begin{Bmatrix} r_x/R \\ r_y/R \\ v_y \\ v_p \\ v_r \end{Bmatrix} = \sum_j \begin{Bmatrix} \gamma_j/R \\ \zeta_j/R \\ \frac{d\zeta_j}{dy} \\ \phi_j \\ -\frac{d\gamma_j}{dy} \end{Bmatrix}_{y=L} q_j(t)$$

$$= [T] \{q(t)\} \qquad (4.10)$$

where

$$[T] = \begin{bmatrix} \gamma_1/R & \gamma_2/R & \cdots & \gamma_n/R \\ \zeta_1/R & \zeta_2/R & \cdots & \zeta_n/R \\ \frac{d\zeta_1}{dy} & \frac{d\zeta_2}{dy} & \cdots & \frac{d\zeta_n}{dy} \\ \phi_1 & \phi_2 & \cdots & \phi_n \\ -\frac{d\gamma_1}{dy} & -\frac{d\gamma_2}{dy} & \cdots & -\frac{d\gamma_n}{dy} \end{bmatrix} \qquad (4.11)$$

$$\{a(t)\} = \begin{Bmatrix} a_1(t) \\ a_2(t) \\ \vdots \\ a_n(t) \end{Bmatrix}$$

The wing coupled modes are normalized as

$$\int_0^L \left\{ m_w(\gamma_j^2 + \zeta_j^2) + I_w \phi_j^2 + 2 S_w \gamma_j \phi_j \right\} dy$$

$$+ \left[M_p(\gamma_j^2 + \zeta_j^2) + I_{p_y}\left(\frac{d\zeta_j}{dy}\right)^2 + I_{p_p}\phi_j^2 + I_{p_r}\left(\frac{d\gamma_j}{dy}\right)^2 \right]_{y=L}$$

$$+ N M_B \left[(\gamma_j + k\phi_j)^2 + k^2\left(\frac{d\zeta_j}{dy}\right)^2 + \zeta_j^2 \right]_{y=L}$$

$$+ \frac{N I_B}{2} \left[2\left(\frac{d\gamma_j}{dy}\right)^2 + \left(\frac{d\zeta_j}{dy}\right)^2 + \phi_j^2 \right]_{y=L}$$

$$= 1 \qquad (4.12)$$

Hence,

$$\int_0^L \Big[\Big\{ (EI_w)_c \sin^2\theta_w + (EI_w)_B \cos^2\theta_w \Big\} \Big(\frac{d^2\gamma_i}{dy^2} \Big) \Big(\frac{d^2\gamma_j}{dy^2} \Big)$$

$$+ \Big\{ (EI_w)_c \cos^2\theta_w + (EI_w)_B \sin^2\theta_w \Big\} \Big(\frac{d^2\zeta_i}{dy^2} \Big) \Big(\frac{d^2\zeta_j}{dy^2} \Big)$$

$$+ \frac{1}{2} \Big\{ (EI_w)_c - (EI_w)_B \Big\} \sin\theta_w \cos\theta_w \Big(\frac{d^2\gamma_i}{dy^2} \frac{d^2\zeta_j}{dy^2} + \frac{d^2\gamma_j}{dy^2} \frac{d^2\zeta_i}{dy^2} \Big)$$

$$+ (GJ_w) \frac{d\phi_i}{dy} \frac{d\phi_j}{dy} \Big] dy$$

$$= \begin{cases} \Lambda_j^2 & i = j \\ 0 & i \neq j \end{cases} \qquad (4.13)$$

where Λ_j is the jth wing undamped natural frequency.

4.3 The Variational Functional Described in Modal Form

The simplified variational functional expressed in terms of natural frequencies is

$$\pi = -\frac{1}{2} \sum_{n=1}^{N} \Big[\sum_j \big(\lambda_j^2 q_{nj}^2 \big) \Big]_n + \frac{1}{2} \sum_{n=1}^{N} \Big[\sum_j \dot{q}_{nj}^2 \Big]_n$$

$$+ \sum_{n=1}^{N} \Big[\frac{1}{2} \int_0^R m \Big(r \Big\{ \sum_j V_j \dot{q}_{nj} \Big\} \Big\{ - \sum_i \frac{d\gamma_i}{dy} \dot{a}_i \Big\}_{y=L}$$

$$- \Big\{ \sum_j V_j \big(q_{nj} \dot{\sin\psi_n} \big) \Big\} \Big\{ \sum_i (\gamma_i + h\phi_j) \dot{a}_i \Big\}_{y=L}$$

$$+ \Big(\sum_j W_j \dot{q}_{nj} \Big) \Big(\sum_i \zeta_i \dot{a}_i \Big)_{y=L} - h \Big\{ \sum_j V_j \big(q_{nj} \dot{\cos\psi_n} \big) \Big\} \Big(\sum_i \frac{d\zeta_i}{dy} \dot{a}_i \Big)_{y=L}$$

$$
\begin{aligned}
&+ r\left\{\sum_j W_j \left(q_{nj}\dot{\sin\psi_n}\right)\right\}\left(\sum_i \frac{dz_i}{dy}\dot{a}_i\right)_{y=L} \\
&- r\left\{\sum_j W_j \left(q_{nj}\dot{\cos\psi_n}\right)\right\}\left(\sum_i \phi_i \dot{a}_i\right)_{y=L} \\
&- 2r\Omega\left(\sum_j W_j q_{nj}\right)\left(\sum_i \frac{dz_i}{dy}\dot{a}_i\right)_{y=L}\cos\psi_n \\
&- 2r\Omega\left(\sum_j W_j q_{nj}\right)\left(\sum_i \phi_i \dot{a}_i\right)_{y=L}\sin\psi_n \Big) dr \Big]_n \\
&- \frac{1}{2}\sum_i \left(\Lambda_i^2 a_i^2\right) + \frac{1}{2}\sum_i \dot{a}_i^2 + I_B N\Omega\left(\sum_i \phi_i a_i\right)_{y=L}\left(\sum_i \frac{dz_i}{dy}\dot{a}_i\right)_{y=L} \\
&+ \sum_{n=1}^{N}\left[\int_0^R P_z\left(\sum_j W_j q_{nj}\right) dr\right]_n \\
&+ \sum_{n=1}^{N}\left[\int_0^R P_\theta\left(\sum_j V_j q_{nj}\right) dr\right]_n \\
&+ W_{WB} \quad + W_{WW}
\end{aligned}
\tag{4.14}
$$

where W_{WB} denotes the work on the wing done by rotor aerodynamic forces and W_{WW} the work on the wing done by wing aerodynamic forces. Details are discussed in Subsection 4.5.

The principle of virtual work is applied to Eq. 4.14 to obtain the modal equation for the blade and wing.

For the blade the modal equation can be expressed as

$$
\ddot{q}_{nj} + \lambda_j^2 q_{nj} + V_{ij}\ddot{\nu}_r - V_{oj}\left(\frac{\ddot{r}_x}{R} + \overline{h}\,\ddot{\nu}_p\right)\sin\psi_n
$$

$$+ W_{oj}\frac{\ddot{r}_z}{R} - \bar{k}\, V_{oj}\ddot{\nu}_y \cos\psi_n + W_{ij}\ddot{\nu}_y \sin\psi_n$$

$$- W_{ij}\ddot{\nu}_p \cos\psi_n + 2\Omega W_{ij}\dot{\nu}_y \cos\psi_n$$

$$+ 2\Omega W_{ij}\dot{\nu}_p \sin\psi_n$$

$$= P_{oj} + P_{zj} \qquad (4.15)$$

where

$$W_{ij} = R^{1-i}\left[\int_0^R m r^i W_j\, dr\right] \qquad (i = 0, 1)$$

$$V_{ij} = R^{1-i}\left[\int_0^R m r^i V_j\, dr\right] \qquad (i = 0, 1) \qquad (4.16)$$

$$P_{oj} = \int_0^R P_o V_j\, dr$$

$$P_{zj} = \int_0^R P_z W_j\, dr \qquad (4.17)$$

For the wing modal equation can be expressed as

$$\ddot{a}_i + \Lambda_i^2 a_i + I_B N\Omega\left[\sum_j\left(\frac{d\beta_i}{dy}\phi_j - \phi_i\frac{d\beta_i}{dy}\right)\dot{a}_i\right]_{y=L}$$

$$+\sum_{n=1}^{N}\sum_j\Big[-V_{ij}\ddot{q}_{nj}\left(\frac{d\delta_i}{dy}\right)_{y=L} - V_{oj}\left(q_{nj}\ddot{\sin}\psi_n\right)\left(\frac{\gamma_i}{R}+\bar{h}\phi_i\right)_{y=L}$$

$$+W_{oj}\ddot{q}_{nj}\left(\frac{\beta_i}{R}\right)_{y=L} - \bar{h}\,V_{oj}\left(q_{nj}\ddot{\cos}\psi_n\right)\left(\frac{d\beta_i}{dy}\right)_{y=L}$$

$$-W_{ij}\left(q_{nj}\ddot{\sin}\psi_n\right)\left(\frac{d\beta_i}{dy}\right)_{y=L} - W_{ij}\left(q_{nj}\ddot{\cos}\psi_n\right)(\phi_i)_{y=L}$$

$$-2\Omega W_{ij}\left(q_{nj}\dot{\cos}\psi_n\right)\left(\frac{d\beta_i}{dy}\right)_{y=L} - 2\Omega W_{ij}\left(q_{nj}\dot{\sin}\psi_n\right)(\phi_i)_{y=L}\Big]_n$$

$$= f_i + g_i \qquad (4.18)$$

where f_i denotes the loading due to the rotor aerodynamic forces derived from the work W_{WB}, and g_i the loading due to wing aerodynamic forces derived from the work W_{WW}.

4.4 Rotor Non-Rotating Coordinate System

4.4.1 Rotor Non-Rotating Coordinate System

The equations of motion 4.15 and 4.18 of the blade and wing have periodic coefficients because of the appearance of $\sin\psi_n$ and $\cos\psi_n$. To avoid difficulties due to these periodic coefficients, the Fourier-type coordinate system will be chosen to describe the motion in the non-rotating system instead of the rotating system (Ref. 16).

(a) For the hingeless rotor, the Fourier coordinate system is described in general as

$$q_{nj} = Q_{j0} + \sum_m\left[Q_{jc(m)}\cos(m\psi_n) + Q_{js(m)}\sin(m\psi_n)\right] + Q_{j\frac{N}{2}}(-1)^n \qquad (4.19)$$

where Q_{jo} is the collective motion, $Q_{jc(m)}$ and $Q_{js(m)}$ are cyclic motion of mth order, defining tilting or warping of the rotor plane and $Q_{j\frac{N}{2}}$ is differential collective motion (only occurring for even N-bladed rotors).

Since many recent proprotor designs have three-bladed rotors, this study is concentrated on the odd N-bladed rotor model. Therefore, the last term $Q_{j\frac{N}{2}}$ of Eq. 4.19, the differential collective motion, will be dropped hereafter. In addition to this, the higher order terms $Q_{jc(2)}, Q_{js(2)}, \cdots Q_{jc(m)}, Q_{js(m)}$ are not coupled with pylon motion. They represent internal rotor motion and usually make only a small contribution to rotor motion. Therefore they are also truncated in this study. Hence,

$$q_{nj} = Q_{jo} + Q_{jc}\cos\psi_n + Q_{js}\sin\psi_n \tag{4.20}$$

By inverting the system of Eq. 4.20, the new degrees of freedom of the non-rotating system can be obtained:

$$\begin{aligned} Q_{jo} &= \frac{1}{N}\sum_{n=1}^{N} q_{nj} \\ Q_{jc} &= \frac{2}{N}\sum_{n=1}^{N} q_{nj}\cos\psi_n \\ Q_{js} &= \frac{2}{N}\sum_{n=1}^{N} q_{nj}\sin\psi_n \end{aligned} \tag{4.21}$$

The same approach may be applied for the rotor generalized force due to periodic aerodynamic forces.

$$\begin{aligned} (P_{\theta j} + P_{zj})_o &= \frac{1}{N}\sum_{n=1}^{N}(P_{\theta j} + P_{zj}) \\ (P_{\theta j} + P_{zj})_c &= \frac{2}{N}\sum_{n=1}^{N}(P_{\theta j} + P_{zj})\cos\psi_n \\ (P_{\theta j} + P_{zj})_s &= \frac{2}{N}\sum_{n=1}^{N}(P_{\theta j} + P_{zj})\sin\psi_n \end{aligned} \tag{4.22}$$

(b) For the gimballed rotor, special care must be taken since it has both collective mode shapes (symmetrical modes with clamped boundary condition at the root) and cyclic mode shapes (antisymmetrical mode shapes with hinged boundary condition), while in the hingeless rotor case both collective mode shapes and cyclic mode shapes are the same. Therefore, collective motion is described with collective mode shapes W_j^o, V_j^o and cyclic motion with cyclic mode shapes W_j^c, V_j^c.

$$\begin{Bmatrix} w_n \\ v_n \end{Bmatrix} = \sum_j \left[\begin{Bmatrix} W_j^o \\ V_j^o \end{Bmatrix} Q_{jo} + \begin{Bmatrix} W_j^c \\ V_j^c \end{Bmatrix} (Q_{jc} \cos\psi_n + Q_{js} \sin\psi_n) \right] \qquad (4.23)$$

This expression is consistent with the derivation of equations of motion up to now, if mode shapes W_j, V_j of the coefficients of the blade collective motion are replaced by the collective mode shapes W_j^o, V_j^o in Eq. 4.15 and 4.18, and those of cyclic motion are replaced by the cyclic mode shapes W_j^c, V_j^c. Therefore, the derivation of equations of motion hereafter is based on the hingeless rotor case, and those equations can be applied to the gimballed rotor case as stated before without confusion. The coefficients associated with collective mode shapes are denoted by superscript 0 and those with cyclic mode shapes by superscript c.

The truncation of higher order terms and of the differential collective motion in Eq. 4.19 is also applied to the gimballed rotor case by the same reasoning as for the hingeless rotor case.

The orthogonality condition for the gimballed rotor case is different from the hingeless orthogonality condition. The entire rotor system including periodic functions $\sin\psi_n$ and $\cos\psi_n$ must be considered. For example, the orthogonality condition between the collective mode and the cyclic sine mode is described as

$$\sum_{n=1}^{N} \int_0^R m \left\{ W_j^o W_j^c \sin\psi_n + V_j^o V_j^c \sin\psi_n \right\} dr$$

$$= \left\{ \int_0^R m \left(W_j^o W_j^c + V_j^o V_j^c \right) dr \right\} \left\{ \sum_{n=1}^{N} \sin\psi_n \right\}$$

$$= 0 \qquad (4.24)$$

Since ψ_n is the phase angle defined in Eq. 2.3, the summation over n=1, ... N of $\sin\psi_n$ becomes zero.

4.4.2 Pitch-Flap Coupling in the Non-Rotating Coordinate System

Pitch-Flap Coupling is expressed in Eq. 3.25 as

$$\theta_{PF} = - \left. \frac{\partial w_n}{\partial r} \right|_{r=0} \tan\delta_3 \qquad (3.25)$$

The substitution of mode shapes into this expression gives

$$\theta_{PF} = \sum_i \left[- \left. \frac{dW_i}{dr} \right|_{r=0} \tan\delta_3 \left\{ Q_{i0} + Q_{ic} \cos\psi_n + Q_{is} \sin\psi_n \right\} \right]$$

$$= \sum_i K_{pi} \left\{ Q_{i0} + Q_{ic} \cos\psi_n + Q_{is} \sin\psi_n \right\} \qquad (4.25)$$

where

$$K_{pi} = - \left. \frac{dW_i}{dr} \right|_{r=0} \tan\delta_3 \qquad (4.26)$$

For the hingeless rotor case considered here, K_{pi} is always zero because the slopes of blade mode shapes at the root are zero, due to the clamped boundary condition.

For the gimballed rotor case, Eq. 4.25 is rewritten as

$$\theta_{PF} = \sum_i \left[K_{pi}^{o} Q_{io} + K_{pi}^{c} (Q_{ic} \cos \psi_n + Q_{is} \sin \psi_n) \right] \tag{4.27}$$

where

$$K_{pi}^{o} = - \left. \frac{dW_i^o}{dr} \right|_{r=0} \tan \delta_3$$

$$K_{pi}^{c} = - \left. \frac{dW_i^c}{dr} \right|_{r=0} \tan \delta_3 \tag{4.28}$$

From the definition of the collective mode shapes, K_{pi}^{o} is zero. Therefore, for the gimballed rotor case the pitch-flap coupling contributes only to the cyclic motion of the rotor, not to the collective motion.

4.5 Aerodynamic Forces Described in Modal Form

4.5.1 Blade Aerodynamic Forces

From Eq. 4.17 blade aerodynamic force is described as

$$P_{oj} + P_{zj} = \int_0^R (P_\theta V_j + P_z W_j) \, dr \tag{4.29}$$

The application of Eq. 4.22, accompanied by the substitution Eq. 4.21 into Eq. 3.13 yields

$$(P_{Qj} + P_{Tj})_o = \tfrac{1}{2}\gamma I_B \Omega^2 \Big[\sum_i G_{ji} \overset{\circ}{Q}_{io} + G_{IIj} \overset{\circ}{\nu}_r + G_{IIIj} \frac{\overset{\circ}{r}_x}{R} + \bar{\lambda}\, G_{IIIj} \frac{u_G}{V} + G_{Vj} \sum_i K_{Pi} Q_{io} + G_{Vj} \theta_o \Big] \tag{4.30}$$

$$(P_{Qj} + P_{Tj})_c = \tfrac{1}{2}\gamma I_B \Omega^2 \Big[\sum_i G_{ji} \overset{\circ}{Q}_{ic} + \bar{\Omega} \sum_i G_{ji} Q_{is} - \bar{h}\, G_{Tj} \overset{\circ}{\nu}_y + \bar{\lambda}\, G_{Tj} \nu_y - G_{Wj} \overset{\circ}{\nu}_p + \bar{\lambda}\, G_{Tj} \frac{v_G}{V} + G_{Vj} \sum_i K_{Pi} Q_{ic} + G_{Vj} \theta_c \Big] \tag{4.31}$$

$$(P_{Qj} + P_{Tj})_s = \tfrac{1}{2}\gamma I_B \Omega^2 \Big[\sum_i G_{ji} \overset{\circ}{Q}_{is} \bar{\Omega} \sum_i G_{ji} Q_{ic} - G_{Tj} \frac{\overset{\circ}{r}_x}{R} - \bar{h}\, G_{Tj} \overset{\circ}{\nu}_p + \bar{\lambda}\, G_{Tj} \nu_p + G_{Wj} \overset{\circ}{\nu}_y + \bar{\lambda}\, G_{Tj} \frac{u_G}{V} + G_{Vj} \sum_i K_{Pi} Q_{is} + G_{Vj} \theta_{is} \Big] \tag{4.32}$$

where

$$G_{ji} = \int_0^1 \left(F_{\theta 1} \frac{V_j V_i}{R^2} + F_{z1} \frac{W_j V_i}{R^2} + F_{\theta 2} \frac{V_j W_i}{R^2} + F_{z2} \frac{W_j W_i}{R^2} \right) dx$$

$$G_{Ij} = \int_0^1 \left(F_{\theta 1} \frac{V_j}{R} + F_{z1} \frac{W_j}{R} \right) dx$$

$$G_{IIj} = \int_0^1 \left(F_{\theta 1} \frac{V_j}{R} + F_{z1} \frac{W_j}{R} \right) x\, dx$$

$$G_{IIIj} = \int_0^1 \left(F_{\theta 2} \frac{V_j}{R} + F_{z2} \frac{W_j}{R} \right) dx$$

$$G_{IVj} = \int_0^1 \left(F_{\theta 2} \frac{V_j}{R} + F_{z2} \frac{W_j}{R} \right) x\, dx$$

$$G_{Vj} = \int_0^1 \left(F_{\theta 3} \frac{V_j}{R} + F_{z3} \frac{W_j}{R} \right) dx \qquad (4.33)$$

$$F_{\theta 0} = P_{\theta 0} \Big/ \left[\tfrac{1}{2} \gamma I_B \left(\frac{\Omega}{R} \right)^2 \right]$$

$$F_{\theta 1} = \left(\frac{\partial P_\theta}{\partial U_r} \right)_0 \Big/ \left[\tfrac{1}{2} \gamma I_B \frac{|\Omega|}{R^3} \right]$$

$$F_{\theta 2} = \left(\frac{\partial P_\theta}{\partial U_p} \right)_0 \Big/ \left[\tfrac{1}{2} \gamma I_B \frac{|\Omega|}{R^3} \right]$$

$$F_{\theta 3} = \left(\frac{\partial P_\theta}{\partial \theta} \right)_0 \Big/ \left[\tfrac{1}{2} \gamma I_B \left(\frac{\Omega}{R} \right)^2 \right]$$

$$F_{z0} = P_{z0} \Big/ \left[\tfrac{1}{2} \gamma I_B \left(\frac{\Omega}{R} \right)^2 \right]$$

$$F_{z1} = \left(\frac{\partial P_z}{\partial U_r} \right)_0 \Big/ \left[\tfrac{1}{2} \gamma I_B \frac{|\Omega|}{R^3} \right]$$

$$F_{z2} = \left(\frac{\partial P_z}{\partial U_p} \right)_0 \Big/ \left[\tfrac{1}{2} \gamma I_B \frac{|\Omega|}{R^3} \right]$$

$$F_{z3} = \left(\frac{\partial P_z}{\partial \theta} \right)_0 \Big/ \left[\tfrac{1}{2} \gamma I_B \frac{|\Omega|}{R^3} \right] \qquad (4.34)$$

4.5.2 Wing-Loading Due to Blade Aerodynamic Forces

The virtual work done by wing loading due to blade aerodynamic forces is described as

$$\delta W_{wb} = \left[\delta r_x \quad \delta r_z \quad \delta \nu_y \quad \delta \nu_p \quad \delta \nu_r \right] \times$$

$$\begin{bmatrix} -P_\Theta \sin\Phi_n + \nu_p P_z \\ \nu_p P_\Theta \sin\psi_n + \nu_y P_\Theta \cos\psi_n + P_z \\ -h(P_\Theta \cos\Phi_n - \nu_y P_z) + \nu_p r P_\Theta + r P_z \sin\Phi_n + P_z v_n \cos\psi_n - P_\Theta w_n \cos\psi_n \\ h(-P_\Theta \sin\Phi_n + \nu_p P_z) - P_\Theta w_n \sin\psi_n + P_z v_n \sin\psi_n - P_z r \cos\Phi_n \\ r P_\Theta \end{bmatrix} \quad (4.35)$$

The application of the blade mode shapes and non-rotating coordinate system gives

$$\delta W_{wb} = \Omega^2 \begin{Bmatrix} \delta r_x/R \\ \delta r_z/R \\ \delta \nu_y \\ \delta \nu_p \\ \delta \nu_r \end{Bmatrix}^T \left[\kappa \left[A_{\dot{a}}^{(2)} \right] \begin{Bmatrix} \overset{o}{r_x}/R \\ \overset{o}{r_z}/R \\ \overset{o}{\nu}_y \\ \overset{o}{\nu}_p \\ \overset{o}{\nu}_r \end{Bmatrix} + \kappa \left[A_a^{(2)} \right] \begin{Bmatrix} r_x/R \\ r_z/R \\ \nu_y \\ \nu_p \\ \nu_r \end{Bmatrix} \right.$$

$$+ \sum_i \kappa \left[A_{\dot{q}_i}^{(2)} \right] \left\{ \overset{o}{Q}_i \right\} + \sum_i \kappa \left[A_{q_i}^{(2)} \right] \left\{ Q_i \right\}$$

$$\left. + \kappa \left[A_c^{(2)} \right] \begin{Bmatrix} u_g/V \\ v_g/V \\ w_g/V \\ \theta_0 \\ \theta_{1c} \\ \theta_{1s} \end{Bmatrix} \right] \quad (4.36)$$

where κ is an integral operator defined as

$$\kappa = \frac{N}{2}\gamma I_B \int_0^1 \quad d\chi \tag{4.37}$$

and integrand matrices are

$$[A_a^{(2)}] = \left[\begin{array}{c|c|c} \frac{1}{2}F_{\theta 1} & 0 & -\frac{1}{2}\chi F_{\theta 2} \\ \hline 0 & F_{z_2} & 0 \\ \hline -\frac{1}{2}\chi F_{\theta 1} & 0 & \frac{1}{2}(\bar{k}^2 F_{\theta 1} + \chi^2 F_{z_2}) \\ \hline \frac{1}{2}\bar{k} F_{\theta 1} & 0 & \frac{1}{2}\bar{k}\chi(-F_{\theta 2} + F_{z_1}) \\ \hline 0 & \chi F_{\theta 2} & 0 \end{array}\right.$$

$$\left.\begin{array}{c|c} \frac{1}{2}\bar{k} F_{\theta 1} & 0 \\ \hline 0 & \chi F_{z_1} \\ \hline \frac{1}{2}\bar{k}\chi(F_{\theta 2} - F_{z_1}) & 0 \\ \hline \frac{1}{2}(\bar{k}^2 F_{\theta 1} + \chi^2 F_{z_2}) & 0 \\ \hline 0 & \chi^2 F_{\theta 1} \end{array}\right] \tag{4.38a}$$

$$[A_a^{(2)}] = \left[\begin{array}{c|c|c|c|c} 0 & 0 & 0 & -\frac{\bar{\lambda}}{2}F_{\theta 1} + F_{z_0} & 0 \\ \hline 0 & 0 & 0 & 0 & 0 \\ \hline 0 & 0 & \bar{k}(F_{z_0} - \frac{\bar{\lambda}}{2}F_{\theta 1}) & \frac{\bar{\lambda}}{2}\chi F_{z_1} + \chi F_{\theta_0} & 0 \\ \hline 0 & 0 & -\frac{\bar{\lambda}}{2}\chi F_{z_1} & \bar{k}(F_{z_0} - \frac{\bar{\lambda}}{2}F_{\theta 1}) & 0 \\ \hline 0 & 0 & 0 & 0 & 0 \end{array}\right] \tag{4.38b}$$

$$[A^{(2)}_{\dot{q}_i}] = \begin{bmatrix} 0 & 0 & -\frac{1}{2}\left(\frac{V_i}{R}F_{\theta_1} + \frac{W_i}{R}F_{\theta_2}\right) \\ \frac{V_i}{R}F_{z_1} + \frac{W_i}{R}F_{z_2} & 0 & 0 \\ 0 & -\frac{\bar{\rho}}{2}\left(\frac{V_i}{R}F_{\theta_1} + \frac{W_i}{R}F_{\theta_2}\right) & \frac{\alpha}{2}\left(\frac{V_i}{R}F_{z_1} + \frac{W_i}{R}F_{z_2}\right) \\ 0 & -\frac{\alpha}{2}\left(\frac{V_i}{R}F_{z_1} + \frac{W_i}{R}F_{z_2}\right) & -\frac{\bar{\rho}}{2}\left(\frac{V_i}{R}F_{\theta_1} + \frac{W_i}{R}F_{\theta_2}\right) \\ \alpha\left(\frac{V_i}{R}F_{\theta_1} + \frac{W_i}{R}F_{\theta_2}\right) & 0 & 0 \end{bmatrix}$$

(4.38c)

$$[A^{(3)}_{q_i}] = \begin{bmatrix} 0 & \frac{\bar{\Omega}}{2}\left(\frac{V_i}{R}F_{\theta_1} + \frac{W_i}{R}F_{\theta_2}\right) & \frac{1}{2}K_{p_i}F_{\theta_3} \\ K_{p_i}F_{z_3} & 0 & 0 \\ 0 & \frac{1}{2}\left[\left(\frac{V_i}{R}F_{z_0} - \frac{W_i}{R}F_{\theta_0}\right) - \bar{\Omega}\alpha\left(\frac{V_i}{R}F_{\theta_1} + \frac{W_i}{R}F_{z_2}\right)\right] - \frac{1}{2}\bar{\ell}K_{p_i}F_{\theta_3} & -\frac{\bar{\Omega}}{2}\bar{\ell}\left(\frac{V_i}{R}F_{\theta_1} + \frac{W_i}{R}F_{\theta_2}\right) + \frac{1}{2}K_{p_i}\alpha F_{z_3} \\ 0 & \frac{\bar{\Omega}}{2}\bar{\ell}\left(\frac{V_i}{R}F_{\theta_1} + \frac{W_i}{R}F_{\theta_2}\right) - \frac{1}{2}K_{p_i}\alpha F_{z_3} & \frac{1}{2}\left[\left(\frac{V_i}{R}F_{z_0} - \frac{W_i}{R}F_{\theta_0}\right) - \bar{\Omega}\alpha\left(\frac{V_i}{R}F_{z_1} + \frac{W_i}{R}F_{z_3}\right) - \frac{\bar{\rho}}{2}K_{p_i}F_{\theta_3}\right] \\ K_{p_i}\alpha F_{\theta_3} & 0 & 0 \end{bmatrix}$$

(4.38d)

$$[A^{(3)}_{\dot{q}}] = \begin{bmatrix} \frac{\bar{\lambda}}{2}F_{\theta_1} & 0 & 0 & 0 & 0 & \frac{1}{2}F_{\theta_3} \\ 0 & 0 & \bar{\lambda}F_{z_2} & F_{z_3} & 0 & 0 \\ -\frac{\bar{\lambda}}{2}\alpha F_{z_1} & -\frac{\bar{\lambda}}{2}\bar{\ell}F_{\theta_1} & 0 & 0 & -\frac{1}{2}\bar{\rho}F_{\theta_3} & \frac{1}{2}\alpha F_{z_3} \\ \frac{\bar{\lambda}}{2}\bar{\ell}F_{\theta_1} & -\frac{\bar{\lambda}}{2}\alpha F_{z_1} & 0 & 0 & -\frac{1}{2}\bar{\rho}F_{z_3} & -\frac{1}{2}\bar{\rho}F_{\theta_3} \\ 0 & 0 & \bar{\lambda}\alpha F_{\theta_2} & \alpha F_{\theta_3} & 0 & 0 \end{bmatrix}$$

(4.38e)

4.5.3 Wing Aerodynamic Forces

The virtual work done by wing aerodynamic forces is expressed by

$$\delta W_{ww} = \{\delta u_w \quad \delta w_w \quad \delta p_w\} \begin{Bmatrix} F_x \\ F_z \\ M_y \end{Bmatrix} \tag{4.39}$$

The displacements u_w, w_w, p_w are described in terms of the mode shapes as

$$\begin{Bmatrix} u_w \\ w_w \\ p_w \end{Bmatrix} = [S] \begin{Bmatrix} a_1 \\ a_2 \\ \vdots \\ a_n \end{Bmatrix} \tag{4.40}$$

where

$$[S] = \begin{bmatrix} \breve{\alpha}_1(\bar{y}) & \breve{\alpha}_2(y) & \cdots & \breve{\alpha}_n(\bar{y}) \\ \beta_1(y) & \beta_2(y) & \cdots & \beta_n(y) \\ \phi_1(y) & \phi_2(y) & \cdots & \phi_n(y) \end{bmatrix} \tag{4.41}$$

Then, the substitution of Eq. 4.40 into 4.39 gives

$$\delta W_{ww} = \Omega^2 \{\delta a_1 \quad \delta a_2 \cdots \delta a_n\} \left[[A_{\dot{\alpha}}^{(3)}] \begin{Bmatrix} \dot{a}_1 \\ \dot{a}_2 \\ \vdots \\ \dot{a}_n \end{Bmatrix} + [A_{\alpha}^{(3)}] \begin{Bmatrix} a_1 \\ a_2 \\ \vdots \\ a_n \end{Bmatrix} + [A_{\zeta}^{(3)}] \begin{Bmatrix} u_g/V \\ v_g/V \\ w_g/V \\ \theta_0 \\ \theta_{1c} \\ \theta_{1s} \end{Bmatrix} \right] \tag{4.42}$$

where

$$[A_a^{(3)}] = \frac{1}{|\Omega|}\int_0^L [S]^T[A_w][S]\,dy$$

$$[A_a^{(3)}] = \frac{1}{|\Omega|^2}\int_0^L [S]^T[A_w][S]\,dy$$

$$[A_a^{(3)}] = \frac{1}{|\Omega|^2}\int_0^L [S]^T[A_G][S]\,dy \qquad (4.43)$$

The matrices A_w, A_w and A_G are derived from Eq. 3.32 as follows:

$$[A_w] = \begin{bmatrix} -\frac{1}{2}\rho C_w V a_w\left(1+\frac{C_{Dow}}{a_w}\right) & \rho C_w V a_w \alpha_{w_0} & 0 \\ -\frac{1}{2}\rho C_w V a_w \alpha_{w_0} & -\rho C_w V C_{Dow} & 0 \\ -\frac{1}{2}\rho C_w^2 V(C_{m_\alpha}+a_w\bar{e}) & \rho C_w^2 V(C_{m_0}+C_{m_q}\alpha_{w_0} & 0 \\ & +a_w\alpha_{w_0}\bar{e}) & \end{bmatrix} \qquad (4.44a)$$

$$[A_w] = \begin{bmatrix} 0 & 0 & \frac{1}{2}\rho C_w V^2 a_w \\ 0 & 0 & 0 \\ 0 & 0 & \frac{1}{2}\rho C_w^2 V^2(C_{m_q}+a_w\bar{e}) \end{bmatrix} \qquad (4.44b)$$

$$[A_{ij}] = \begin{bmatrix} -\frac{1}{2}\rho C_{w} V^2 a_{w}\left(1+\frac{C_{Dow}}{a_{w}}\right) & 0 & \rho C_{w} V^2 a_{w} \alpha_{w_0} \\ -\frac{1}{2}\rho C_{w} V^2 a_{w} \alpha_{w_0} & 0 & -\rho C_{w} V^2 C_{Dow} \\ -\frac{1}{2}\rho C_{w}^2 V^2 (C_{m_w} + a_{w}\bar{e}) & 0 & \rho C_{w}^2 V^2 (C_{m_0} + C_{m_\alpha}\alpha_{w_0} + a_{w}\alpha_{w_0}\bar{e}) \end{bmatrix}$$

$$\begin{bmatrix} 0 & 0 & 0 \\ 0 & 0 & 0 \\ 0 & 0 & 0 \end{bmatrix} \qquad (4.44c)$$

4.6 Final Equations of Motion

In this part the final equations of motion will be derived. They will be expressed in general format, so that any number of mode shapes both for the blade and wing can be chosen to describe the rotor or wing motion as accurately as required.

4.6.1 Equations of Motion in General Format

The substitution of Eqs. 4.20 and Eq. 4.10 into Eq. 4.15 gives the jth blade modal equations of motion. Note that time derivatives are normalized by rotational speed as in Eq. 3.24.

For the jth blade mode

$$\{\ddot{Q}_j\} + \bar{\Omega}\,[M_{\dot{Q}}]\{\dot{Q}_j\} + [M_Q]_j\{Q_j\} + [M_j][T]\{\ddot{a}\} + \bar{\Omega}[C_j][T]\{\dot{a}\} = \{P_j\} \qquad (4.45)$$

where

$$\{Q_j\} = \begin{Bmatrix} Q_{j_0} \\ Q_{j_c} \\ Q_{j_s} \end{Bmatrix} \quad , \quad \{a\} = \begin{Bmatrix} a_1 \\ a_2 \\ \vdots \\ \vdots \end{Bmatrix} \tag{4.46a}$$

$$[M_{\dot{Q}}] = \begin{bmatrix} 0 & 0 & 0 \\ 0 & 0 & 2 \\ 0 & -2 & 0 \end{bmatrix} \tag{4.46b}$$

$$[M_Q]_j = \begin{bmatrix} \left(\frac{\lambda_j}{\Omega}\right)^2 & 0 & 0 \\ 0 & \left(\frac{\lambda_j}{\Omega}\right)^2 - 1 & 0 \\ 0 & 0 & \left(\frac{\lambda_j}{\Omega}\right)^2 - 1 \end{bmatrix} \tag{4.46c}$$

$$[M_j] = \begin{bmatrix} 0 & W_{0j} & 0 & 0 & V_{1j} \\ 0 & 0 & -\bar{k} V_{0j} & -W_{1j} & 0 \\ -V_{0j} & 0 & W_{1j} & -\bar{k} V_{0j} & 0 \end{bmatrix} \tag{4.46d}$$

$$[C_j] = \begin{bmatrix} 0 & 0 & 0 & 0 & 0 \\ 0 & 0 & 2W_{1j} & 0 & 0 \\ 0 & 0 & 0 & 2W_{1j} & 0 \end{bmatrix} \tag{4.46e}$$

$$\{P_j\} = \frac{1}{\Omega^2} \begin{Bmatrix} (P_{0j} + P_{2j})_0 \\ (P_{0j} + P_{2j})_c \\ (P_{0j} + P_{2j})_s \end{Bmatrix} \tag{4.47}$$

and the matrix [T] is defined in Eq. 4.11.

Substituting Eqs. 4.21 and 4.10 into Eq. 4.18 yields the wing equation.

For the wing mode

$$\{\ddot{a}\} + \bar{\Omega}[W_{\dot{a}}]\{\dot{a}\} + [W_a]\{a\} + \sum_j \left([T]^T [M_j]^T [K] \{\ddot{Q}_j\} - \bar{\Omega} [T]^T [C_j]^T [K] \{\dot{Q}_j\} \right) = \{F\} \tag{4.48}$$

where

$$[W_{\dot{a}}] = NI_0 \left[\begin{Bmatrix} \frac{\partial \zeta_1}{\partial y} \\ \frac{\partial \zeta_2}{\partial y} \\ \vdots \end{Bmatrix}_{y=L} \{\phi_1 \ \phi_2 \ \cdots\}_{y=L} - \begin{Bmatrix} \phi_1 \\ \phi_2 \\ \vdots \end{Bmatrix}_{y=L} \left\{ \frac{\partial \zeta_1}{\partial y} \ \frac{\partial \zeta_2}{\partial y} \ \cdots \right\}_{y=L} \right]$$

$$[W_a] = \begin{bmatrix} \left(\frac{\Lambda_1}{\Omega}\right)^2 & & 0 \\ & \left(\frac{\Lambda_2}{\Omega}\right)^2 & \\ 0 & & \ddots \end{bmatrix} \quad : \text{diagonal matrix}$$

(4.49)

$$[K] = \begin{bmatrix} N & 0 & 0 \\ 0 & \frac{N}{2} & 0 \\ 0 & 0 & \frac{N}{2} \end{bmatrix}$$

Loading matrix $\{F\}$ for the wing consists of aerodynamic forces f_i due to the rotor, and aerodynamic forces g_i due to wing motion itself.

$$\{F\} = \begin{Bmatrix} f_1 + g_1 \\ f_2 + g_2 \\ \vdots \\ \vdots \\ \vdots \end{Bmatrix} \tag{4.50}$$

Similarly, aerodynamic forces are derived.

For rotor aerodynamic forces

$$\{P_j\} = \frac{1}{\Omega^2} \begin{Bmatrix} (P_{\theta_j} + P_{z_j})_0 \\ (P_{\theta_j} + P_{z_j})_c \\ (P_{\theta_j} + P_{z_j})_s \end{Bmatrix}$$

$$= \sum_i \left[A^{(\omega)}_{\dot{Q}_i}\right]_j \{\dot{Q}_i\} + \sum_i \left[A^{(\omega)}_{Q_i}\right]_j \{Q_i\}$$

$$+ \left[A^{(\omega)}_{\dot{a}}\right]_j [T]\{\dot{a}\} + \left[A^{(\omega)}_{a}\right]_j [T]\{a\}$$

$$+ \left[A^{(\omega)}_{e}\right]_j \{e\} \tag{4.51}$$

where

$$\left[A^{(i)}_{\dot{q}_i}\right]_j = \frac{1}{2}\gamma I_B \begin{bmatrix} G_{ji} & 0 & 0 \\ 0 & G_{ji} & 0 \\ 0 & 0 & G_{ji} \end{bmatrix} \tag{4.52a}$$

$$\left[A^{(i)}_{q_i}\right]_j = \frac{1}{2}\gamma I_B \begin{bmatrix} K_{pi}\, G_{vj} & 0 & 0 \\ 0 & K_{pi}\, G_{vj} & \bar{\Omega}\, G_{ji} \\ 0 & -\bar{\Omega}\, G_{ji} & K_{pi}\, G_{vj} \end{bmatrix} \tag{4.52b}$$

$$\left[A^{(i)}_{\dot{a}}\right]_j = \frac{1}{2}\gamma I_B \begin{bmatrix} 0 & G_{III_j} & 0 & 0 & G_{II_j} \\ 0 & 0 & -\bar{k}\, G_{I_j} & -G_{IV_j} & 0 \\ -G_{I_j} & 0 & G_{IV_j} & -\bar{k}\, G_{I_j} & 0 \end{bmatrix} \tag{4.52c}$$

$$\left[A^{(i)}_{a}\right]_j = \frac{1}{2}\gamma I_B \begin{bmatrix} 0 & 0 & 0 & 0 & 0 \\ 0 & 0 & \bar{\lambda}\, G_{I_j} & 0 & 0 \\ 0 & 0 & 0 & \bar{\lambda}\, G_{I_j} & 0 \end{bmatrix} \tag{4.52d}$$

$$\left[A_e^{(i)}\right]_j = \frac{1}{2}\gamma I_\beta \begin{bmatrix} 0 & 0 & \bar{\lambda} G_{\beta j} & G_{vj} & 0 & 0 \\ 0 & \bar{\lambda} G_{\zeta j} & 0 & 0 & G_{vj} & 0 \\ -\bar{\lambda} G_{\zeta j} & 0 & 0 & 0 & 0 & G_{vj} \end{bmatrix} \tag{4.52e}$$

The excitation vector {e} is expressed as

$$\{e\} = \begin{Bmatrix} \frac{u_g}{V} \\ \frac{v_g}{V} \\ \frac{w_g}{V} \\ \theta_0 \\ \theta_{1c} \\ \theta_{1s} \end{Bmatrix} \tag{4.53}$$

For wing aerodynamic forces

From Eq. 4.50

$$\{F\} = \{f + g\} \tag{4.54}$$

Loading to the wing due to rotor aerodynamic forces f_i corresponding to a_i is expressed from Eq. 4.36 as

$$\{f\} = \kappa[T]^T[A_{\dot{a}}^{(2)}][T]\{\overset{\circ}{a}\} + \kappa[T]^T[A_a^{(2)}][T]\{a\}$$
$$+ \sum_i \kappa[T]^T[A_{\dot{a}_i}^{(2)}]\{\overset{\circ}{Q}_i\}$$
$$+ \sum_i \kappa[T]^T[A_{Q_i}^{(2)}]\{Q_i\}$$
$$+ \kappa[T]^T[A_e^{(2)}]\{e\} \qquad (4.55)$$

Loading due to wing aerodynamic forces g_i is described from Eq. 4.42 as

$$\{g\} = [A_{\dot{a}}^{(3)}]\{\overset{\circ}{a}\} + [A_a^{(3)}]\{a\} + [A_e^{(3)}]\{e\} \qquad (4.56)$$

4.6.2 Equations of Motion for Nine Degrees of Freedom

For a typical case, nine degrees of freedom are considered here. These degrees are rotor flapping motion (collective flapping motion Q_{10}, cyclic flapping motion Q_{1c} and Q_{1s}), rotor lagging motion (collective lagging motion Q_{20}, cyclic lagging motion Q_{2c} and Q_{2s}), wing vertical bending motion a_1, wing chordwise bending motion a_2 and wing torsion a_3.

These mode shapes are natural modes, therefore they are coupled.

The final equations in matrix form are

$$[A]\{\overset{\circ\circ}{x}\} + [B]\{\overset{\circ}{x}\} + [C]\{x\} = [D]\{e\} \qquad (4.57)$$

where

$$\{x\} = \begin{Bmatrix} Q_{1_0} \\ Q_{1C} \\ Q_{1S} \\ Q_{2_0} \\ Q_{2C} \\ Q_{2S} \\ a_1 \\ a_2 \\ a_3 \end{Bmatrix}, \qquad \{e\} = \begin{Bmatrix} \frac{\mu_G}{V} \\ \frac{\mu_F}{V} \\ \frac{w_G}{V} \\ \Theta_0 \\ \Theta_{1C} \\ \Theta_{1S} \end{Bmatrix} \tag{4.58}$$

The coefficient matrices [A], [B] and [C] are 9 x 9 matrices, and [D] is a 9 x 6 matrix, as given below.

$$[A] = \begin{bmatrix} [I] & [0] & [M_1][T] \\ [0] & [I] & [M_2][T] \\ [T]^T[M_1][K] & [T]^T[M_2][K] & [I] \end{bmatrix} \tag{4.59a}$$

$$[B] = \begin{bmatrix} \bar{\Omega}^2[M_{\theta\theta}] - [A^{(0)}_{\theta\theta_1}]_1 & -[A^{(0)}_{\theta\theta_2}]_1 & \bar{\Omega}[C_1][T] - [A^{(1)}_{\theta a}]_1[T] \\ -[A^{(0)}_{a\theta_1}]_2 & \bar{\Omega}^2[M_{aa}] - [A^{(0)}_{aa_1}]_2 & \bar{\Omega}[C_2][T] - [A^{(0)}_{aa}]_2[T] \\ -\bar{\Omega}[T]^T[C_1]^T[K] - \kappa[T]^T[A^{(0)}_{\theta\theta_1}][T] & -\bar{\Omega}[T]^T[C_2][K] - \kappa[T]^T[A^{(0)}_{\theta a_2}][T] & \bar{\Omega}^2[W_{aa}] - \kappa[T]^T[A^{(0)}_{aa}][T] - [A^{(0)}_{aa}] \end{bmatrix} \qquad (4.59b)$$

$$[C] = \begin{bmatrix} [M_{\theta\theta}]_1 - [A^{(0)}_{\theta\theta_1}]_1 & -[A^{(0)}_{\theta\theta_2}]_1 & -[A^{(0)}_{\theta a}]_1[T] \\ -[A^{(0)}_{a\theta_1}]_2 & [M_{aa}]_2 - [A^{(0)}_{aa_2}]_2 & -[A^{(0)}_{aa}]_2[T] \\ -\kappa[T]^T[A^{(0)}_{\theta\theta_1}] & -\kappa[T]^T[A^{(0)}_{\theta a_2}] & [W_{aa}] - \kappa[T]^T[A^{(0)}_{aa}][T] - [A^{(0)}_{aa}] \end{bmatrix} \qquad (4.59c)$$

$$[D] = \begin{bmatrix} [A_e^{(1)}]_1 & & \\ & [A_e^{(1)}]_2 & \\ & & K[T]^T[A_e^{(2)}] + [A_e^{(3)}] \end{bmatrix} \tag{4.59d}$$

4.6.3 Equations of Motion for Nine Degrees of Freedom with Uncoupled Modes

In order to have a better understanding of tilting prop-rotor dynamics, a simple special case was considered. This case is based on the assumption that the mode shapes are uncoupled. Therefore, rotor motion is expressed as

$$\begin{Bmatrix} w_n \\ v_n \end{Bmatrix} = \begin{Bmatrix} W_1 \\ 0 \end{Bmatrix} (Q_{1o} + Q_{1c}\cos\psi_n + Q_{1s}\sin\psi_n) + \begin{Bmatrix} 0 \\ V_2 \end{Bmatrix} (Q_{2o} + Q_{2c}\cos\psi_n + Q_{2s}\sin\psi_n) \tag{4.60}$$

The wing motion is also,

$$\begin{Bmatrix} u_w \\ w_w \\ p_w \end{Bmatrix} = \begin{Bmatrix} \gamma_1 \\ 0 \\ 0 \end{Bmatrix} a_1 + \begin{Bmatrix} 0 \\ \gamma_2 \\ 0 \end{Bmatrix} a_2 + \begin{Bmatrix} 0 \\ 0 \\ \phi_3 \end{Bmatrix} a_3 \tag{4.61}$$

The substitution of Eq. 4.60 and 4.61 into Eq. 4.59 gives the following matrices for the same nine degrees of freedom

equation as Eq. 4.57.

$$[A] =$$

$$\begin{bmatrix}
1 & 0 & 0 & 0 & 0 & 0 & 0 & W_{01}\frac{W_c}{R} & 0 \\
0 & 1 & 0 & 0 & 0 & 0 & 0 & 0 & -W_{11}\Phi \\
0 & 0 & 1 & 0 & 0 & 0 & 0 & W_{11}W_c' & 0 \\
0 & 0 & 0 & 1 & 0 & 0 & -V_{12}W_B' & 0 & 0 \\
0 & 0 & 0 & 0 & 1 & 0 & 0 & -\bar{h}V_{02}W_c' & 0 \\
0 & 0 & 0 & 0 & 0 & 1 & -V_{02}\frac{W_B}{R} & 0 & -\bar{h}V_{02}\Phi \\
0 & 0 & 0 & -NV_{12}W_B' & 0 & -\frac{N}{2}V_{02}\frac{W_B}{R} & 1 & 0 & 0 \\
NW_{01}\frac{W_c}{R} & 0 & \frac{N}{2}W_{11}W_c & 0 & -\frac{N}{2}\bar{h}V_{02}W_c' & 0 & 0 & 1 & 0 \\
0 & -\frac{N}{2}W_{11}\Phi & 0 & 0 & 0 & -\frac{N}{2}\bar{h}V_{02}\Phi & 0 & 0 & 1
\end{bmatrix}$$

(4.62a)

$$[B] =$$

$$\begin{bmatrix}
F_{\hat{\rho}\hat{\rho}} & 0 & 0 & F_{\hat{\zeta}\hat{\rho}} & 0 & 0 & -F^{+}_{T\hat{\rho}} W_B' & +F_{P\hat{\rho}} \frac{W_c}{R} & 0 \\
0 & F_{\hat{\rho}\hat{\rho}} & 2\bar{\Omega} & 0 & F_{\hat{\zeta}\hat{\rho}} & 0 & 0 & 2\bar{\Omega} W_{11} W_c' - \bar{k} F_{T\hat{\rho}} W_c' & -F^{+}_{P\hat{\rho}} \Phi \\
0 & -2\bar{\Omega} & F_{\hat{\rho}\hat{\rho}} & 0 & 0 & F_{\hat{\zeta}\hat{\rho}} & -F_{T\hat{\rho}} \frac{W_B}{R} & F^{+}_{P\hat{\rho}} W_c' & 2\bar{\Omega} W_{11} \Phi - \bar{k} F_{T\hat{\rho}} \Phi \\
L_{\hat{\rho}\hat{\zeta}} & 0 & 0 & L_{\hat{\zeta}\hat{\zeta}} & 0 & 0 & -L^{+}_{T\hat{\zeta}} W_B' & L_{P\hat{\zeta}} \frac{W_c}{R} & 0 \\
0 & L_{\hat{\rho}\hat{\zeta}} & 0 & 0 & L_{\hat{\zeta}\hat{\zeta}} & 2\bar{\Omega} & 0 & -\bar{k} L_{T\hat{\zeta}} W_c' & -L^{+}_{P\hat{\zeta}} \Phi \\
0 & 0 & L_{\hat{\rho}\hat{\zeta}} & 0 & -2\bar{\Omega} & L_{\hat{\zeta}\hat{\zeta}} & -L_{T\hat{\zeta}} \frac{W_B}{R} & L^{+}_{P\hat{\zeta}} W_c' & -\bar{k} L_{T\hat{\zeta}} \Phi \\
-N L^{+}_{P\hat{\rho}} W_B' & 0 & -\frac{N}{2} L_{P\hat{\rho}} \frac{W_B}{R} & -N L^{+}_{T\hat{\zeta}} W_B' & 0 & -\frac{N}{2} L_{T\hat{\zeta}} \frac{W_B}{R} & C\dot{a}_{11} + C\dot{\Theta}_{11} & C\dot{a}_{12} + C\dot{\Theta}_{12} & C\dot{\Theta}_{13} \\
N F_{P\hat{\rho}} \frac{W_c}{R} & -\bar{\Omega} N W_{11} W_c' - \frac{N}{2} \bar{k} L_{P\hat{\rho}} W_c' & \frac{N}{2} F^{+}_{P\hat{\rho}} W_c & N F_{T\hat{\zeta}} \frac{W_c}{R} & -\frac{N}{2} \bar{k} L_{T\hat{\zeta}} W_c' & \frac{N}{2} F^{+}_{T\hat{\zeta}} W_c' & C\dot{a}_{21} + C\dot{\Theta}_{21} & C\dot{a}_{22} + C\dot{\Theta}_{21} & \bar{\Omega} I_B N W_c' \Phi + C\dot{\Theta}_{23} \\
0 & -\frac{N}{2} F^{+}_{P\hat{\rho}} \Phi & -\bar{\Omega} N W_{11} \Phi - \frac{N}{2} \bar{k} L_{P\hat{\rho}} \Phi & 0 & -\frac{N}{2} F^{+}_{T\hat{\zeta}} \Phi & -\frac{N}{2} \bar{k} L_{T\hat{\zeta}} \Phi & C\dot{a}_{31} + C\dot{\Theta}_{31} & -\bar{\Omega} I_B N W_c' \Phi + C\dot{a}_{32} + C\dot{\Theta}_{32} & C\dot{\Theta}_{33}
\end{bmatrix}$$

(4.62b)

$$[C] =$$

$$\begin{bmatrix}
\left(\frac{\lambda_\theta}{\Omega}\right)^2 & 0 & 0 & 0 & 0 & 0 & 0 & 0 & 0 \\
0 & \left(\frac{\lambda_\theta}{\Omega}\right)^2 - 1 + K_p F_{\theta\dot{\theta}} & \bar{\Omega} F_{\dot{\theta}\dot{\theta}} & 0 & 0 & \bar{\Omega} F_{\dot{\zeta}\dot{\theta}} & 0 & \lambda F_{T\dot{\theta}} \bar{W}_c' & 0 \\
0 & -\bar{\Omega} F_{\dot{\theta}\dot{\theta}} & \left(\frac{\lambda_\theta}{\Omega}\right)^2 - 1 + K_p F_{\theta\dot{\theta}} & 0 & -\bar{\Omega} F_{\dot{\zeta}\dot{\theta}} & 0 & 0 & 0 & \lambda F_{T\dot{\theta}} \bar{\Phi} \\
0 & 0 & 0 & \left(\frac{\lambda_\zeta}{\Omega}\right)^2 & 0 & 0 & 0 & 0 & 0 \\
0 & K_p L_{\theta\dot{\zeta}} & \bar{\Omega} L_{\dot{\theta}\dot{\zeta}} & 0 & \left(\frac{\lambda_\zeta}{\Omega}\right)^2 - 1 & \bar{\Omega} L_{\dot{\zeta}\dot{\zeta}} & 0 & \lambda L_{T\dot{\zeta}} \bar{W}_c' & 0 \\
0 & -\bar{\Omega} L_{\dot{\theta}\dot{\zeta}} & K_p L_{\theta\dot{\zeta}} & 0 & -\bar{\Omega} L_{\dot{\zeta}\dot{\zeta}} & \left(\frac{\lambda_\zeta}{\Omega}\right)^2 - 1 & 0 & 0 & \lambda L_{T\dot{\zeta}} \bar{\Phi} \\
0 & \frac{\bar{\Omega}}{2} N L_{p\dot{\theta}} \frac{W_0}{R} & \frac{1}{2} N K_p L_{\theta} \frac{W_0}{R} & 0 & \frac{\bar{\Omega}}{2} N L_{T\dot{\zeta}} \frac{W_0}{R} & 0 & \left(\frac{\Lambda_1}{\Omega}\right)^2 & 0 & C_{Q_{13}} + C_{a_{13}} \\
0 & \frac{N}{2}\left[L_\sigma - \bar{\Omega} F_{p\dot{\theta}}^+ - \bar{k} K_p L_{\theta}\right] \bar{W}_c' & \frac{N}{2}\left[-\bar{k}\bar{\Omega} L_{p\dot{\theta}} + K_p F_{\theta}^+\right] \bar{W}_c' & 0 & \frac{N}{2}\left[F_0 - \bar{\Omega} F_{T\dot{\zeta}}^+\right] \bar{W}_c' & -\frac{N}{2}\bar{k}\bar{\Omega} L_{T\dot{\zeta}} \bar{W}_c' & 0 & \left(\frac{\Lambda_2}{\Omega}\right)^2 + C_{a_{22}} & C_{Q_{23}} \\
0 & \frac{N}{2}\left[\bar{k}\bar{\Omega} L_{p\dot{\theta}} - K_p F_{\theta}^+\right] \bar{\Phi} & \frac{N}{2}\left[L_\sigma - \bar{\Omega} F_{p\dot{\theta}}^+ - \bar{k} K_p L_{\theta}\right] \bar{\Phi} & 0 & \frac{N}{2} \bar{k}\bar{\Omega} L_{T\dot{\zeta}} \bar{\Phi} & \frac{N}{2}\left[F_0 - \bar{\Omega} F_{T\dot{\zeta}}^+\right] \bar{\Phi} & 0 & C_{Q_{32}} & \left(\frac{\Lambda_3}{\Omega}\right)^2 + C_{Q_{33}} + C_{a_{33}}
\end{bmatrix}$$

(4.62c)

$$[D] = \begin{bmatrix}
0 & 0 & \bar{\lambda} F_{P\dot{\beta}} & F_{\theta\dot{\beta}} & 0 & 0 \\
0 & \bar{\lambda} F_{T\dot{\beta}} & 0 & 0 & F_{\theta\dot{\beta}} & 0 \\
-\bar{\lambda} F_{T\dot{\beta}} & 0 & 0 & 0 & 0 & F_{\theta\dot{\beta}} \\
0 & 0 & \bar{\lambda} L_{P\dot{\zeta}} & L_{\theta\dot{\zeta}} & 0 & 0 \\
0 & \bar{\lambda} L_{T\dot{\zeta}} & 0 & 0 & L_{\theta\dot{\zeta}} & 0 \\
-\bar{\lambda} L_{T\dot{\zeta}} & 0 & 0 & 0 & 0 & L_{\theta\dot{\zeta}} \\
\frac{N}{2}\bar{\lambda} L_T \frac{W_B}{R} + C_{G_{11}} & 0 & -N\bar{\lambda} L_P^t W_B' + C_{G_{13}} & -N L_\theta^t W_B' & 0 & \frac{N}{2} L_\theta \frac{W_B}{R} \\
-\frac{N}{2}\bar{\lambda} F_T^t W_C' + C_{G_{21}} & -\frac{N}{2}\bar{\lambda}\bar{\ell} L_T W_C'' & N\bar{\lambda} F_P \frac{W_C}{R} + C_{G_{23}} & N F_\theta \frac{W_C}{R} & -\frac{N}{2}\bar{\ell} L_\theta W_C' & \frac{N}{2} F_\theta^t W_C' \\
\frac{N}{2}\bar{\lambda}\bar{\ell} L_T \Phi + C_{G_{31}} & -\frac{N}{2}\bar{\lambda} F_T^t \Phi & C_{G_{33}} & 0 & -\frac{N}{2}\bar{\ell} F_\theta^t \Phi & -\frac{N}{2}\bar{\ell} L_\theta \Phi
\end{bmatrix} \tag{4.62d}$$

New symbols will be defined below, but all these symbols can be derived by applying the uncoupled mode shapes to the general equations.

Pylon Motions

$$
\begin{aligned}
W_B &= \gamma_1 \quad \text{at} \quad y = L \\
W_C &= \zeta_2 \quad \text{at} \quad y = L \\
W_C' &= \frac{d\zeta_2}{dy} \quad \text{at} \quad y = L \\
\Phi &= \Phi_3 \quad \text{at} \quad y = L \\
W_B' &= \frac{d\gamma_1}{dy} \quad \text{at} \quad y = L
\end{aligned}
\tag{4.63}
$$

Therefore the matrix [T] in Eq. 4.10 is described as

$$
[T] = \begin{bmatrix}
\frac{W_B}{R} & 0 & 0 \\
0 & \frac{W_C}{R} & 0 \\
0 & W_C' & 0 \\
0 & 0 & \Phi \\
-W_B' & 0 & 0
\end{bmatrix}
\tag{4.64}
$$

Aerodynamic Forces

(a) Rotor Aerodynamic Forces

$$
\begin{aligned}
F_{\dot\beta\dot\beta} &= -\frac{1}{2}\gamma I_B \int_0^1 (F_{z_1}) \frac{W_1^2}{R^2} dx \\
F_{\dot\zeta\dot\beta} &= -\frac{1}{2}\gamma I_B \int_0^1 (F_{z_1}) \frac{W_1 V_3}{R^2} dx \\
L_{\dot\beta\dot\zeta} &= -\frac{1}{2}\gamma I_B \int_0^1 (F_{\theta_2}) \frac{W_1 V_2}{R^2} dx \\
L_{\dot\zeta\dot\zeta} &= -\frac{1}{2}\gamma I_B \int_0^1 (F_{\theta_1}) \frac{V^2}{R^2} dx
\end{aligned}
\tag{4.65a}
$$

$$F_{T\dot{\rho}} = -\tfrac{1}{2}\gamma I_B \int_0^1 (F_{z_1}) \frac{W_1}{R}\, dx$$

$$F_{P\dot{\beta}} = -\tfrac{1}{2}\gamma I_B \int_0^1 (F_{z_2}) \frac{W_1}{R}\, dx$$

$$F^{+}_{T\dot{\beta}} = -\tfrac{1}{2}\gamma I_B \int_0^1 (F_{z_1}) \frac{W_1}{R}\, x\, dx$$

$$F^{+}_{P\dot{\beta}} = -\tfrac{1}{2}\gamma I_B \int_0^1 (F_{z_2}) \frac{W_1}{R}\, x\, dx$$

$$F_{\theta\dot{\rho}} = -\tfrac{1}{2}\gamma I_B \int_0^1 (F_{z_3}) \frac{W_1}{R}\, dx \qquad (4.65b)$$

$$F_{T\dot{\zeta}} = -\tfrac{1}{2}\gamma I_B \int_0^1 (F_{\theta_1}) \frac{V_2}{R}\, dx$$

$$F^{+}_{T\dot{\zeta}} = -\tfrac{1}{2}\gamma I_B \int_0^1 (F_{\theta_1}) \frac{V_2}{R}\, x\, dx \qquad (4.65c)$$

$$L_{T\dot{\zeta}} = -\tfrac{1}{2}\gamma I_B \int_0^1 (F_{\theta_1}) \frac{V_2}{R}\, dx$$

$$L_{P\dot{\zeta}} = -\tfrac{1}{2}\gamma I_B \int_0^1 (F_{\theta_2}) \frac{V_2}{R}\, dx$$

$$L^{+}_{T\dot{\zeta}} = -\tfrac{1}{2}\gamma I_B \int_0^1 (F_{\theta_1}) \frac{V_2}{R}\, x\, dx$$

$$L^{+}_{P\dot{\zeta}} = -\tfrac{1}{2}\gamma I_B \int_0^1 (F_{\theta_2}) \frac{V_2}{R}\, x\, dx$$

$$L_{\theta\dot{\zeta}} = -\tfrac{1}{2}\gamma I_B \int_0^1 (F_{\theta_3}) \frac{V_2}{R}\, dx \qquad (4.65d)$$

$$L_{P\dot{\beta}} = -\tfrac{1}{2}\gamma I_B \int_0^1 (F_{\theta_2}) \frac{W_1}{R}\, dx$$

$$L^{+}_{P\dot{\rho}} = -\tfrac{1}{2}\gamma I_B \int_0^1 (F_{\theta_2}) \frac{W_1}{R}\, x\, dx \qquad (4.65e)$$

where in general F,L expresses the forces corresponding to the direction of flapping motion and lagging motion respectively. Subscripts β and ζ describe the mode shape contributions to the aerodynamic forces; T and P show the derivatives for the perturbation expression with respect to inplane velocity U_T and out-of-plane velocity U_p; superscript + expresses the moment at the blade root.

$$
\begin{aligned}
F_0 &= \tfrac{1}{2}\gamma I_\beta \int_0^1 (F_{z0})\,dx \\
F_T &= \tfrac{1}{2}\gamma I_\beta \int_0^1 (F_{z1})\,dx & F_T^+ &= \tfrac{1}{2}\gamma I_\beta \int_0^1 (F_{z1})\,x\,dx \\
F_P &= \tfrac{1}{2}\gamma I_\beta \int_0^1 (F_{z2})\,dx & F_P^{++} &= \tfrac{1}{2}\gamma I_\beta \int_0^1 (F_{z2})\,x^2 dx \\
F_\theta &= \tfrac{1}{2}\gamma I_\beta \int_0^1 (F_{z3})\,dx & F_\theta^+ &= \tfrac{1}{2}\gamma I_\beta \int_0^1 (F_{z3})\,x\,dx \\
L_0 &= \tfrac{1}{2}\gamma I_\beta \int_0^1 (F_{\theta 0})\,dx & L_0^+ &= \tfrac{1}{2}\gamma I_\beta \int_0^1 (F_{\theta 0})\,x\,dx \\
L_T &= \tfrac{1}{2}\gamma I_\beta \int_0^1 (F_{\theta 1})\,dx & L_T^{++} &= \tfrac{1}{2}\gamma I_\beta \int_0^1 (F_{\theta 1})\,x^2 dx \\
L_P &= \tfrac{1}{2}\gamma I_\beta \int_0^1 (F_{\theta 2})\,dx & L_P^+ &= \tfrac{1}{2}\gamma I_\beta \int_0^1 (F_{\theta 2})\,x\,dx \\
L_\theta &= \tfrac{1}{2}\gamma I_\beta \int_0^1 (F_{\theta 3})\,dx & L_\theta^+ &= \tfrac{1}{2}\gamma I_\beta \int_0^1 (F_{\theta 3})\,x\,dx
\end{aligned}
\qquad (4.66)
$$

$$
\begin{aligned}
C\dot{Q}_{11} &= -N\left[\tfrac{1}{2}L_T\left(\frac{W_\beta}{R}\right)^2 - L_T^{++}(W_\beta')^2\right] \\
C\dot{Q}_{12} &= -N\left[-L_P^+ W_\beta' \frac{W_\zeta}{R} - \tfrac{1}{2}L_P^+ \frac{W_\beta}{R} W_c'\right] \\
C\dot{Q}_{13} &= -N\left[\tfrac{1}{2}\bar{k} L_T \frac{W_\beta}{R}\Phi\right] \\
C\dot{Q}_{21} &= -N\left[-\tfrac{1}{2}F_T^+ W_c' \frac{W_\beta}{R} - F_T^+ \frac{W_c}{R} W_\beta'\right] \\
C\dot{Q}_{22} &= -N\left[F_P\left(\frac{W_c}{R}\right)^2 + \tfrac{1}{2}\left\{\bar{k}^2 L_T + F_P^{++}\right\}(W_c')^2\right] \\
C\dot{Q}_{23} &= -N\left[\tfrac{1}{2}\bar{k}\,(L_P^+ - F_T^+)\,W_c'\Phi\right] \\
C\dot{Q}_{31} &= -N\left[\tfrac{1}{2}\bar{k} L_T \Phi \frac{W_\beta}{R}\right]
\end{aligned}
\qquad (4.67a)
$$

$$C_{\dot{a}_{32}} = -N\left[\frac{1}{2}\bar{R}\left(-L_p^+ + F_T^+\right)\Phi W_c'\right]$$
$$C_{\dot{a}_{33}} = -N\left[\frac{1}{2}\left\{\bar{R}^2 L_T + F_p^{++}\right\}\Phi^2\right]$$

$$C_{Q_{13}} = -N\left[\left\{F_0 - \frac{\bar{\lambda}}{2}L_T\right\}\frac{W_p}{R}\Phi\right]$$
$$C_{Q_{22}} = -N\left[\bar{R}\left(F_0 - \frac{\bar{\lambda}}{2}L_T\right)(W_c')^2\right]$$
$$C_{Q_{23}} = -N\left[\left(\frac{\bar{\lambda}}{2}F_T^+ + L_0^+\right)W_c'\Phi\right]$$
$$C_{Q_{32}} = -N\left[-\frac{\bar{\lambda}}{2}F_T^+\Phi W_c'\right]$$
$$C_{Q_{33}} = -N\left[\bar{R}\left(F_0 - \frac{\bar{\lambda}}{2}L_T\right)\Phi^2\right] \qquad (4.67b)$$

(b) Wing Aerodynamic Forces

$$C_{\dot{a}_{11}} = -\frac{1}{|\Omega|}\int_0^L A\dot{w}_{11}(\gamma_1)^2\,dy$$
$$C_{\dot{a}_{12}} = -\frac{1}{|\Omega|}\int_0^L A\dot{w}_{12}\gamma_1\zeta_2\,dy$$
$$C_{\dot{a}_{21}} = -\frac{1}{|\Omega|}\int_0^L A\dot{w}_{21}\zeta_2\gamma_1\,dy \qquad (4.68a)$$
$$C_{\dot{a}_{22}} = -\frac{1}{|\Omega|}\int_0^L A\dot{w}_{22}(\zeta_2)^2\,dy$$

$$C_{\dot{a}_{21}} = -\frac{1}{|\Omega|}\int_0^L A_{\dot{w}_{21}}\Phi_2\gamma_1\,dy$$

$$C_{\dot{a}_{32}} = -\frac{1}{|\Omega|}\int_0^L A_{\dot{w}_{32}}\Phi_3\zeta_2\,dy$$

$$C_{a_{12}} = -\frac{1}{\Omega^2}\int_0^L A_{w_{12}}\gamma_1\Phi_2\,dy$$

$$C_{a_{33}} = -\frac{1}{\Omega^2}\int_0^L A_{w_{33}}(\Phi_3)^2\,dy \qquad (4.68b)$$

$$C_{G_{11}} = \frac{1}{\Omega^2}\int_0^L A_{G_{11}}\gamma_1\,dy$$

$$C_{G_{13}} = \frac{1}{\Omega^2}\int_0^L A_{G_{13}}\gamma_1\,dy$$

$$C_{G_{21}} = \frac{1}{\Omega^2}\int_0^L A_{G_{21}}\zeta_2\,dy$$

$$C_{G_{23}} = \frac{1}{\Omega^2}\int_0^L A_{G_{23}}\zeta_2\,dy \qquad (4.68c)$$

$$C_{G_{31}} = \frac{1}{\Omega^2}\int_0^L A_{G_{31}}\Phi_3\,dy$$

$$C_{G_{33}} = \frac{1}{\Omega^2}\int_0^L A_{G_{33}}\Phi_3\,dy$$

where $A_{\dot{w}_{ij}}$, $A_{w_{ij}}$, and $A_{G_{ij}}$ are components of matrix $[A_{\dot{w}}]$, $[A_w]$, and $[A_G]$ respectively in Eq. 4.44.

Pitch-Flap Coupling

The pitch-flap coupling coefficient is expressed as

$$K_p = -\left.\frac{dw_i}{dr}\right|_{r=0} \tan\delta_3 \tag{4.69}$$

The rotor collective mode shape has zero slope at the root. Therefore, pitch-flap coupling appears only in cyclic motion.

Natural frequencies

λ_β : blade flapping natural frequency

λ_ζ : blade lagging natural frequency

Λ_1 : wing vertical bending natural frequency

Λ_2 : wing chordwise bending natural frequency

Λ_3 : wing torsion natural frequency

4.7 Equations for Gimballed Rotor

As discussed in Subsection 4.4, equations of motion (Eqs. 4.45 and 4.48) are applicable to the gimballed rotor. The significant difference between the gimballed rotor and the hingeless rotor lies in the application of the blade mode shapes to the rotor motion. The gimballed rotor has independent collective mode shapes for the collective motion and cyclic mode shapes for the cyclic motion. Therefore, the above distinction is found in the following matrices:

For blade equations

$$[M_{\Theta}]_j = \begin{bmatrix} \left(\frac{\lambda_j^{(s)}}{\Omega}\right)^2 & 0 & 0 \\ 0 & \left(\frac{\lambda_j^{(c)}}{\Omega}\right)^2 - 1 & 0 \\ 0 & 0 & \left(\frac{\lambda_j^{(s)}}{\Omega}\right)^2 - 1 \end{bmatrix}$$

$$[M_j] = \begin{bmatrix} 0 & W_{0j}^{(s)} & 0 & 0 & V_{ij}^{(s)} \\ 0 & 0 & -\bar{R} V_{0j}^{(s)} & -W_{ij}^{(c)} & 0 \\ -V_{0j}^{(c)} & 0 & W_{ij}^{(c)} & -\bar{R} V_{0j}^{(c)} & 0 \end{bmatrix} \qquad (4.70)$$

$$[C_j] = \begin{bmatrix} 0 & 0 & 0 & 0 & 0 \\ 0 & 0 & 2W_{ij}^{(c)} & 0 & 0 \\ 0 & 0 & 0 & 2W_{ij}^{(s)} & 0 \end{bmatrix}$$

For Rotor Aerodynamic Forces

$$\left[A_{\dot{\Theta}_i}^{(1)}\right]_j = \frac{1}{2}\gamma I_B \begin{bmatrix} G_{ji}^{(s)} & 0 & 0 \\ 0 & G_{ji}^{(c)} & 0 \\ 0 & 0 & G_{ji}^{(c)} \end{bmatrix} \qquad (4.71a)$$

$$\left[A_{\Theta_i}^{(1)}\right]_j = \frac{1}{2}\gamma I_B \begin{bmatrix} K_{Pi}^{(s)} G_{Vj}^{(s)} & 0 & 0 \\ 0 & K_{Pi}^{(c)} G_{Vj}^{(c)} & \bar{\Omega} G_{ji}^{(c)} \\ 0 & -\bar{\Omega} G_{ji}^{(s)} & K_{Pi}^{(c)} G_{Vj}^{(c)} \end{bmatrix} \qquad (4.71b)$$

$$[A_a^{(i)}]_j = \frac{1}{2}\gamma I_B \begin{bmatrix} 0 & G_{II_j}^{(o)} & 0 & 0 & G_{II_j}^{(e)} \\ 0 & 0 & -\bar{k}G_{I_j}^{(c)} & -G_{III_j}^{(c)} & 0 \\ -G_{I_j}^{(c)} & 0 & G_{III_j}^{(c)} & -\bar{k}G_{I_j}^{(c)} & 0 \end{bmatrix} \qquad (4.71c)$$

$$[A_a^{(i)}]_j = \frac{1}{2}\gamma I_B \begin{bmatrix} 0 & 0 & 0 & 0 & 0 \\ 0 & 0 & \bar{\lambda}G_{I_j}^{(c)} & 0 & 0 \\ 0 & 0 & 0 & \bar{\lambda}G_{I_j}^{(c)} & 0 \end{bmatrix} \qquad (4.71d)$$

$$[A_a^{(i)}]_j = \frac{1}{2}\gamma I_B \begin{bmatrix} 0 & 0 & \bar{\lambda}G_{III_j}^{(o)} & G_{IV_j}^{(o)} & 0 & 0 \\ 0 & \bar{\lambda}G_{I_j}^{(c)} & 0 & 0 & G_{IV_j}^{(c)} & 0 \\ -\bar{\lambda}G_{I_j}^{(c)} & 0 & 0 & 0 & 0 & G_{IV_j}^{(c)} \end{bmatrix} \qquad (4.71e)$$

$$[A_{Q_i}^{(s)}] = \begin{bmatrix} 0 & 0 & -\frac{1}{2}\left(\frac{V_i^{(c)}}{R}F_{\theta_1} + \frac{W_i^{(c)}}{R}F_{\theta_2}\right) \\ \frac{V_i^{(o)}}{R}F_{x_1} + \frac{W_i^{(o)}}{R}F_{z_1} & 0 & 0 \\ 0 & -\frac{1}{2}\bar{k}\left(\frac{V_i^{(c)}}{R}F_{\theta_1} + \frac{W_i^{(c)}}{R}F_{\theta_2}\right) & \frac{1}{2}\chi\left(\frac{V_i^{(c)}}{R}F_{z_1} + \frac{W_i^{(c)}}{R}F_{z_2}\right) \\ 0 & -\frac{1}{2}\chi\left(\frac{V_i^{(c)}}{R}F_{z_1} + \frac{W_i^{(c)}}{R}F_{z_2}\right) & -\frac{1}{2}\bar{k}\left(\frac{V_i^{(c)}}{R}F_{\theta_1} + \frac{W_i^{(c)}}{R}F_{\theta_2}\right) \\ \chi\left(\frac{V_i^{(o)}}{R}F_{\theta_1} + \frac{W_i^{(o)}}{R}F_{\theta_2}\right) & 0 & 0 \end{bmatrix} \qquad (4.71f)$$

$$\left[A_{a_i}^{(a)}\right] =$$

$$\begin{bmatrix}
0 & \frac{\bar{\Omega}}{2}\left(\frac{V_i^{(c)}}{R}F_{\theta_1} + \frac{W_i^{(c)}}{R}F_{\theta_2}\right) \\
K_{p_i}^{(a)}F_{z_3} & 0 \\
0 & \frac{1}{2}\left[\left(\frac{V_i^{(c)}}{R}F_{z_0} - \frac{W_i^{(c)}}{R}F_{\theta_0}\right) - \bar{\Omega}\,x\left(\frac{V_i^{(c)}}{R}F_{z_1} + \frac{W_i^{(c)}}{R}F_{z_2}\right)\right] - \frac{1}{2}\bar{\ell}\,K_{p_i}^{(c)}F_{\theta_3} \\
0 & \frac{\bar{\Omega}}{2}\bar{\ell}\left(\frac{V_i^{(c)}}{R}F_{\theta_1} + \frac{W_i^{(c)}}{R}F_{\theta_2}\right) - \frac{1}{2}K_{p_i}^{(c)}\,x\,F_{z_3} \\
K_{p_i}^{(a)}\,x F_{\theta_3} & 0
\end{bmatrix}$$

$$\begin{bmatrix}
\frac{1}{2}K_{p_i}^{(c)}F_{\theta_3} \\
0 \\
-\frac{\bar{\Omega}}{2}\bar{\ell}\left(\frac{V_i^{(c)}}{R}F_{\theta_1} + \frac{W_i^{(c)}}{R}F_{\theta_2}\right) + \frac{1}{2}K_{p_i}^{(c)}\,x\,F_{z_3} \\
\frac{1}{2}\left[\left(\frac{V_i^{(c)}}{R}F_{z_0} - \frac{W_i^{(c)}}{R}F_{\theta_0}\right) - \bar{\Omega}\,x\left(\frac{V_i^{(c)}}{R}F_{z_1} + \frac{W_i^{(c)}}{R}F_{z_2}\right) - \frac{1}{2}\bar{\ell}\,K_{p_i}^{(c)}F_{\theta_3}\right. \\
0
\end{bmatrix} \tag{4.71g}$$

SECTION 5

NATURAL FREQUENCIES AND MODE SHAPES OF THE ROTOR AND WING

5.1 Rigid Rotor

In order to obtain the natural frequencies and corresponding mode shapes of the free vibration of the rotating blade, the equations of motion are derived neglecting aerodynamic forces and pylon motions in Eqs. 2.3 and 2.4.

$$\frac{\partial^2}{\partial r^2}\left[\left\{(EI)_C \sin^2\theta_B + (EI)_B \cos^2\theta_B\right\}\frac{\partial^2 w_n}{\partial r^2}\right]$$

$$+\frac{\partial^2}{\partial r^2}\left[\left\{(EI)_C - (EI)_B\right\}\sin\theta_B\cos\theta_B\frac{\partial^2 v_n}{\partial r^2}\right]$$

$$-\frac{\partial}{\partial r}\left(T\frac{\partial w_n}{\partial r}\right) + m\ddot{w}_n = 0$$

$$\frac{\partial^2}{\partial r^2}\left[\left\{(EI)_C \cos^2\theta_B + (EI)_B \sin^2\theta_B\right\}\frac{\partial^2 v_n}{\partial r^2}\right]$$

$$+\frac{\partial^2}{\partial r^2}\left[\left\{(EI)_C - (EI)_B\right\}\sin\theta_B\cos\theta_B\frac{\partial^2 w_n}{\partial r^2}\right]$$

$$-\frac{\partial}{\partial r}\left(T\frac{\partial v_n}{\partial r}\right) + m\ddot{v}_n - m\Omega^2 v_n = 0 \qquad (5.1)$$

These equations of motion are rewritten as a usual eigenvalue problem to find eigenvalues and/or eigenvectors.

Boundary conditions for the rigid rotor are

at the root:

$$w_n = 0 \qquad \frac{\partial w_n}{\partial r} = 0$$

$$v_n = 0 \qquad \frac{\partial v_n}{\partial r} = 0 \qquad (5.2)$$

at the tip:

$$\frac{\partial^2 w_n}{\partial r^2} = 0 \qquad \frac{\partial^3 w_n}{\partial r^3} = 0$$

$$\frac{\partial^2 v_n}{\partial r^2} = 0 \qquad \frac{\partial^3 v_n}{\partial r^3} = 0 \tag{5.3}$$

As a typical hingeless rotor, the Boeing rotor is chosen in this study. Mass, stiffness distributions and built-in angle of twist are shown in Fig. 8.

Nonrotating natural frequencies of the blade are shown in Fig. 9. Almost no influence of the collective pitch change on the natural frequency is found in the case of the rigid rotor.

In Figs. 10a and 10b, the first and second natural frequencies of the rotating blade are shown versus rotor rotational speed and inflow ratio. Inflow ratio is related to the collective pitch as described in Eq. 3.9. At normal rotational speed (in this case Ω = 386 R.P.M.) the natural frequency variation due to collective pitch change is shown in Fig. 11. Typical mode shapes up to the 4th mode are shown in Figs. 12a through 12d. Blade mode shapes are normalized with respect to the blade radius at the point of maximum deflection in either out-of-plane or inplane bending.

5.2 Gimballed Rotor

In the case of the gimballed rotor, rotor motion is expressed by collective modes and cyclic modes (in Ref. 17 and 18). Hence, based on Eq. 5.1, the eigenvalue problem should be solved with boundary conditions for collective modes and cyclic modes for the powered flight, respectively.

Boundary conditions for collective modes are defined to yield symmetrical modes for flapping and lagging. Therefore,

at the root:

$$w_n = 0 \qquad \frac{\partial w_n}{\partial r} = 0$$

$$v_n = 0 \qquad \frac{\partial v_n}{\partial r} = 0 \tag{5.4}$$

at the tip:

$$\frac{\partial^2 w_n}{\partial r^2} = 0 \qquad \frac{\partial^3 w_n}{\partial r^3} = 0$$

$$\frac{\partial^2 v_n}{\partial r^2} = 0 \qquad \frac{\partial^3 v_n}{\partial r^3} = 0 \tag{5.5}$$

Boundary conditions for cyclic modes which consist of anti-symmetrical modes for flapping motion and symmetrical modes for lagging motion are expressed as:

at the root:

$$w_n = 0 \qquad \frac{\partial^2 w_n}{\partial r^2} = 0$$

$$v_n = 0 \qquad \frac{\partial v_n}{\partial r} = 0 \tag{5.6}$$

at the tip:

$$\frac{\partial^2 w_n}{\partial r^2} = 0 \qquad \frac{\partial^3 w_n}{\partial r^3} = 0$$

$$\frac{\partial^2 v_n}{\partial r^2} = 0 \qquad \frac{\partial^3 v_n}{\partial r^3} = 0 \tag{5.7}$$

As a typical case, the Bell design is considered here. Mass, stiffness distributions and built-in angle of twist are shown in Fig. 8.

Blade nonrotating natural frequencies for the gimballed rotor are shown in Fig. 13. In Fig. 13b, the first natural frequency for rigid body flapping motion has non-zero natural frequency due to the rubber hub spring, which is intended to increase control power and damping.

In Figs. 14 and 15 it is shown that collective pitch change has a large influence on the natural frequency variation except for the first cyclic mode natural frequency (rigid body mode). Mode shapes for the gimballed rotor are shown in Figs. 16 and 17. The normalization system is the same as that of the rigid rotor.

5.3 Wing

The equations of motion for free vibration of the wing are the same as Eq. 2.5, 2.6, and 2.7 when the aerodynamic forces F_x, F_z, and M_y are eliminated from these equations. Boundary conditions are as follows:

(a) at the root:

$$u_w = 0 \qquad \frac{\partial u_w}{\partial y} = 0$$
$$w_w = 0 \qquad \frac{\partial w_w}{\partial y} = 0$$
$$\rho_w = 0 \tag{5.8}$$

(b) at the wing tip:

$$M_p \ddot{r}_x - \frac{\partial}{\partial y}\left[\left\{(EI_w)_c \sin^2\theta_w + (EI_w)_B \cos^2\theta\right\} \frac{\partial^2 u_w}{\partial y^2}\right]_{y=L}$$
$$- \frac{\partial}{\partial y}\left[\left\{(EI_w)_c - (EI_w)_B\right\} \sin\theta_w \cos\theta_w \frac{\partial^2 w_w}{\partial y^2}\right]_{y=L}$$
$$+ N M_B \ddot{r}_x + N M_B h \ddot{\nu}_p = 0 \tag{5.9a}$$

$$M_p \ddot{r}_z - \frac{\partial}{\partial y}\left[\left\{(EI_w)_c \cos^2\theta_w + (EI_w)_B \sin^2\theta_w\right\} \frac{\partial^2 w_w}{\partial y^2}\right]_{y=L}$$
$$- \frac{\partial}{\partial y}\left[\left\{(EI_w)_c - (EI_w)_B\right\} \sin\theta_w \cos\theta_w \frac{\partial^2 u_w}{\partial y^2}\right]_{y=L}$$
$$+ N M_B \ddot{r}_z = 0 \tag{5.9b}$$

$$I_{py} \ddot{\nu}_y + \left[\left\{(EI_w)_c \cos^2\theta_w + (EI_w)_B \sin^2\theta_w\right\} \frac{\partial^2 w_w}{\partial y^2}\right]_{y=L}$$
$$+ \left[\left\{(EI_w)_c - (EI_w)_B\right\} \sin\theta_w \cos\theta_w \frac{\partial^2 u_w}{\partial y^2}\right]_{y=L}$$
$$+ N M_B h^2 \ddot{\nu}_y + \frac{N}{2} I_B \ddot{\nu}_y = 0 \tag{5.9c}$$

$$I_{pp}\ddot{\nu}_p + \left[(GJ)_w \frac{\partial \theta_w}{\partial y}\right]_{y=L} + NM_B h \ddot{r}_x + NM_B h \ddot{\nu}_p + \frac{N}{2} I_B \ddot{\nu}_p = 0 \qquad (5.9d)$$

$$I_{pr}\ddot{\nu}_r - \left[\left\{(EI_w)_c \sin^2\theta_w + (EI_w)_B \cos^2\theta_w\right\} \frac{\partial^2 u_w}{\partial y^2}\right]_{y=L} - \left[\left\{(EI_w)_c - (EI_w)_B\right\} \sin\theta_w \cos\theta_w \frac{\partial^2 v_w}{\partial y^2}\right]_{y=L} + N I_B \ddot{\nu}_r = 0 \qquad (5.9e)$$

The relationship between pylon motions and wing deflections is defined in Eq. 2.8. The rotor and the pylon are treated as lumped masses at the wing tip in these equations; as in the actual structural dynamic test, the proprotor blades will be removed and replaced by equivalent weights. Note that in Eq. 5.9 the blade is treated as a lumped mass which has equivalent weight and equivalent blade flapping inertia I_B. This flapping inertia leads to lower wing frequencies, especially in torsion, than when the blade is treated as a lumped mass with equivalent mass and without equivalent blade flapping inertia.

The same wing is used for the Boeing and the Bell design; mass and stiffness properties are shown in Fig. 18. The differences appear in the pylon and blade mass properties shown in Table 1. No built-in angle of twist, dihedral angle, and sweep angle are considered here.

Natural frequencies of both cases are listed in Table 1, and mode shapes are described in Fig. 19 for the Boeing case and in

Fig. 20 for the Bell case. Wing mode shapes are normalized with respect to the wing semispan at the point of maximum deflection in either vertical bending or in chordwise bending. However, the mode shape corresponding to the third natural frequency of the wing, which is predominantly one of wing torsional deflection, is normalized at the point of maximum torsional deflection.

SECTION 6

PROPROTOR DYNAMIC CHARACTERISTICS

6.1 Introduction

In this section the eigenvalues and frequency response of the system will be discussed. The results are compared with those of Ref. 13. The analyses were conducted for two types of proprotor design: the hingeless rotor Boeing design, and the gimballed rotor Bell design. The case selected to be investigated is cruising flight in the airplane mode for each design. The data for the calculation are listed in Table 1. One should notice that the equations of motion shown in Eq. 4.57 were derived based on mass-normalized coupled modes. However, for the sake of aiding physical understanding of the frequency response and eigenvalue analysis, those results are based on physical mode shapes, as presented in Figs. 12, 16, 17, 19, and 20.

The primary differences between the Ref. 13 analysis and this report are tabulated below.

	This Report	Ref. 13
Natural Frequencies	Calculated Data	Experimental Data
Mode Shapes		
Wing	Coupled Modes	Uncoupled Modes
Rotor	Coupled Modes	Uncoupled Elastic Modes for Inertia Terms; Rigid-Body Mode for Aerodynamic Terms
Structural Damping	No	Yes

The case studies done in the present study are tabulated below:

Degree-of-Freedom	9 Degree-of-Freedom		18 Degree-of-Freedom	
Mode Shapes				
Blade	Rigid Body	Uncoupled Elastic	Coupled	Coupled
Wing	Coupled	Coupled	Coupled	Coupled
Analysis	Eigenvalue	Eigenvalue	Eigenvalue and Eigenvector Frequency Response to u_G, v_G, w_G, θ_{ls}	Eigenvalue

The general symbols Q_{jo}, Q_{jc}, Q_{js}, and a_i for blade and wing motions are convenient for the theoretical derivation of the equations, but from the physical understanding aspect, it would be better to choose other symbols. For this section, except for the eigenvalue analysis, the following system will be used to express blade and wing motion for the 9 degree-of-freedom system: flapping and lagging motions which are designated as β and ζ, respectively, and wing motions are q_1, q_2, and p, which express the vertical bending, chordwise bending, and torsion, respectively.

The correspondence between these sets of symbols is tabulated below:

New Symbols		General Symbols	
		Bell Design	Boeing Design
β_o	Predominant Flapping Motion	Q_{20}	Q_{2o}
β_{1c}		Q_{1c}	Q_{2c}
β_{1s}		Q_{1s}	Q_{2s}
ζ_o	Predominant Lagging Motion	Q_{10}	Q_{10}
ζ_{1c}		Q_{2c}	Q_{1c}
ζ_{1s}		Q_{2s}	Q_{1s}
q_1	Wing Vertical Bending	a_1	a_1
q_2	Wing Chordwise Bending	a_2	a_2
p	Wing Torsion	a_3	a_3

6.2 Eigenvalues and Eigenvectors

The system stability characteristics are shown in Figs. 21 through 24.

6.2.1 Addition of Higher Mode Degrees of Freedom

The eigenvalue variation with number of degrees-of-freedom considered is shown in Fig. 21. The 9 degrees-of-freedom include Q_{10}, Q_{1c}, Q_{1s}, Q_{20}, Q_{2c}, Q_{2s}, a_1, a_2, and a_3 (β_o, β_{1c}, β_{1s}, ζ_o, ζ_{1c}, ζ_{1s}, q_1, q_2, and p) corresponding to the blade's first two natural frequencies and the wing's first three natural frequencies. This system has 9 eigenvalues and 9 corresponding eigenvectors. The 9 eigenvalues are denoted by their frequencies, and the participation of the degrees-of-freedom in the eigenvectors is indicated below:

C-2

Present		Ref. 13	
Eigenvalue Symbol	Participation	Bell	Boeing
Q_1^-	Low frequency Q_1	$\beta-1$	$\zeta-1$
Q_1^o	Collective Q_1	ζ	ζ
Q_1^+	High frequency Q_1	$\beta+1$	$\zeta+1$
Q_2^-	Low frequency Q_2	$\zeta-1$	$\beta-1$
Q_2^o	Collective Q_2	β	β
Q_2^+	High frequency Q_2	$\zeta+1$	$\beta+1$
a_1	The first wing frequency	q_1	q_1
a_2	The second wing frequency	q_2	q_2
a_3	The third wing frequency	p	p

In the 18 degree-of-freedom system two higher elastic modes for the blade and three higher elastic modes for the wing are added to the 9 degree-of-freedom system. The same designation system as used for the 9 degree-of-freedom is employed for the higher eigenvalues. The results of the 18 degree-of-freedom analysis show that the addition of more degrees of freedom does not substantially influence the basic system eigenvalues since the added degrees of freedom have large natural frequencies in comparison with the original values (see Table 1). The 18 degree-of-freedom system eigenvalue locations are shown in Fig. 22.

6.2.2 The Sensitivity to Mode Shape

Eigenvalues and damping ratios (the fraction of the critical damping) for three different types of mode shapes for the blade are shown in Fig. 23. One is the rigid-body mode (with spring restraint at the root), another is the elastic uncoupled mode, and the third is the elastic coupled mode, while the wing mode shapes considered are restricted to the elastic coupled mode shapes only.

The results tell that mode-shape types make negligible difference in the frequency of the eigenvalues; however, they influence the damping a lot.

In the Bell design, there is almost no difference between the rigid mode and the elastic mode in the damping ratio. This is due to the similarity between the rigid-body mode and the elastic uncoupled mode. In the elastic coupled mode, a slightly higher damping is obtained.

In the Boeing design, each mode-shape type gives a different damping. For the first natural frequency mode of the blade, the rigid-body mode calculation is conservative rather than that of the elastic coupled mode-shape type, and for the second natural frequency mode, it is nonconservative. This is because the first mode has both positive out-of-plane and inplane deflection, while the second has a positive out-of-plane and a negative inplane deflection as shown in Figs. 12 (a) and (b). The corresponding positive out-of-plane deflection of the first mode increases the damping, while the associated negative inplane deflection of the second mode reduces the damping. This explanation also holds for the Bell case. The damping of the second collective elastic coupled mode of the Bell rotor is lower than that of the rigid-body mode. The second collective mode has a positive out-of-plane deflection and a small positive inplane deflection. However, the rotation direction of the rotor is different for the Bell and the Boeing

designs. Therefore, the positive inplane deflection mode of the Bell rotor is physically the same motion as that of the first mode of the Boeing rotor. The coordinate system related to this is shown in Fig. 5, and the contribution to the damping of the coupled mode shape can be seen in the term G_{ji} in Eq. 4.33.

In conclusion, the use of the elastic coupling mode affects the damping significantly. The coupled mode with a combination of forward out-of-plane deflection (upward in helicopter mode) and inplane deflection opposing the rotor direction of rotation, or vice versa, increases the damping over that of the rigid-body-mode calculation. The coupled mode which has forward out-of-plane deflection and inplane deflection proceeding with rotor direction of rotation, or vice versa, decreases the damping. This holds only for the first beam bending mode; in other words, the coupled mode without nodal points between the root and the tip.

6.3 Frequency Response

The frequency response analysis is dealt with in this subsection. These calculations are all based on mass-normalized coupled modes for both the blade and the wing. However, for convenience in physical understanding, the results of the frequency response calculation are presented in terms of length-normalized mode shapes in Figs. 25 through 32.

6.3.1 Frequency Response to the Gust

Frequency responses to the vertical gust u_G, the lateral gust v_G, and the longitudinal gust w_G for both the Bell and the Boeing designs are shown in Figs. 25 through 30.

As a whole, the behavior of the frequency response is quite similar to that of Ref. 13 in spite of the differences in the theoretical model stated in Subsection 6.1.

The detail characteristics of the frequency response are discussed next.

6.3.1.1 Blade Collective Motion Response (β_o,ζ_o)

Collective motion responses have a close relationship with the wing motions (vertical bending q_1, chordwise bending, q_2, and torsion, p). They have strong resonances with these modes. In the case of u_G and v_G inputs, the static response (ω equal to zero) and the lower-frequency-range response are negligible. However, the response to the longitudinal gust w_G has a significant static and lower frequency range response. Resonances of the collective modes occur in the response to the longitudinal gust input. Comparing the Boeing design with the Bell design, the Boeing has a larger response in collective responses to each gust input.

6.3.1.2 Blade Cyclic Flapping Motion Response (β_{1c} and β_{1s})

For the cyclic inputs (u_G and v_G) there are not strong resonances between cyclic flapping motions and the wing vertical bending motion (q_1). In the upper frequency range, the high frequency flapping mode (β+1 mode) has a significant resonance appearing in the flapping motion. In the lower frequency range, there is a resonance of the low frequency flapping mode (β-1 mode) for the Boeing design and the low frequency lagging mode (ζ-1 mode) for the Bell design.

For the collective input (w_G) the response of the cyclic flapping motion has resonances with the wing motion modes (q_1, q_2, and p) in both designs.

6.3.1.3 Blade Cyclic Lagging Motion Response (ζ_{1c} and ζ_{1s})

In the Bell design there is an evident resonance in the cyclic lagging motion response (ζ_{1c} and ζ_{1s}) to the vertical gust input (u_G) in proximity to the wing vertical bending mode (q_1). To the lateral gust input (v_G), a low frequency lagging mode (ζ-1 mode) resonance appears in the lagging motion response.

In the Boeing design there cannot be seen such obvious resonances in the response to the vertical and lateral gust inputs.

The static response is much larger than that of the Bell design due to the soft inplane design (the blade lagging natural frequency is less than unity).

For the collective input (w_G), the responses of cyclic lagging motion have resonances with the wing motion modes (q_1, q_2, and p) in both designs.

6.3.1.4 Wing Motion Response (q_1, q_2, and p)

The wing motion includes resonances in each wing mode. Although the response magnitude is quite large, it is expected to become rather small if structural damping is included.

6.3.2 Frequency Response to Control Pitch Angle

Frequency responses to longitudinal cyclic pitch input are shown in Figs. 31 and 32.

SECTION 7

CONCLUSIONS AND COMMENTS

7.1 Conclusions

This study has been devoted to the development and evaluation of a theoretical model of the proprotor on a cantilever wing, operating in normal cruising flight. This theory expresses the wing and blade motions in coupled form, and can include any number of mode shapes required to express the motions accurately. It has been applied to an investigation of the dynamic characteristics of the Bell and the Boeing designs.

Based on the theoretical results included in this study, the following conclusions may be stated:

(a) The choice of mode shape (rigid-body mode or elastic-coupled mode) affects the damping significantly. The dependency of the damping on the mode shape can be estimated for the first beam bending mode. The blade inplane deflection opposing the rotor direction of rotation, accompanied by the forward out-of-plane deflection, increases the damping, comparing it with the rigid-body calculation. The inplane deflection proceeding in the rotor direction of rotation decreases the damping. The mode shape has little influence on the frequencies of the system.

(b) The results of the frequency response are quite similar to those of Ref. 13, in spite of the difference in the mode shapes. The amplitude of the response is slightly different, since structural damping was not included in the present calculation, and the mode shapes used were different.

(c) The analysis of the eighteen degree-of-freedom system showed that the higher-frequency degrees of freedom have small influence on the basic degrees of freedom.

7.2 Suggestions for Future Research

A direct and useful extension of the present study would be the stability analysis of the proprotor aircraft, with respect to air resonance and flutter. This theory will be very powerful because the eigenvector components can be compared directly without any adjustment between components. Mach number effects of the blade should be included for the flutter analysis.

Stresses or bending moments of the wing or blade can be predicted from the motions of the wing and blade obtained from this analysis. In addition, this analysis may be applied to the development of an automatic control device to alleviate the gust response of the vehicle.

REFERENCES

1. Brown, D., "Vertol Sees Wide Use of Tilt-Rotor Design". Aviation Week and Space Technology, January 1, 1973, pp. 52-54.

2. Ludi, L.H., "Composite Aircraft Design". Journal of American Helicopter Society, Vol. 13, No. 1, 1968, pp. 1-13.

3. Wernicke, K.G., "Tilt Proprotor Composite Aircraft, Design State of the Art". Journal of American Helicopter Society, Vol. 14, No. 2, 1969, pp. 10-25.

4. Reed, W.H. III, "Propeller-Rotor Whirl Flutter: A State of the Art Review". Journal of Sound and Vibration, Vol. 3, No. 4, 1966, pp. 526-544.

5. Loewy, R.G., "Review of Rotary Wing/V/STOL Dynamic and Aeroelastic Problems". Journal of American Helicopter Society, Vol. 14, No. 3, 1969, pp. 3-23.

6. Taylor, E.S. and Browne, K.A., "Vibration Isolation of Aircraft Power Plants". Journal of the Aeronautical Sciences, Vol. 6, No. 2, 1938, pp. 43-49.

7. Houbolt, J.C. and Reed, W.H. III, "Propeller-Nacelle Whirl Flutter". Journal of the Aerospace Sciences, Vol. 29, No. 3, 1962, pp. 333-346.

8. Hall, E.W. Jr., "Prop-Rotor Stability at High Advance Ratios". Journal of American Helicopter Society, Vol. 11, No. 2, 1966, pp. 11-26.

9. Young, M.I. and Lytwyn, R.I., "The Influence of Blade Flapping Restraint on the Dynamic Stability of Low Disk Loading Propeller-Rotors", Journal of American Helicopter Society, Vol. 2, No. 4, 1968, pp. 38-54.

10. Gaffey, T.M., "The Effect of Positive Pitch-Flap Coupling (Negative δ_3) on Rotor Blade Motion Stability and Flapping".

Journal of American Helicopter Society, Vol. 14, No. 2, 1969, pp. 49-67.

11. Bell Helicopter Company, "V/STOL Tilt-Rotor Study Task II -- Research Aircraft Design". NASA CR 114442, March 1972.

12. Boeing Vertol Company, "V/STOL Tilt-Rotor Aircraft Study Volume II -- Preliminary Design of Research Aircraft". NASA CR 114438, March 1972.

13. Johnson, W., "Dynamics of Tilting Proprotor Aircraft in Cruise Flight". NASA TN-D 7677, May 1974.

14. Johnson, W., "Theory and Comparison with Tests of Two Full-Scale Proprotors". Proceeding of the AHS/NASA-Ames Specialists' Meeting on Rotorcraft Dynamics, Feb., 1974.

15. Bisplinghoff, R.L., Ashley, H., Halfman, R.L., "Aeroelasticity". Addison-Wesley Pub. Co., 1955.

16. Hohenemser, K.H., Yin, S., "Some Applications of the Method of Multiblade Coordinates". Journal of American Helicopter Society, Vol. 17, No. 3, 1972, pp. 3-12.

17. Balke, R.W., Bennett, R.L., Gaffey, T.N., and Lynn, R.R., "Tail Rotor Design Part II: Structural Dynamics". Journal of American Helicopter Society, Vol. 15, No. 4, 1970, pp. 16-30.

18. Blankenship, B.L., and Harvey, K.W., "A Digital Analysis for Helicopter Performance and Rotor Blade Bending Mode", Journal of American Helicopter Society, Vol. 7, No. 4, 1962, pp. 55-68.

19. Wernicke, K.G., and Edenborough, H.K., "Full-Scale Proprotor Development". Journal of American Helicopter Society, Vol. 17, No. 1, 1972, pp. 31-40.

TABLE 1

DESCRIPTION OF THE BELL AND THE BOEING PROPROTOR DESIGNS CONSIDERED IN THIS REPORT

	BELL	BOEING
ROTOR		
Type	gimballed, stiff inplane	cantilever, soft inplane
Number of blades, N	3	3
Radius, R	156 in.	150 in.
Chord, C_B	18.9 in.	14 in.
Lock number, γ	3.83	4.04
Solidity, σ	0.089	0.115
Pitch/flap coupling, δ_3	-15 deg.	0
Collective pitch, θ_D	1.25 deg.	1.0 deg.
Lift-curve slope, a	5.7	5.7
Drag Coefficient, C_{Do}	0.0065	0.0065
Rotor rotation direction, $\bar{\Omega}$	+1	-1
Inflow ratio, λ	0.7	0.7
Rotational speed, $\|\Omega\|$	458 RPM 48.9 rad/sec	386 RPM 40.4 rad/sec
Blade Natural Frequencies		
first, $\lambda_1/\|\Omega\|$	1.02/rev (7.78Hz)	0.827/rev.(5.32Hz)
second, $\lambda_2/\|\Omega\|$	1.34/rev (10.2Hz)	1.32/rev (8.49Hz)
third, $\lambda_3/\|\Omega\|$	4.35/rev (33.2Hz)	3.40/rev (21.9Hz)

TABLE 1 CONTINUED

	BELL	BOEING
ROTOR(cont'd)		
fourth, $\lambda_4/\|\Omega\|$	10.1/rev(77.1Hz)	6.77/rev(43.5Hz)
Collective Natural Frequency		
first, $\lambda_1^{(o)}/\|\Omega\|$	1.31/rev (10.0Hz)	
second, $\lambda_2^{(o)}/\|\Omega\|$	2.12/rev (16.2Hz)	
third, $\lambda_3^{(o)}/\|\Omega\|$	4.93/rev (37.7Hz)	
fourth $\lambda_4^{(o)}/\|\Omega\|$	10.6/rev (80.9Hz)	
Blade flapping inertia, I_B	105 slug-ft^2	150 slug-ft^2
One blade weight, M_B	133 lb	124 lb
WING		
Semispan, L	200 in.	200 in.
Chord, c_w	62.2 in.	62.2 in.
Mast height, h	51.3 in.	51.3 in.
Sweep	0	0
Dihedral	0	0
Lift-curve slope, a_w	5.7	5.7
Drag coefficient, C_{Dow}	0.004	0.004
Moment coefficient C_{mo}	-0.005	-0.005
Aerodynamic center, $\bar{e} = x_{A_w}/C_w$	0.01	0.01
Angle of attack, α_{wo}	2.0 deg	2.0 deg

TABLE 1 CONCLUDED

	BELL	BOEING
WING (cont'd)		
Natural Frequencies		
first, $\Lambda_1/\|\Omega\|$	0.347/rev(2.65Hz)	0.365/rev(2.35Hz)
second, $\Lambda_2/\|\Omega\|$	0.622/rev(4.75Hz)	0.653/rev(4.20Hz)
third, $\Lambda_3/\|\Omega\|$	1.09/rev(8.32Hz)	1.11/rev(7.14Hz)
fourth, $\Lambda_4/\|\Omega\|$	2.37/rev(18.1Hz)	2.47/rev(15.9Hz)
fifth, $\Lambda_5/\|\Omega\|$	3.76/rev(28.7Hz)	3.95/rev(25.4Hz)
sixth, $\Lambda_6/\|\Omega\|$	10.6/rev(80.9Hz)	12.5/rev(80.4Hz)
PYLON		
Weight, M_p	1420 lb	2000 lb
Yaw inertia, I_{py}	164.8 slug-ft^2	250.0 slug-ft^2
Pitch inertia, I_{pp}	190.0 slug-ft^2	250.0 slug-ft^2
Roll inertia, I_{pr}	42.4 slug-ft^2	30.0 slug-ft^2
FLIGHT CONDITION FOR CALCULATIONS, $\lambda = 0.7$		
Cruising speed, V	250 kt	218 kt
Cruising altitude	sea level	sea level

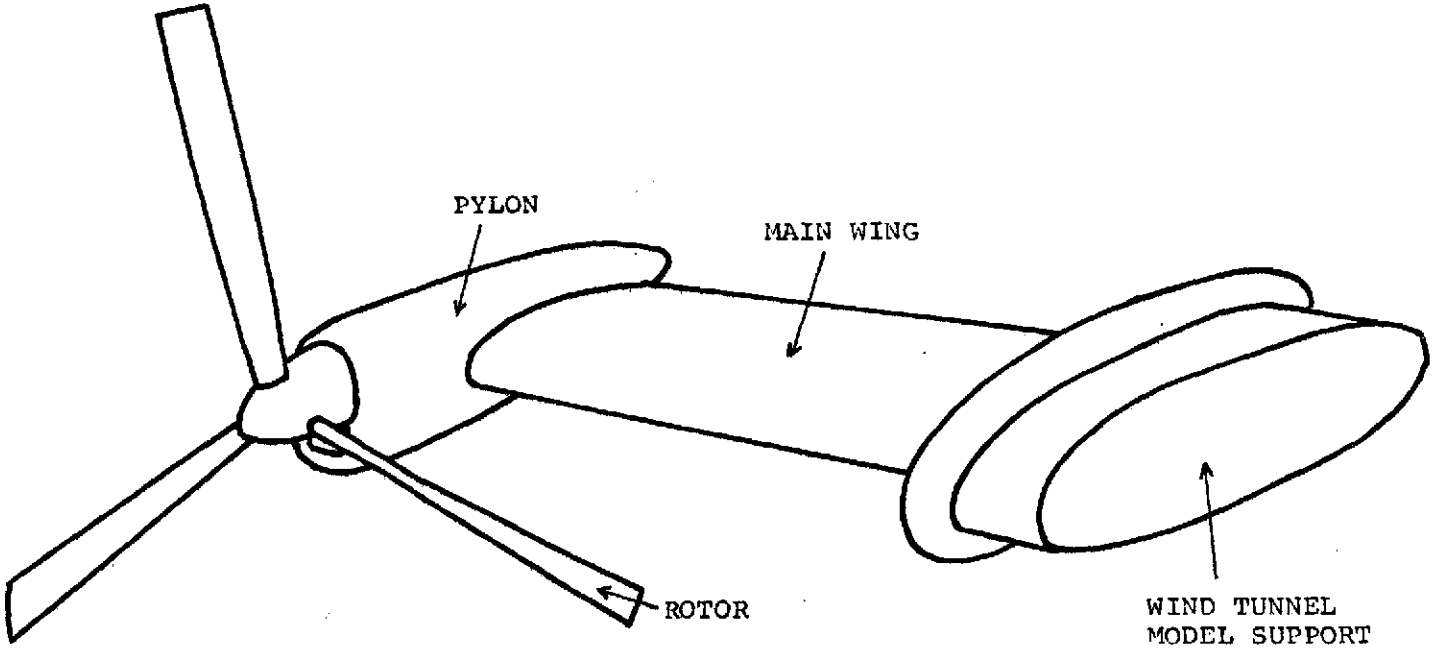

FIG. 1 CONFIGURATION OF ANALYTICAL MODEL, PROPROTOR ON A CANTILEVER WING OPERATING IN THE AIRPLANE MODE

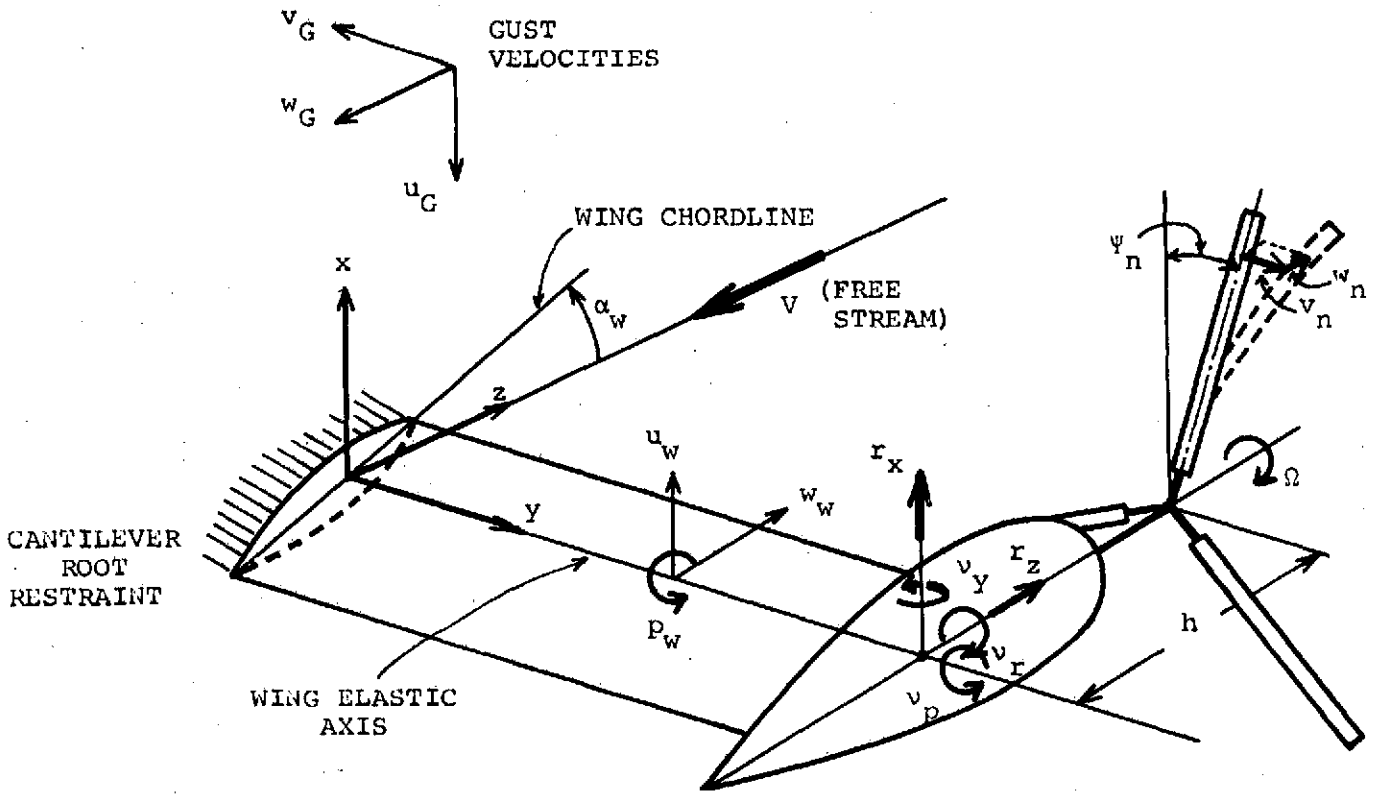

FIG. 2 PROPROTOR GEOMETRY AND MOTION WITH GUST VELOCITY DEFINITION

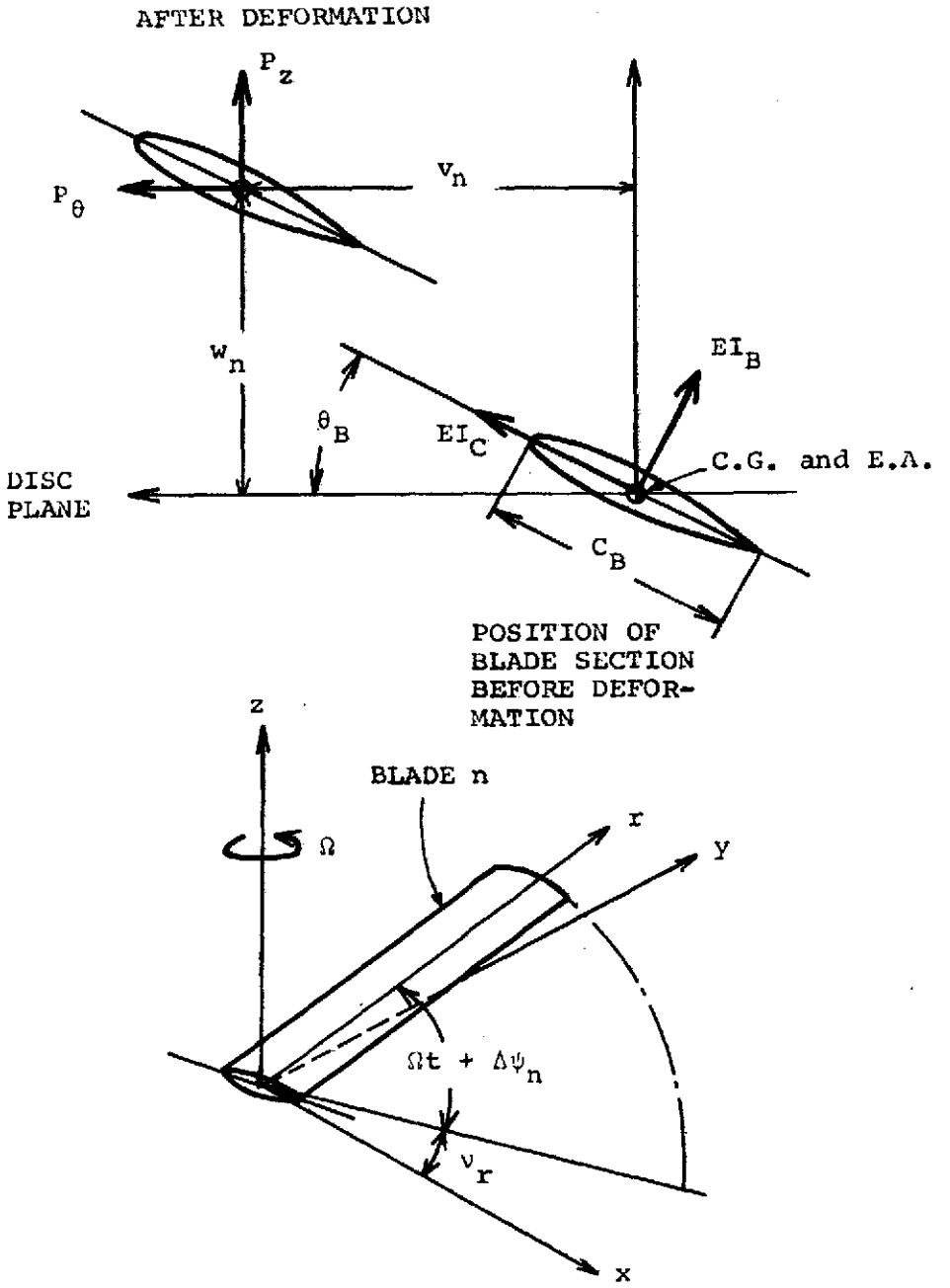

FIG. 3 BLADE GEOMETRY

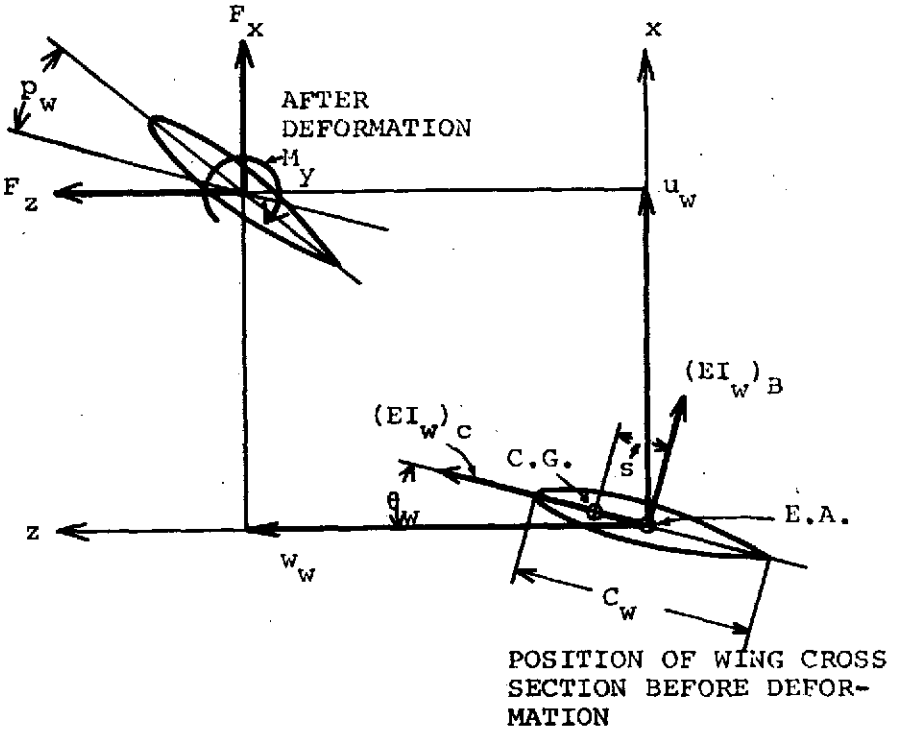

FIG. 4 WING GEOMETRY

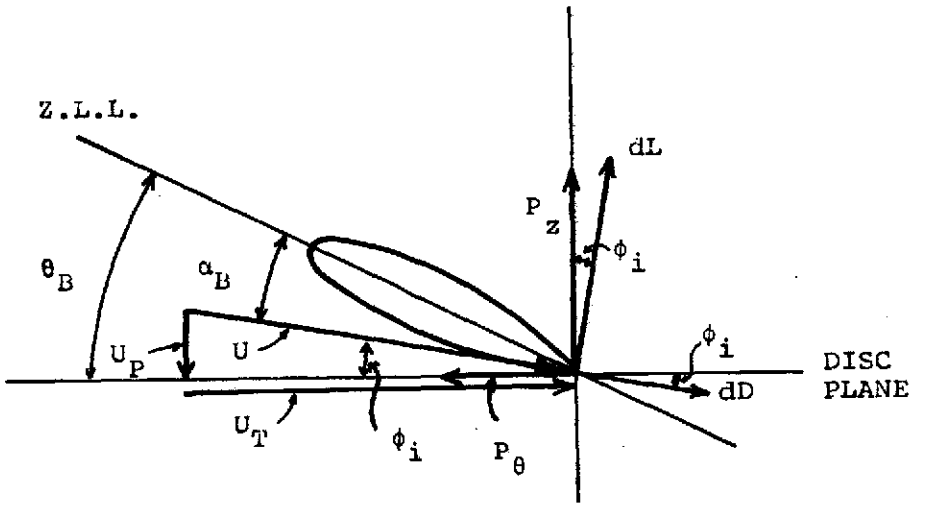

(a) For Clockwise Rotation

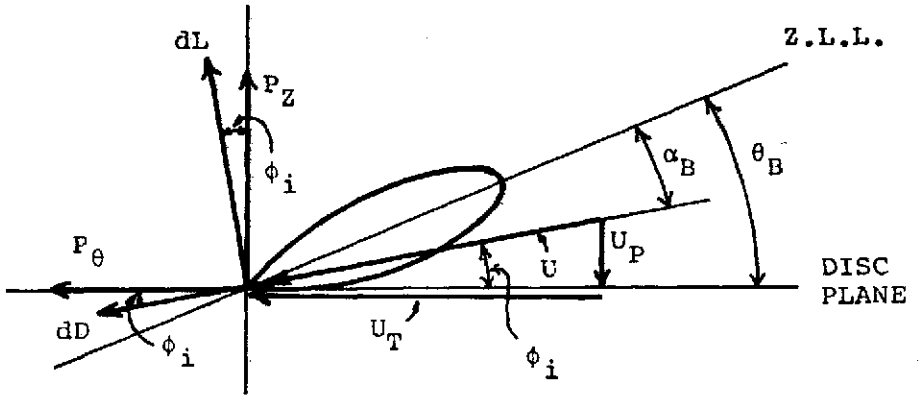

(b) For Counterclockwise Rotation

FIG. 5 VELOCITIES AT THE BLADE ELEMENT AND RESULTING AERODYNAMIC FORCES WHEN LOOKING OUTBOARD

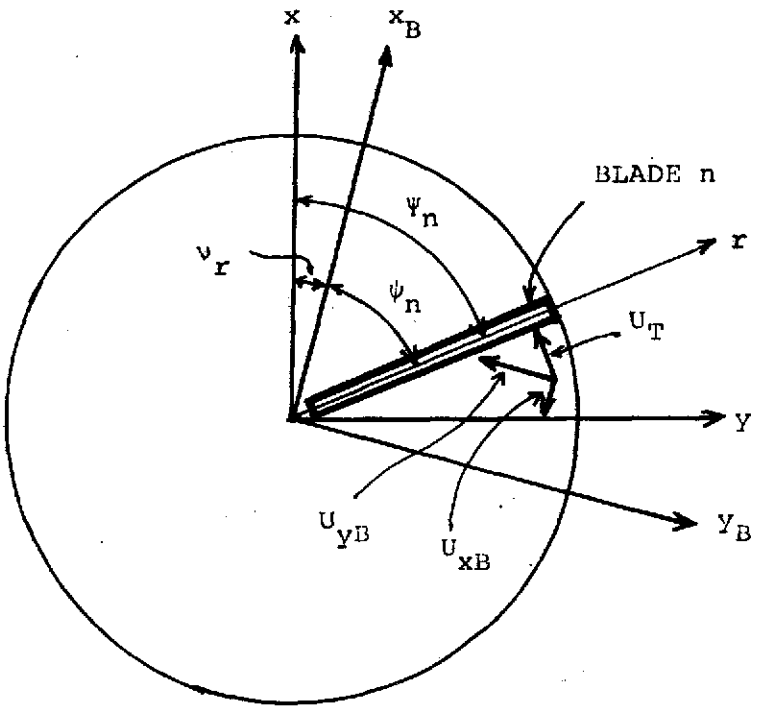

FIG. 6 WIND VELOCITIES IN THE DISC PLANE OF THE ROTOR, LOOKING FORWARD

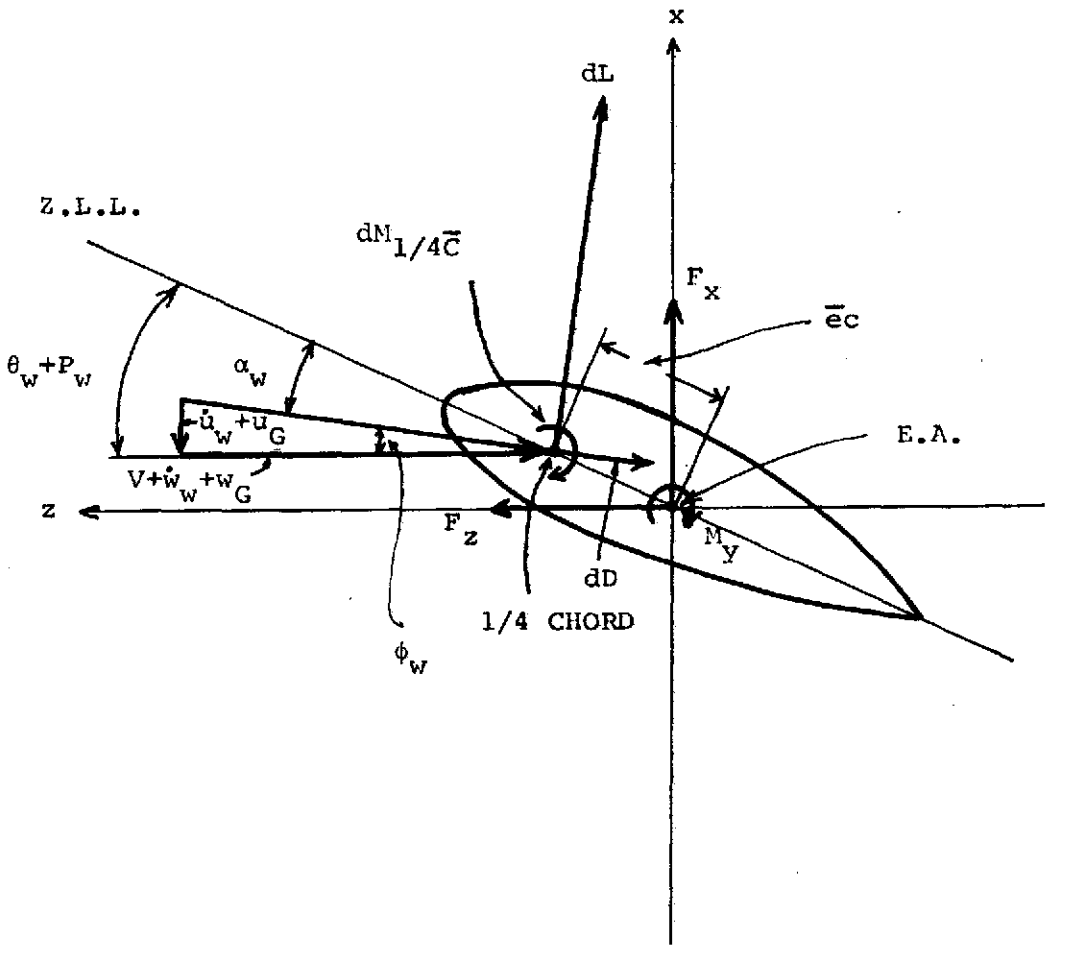

FIG. 7 VELOCITIES AT THE WING ELEMENT AND RESULTING AERODYNAMIC FORCES WHEN LOOKING OUTBOARD

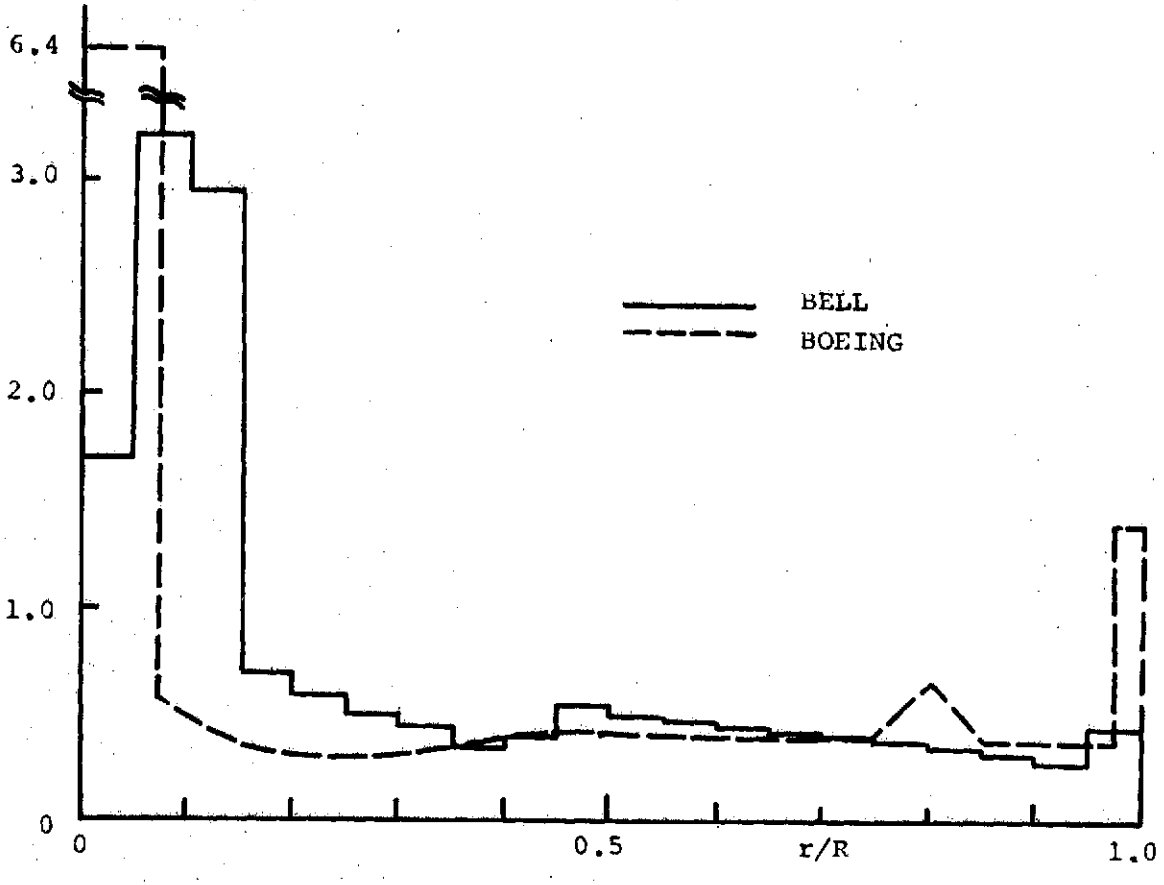

(a) Section Mass Distribution

FIG. 8 STRUCTURAL CHARACTERISTICS OF TWO PROPROTOR BLADES

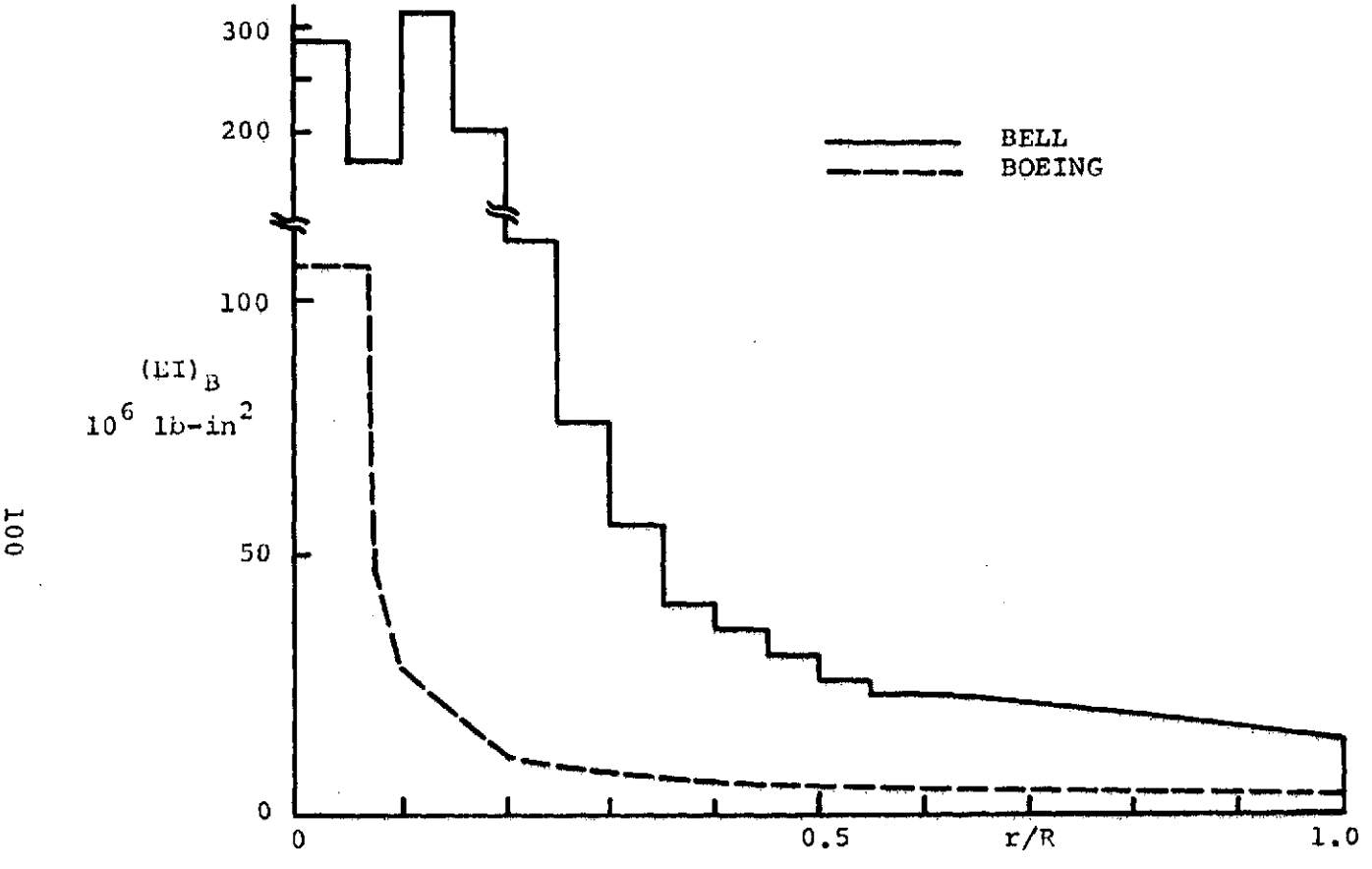

(b) Section Flapwise Bending Stiffness Distribution

FIG. 8 CONTINUED

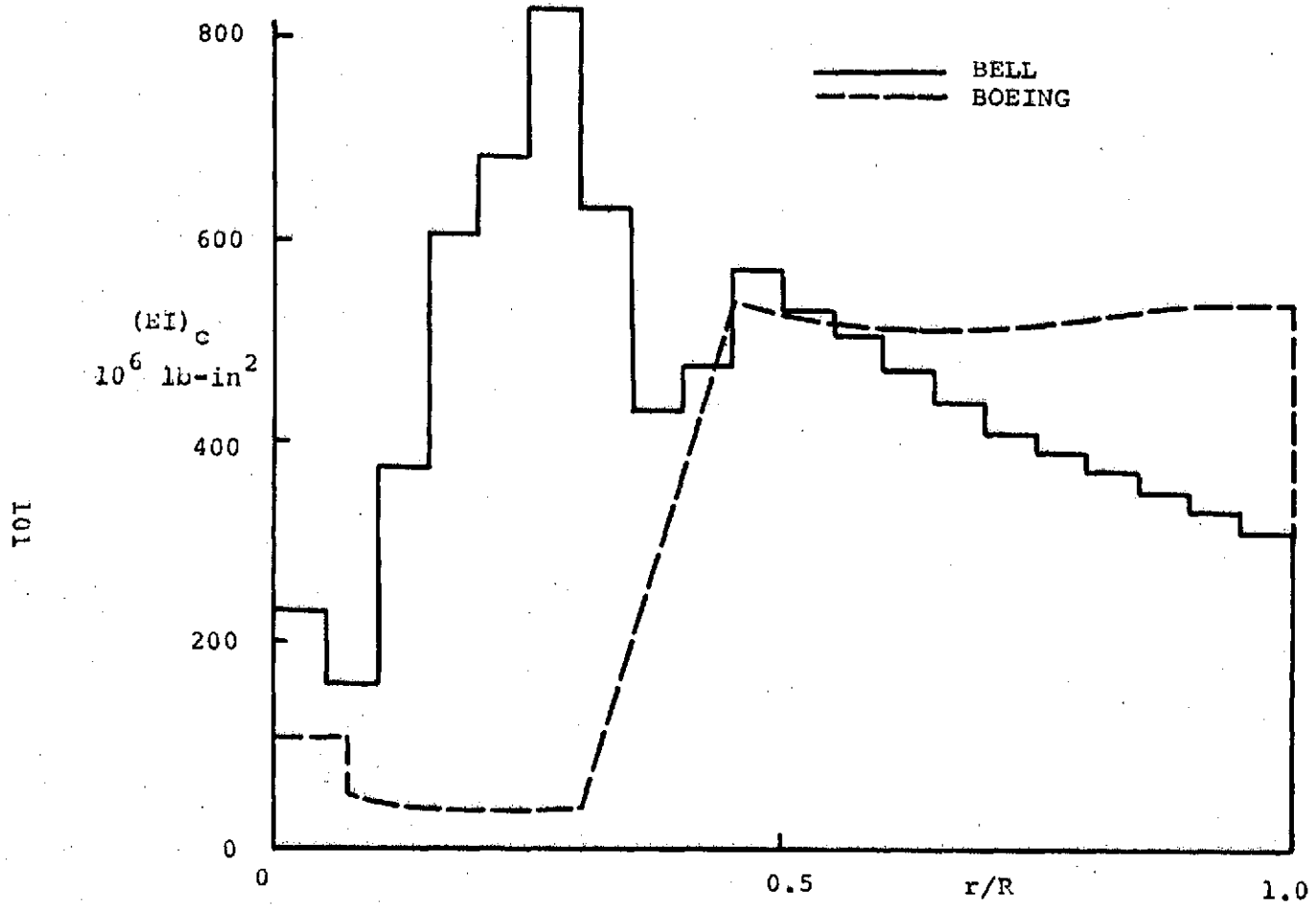

(c) Section Chordwise Bending Stiffness Distribution

FIG. 8 CONTINUED

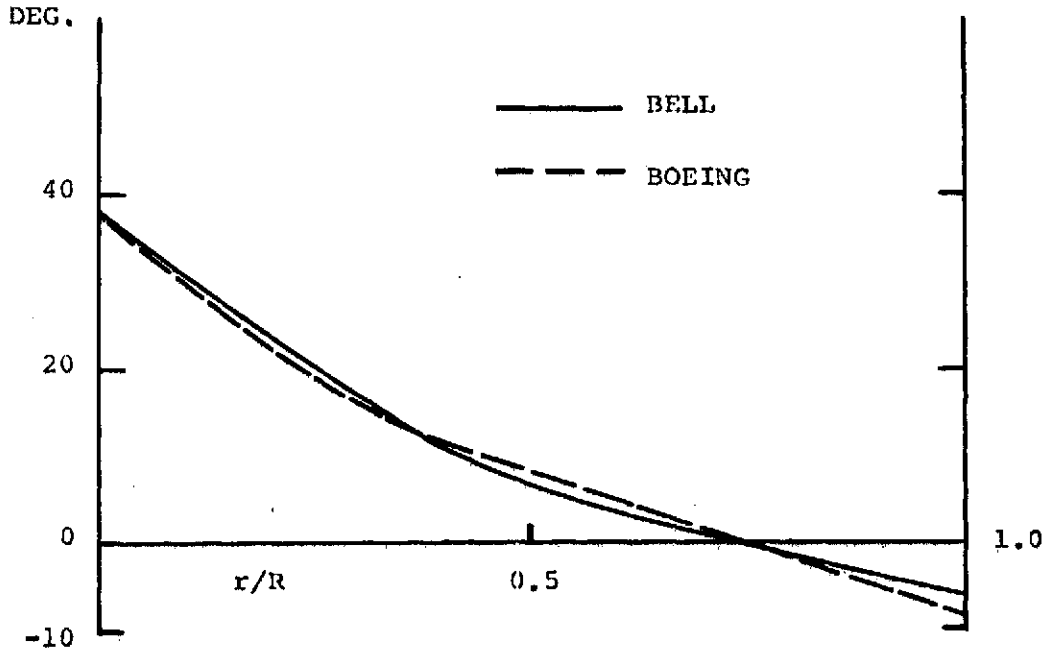

(d) Angle of Twist

FIG. 8 CONCLUDED

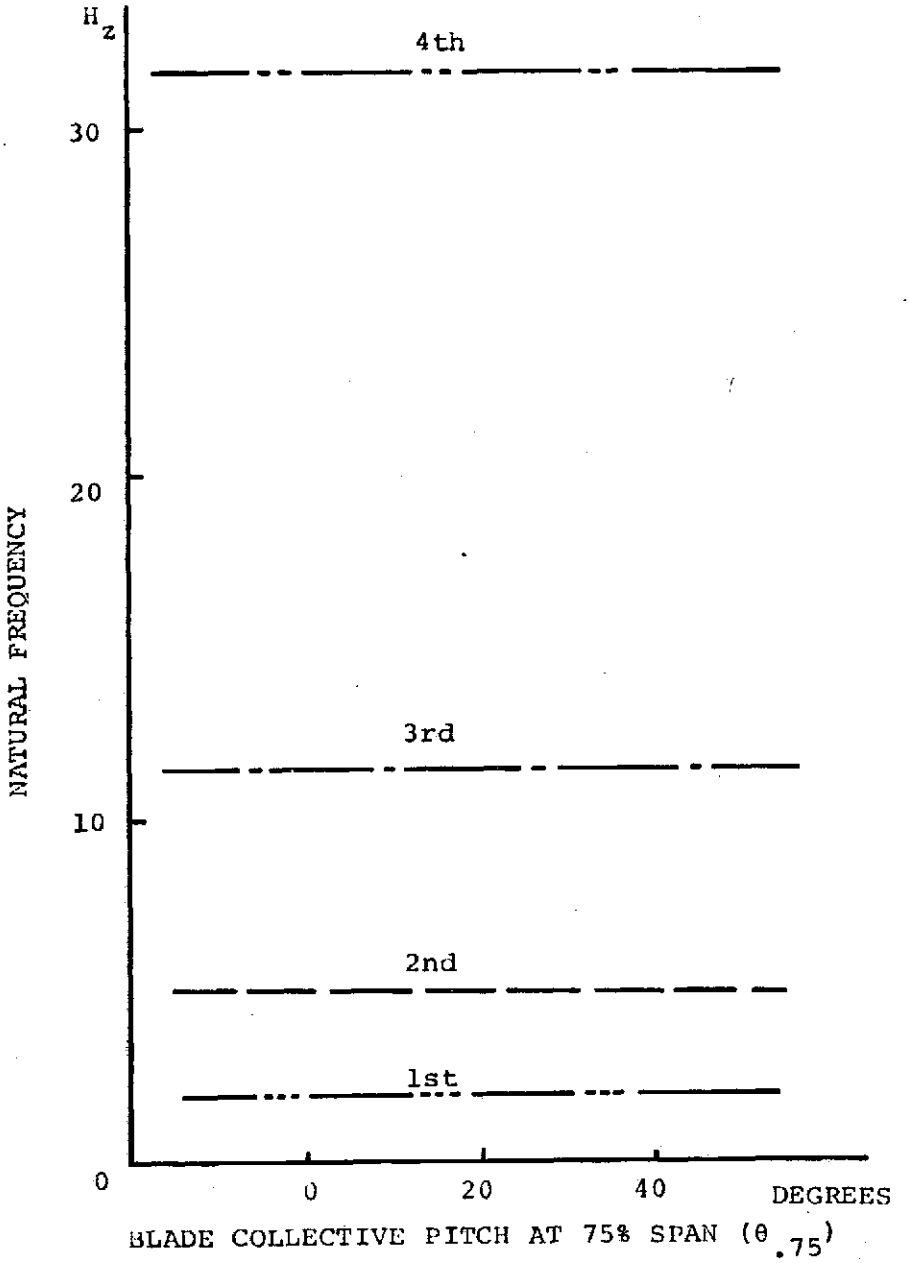

FIG. 9 BLADE NATURAL FREQUENCIES, NONROTATING, FOR BOEING ROTOR

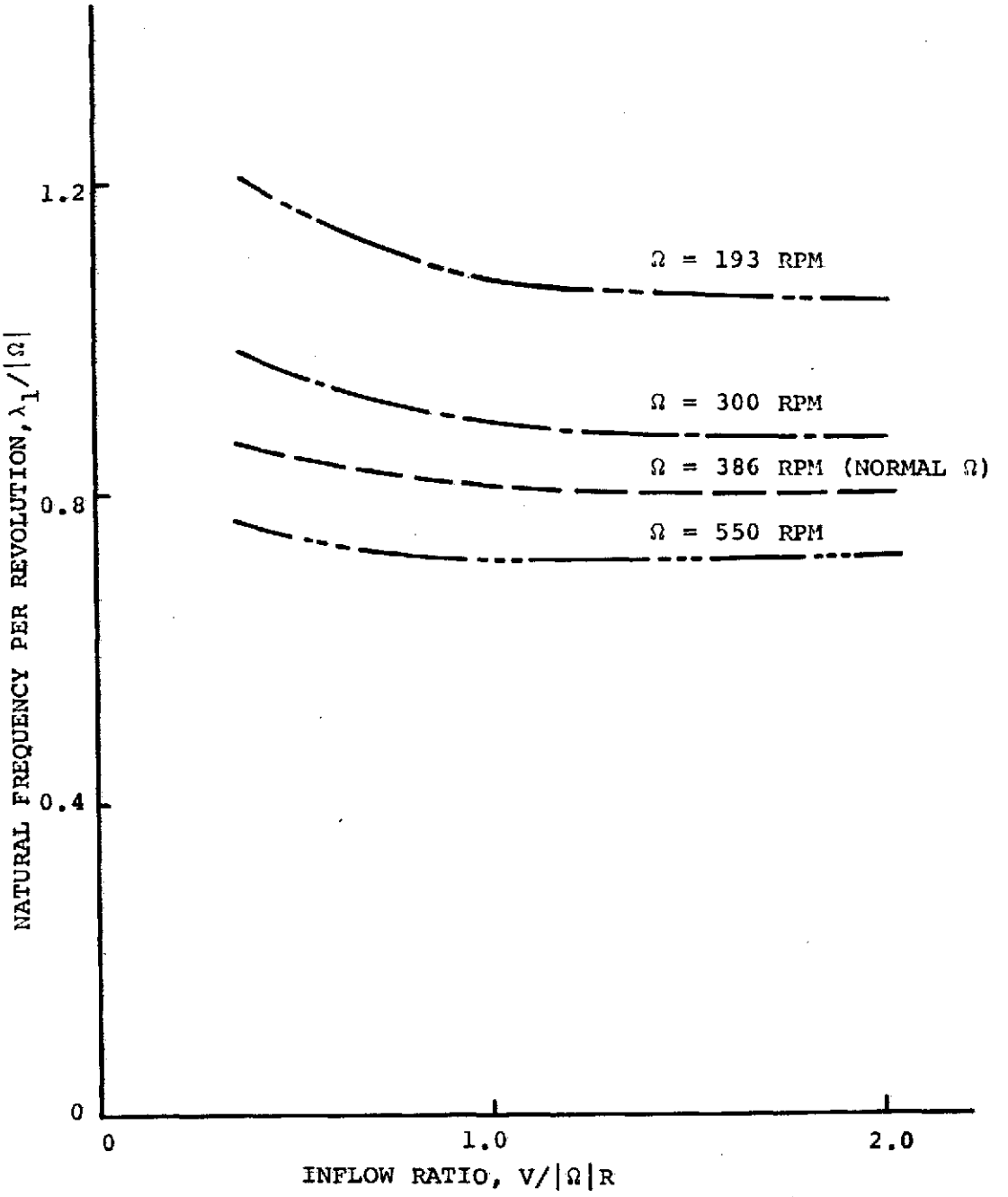

(a) 1st Natural Frequency

FIG. 10 BLADE ROTATING NATURAL FREQUENCIES FOR BOEING ROTOR

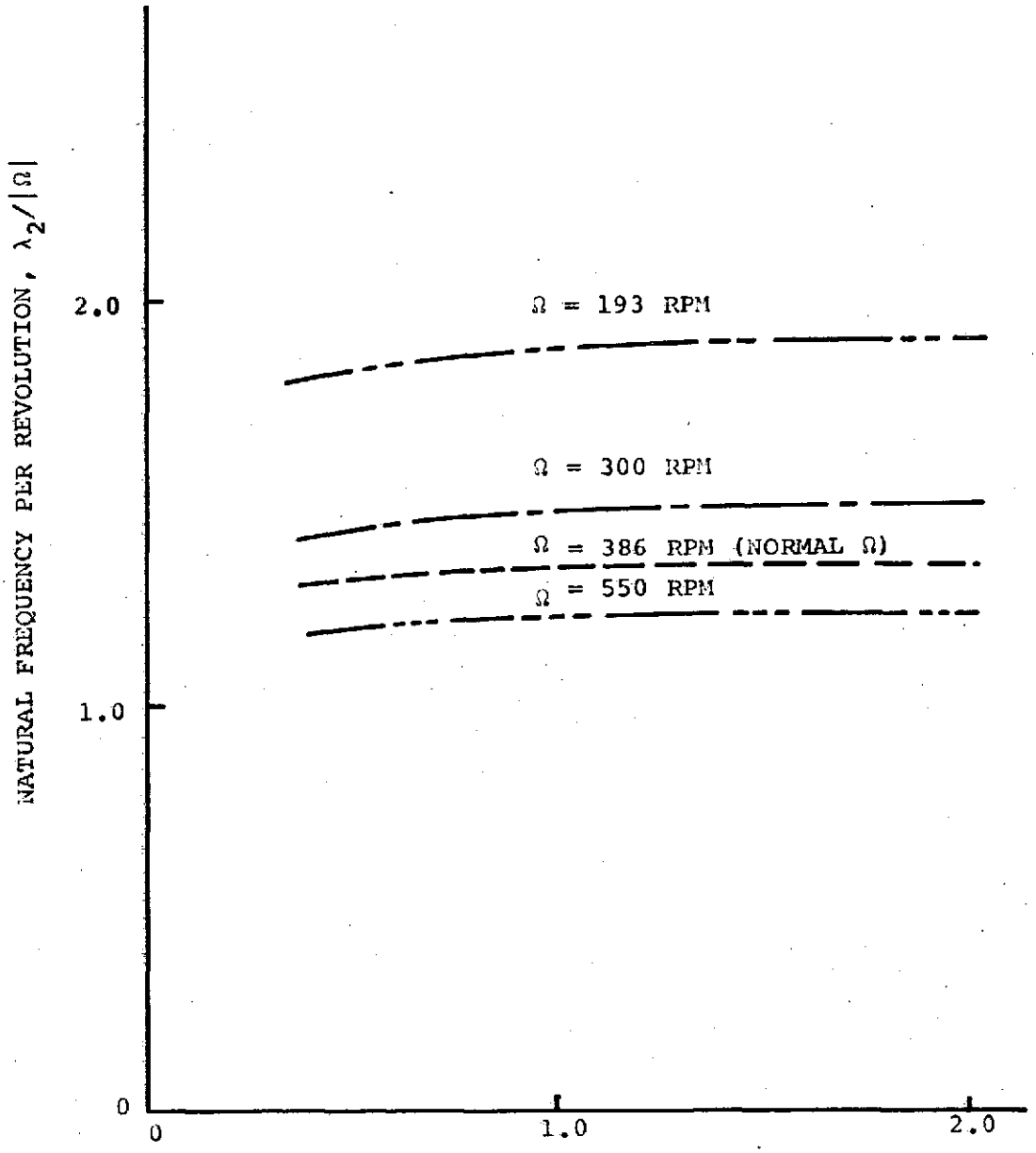

(b) 2nd Natural Frequency

FIG. 10 CONCLUDED

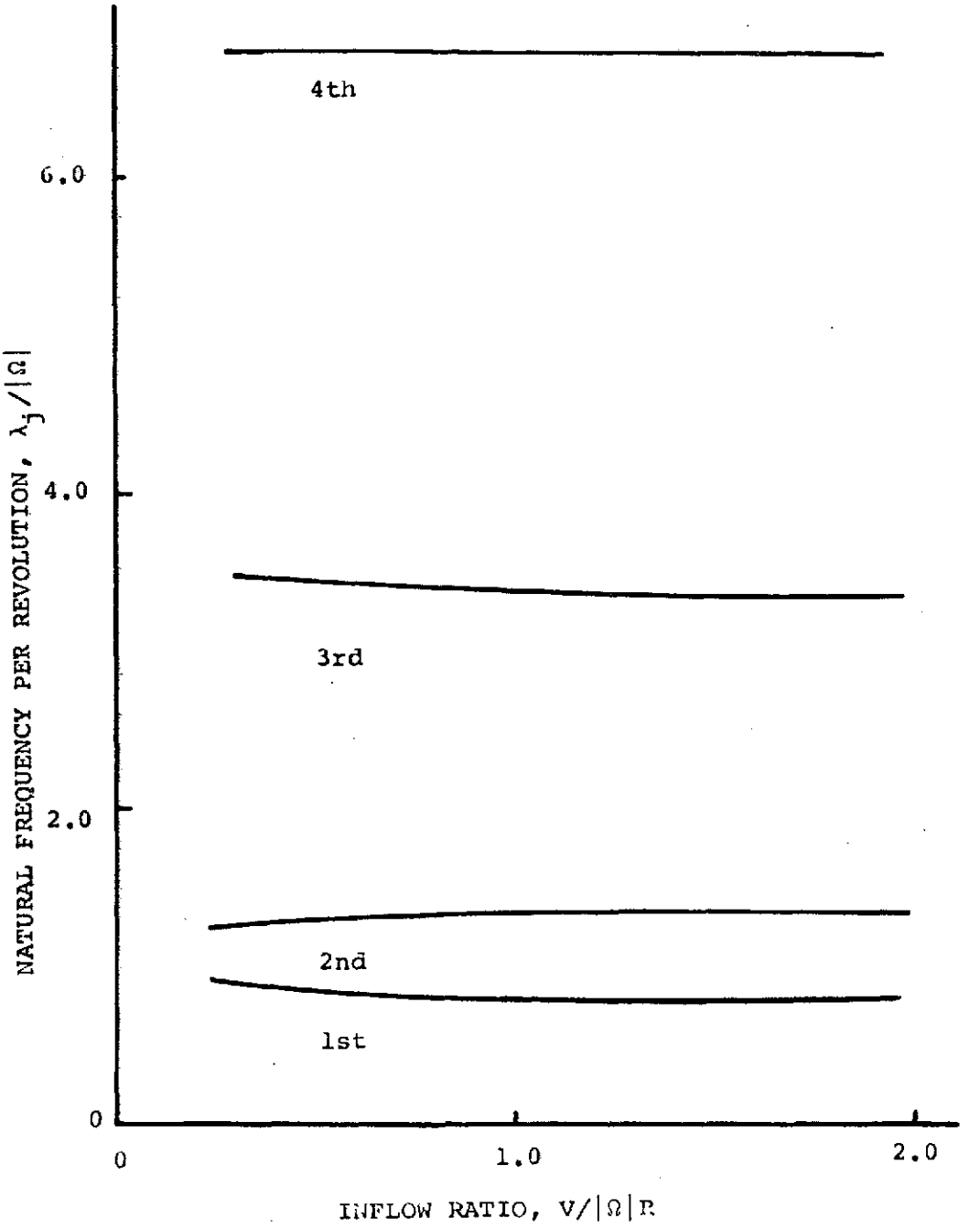

FIG. 11 BLADE NATURAL FREQUENCIES FOR BOEING ROTOR AT CONSTANT ROTATIONAL SPEED (Ω = 386 RPM)

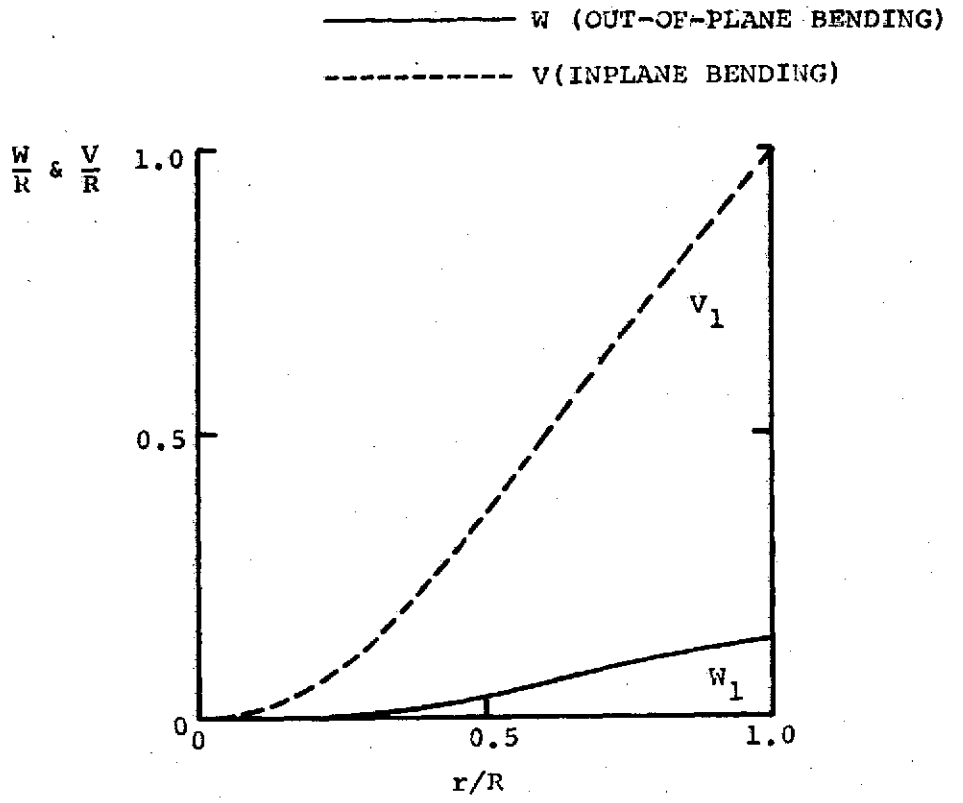

(a) First Mode (Frequency $\lambda_1/\Omega = 0.827$)

FIG. 12 MODE SHAPES FOR BOEING ROTOR AT $\lambda = 0.7$ AND $\Omega = 386$ RPH

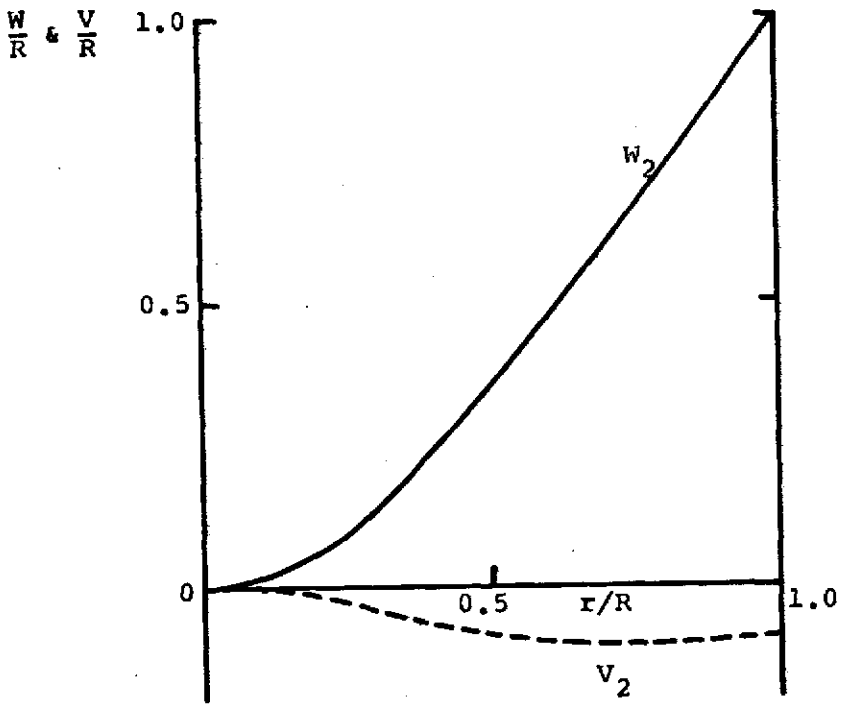

(b) Second Mode (Frequency $\lambda_2/\Omega = 1.32$)

FIG. 12 CONTINUED

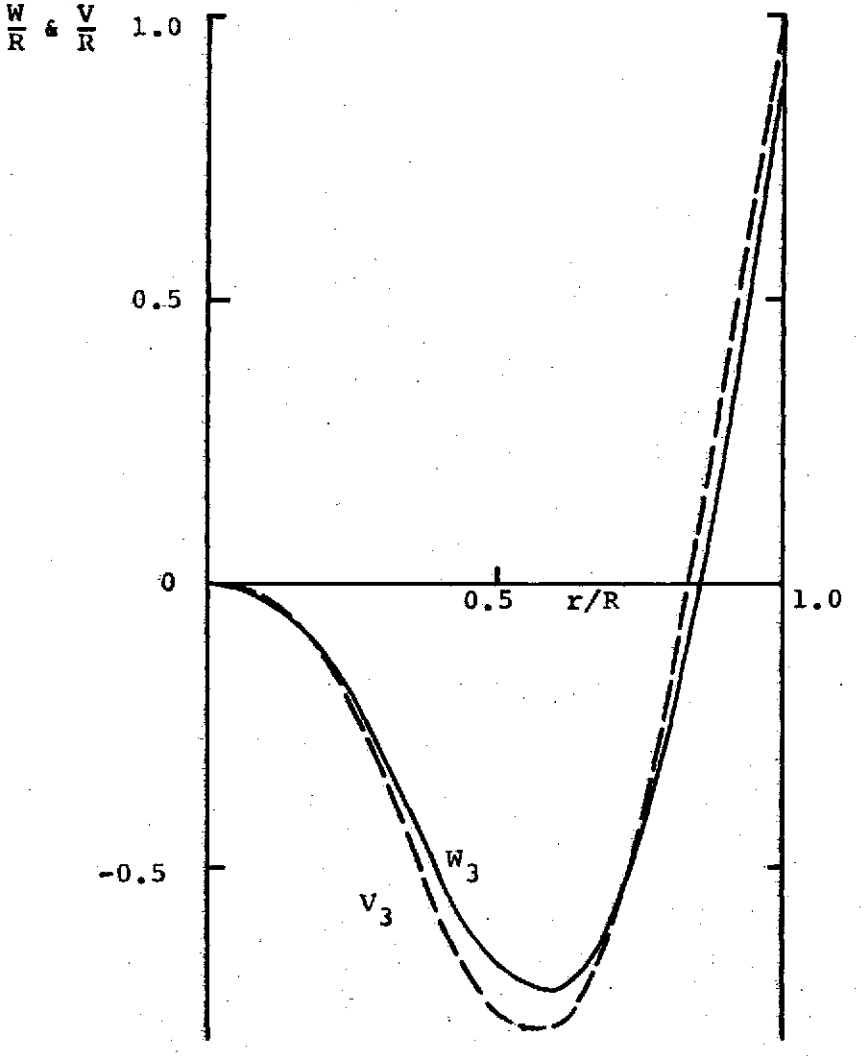

(c) Third Mode (Frequency $\lambda_3/\Omega = 3.40$)

FIG. 12 CONTINUED

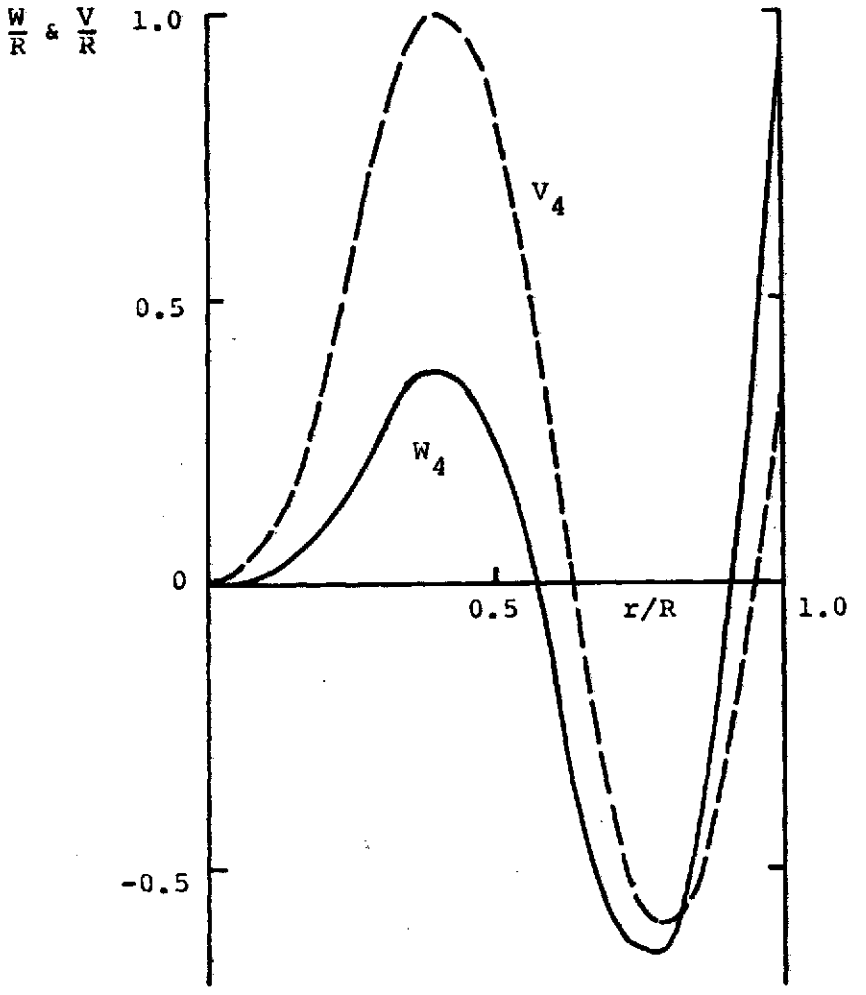

(d) Fourth Mode (Frequency λ_4/Ω = 6.77)

FIG. 12 CONCLUDED

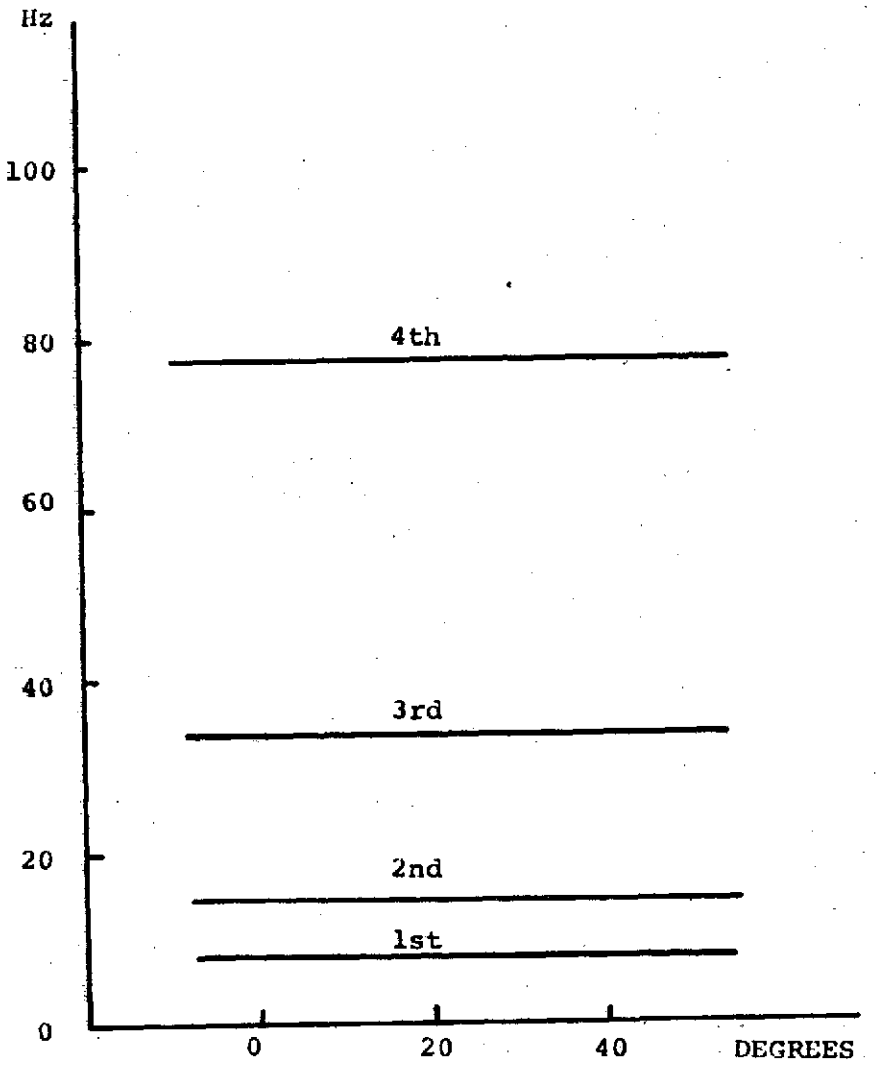

BLADE COLLECTIVE PITCH AT 75% SPAN ($\theta_{.75}$)

(a) Collective Mode

FIG. 13 BLADE NATURAL FREQUENCIES, NONROTATING, FOR BELL ROTOR

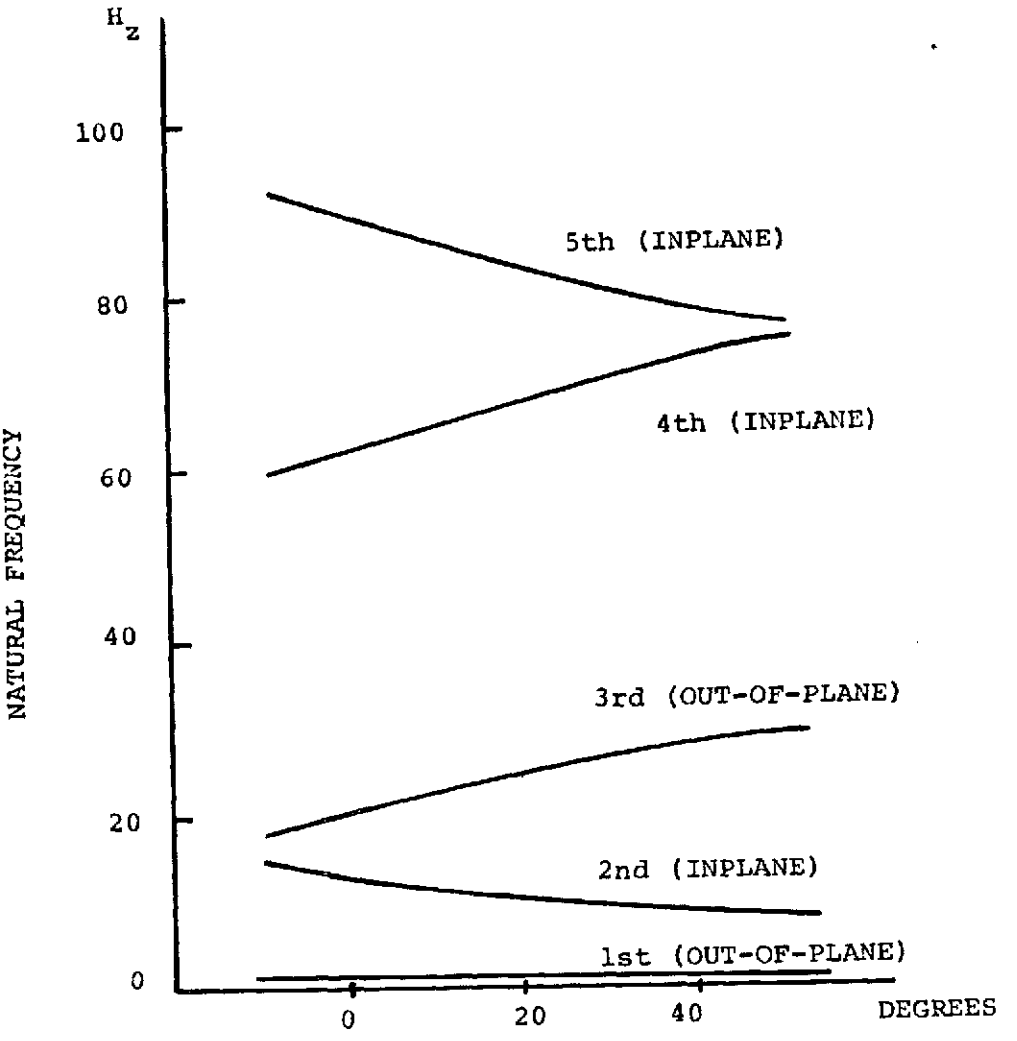

(b) Cyclic Mode

FIG. 13 CONCLUDED

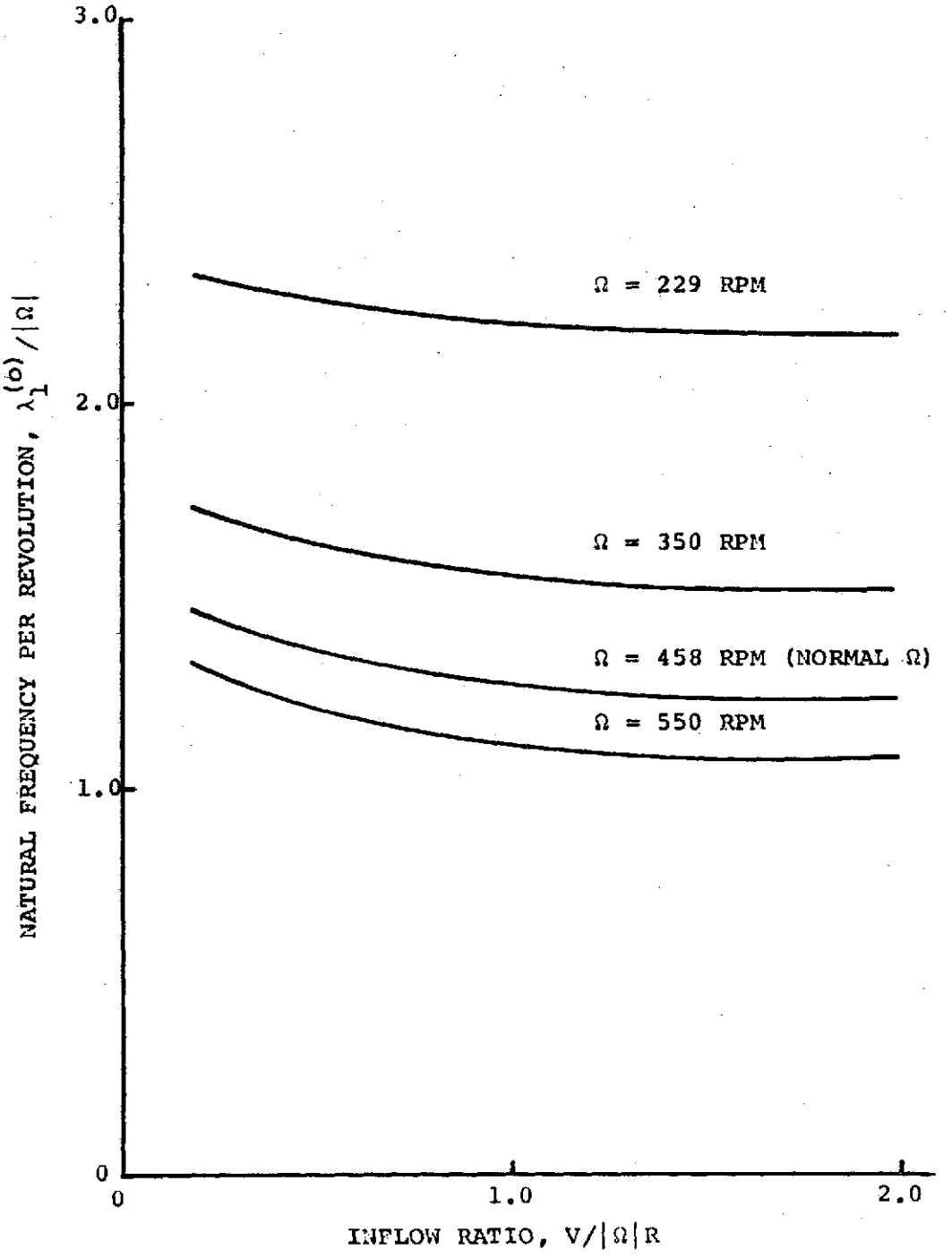

(a) First Collective Mode

FIG. 14 BLADE ROTATING NATURAL FREQUENCIES FOR BELL ROTOR

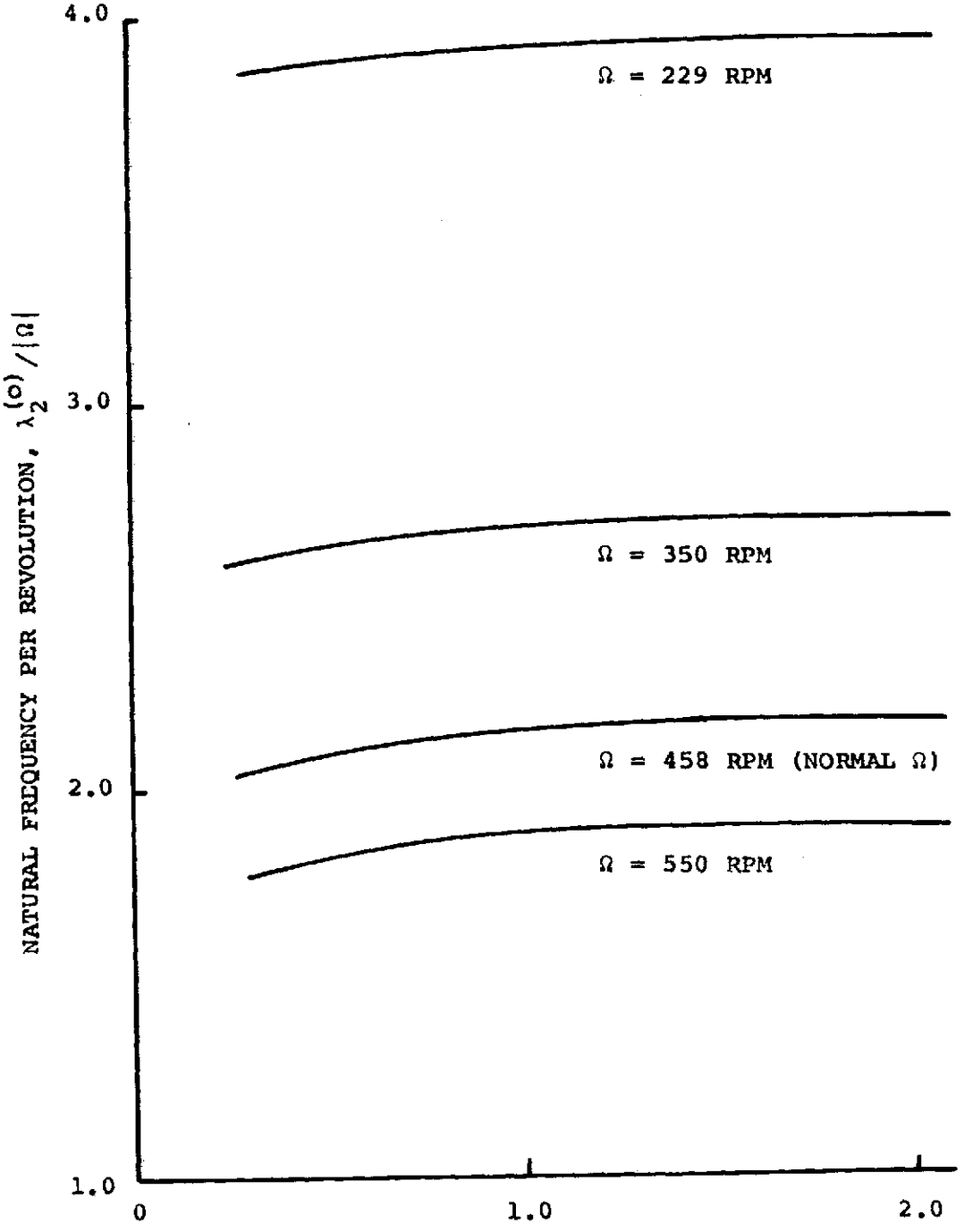

(b) Second Collective Mode

FIG. 14 CONTINUED

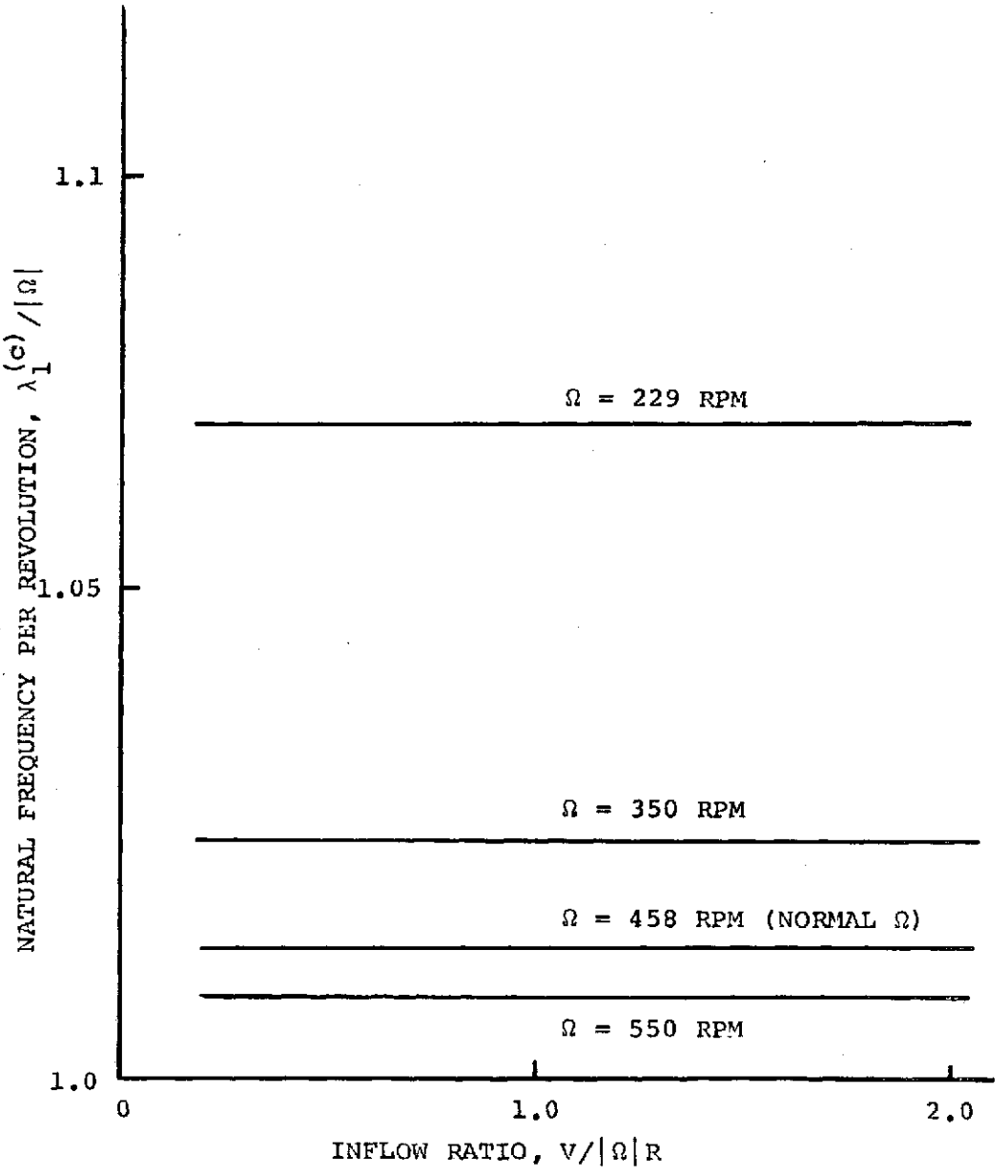

(c) First Cyclic Mode (Out-of-Plane Mode)

FIG. 14 CONTINUED

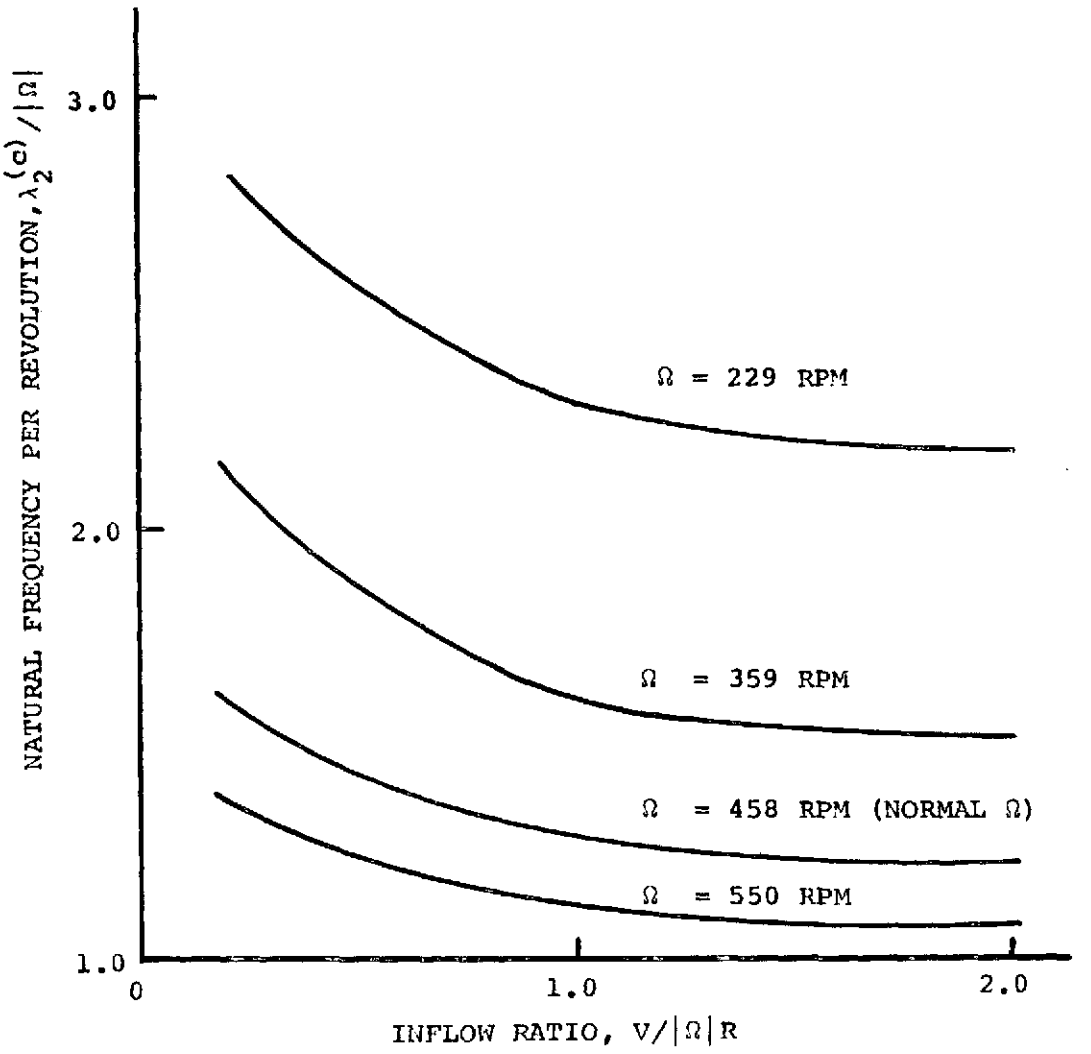

(d) Second Cyclic Mode (Inplane Mode)

FIG. 14 CONCLUDED

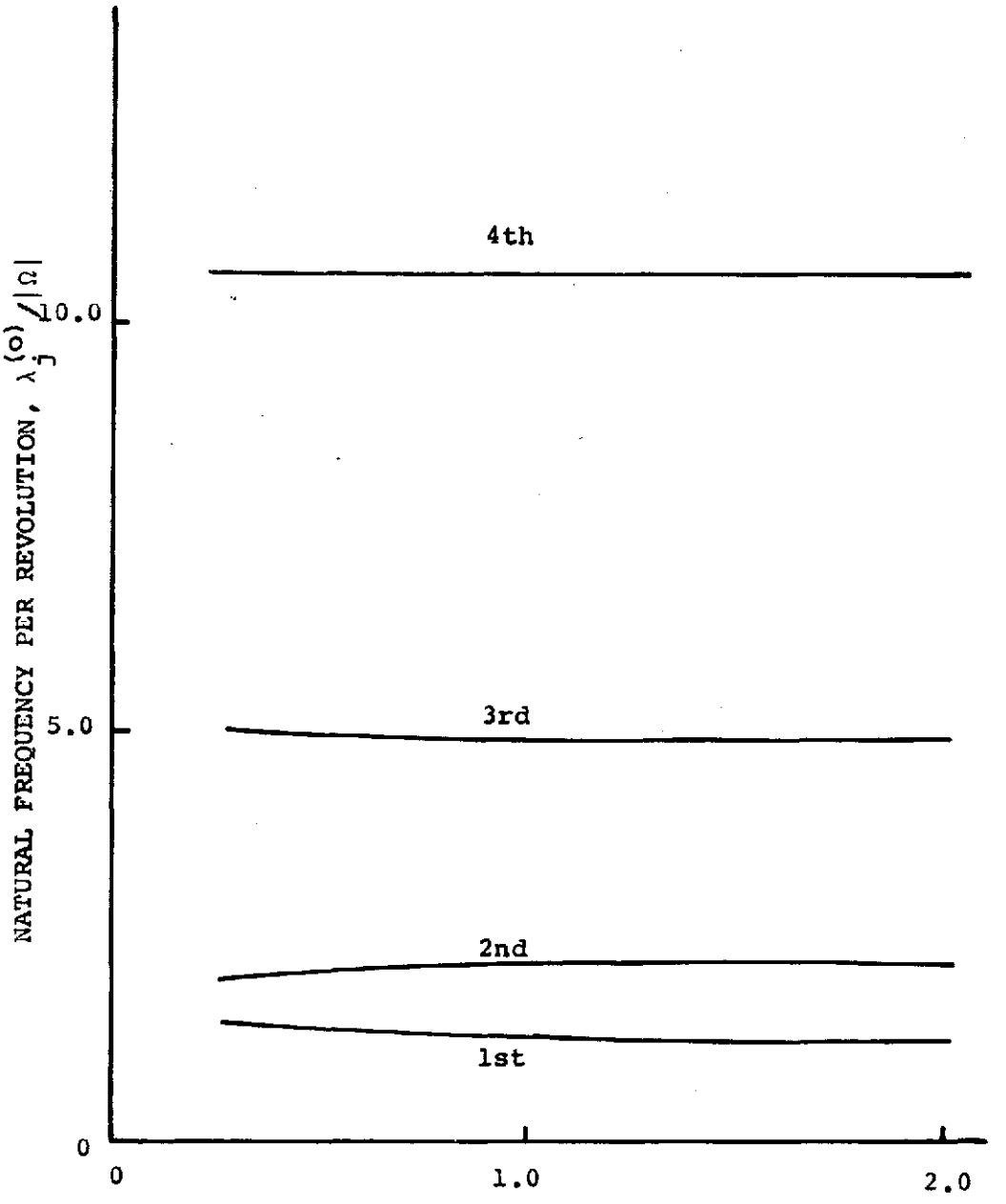

(a) Collective Modes

FIG. 15 BLADE NATURAL FREQUENCIES FOR BELL ROTOR AT CONSTANT ROTATIONAL SPEED (Ω = 458 RPM)

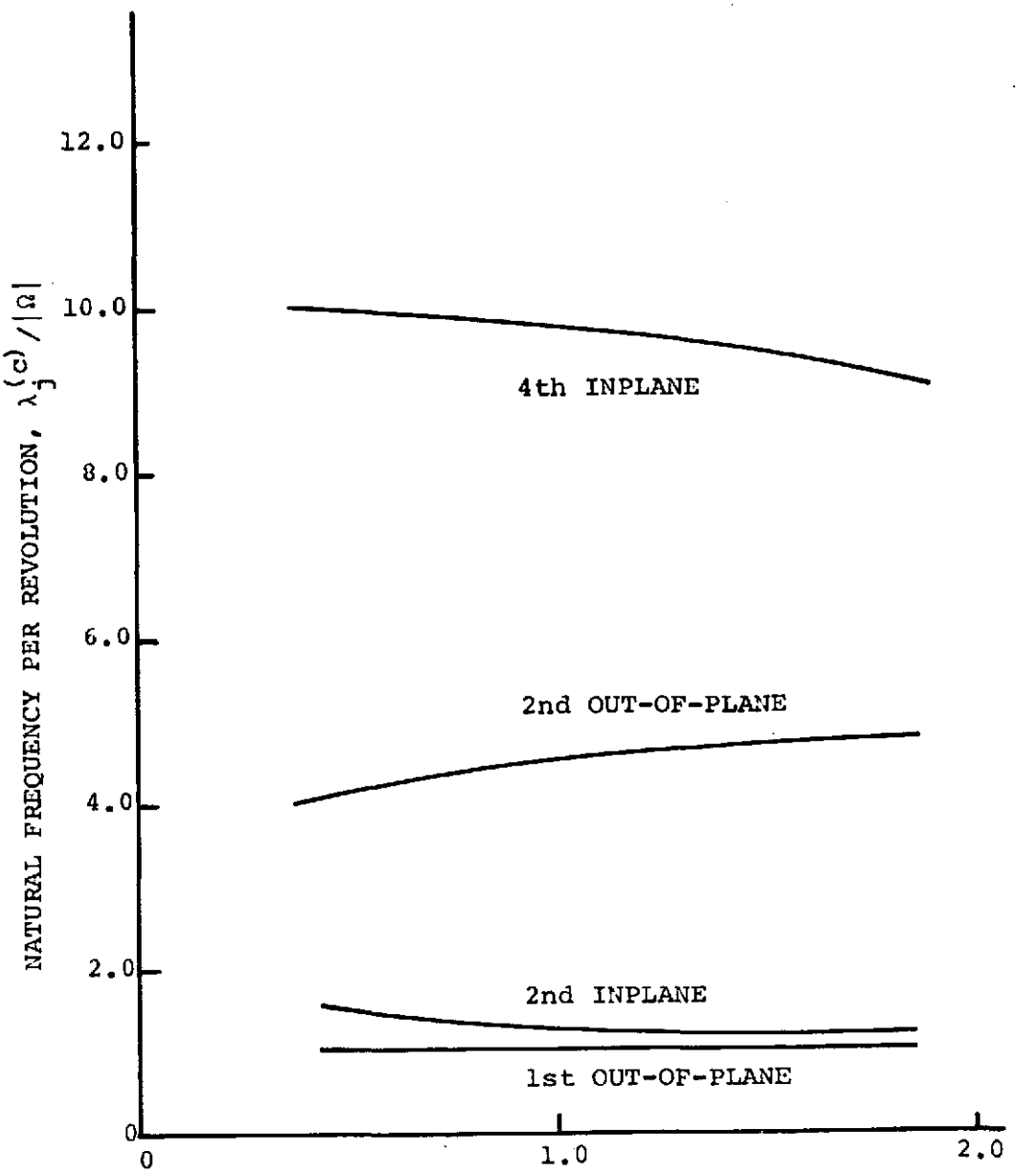

(b) Cyclic Modes

FIG. 15 CONCLUDED

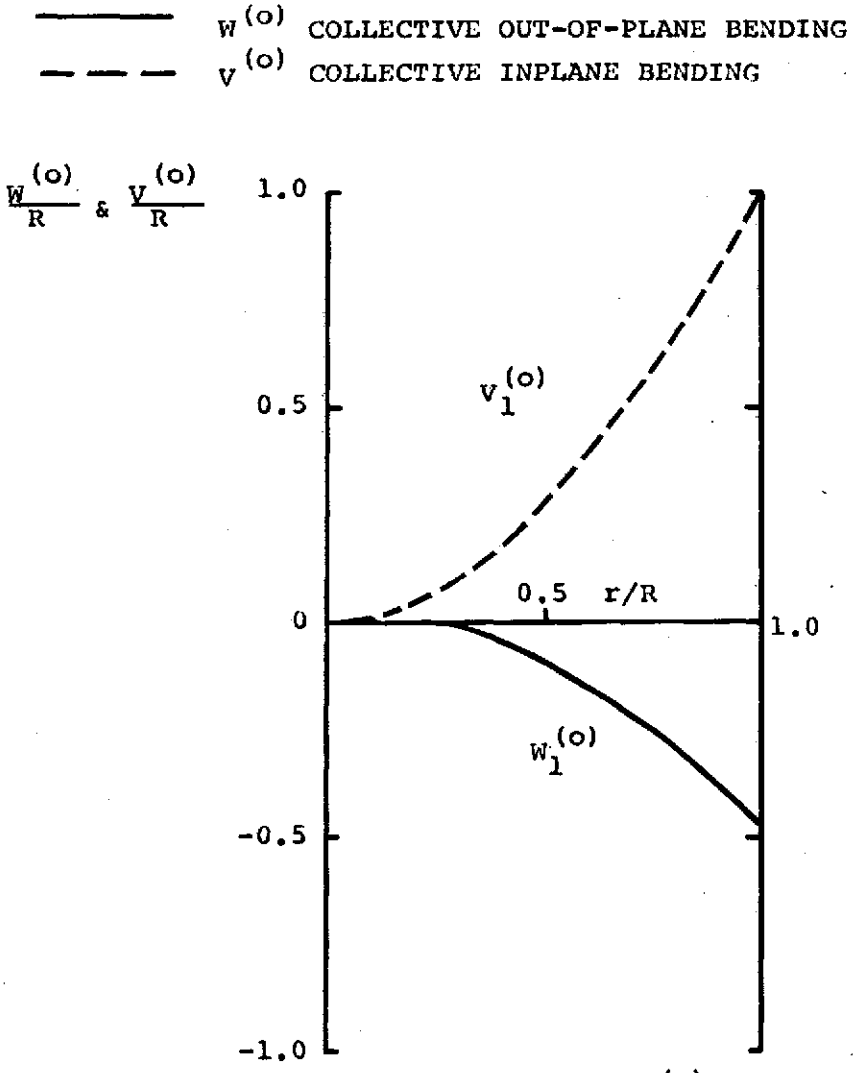

(a) First Mode (Frequency $\lambda_1^{(o)}/|\Omega| = 1.31$)

FIG. 16 COLLECTIVE MODE SHAPES FOR BELL ROTOR AT $\lambda = 0.7$ AND $\Omega = 458$ RPM

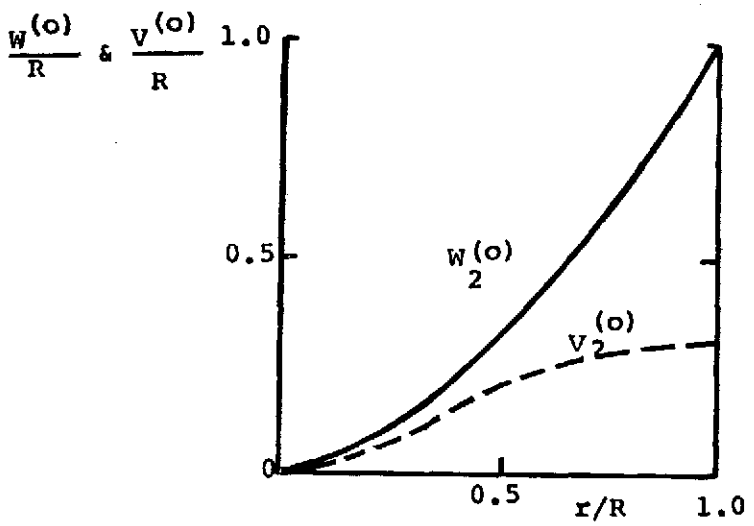

(b) Second Mode (Frequency $\lambda_2^{(o)}/|\Omega| = 2.12$)

FIG. 16 CONTINUED

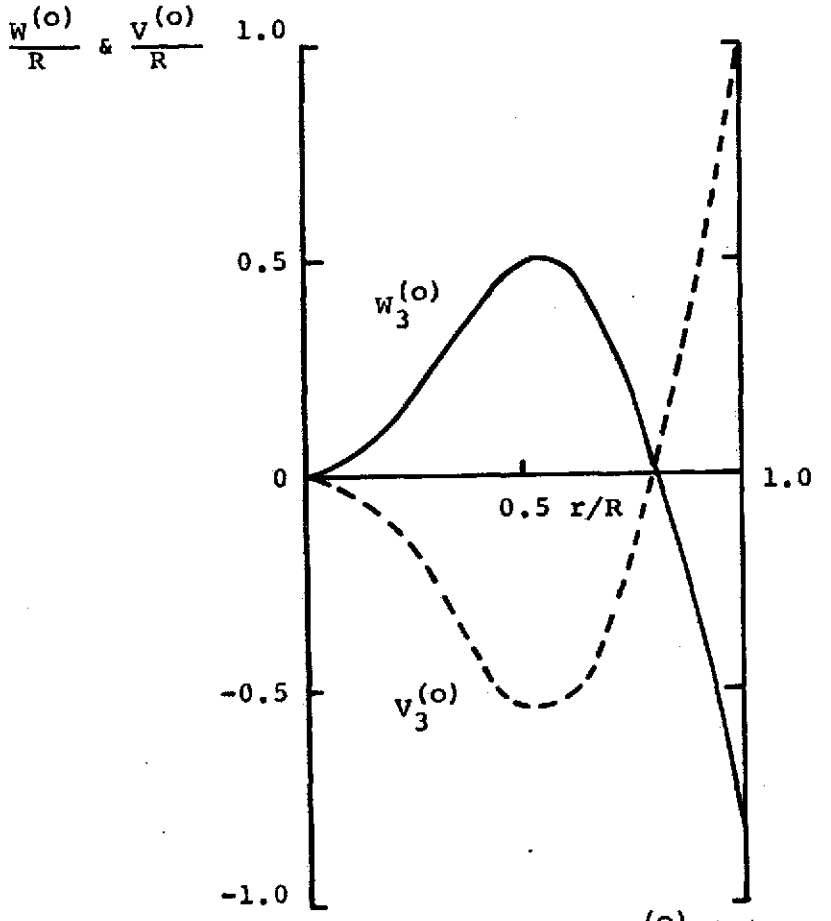

(c) Third Mode (Frequency $\lambda_3^{(o)}/|\Omega| = 4.93$)

FIG. 16 CONTINUED

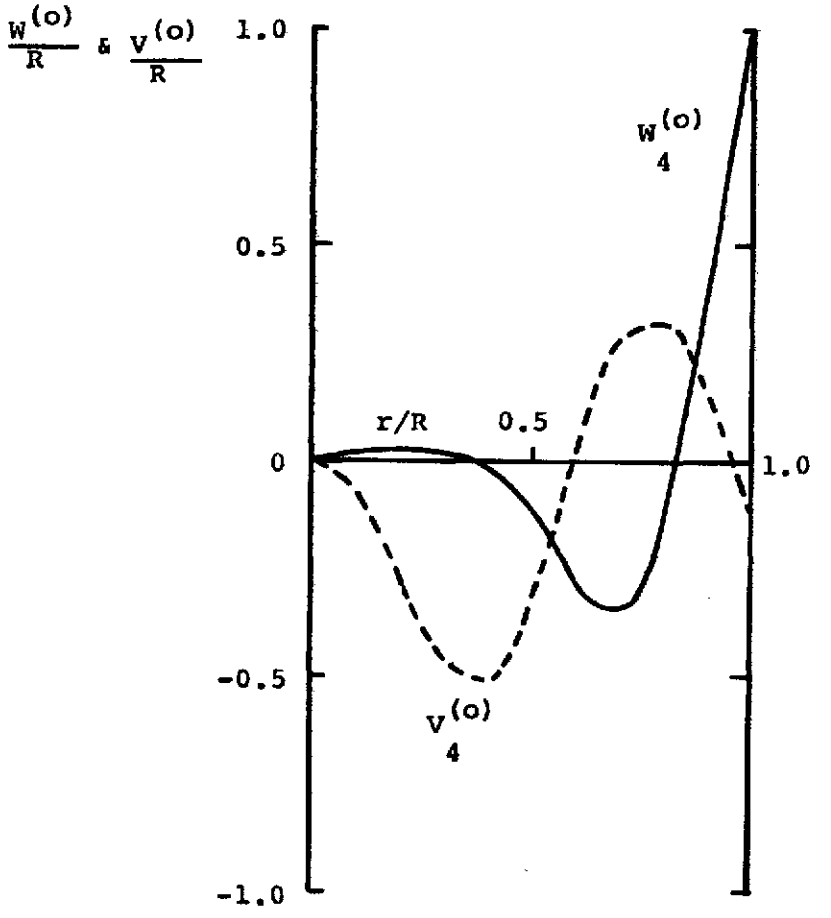

(d) Fourth Mode (Frequency $\lambda_4^{(o)}/|\Omega| = 10.6$)

FIG. 16 CONCLUDED

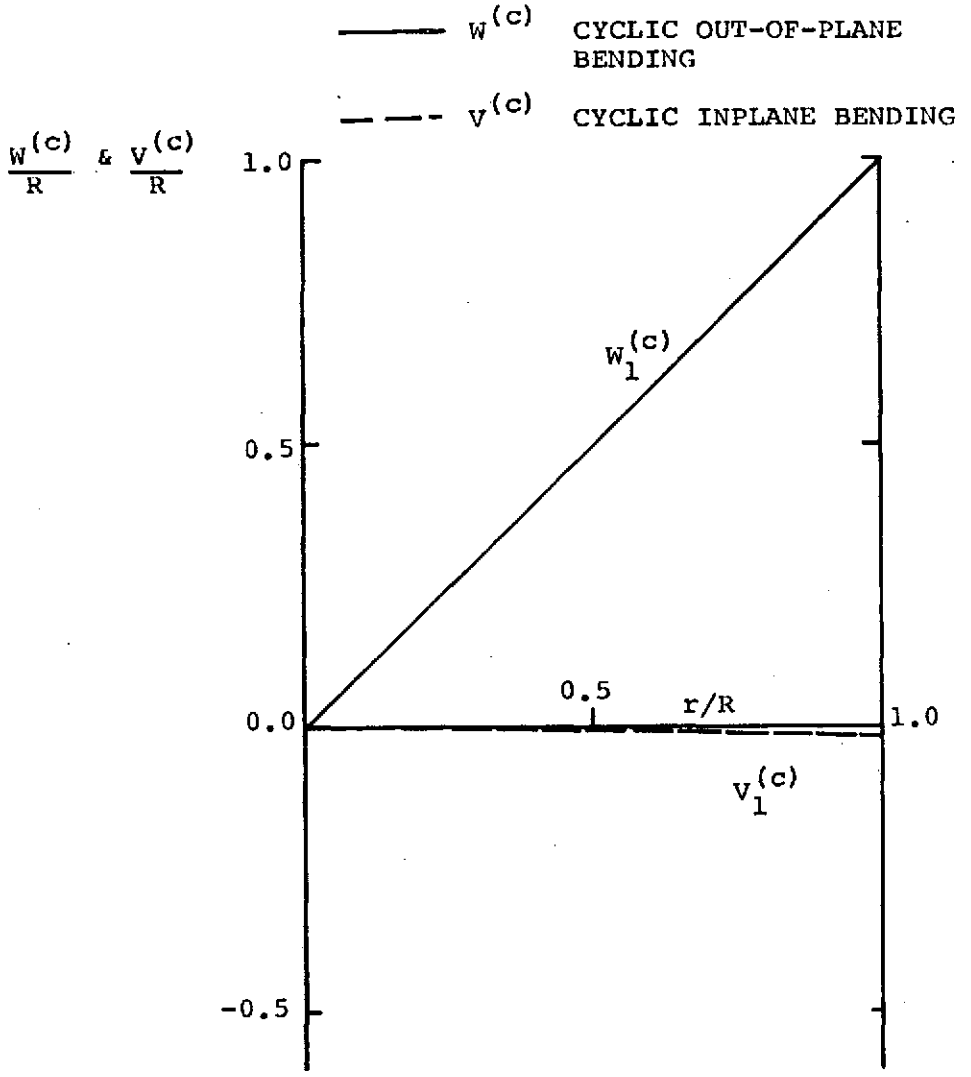

(a) First Mode (Frequency $\lambda_1^{(c)}/|\Omega|$ = 1.016)

FIG. 17 CYCLIC MODE SHAPES FOR BELL ROTOR AT λ = 0.7 AND Ω = 458 RPM

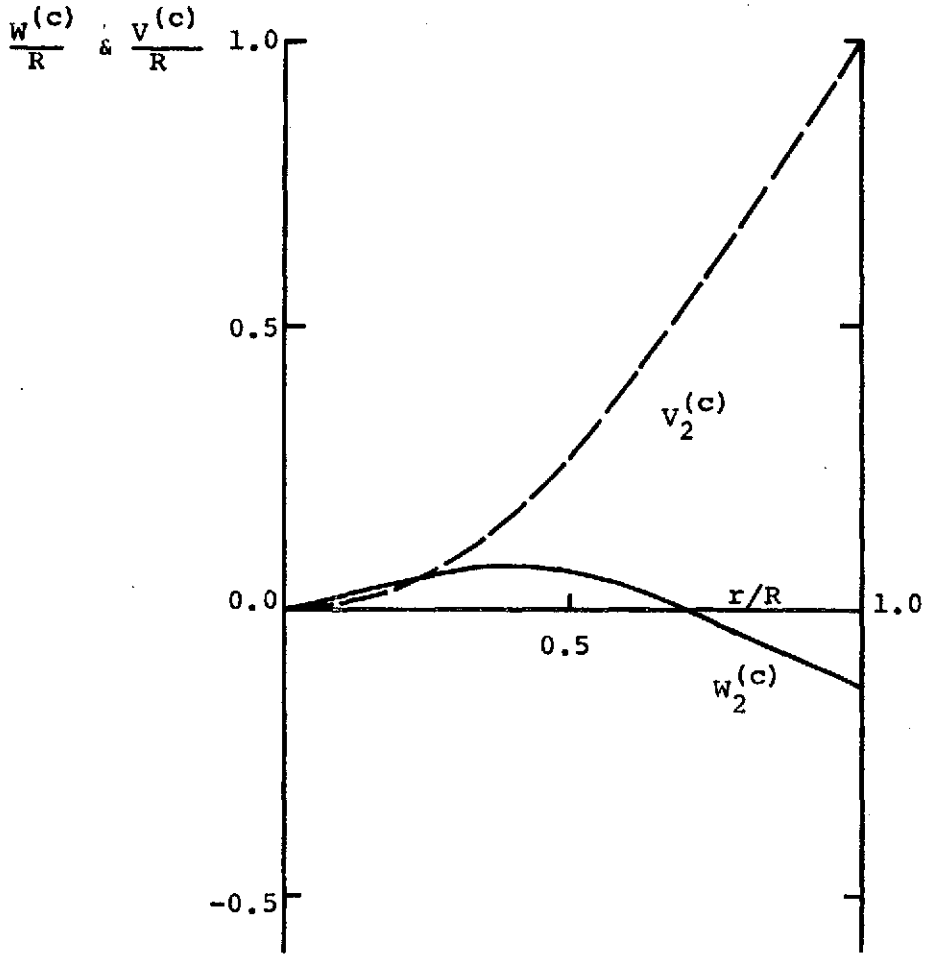

(b) Second Mode (Frequency $\lambda_2^{(c)}/|\Omega| = 1.34$)

FIG. 17 CONTINUED

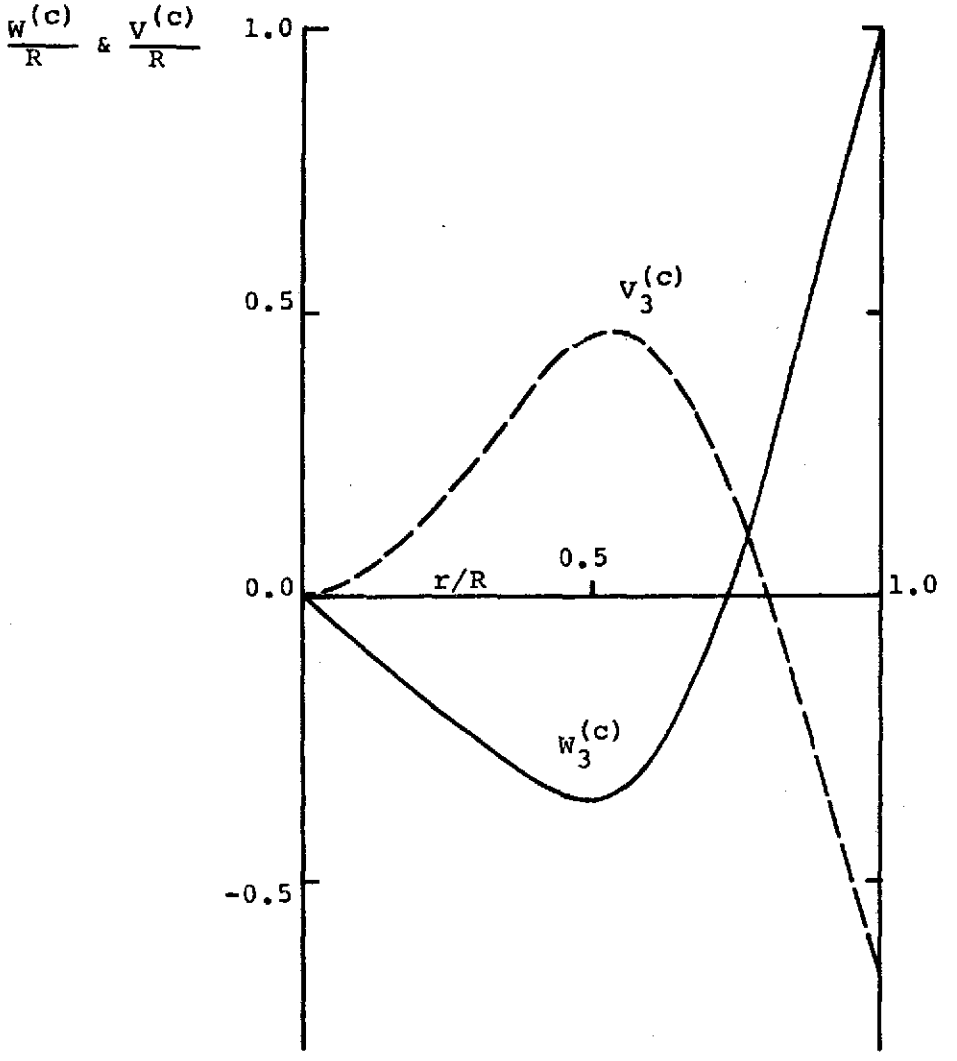

(c) Third Mode (Frequency $\lambda_3^{(c)}/|\Omega| = 4.35$)

FIG. 17 CONTINUED

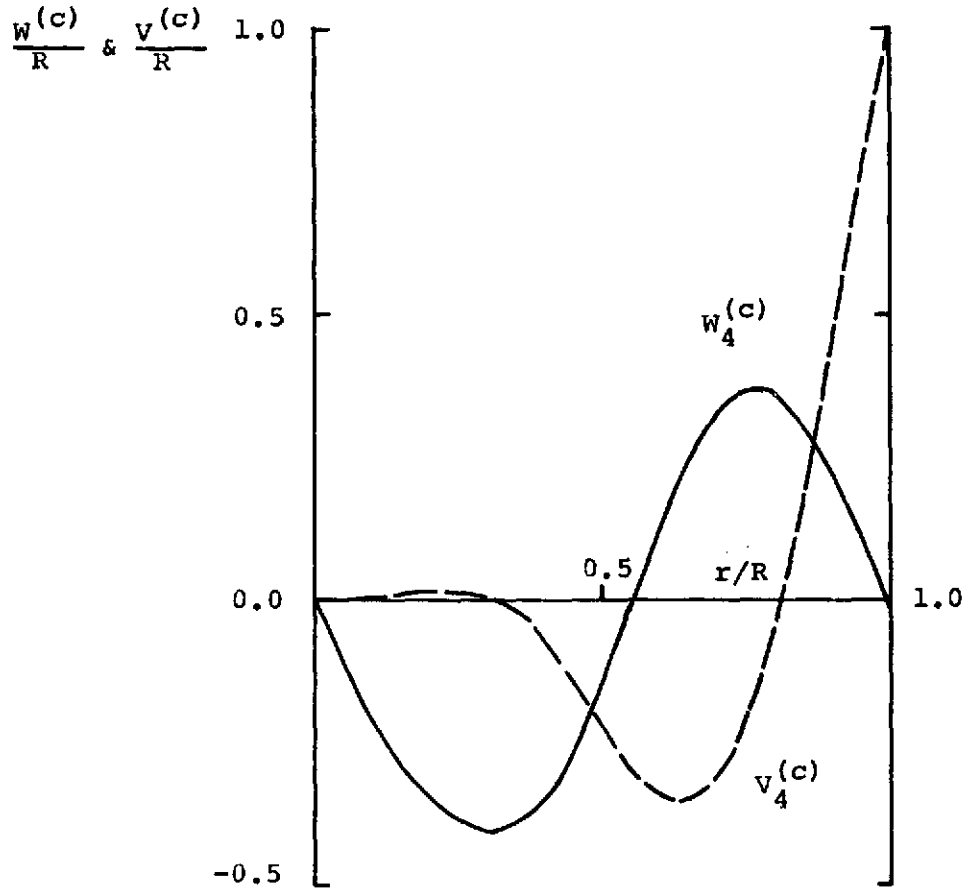

(d) Fourth Mode (Frequency $\lambda_4^{(c)}/|\Omega| = 10.1$)

FIG. 17 CONCLUDED

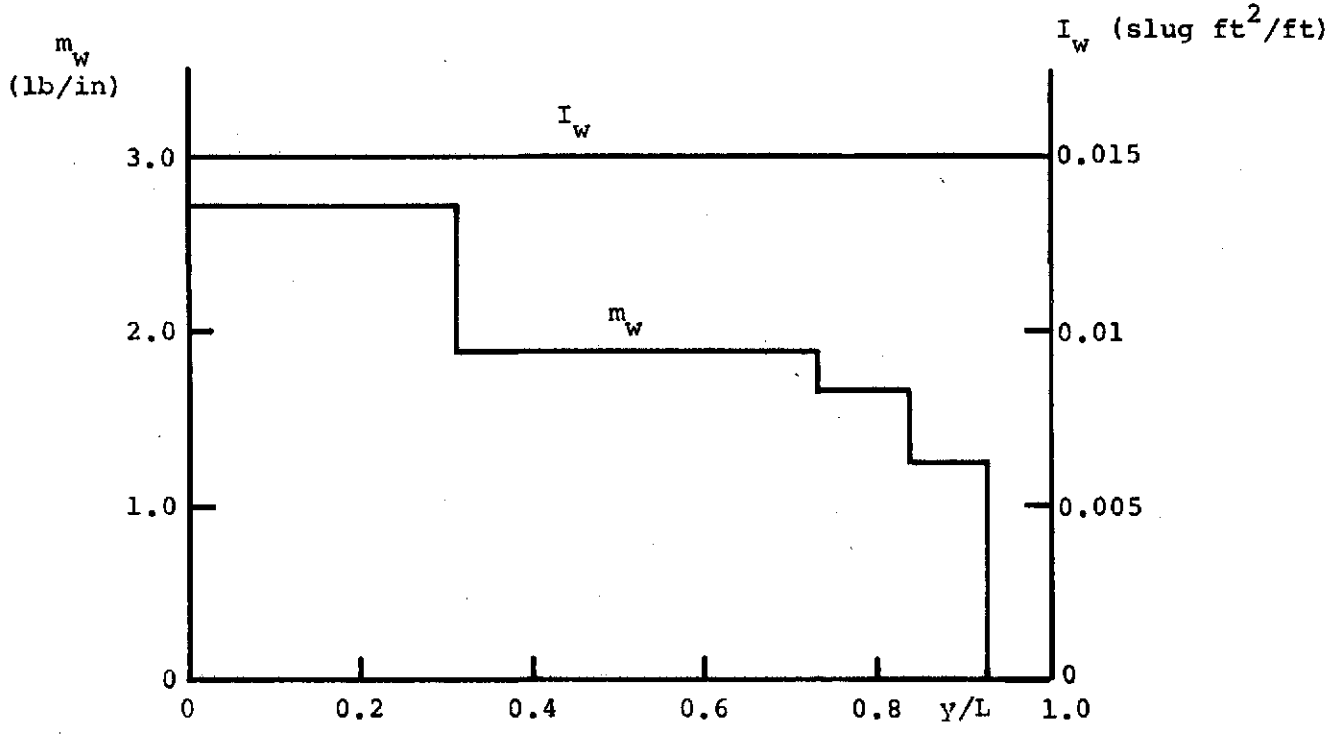

(a) Mass and Cross-Sectional Moment of Inertia Distribution

FIG. 18 STRUCTURAL CHARACTERISTICS OF THE WING (THE SAME WING IS USED BY BOTH BELL AND BOEING)

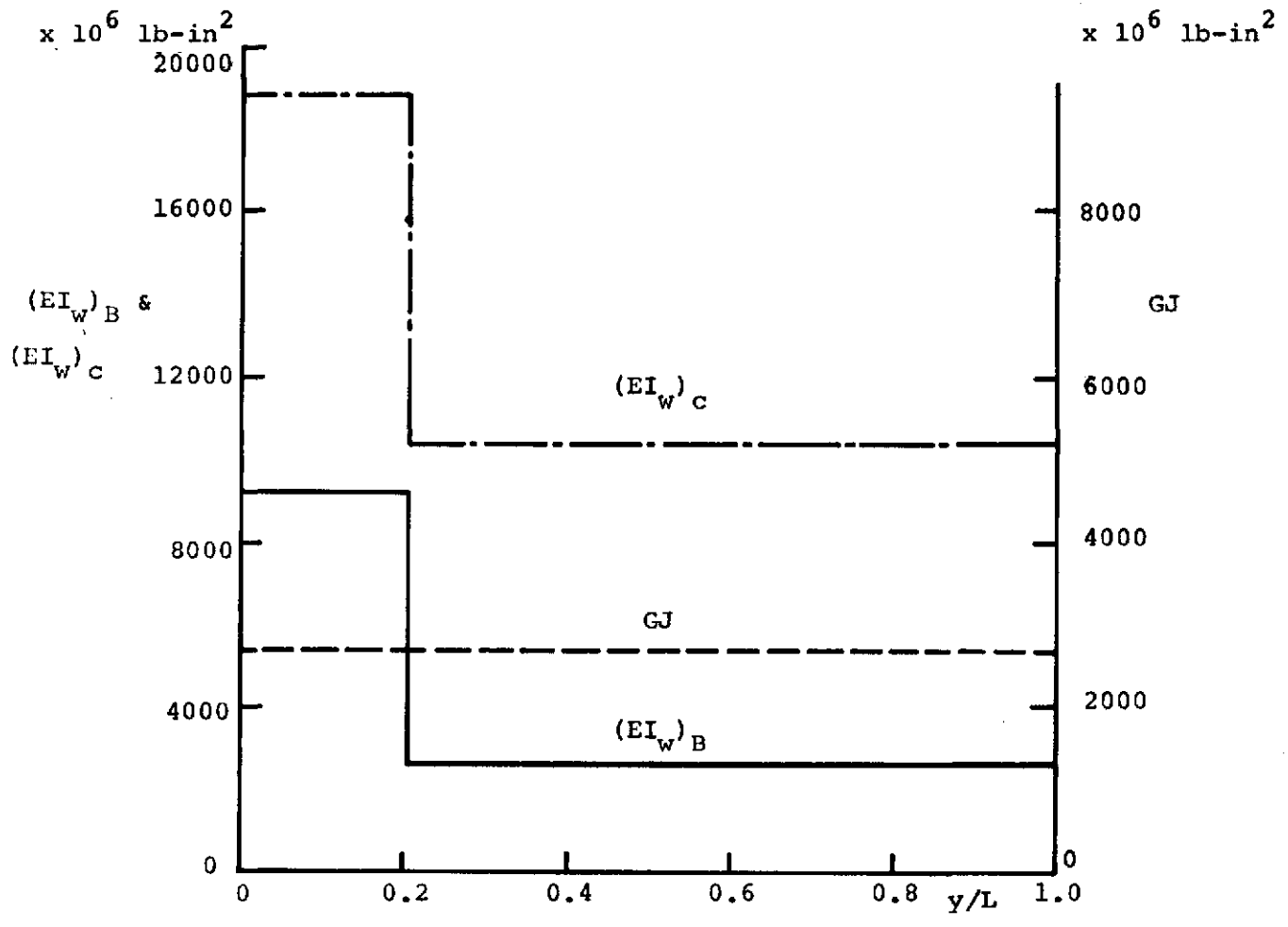

(b) Stiffness Distribution: Vertical Bending Stiffness $(EI_w)_B$, Chordwise Bending Stiffness $(EI_w)_C$, and Torsional Rigidity GJ

FIG. 18 CONCLUDED

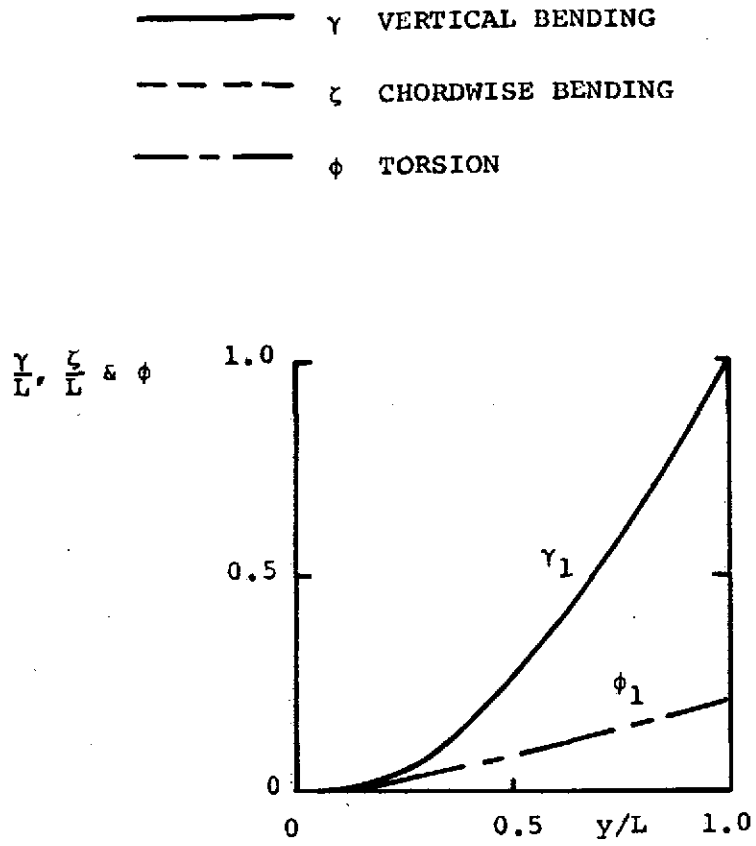

(a) First Mode (2.35 Hz)

FIG. 19 MODE SHAPES FOR BOEING WING

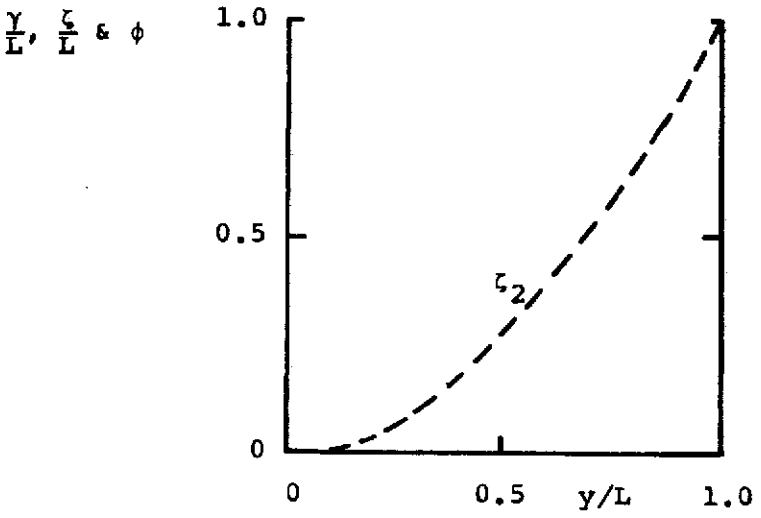

(b) Second Mode (4.18 Hz)

FIG. 19 CONTINUED

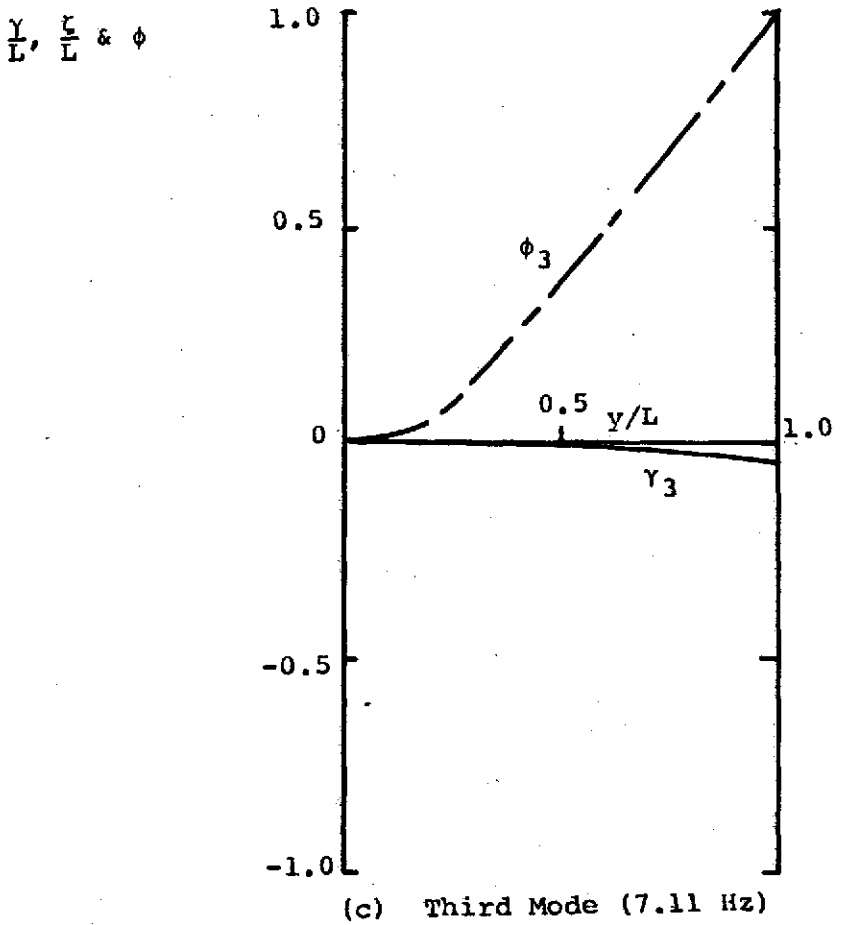

(c) Third Mode (7.11 Hz)

FIG. 19 CONTINUED

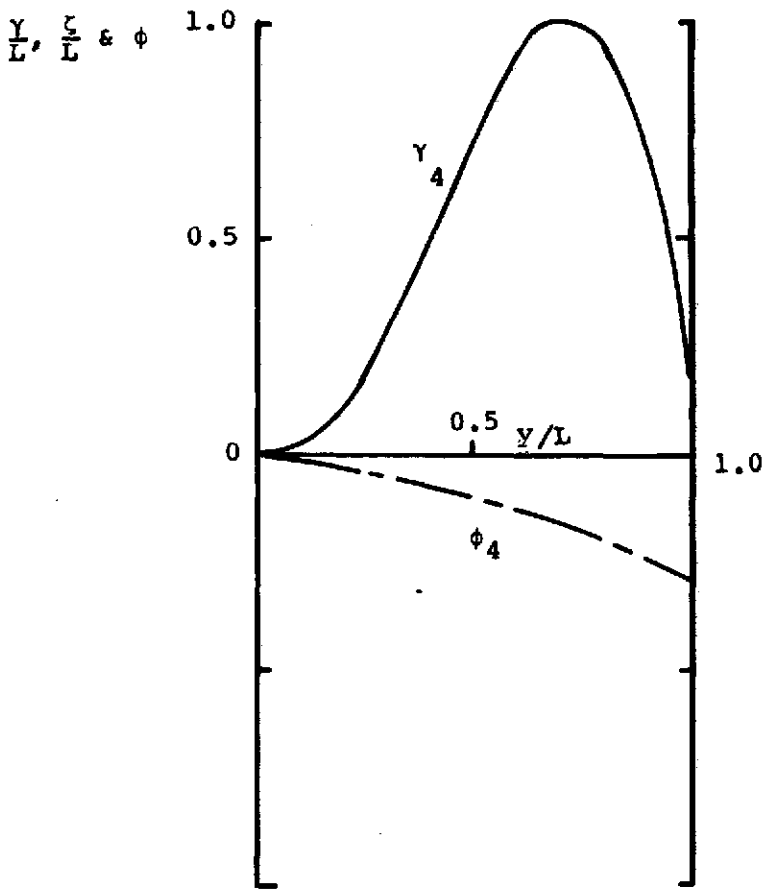

(d) Fourth Mode (15.9 Hz)

FIG. 19 CONTINUED

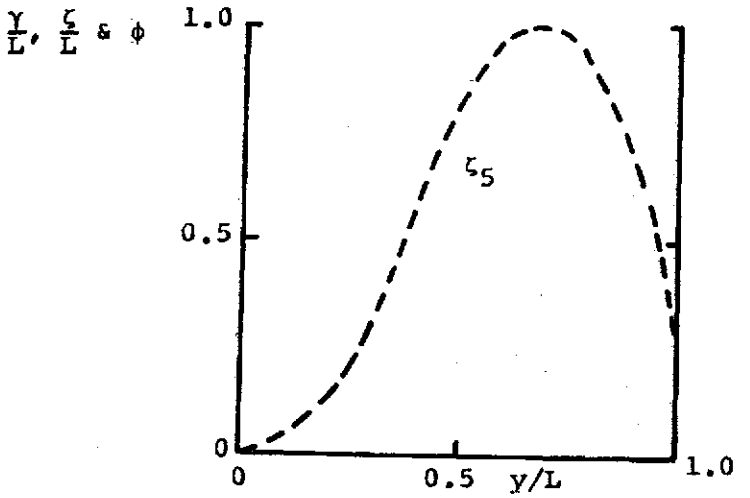

(e) Fifth Mode (25.4 Hz)

FIG. 19 CONTINUED

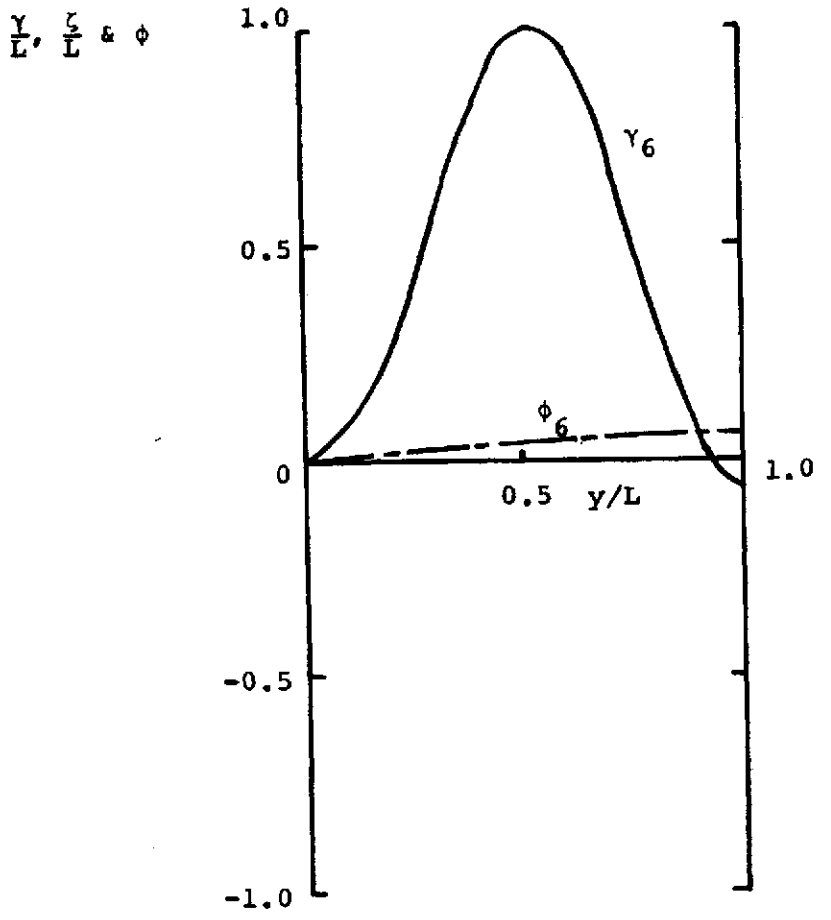

(f) Sixth Mode (89.5 Hz)

FIG. 19 CONCLUDED

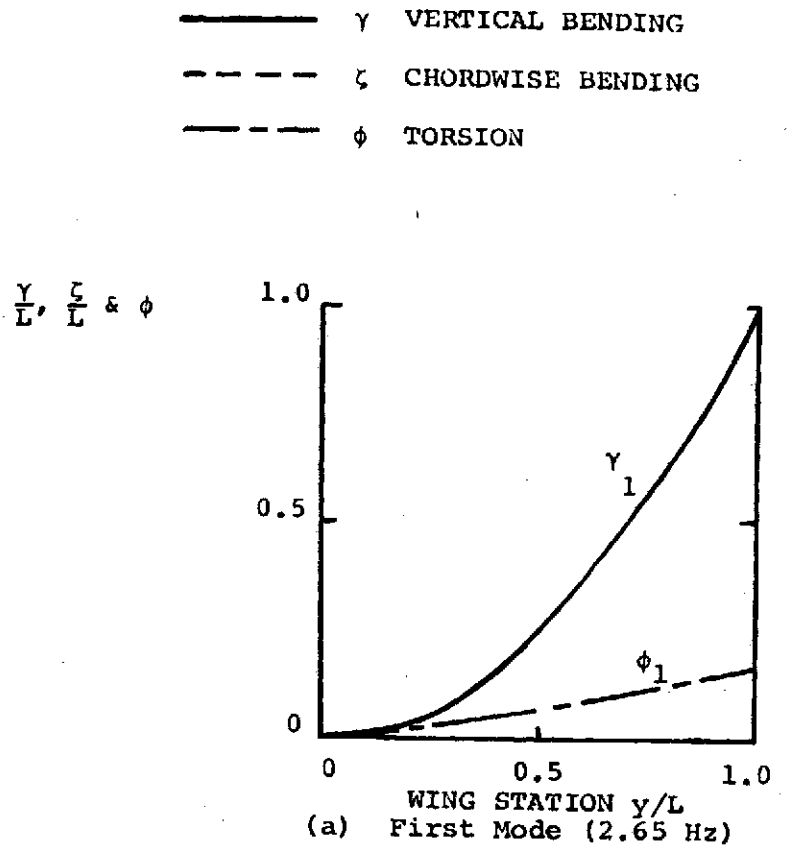

(a) First Mode (2.65 Hz)

FIG. 20 MODE SHAPES FOR BELL WING

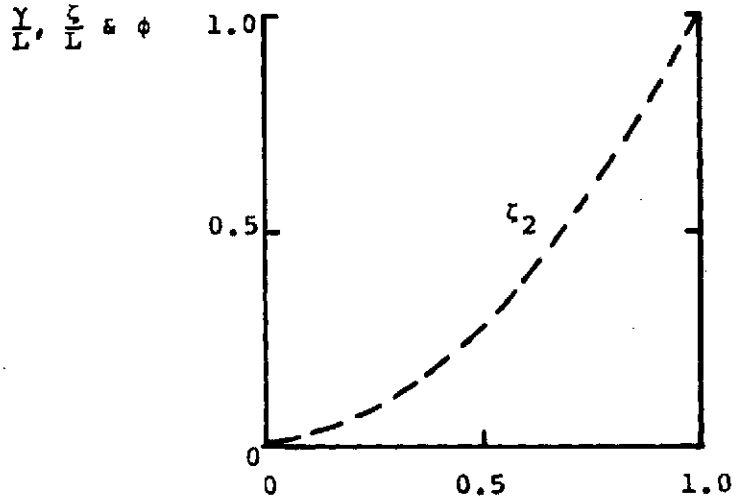

(b) Second Mode (4.72 Hz)

FIG. 20 CONTINUED

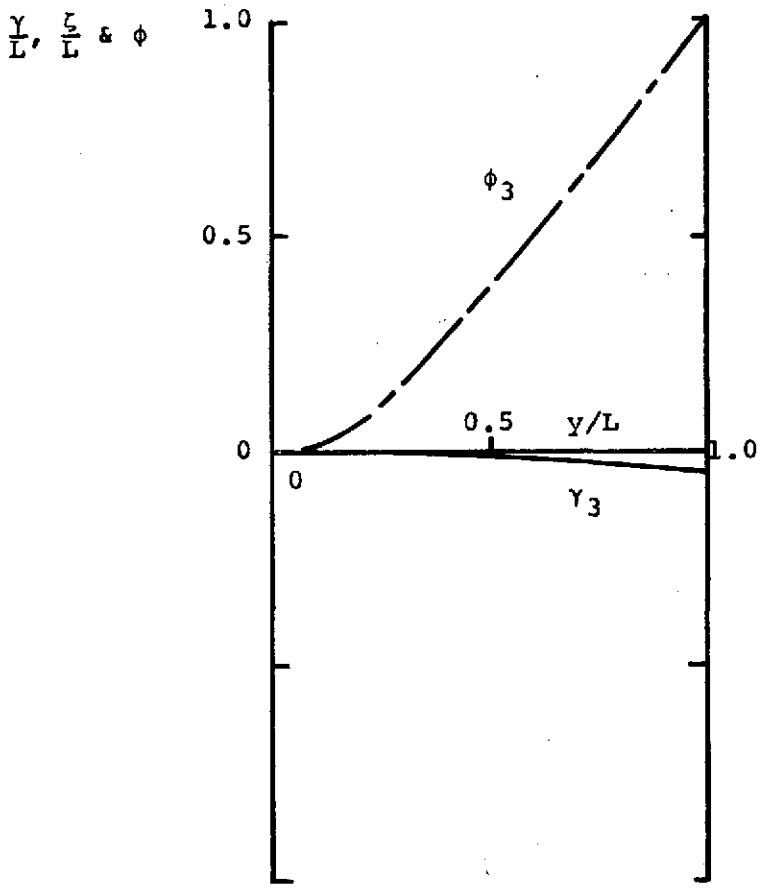

(c) Third Mode (8.3 Hz)

FIG. 20 CONTINUED

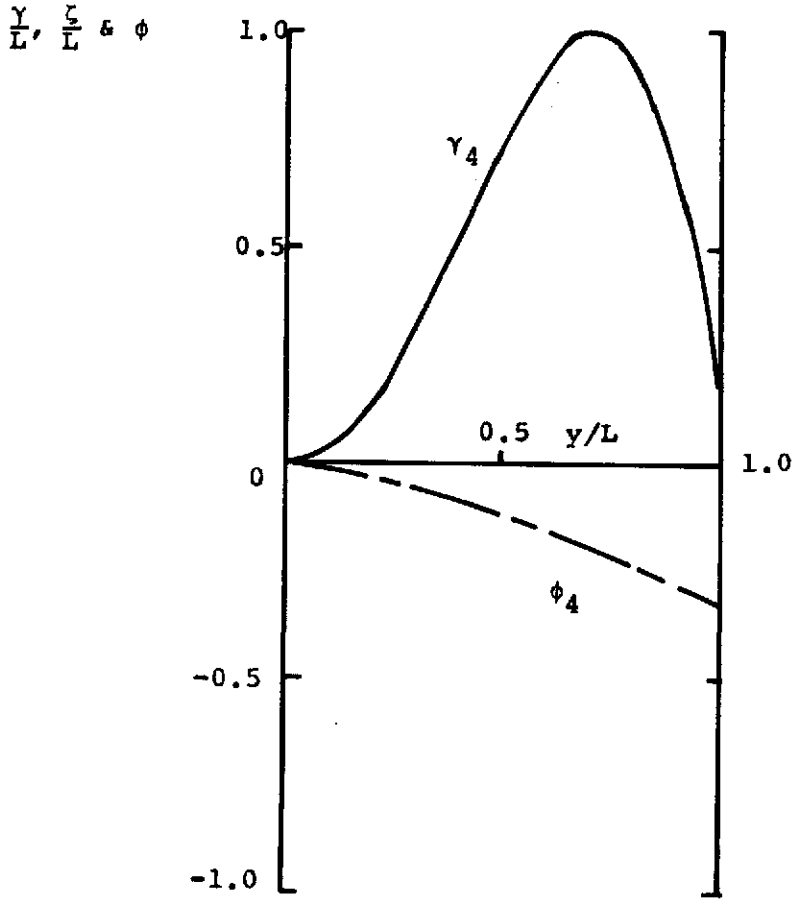

(d) Fourth Mode (8.1 Hz)

FIG. 20 CONTINUED

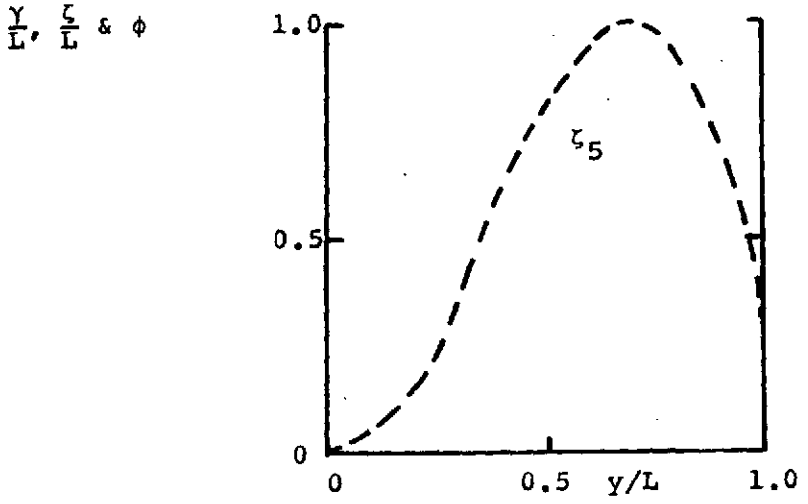

(e) Fifth Mode (28.8 Hz)

FIG. 20 CONTINUED

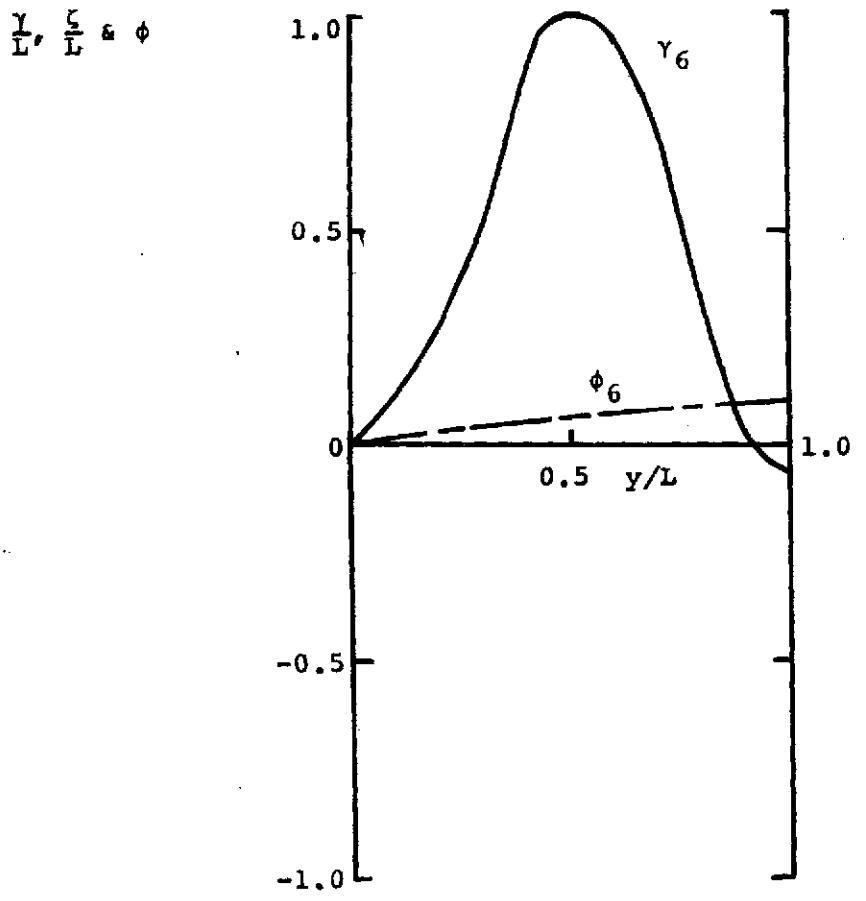

(f) Sixth Mode (80.8 Hz)

FIG. 20 CONCLUDED

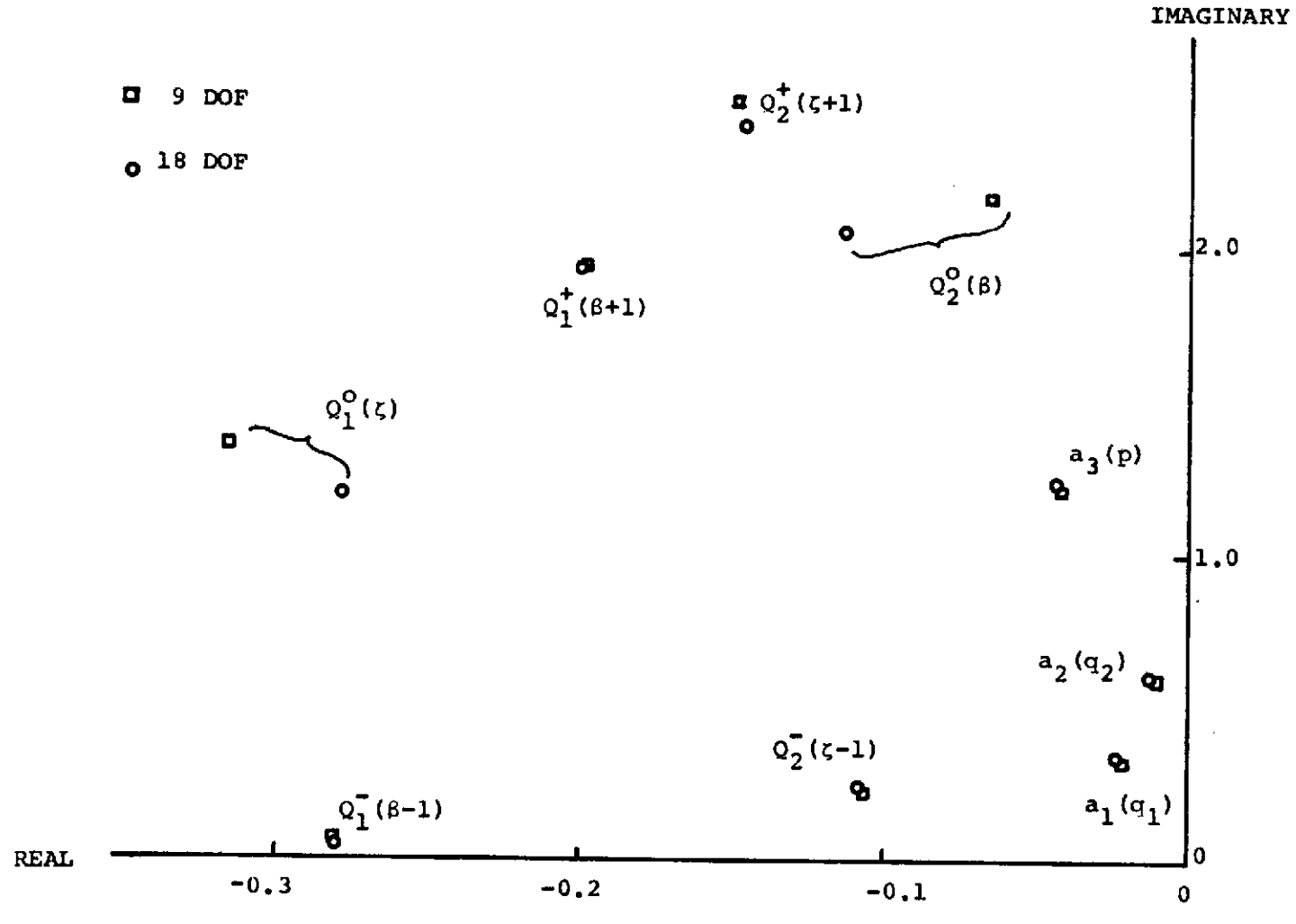

(a) Bell Proprotor

FIG. 21 INFLUENCE OF ADDITION OF HIGHER DEGREES OF FREEDOM ON EIGENVALUES COMPARED WITH BASIC NINE DEGREES OF FREEDOM

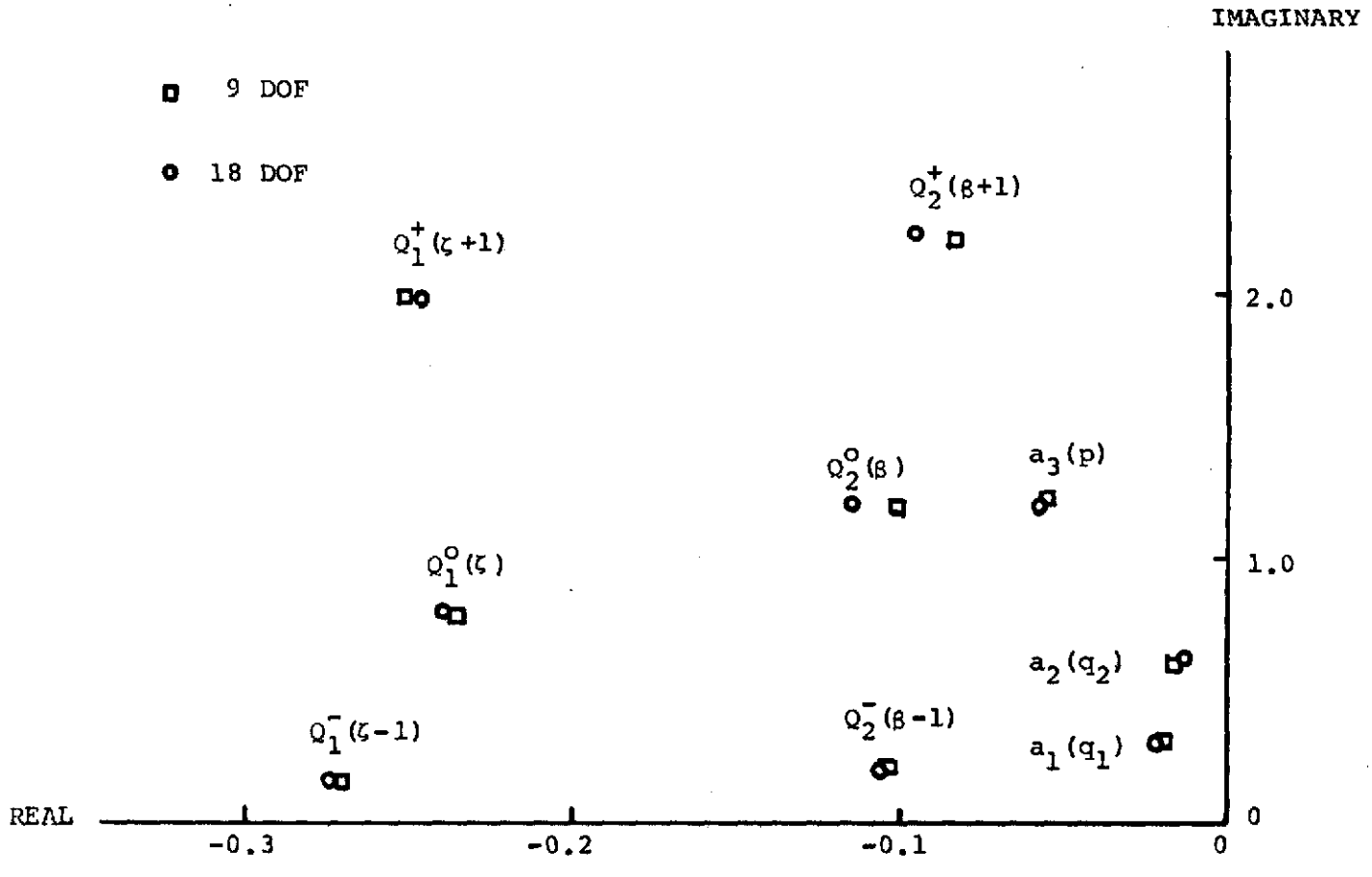

(b) Boeing Proprotor

FIG. 21 CONCLUDED

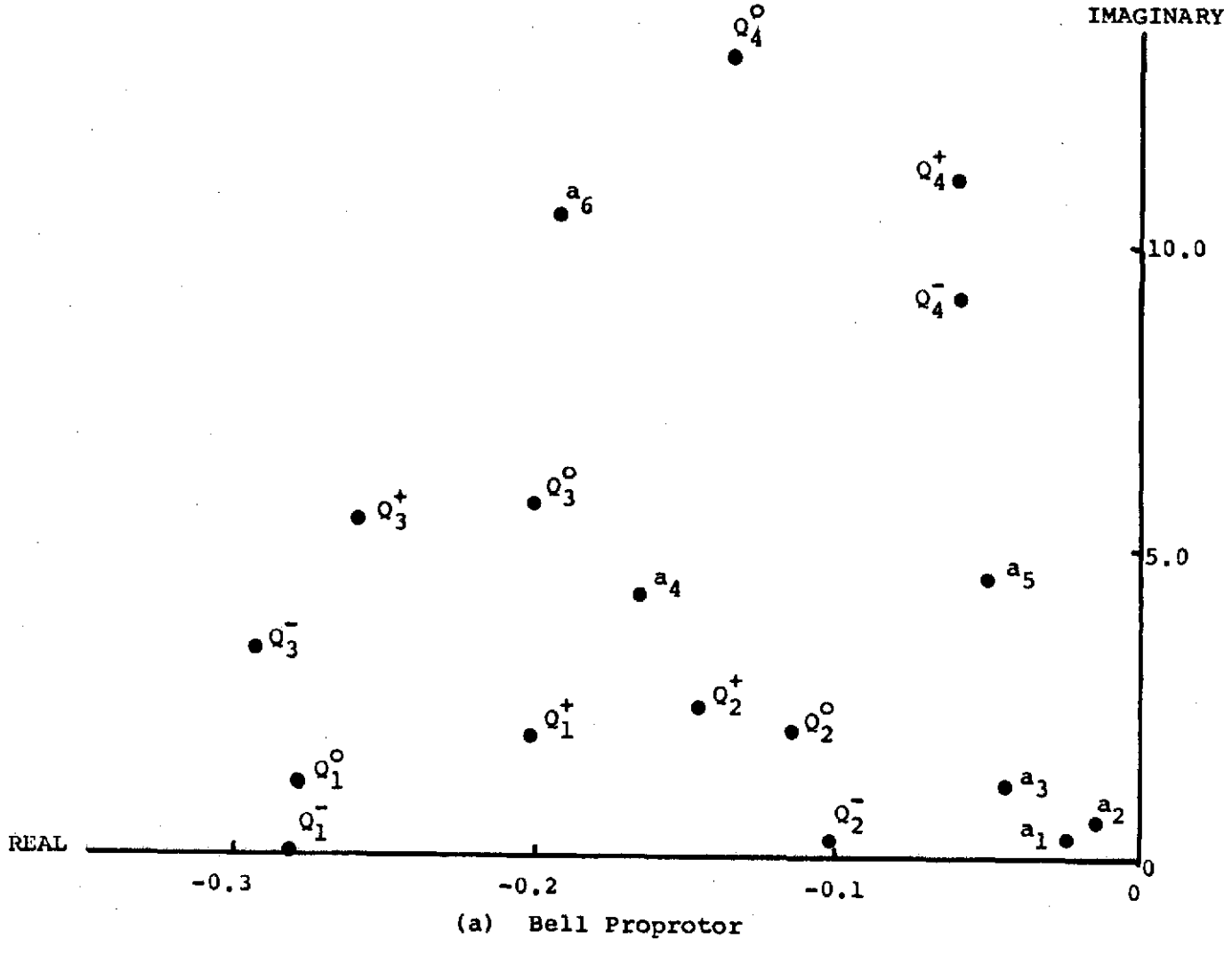

(a) Bell Proprotor

FIG. 22 EIGENVALUES FOR 18 DEGREES OF FREEDOM

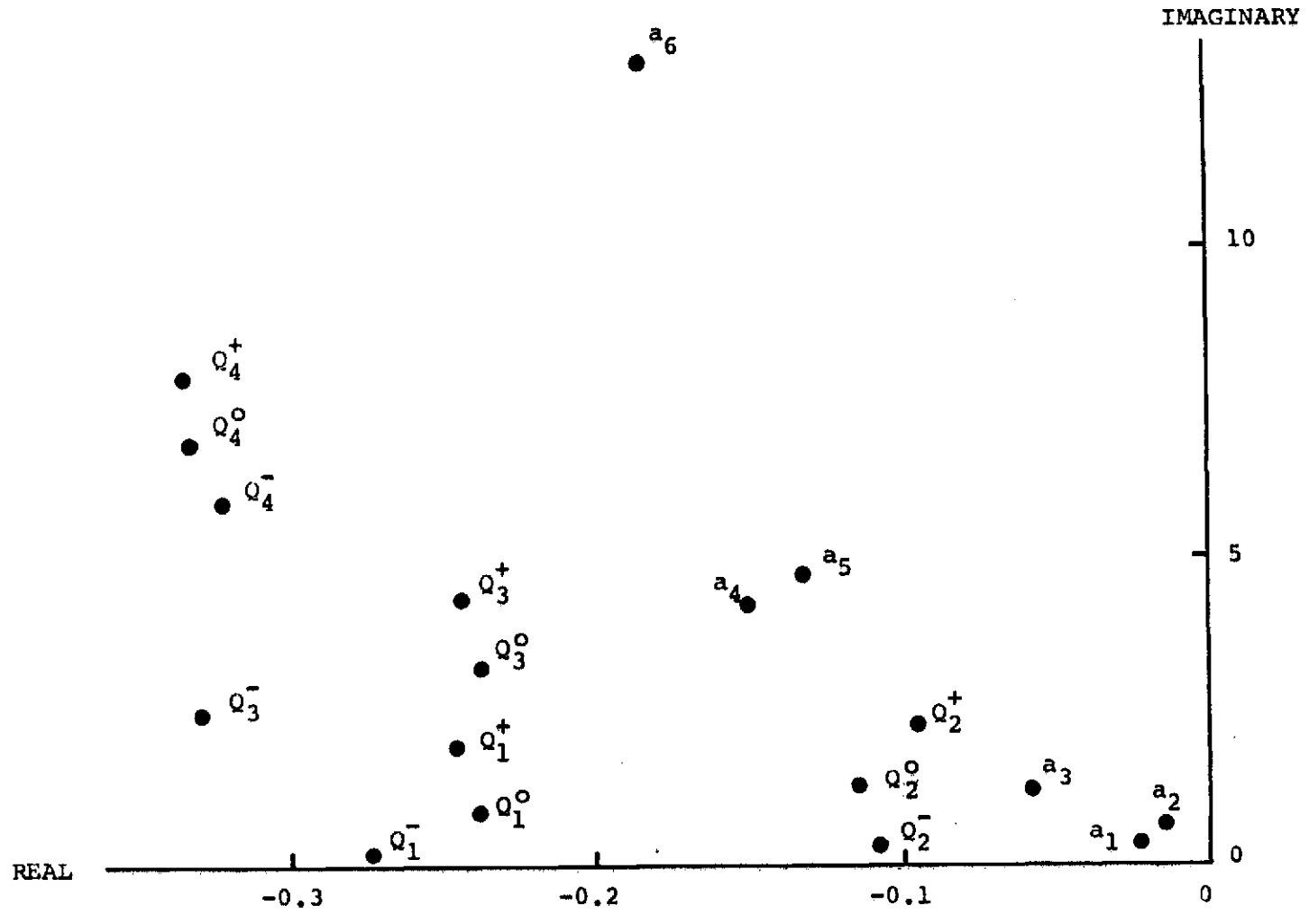

(b) Boeing Proprotor

FIG. 22 CONCLUDED

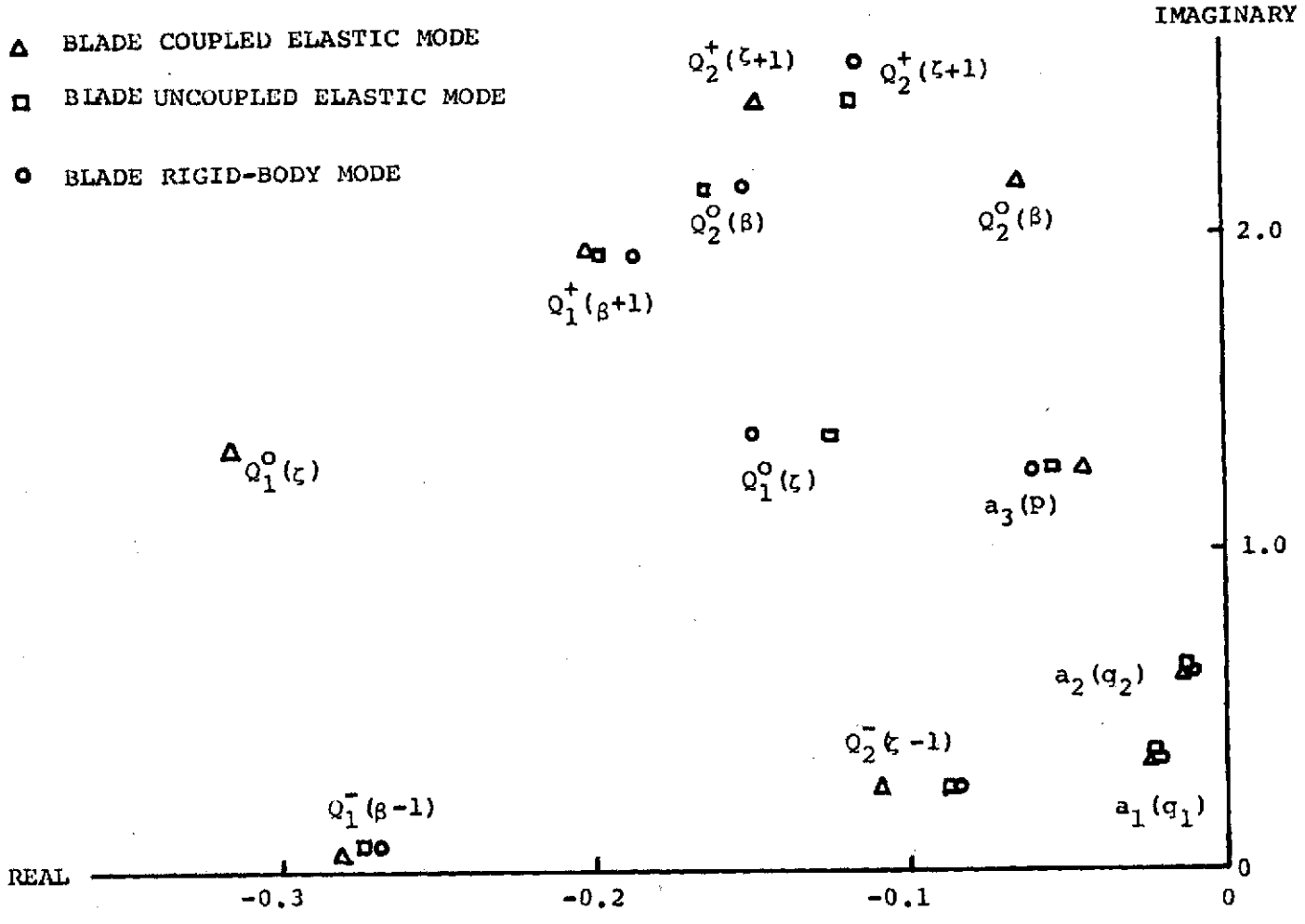

(a) Bell Proprotor Eigenvalues

FIG. 23 INFLUENCE OF BLADE MODE SHAPE TYPES ON PROPROTOR SYSTEM EIGENVALUES AND DAMPING RATIOS FOR COUPLED ELASTIC MODE SHAPES, COMPARED WITH THOSE BASED ON RIGID-BODY MODE SHAPES AND UNCOUPLED ELASTIC MODE SHAPES

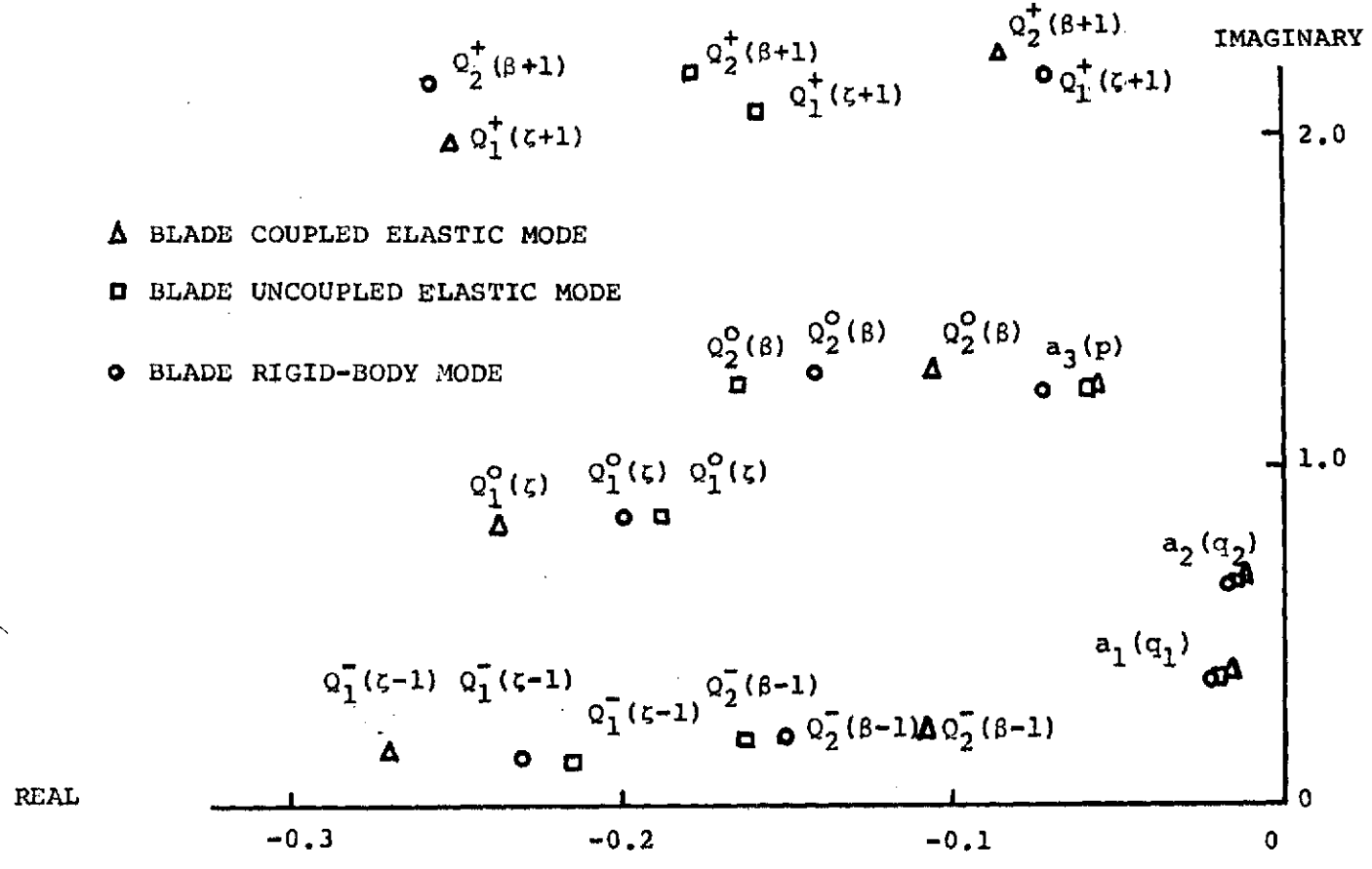

(b) Boeing Proprotor Eigenvalues

FIG. 23 CONTINUED

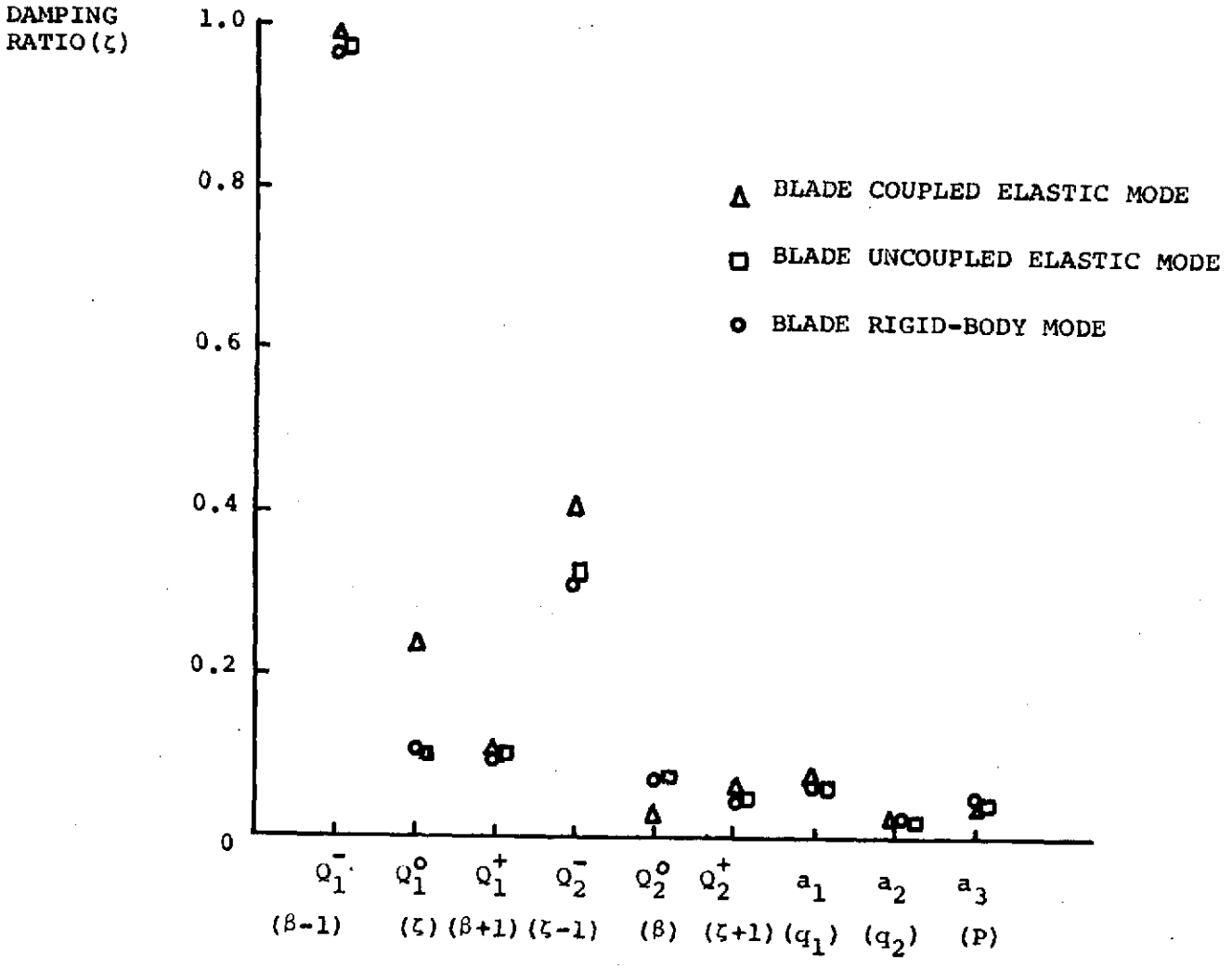

(c) Bell Proprotor Damping Ratios

FIG. 23 CONTINUED

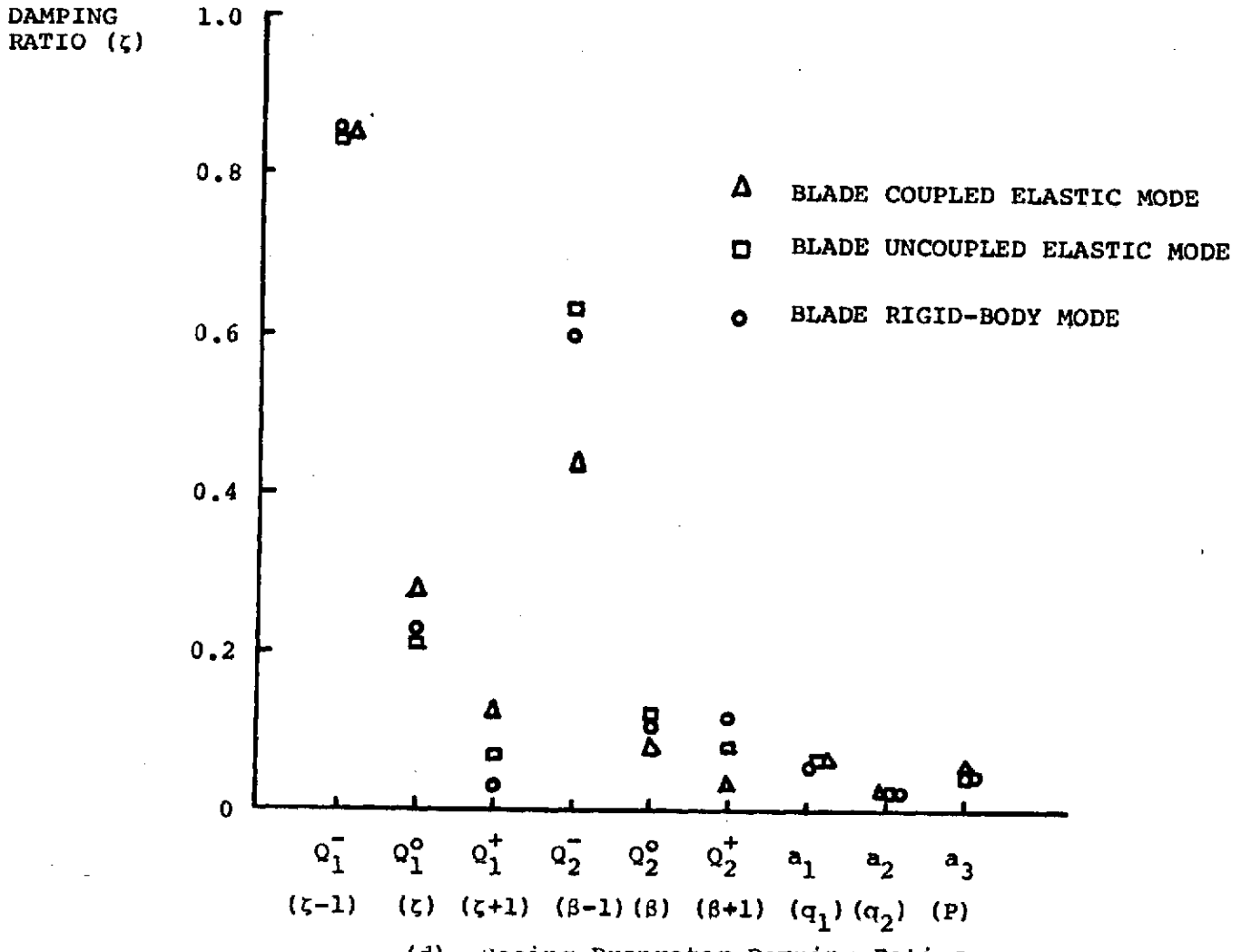

(d) Boeing Proprotor Damping Ratios

FIG. 23 CONCLUDED

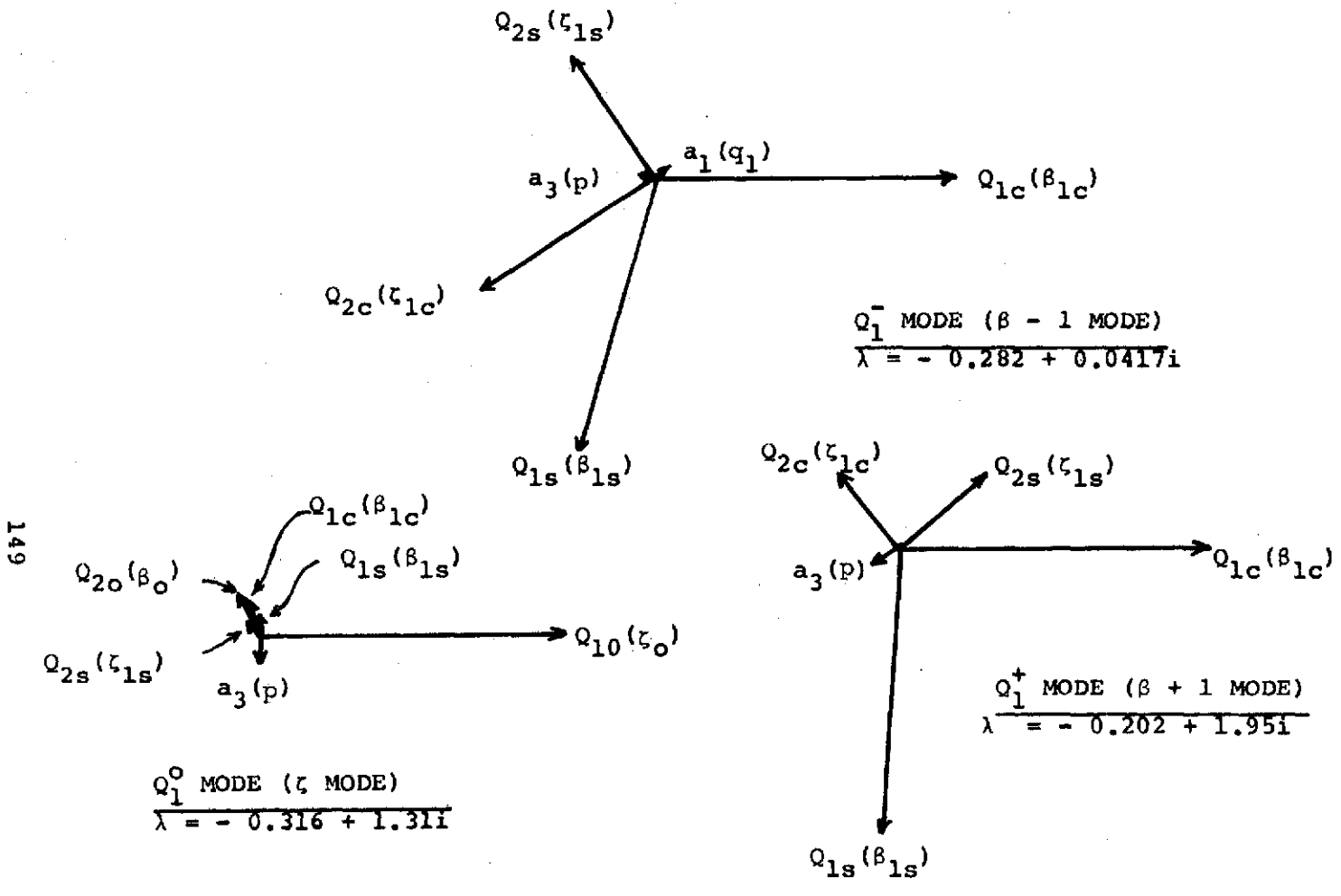

(a) Bell Proprotor

FIG. 24 EIGENVALUES AND EIGENVECTORS FOR NINE DEGREES OF FREEDOM

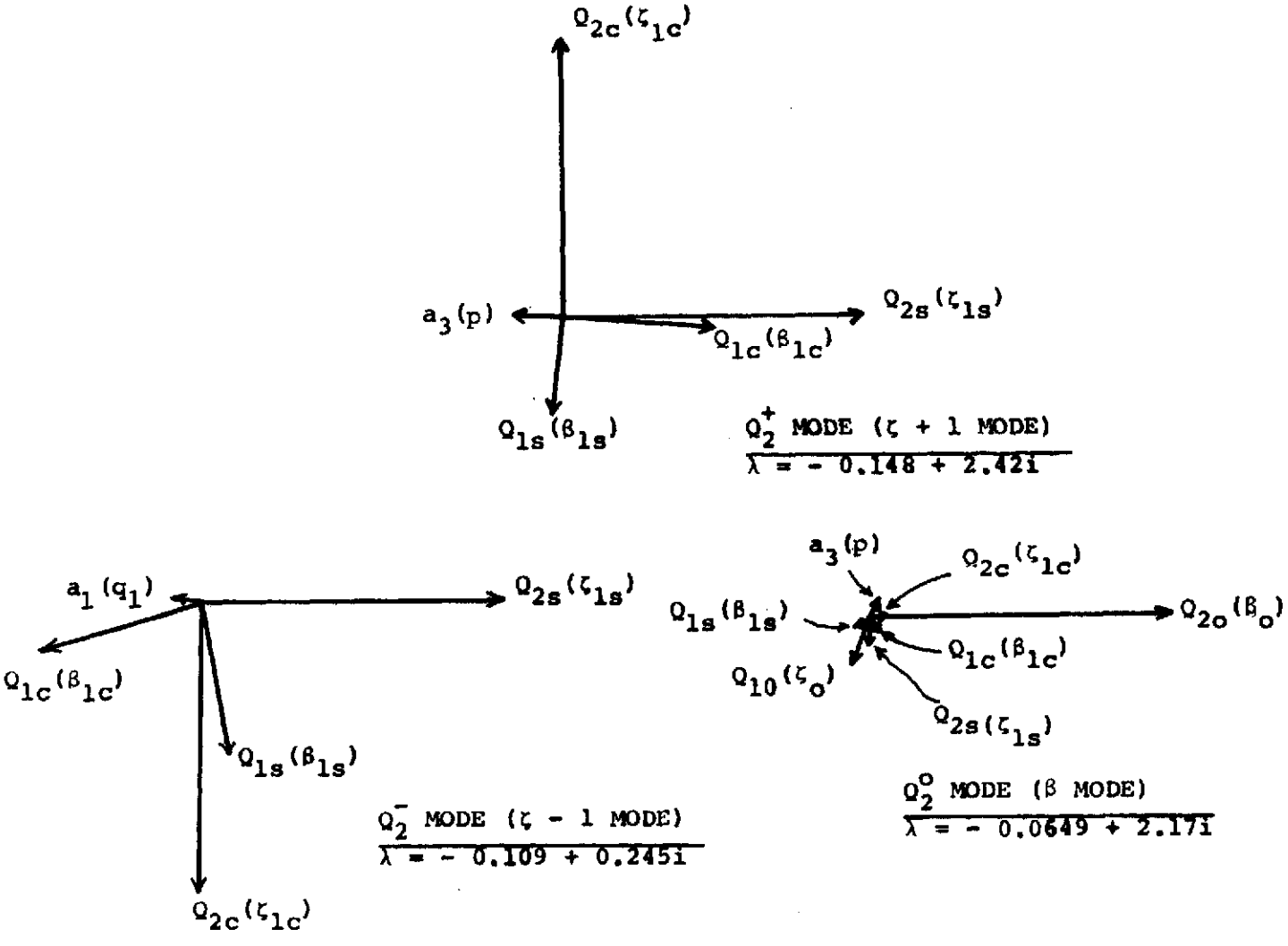

(a) Continued

FIG. 24 CONTINUED

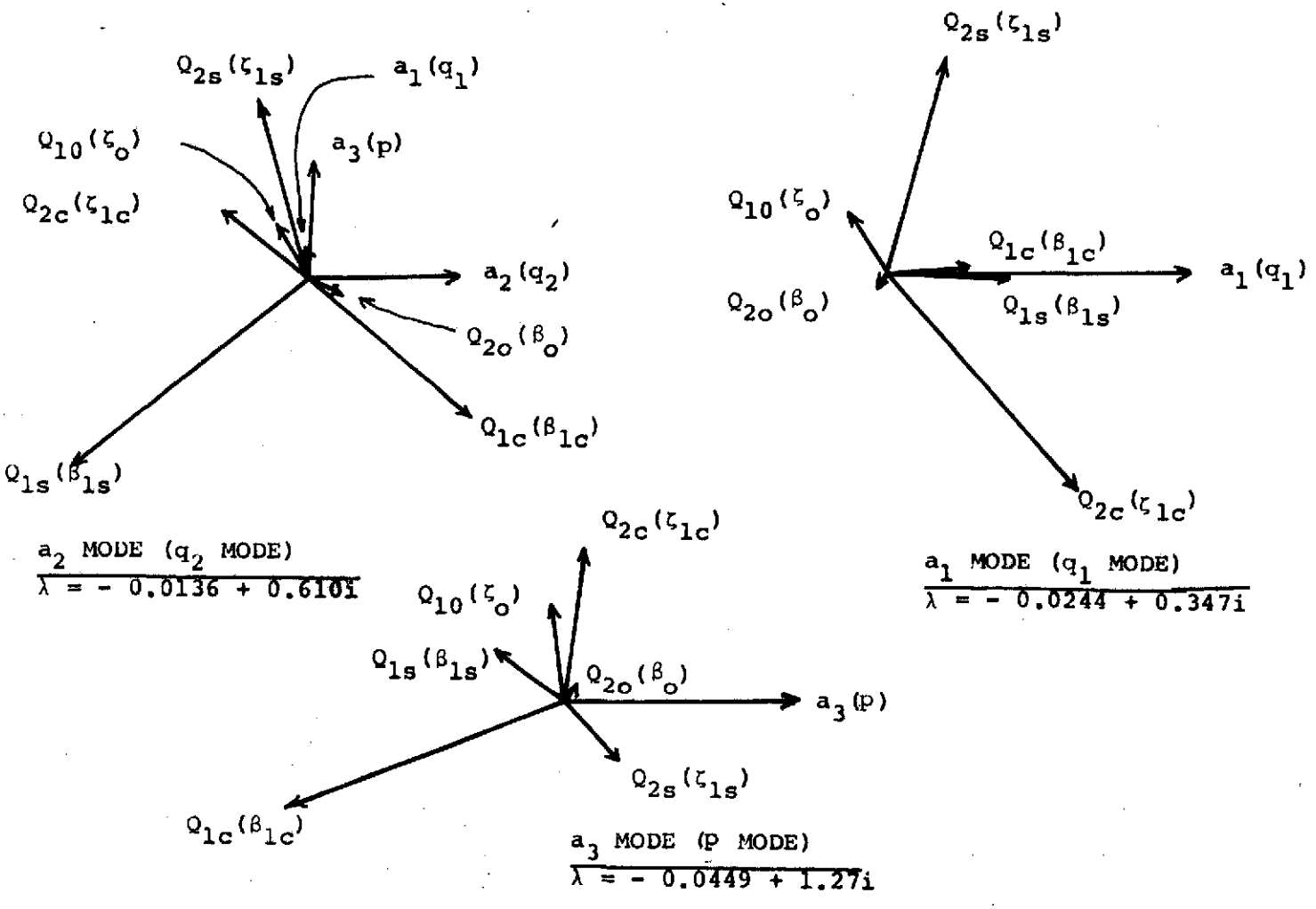

(a) Concluded

FIG. 24 CONCLUDED

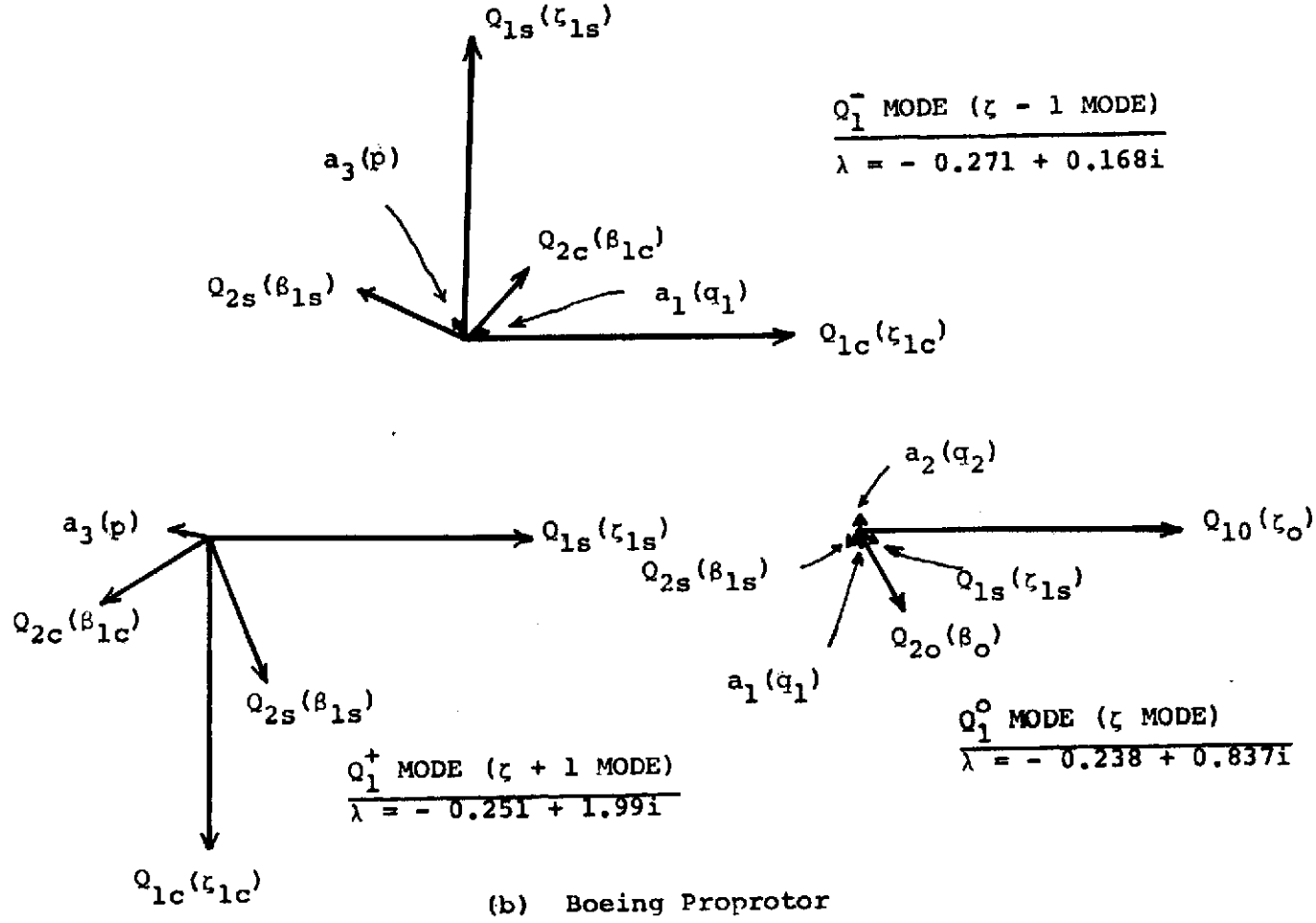

(b) Boeing Proprotor

FIG. 24 CONTINUED

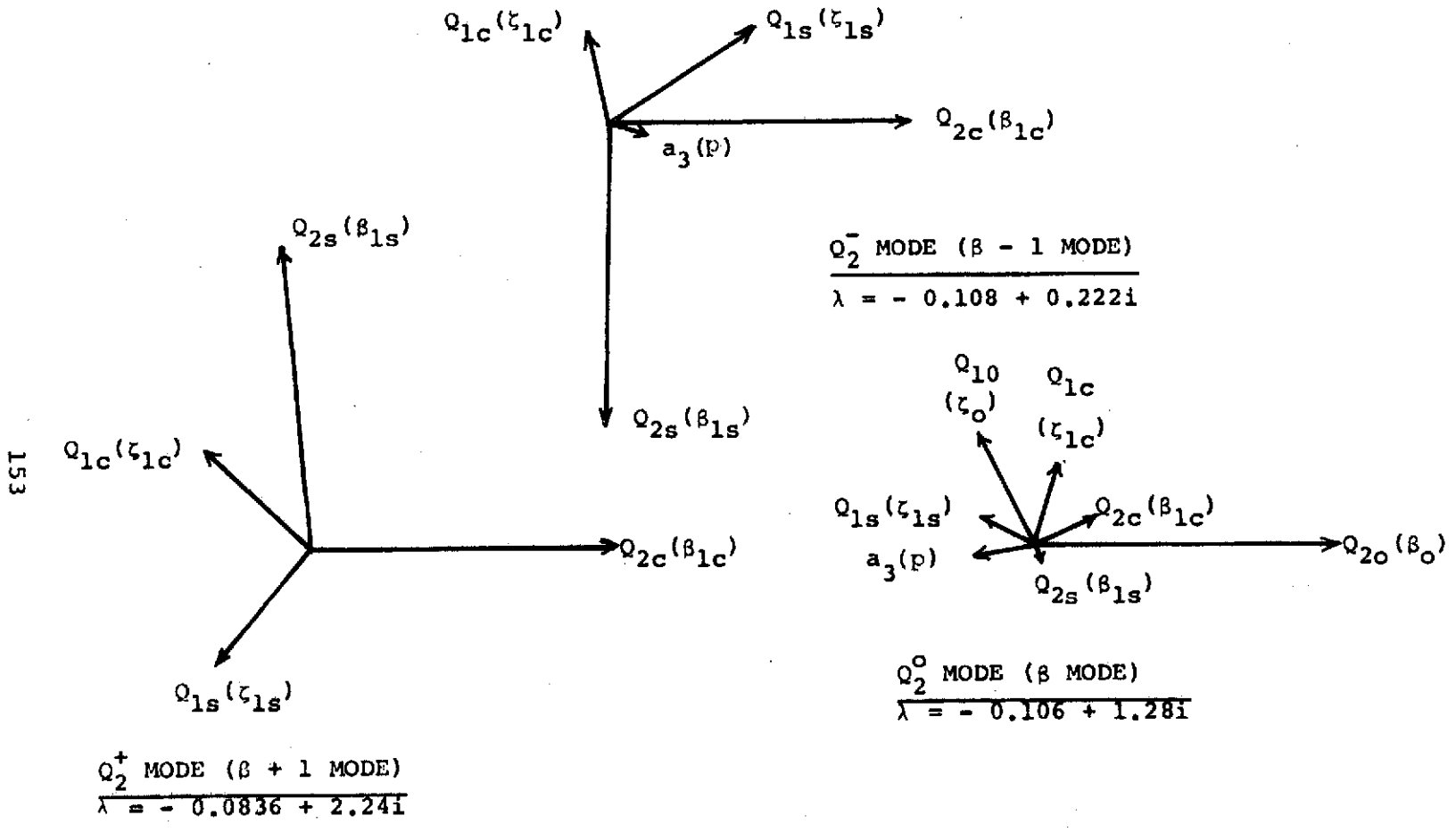

(b) Continued

FIG. 24 CONTINUED

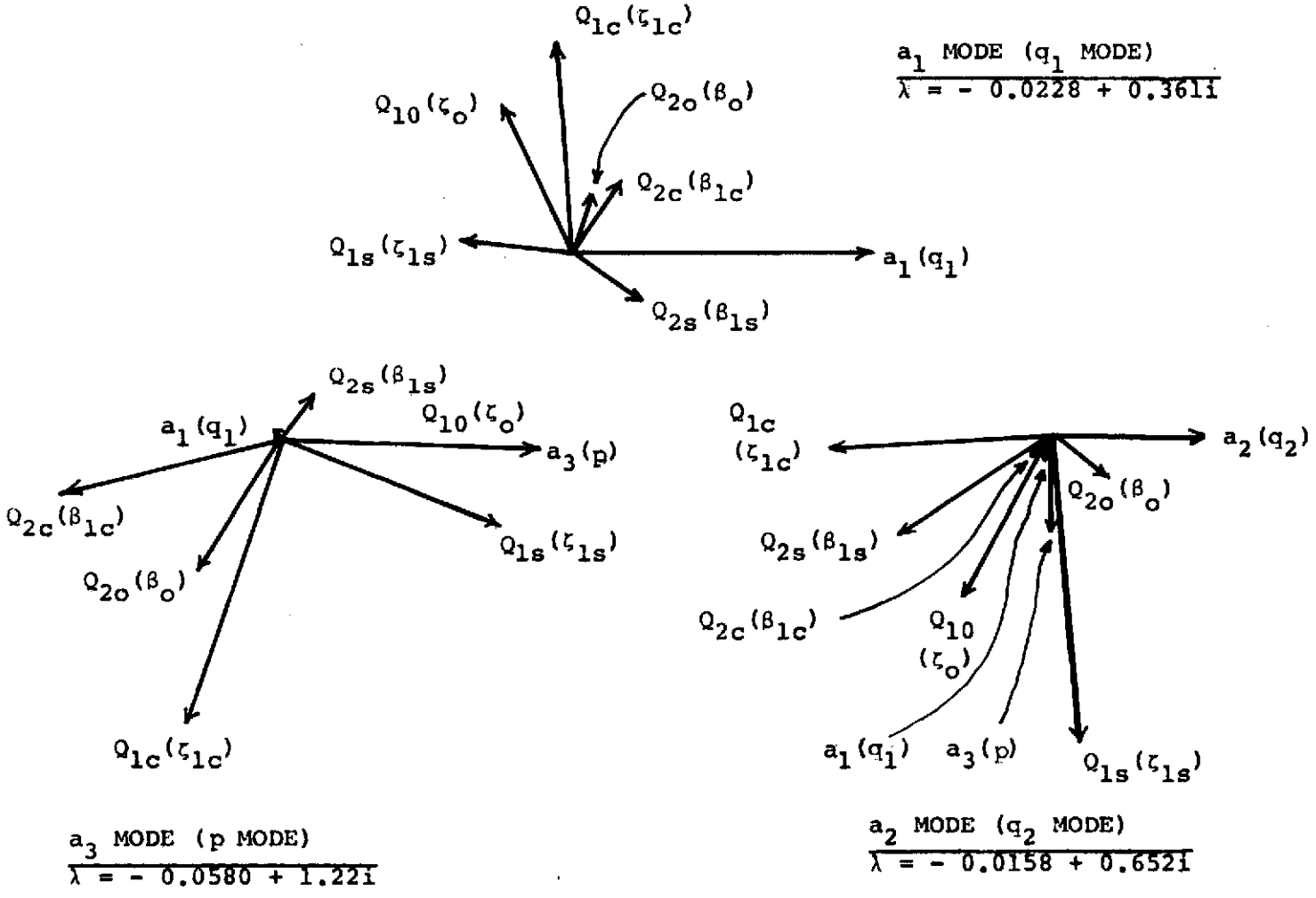

(b) Concluded

FIG. 24 CONCLUDED

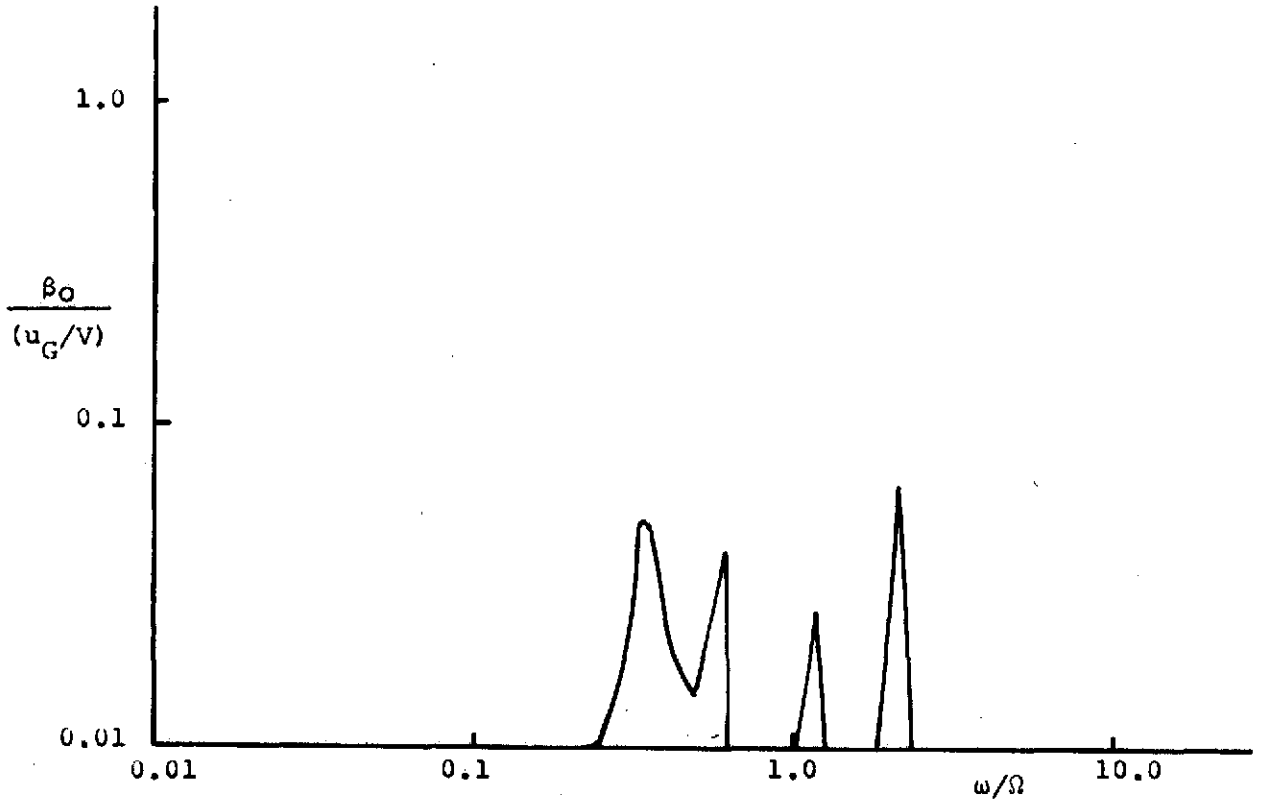

(a) Collective Flapping Motion β_o Response to u_G

FIG. 25 FREQUENCY RESPONSE OF BELL ROTOR TO VERTICAL GUST u_G INPUT AT FREQUENCY ω

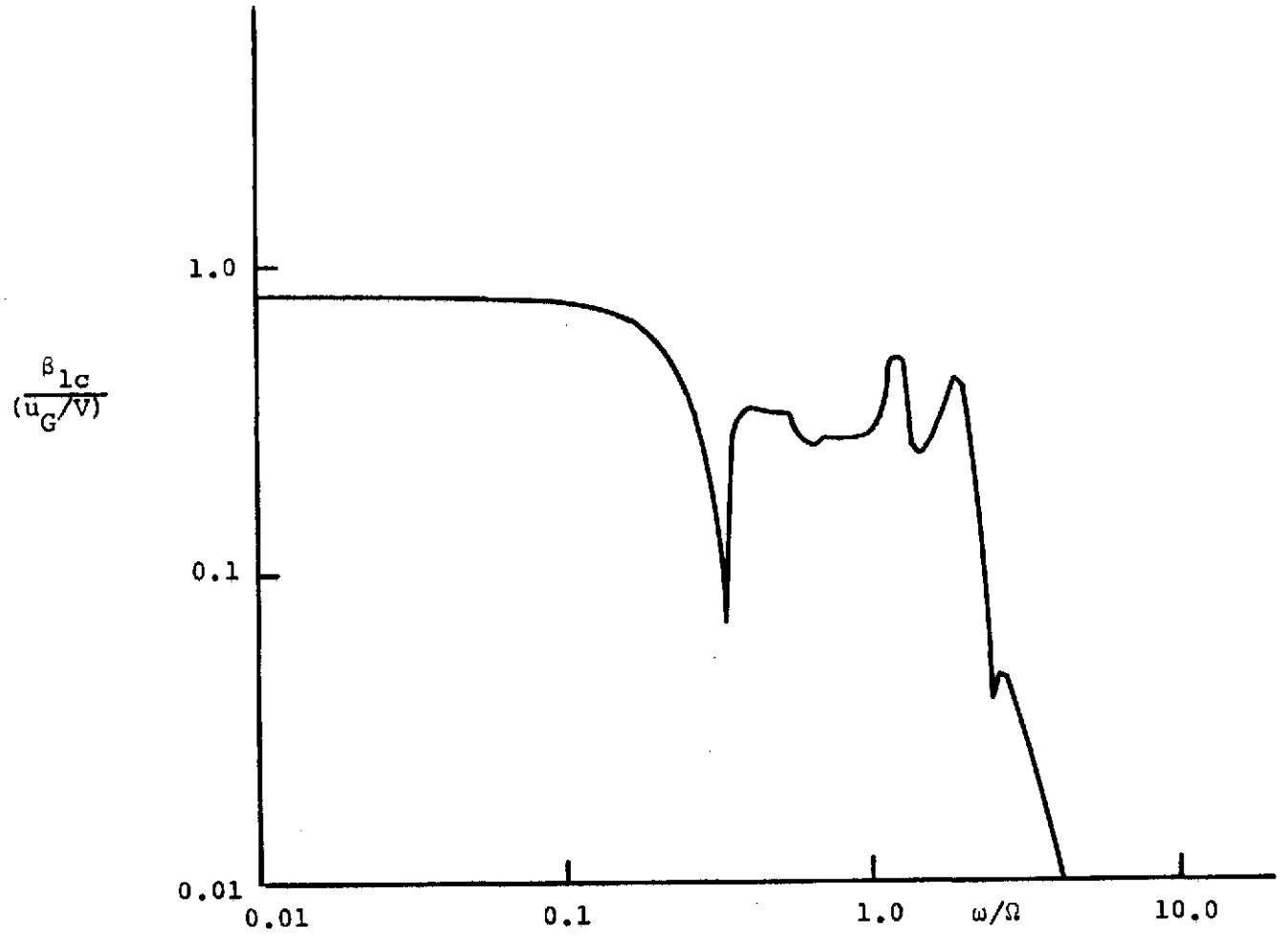

(b) Cyclic Flapping Motion β_{1c} Response to u_G

FIG. 25 CONTINUED

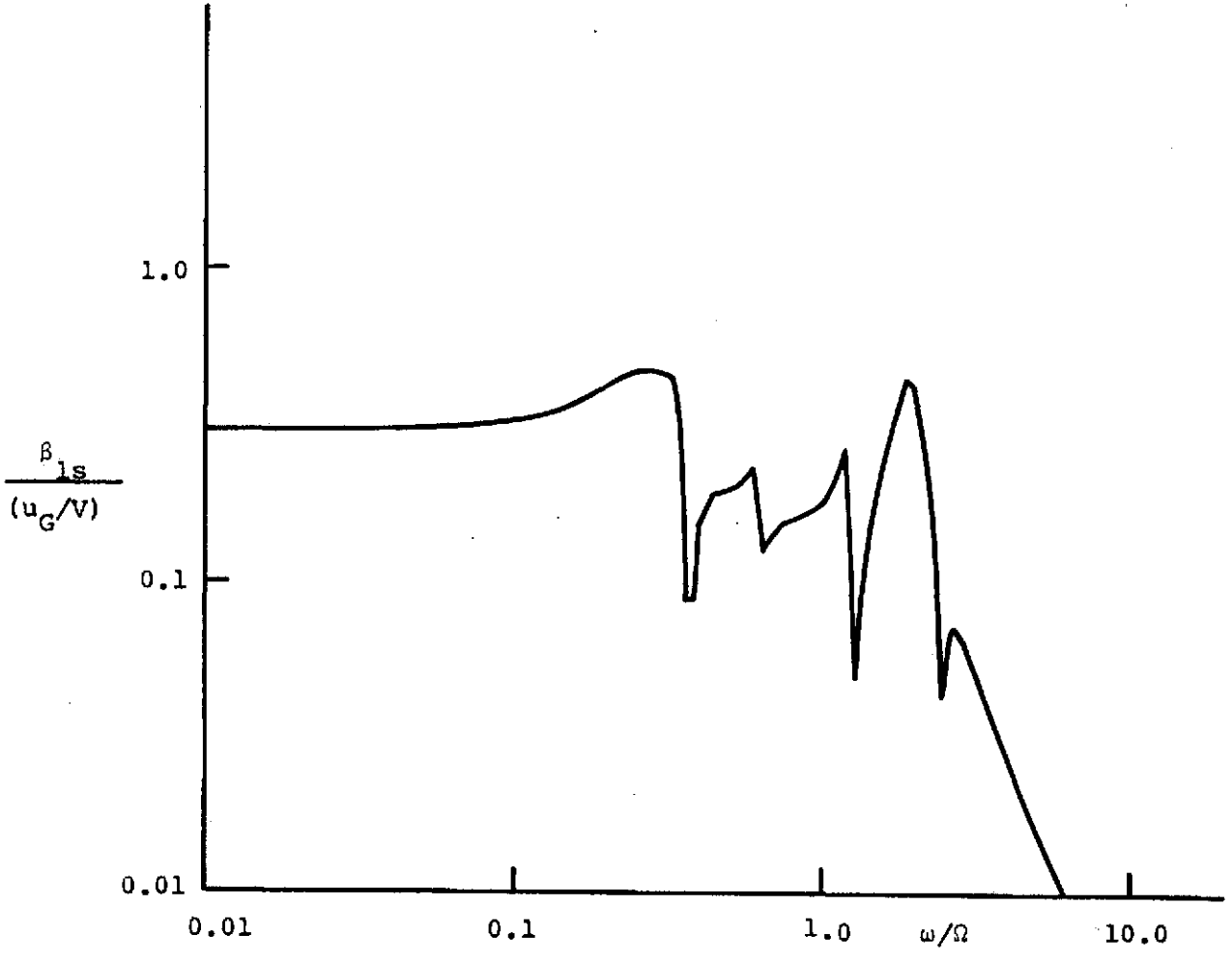

(c) Cyclic Flapping Motion β_{1s} Response to u_G

FIG. 25 CONTINUED

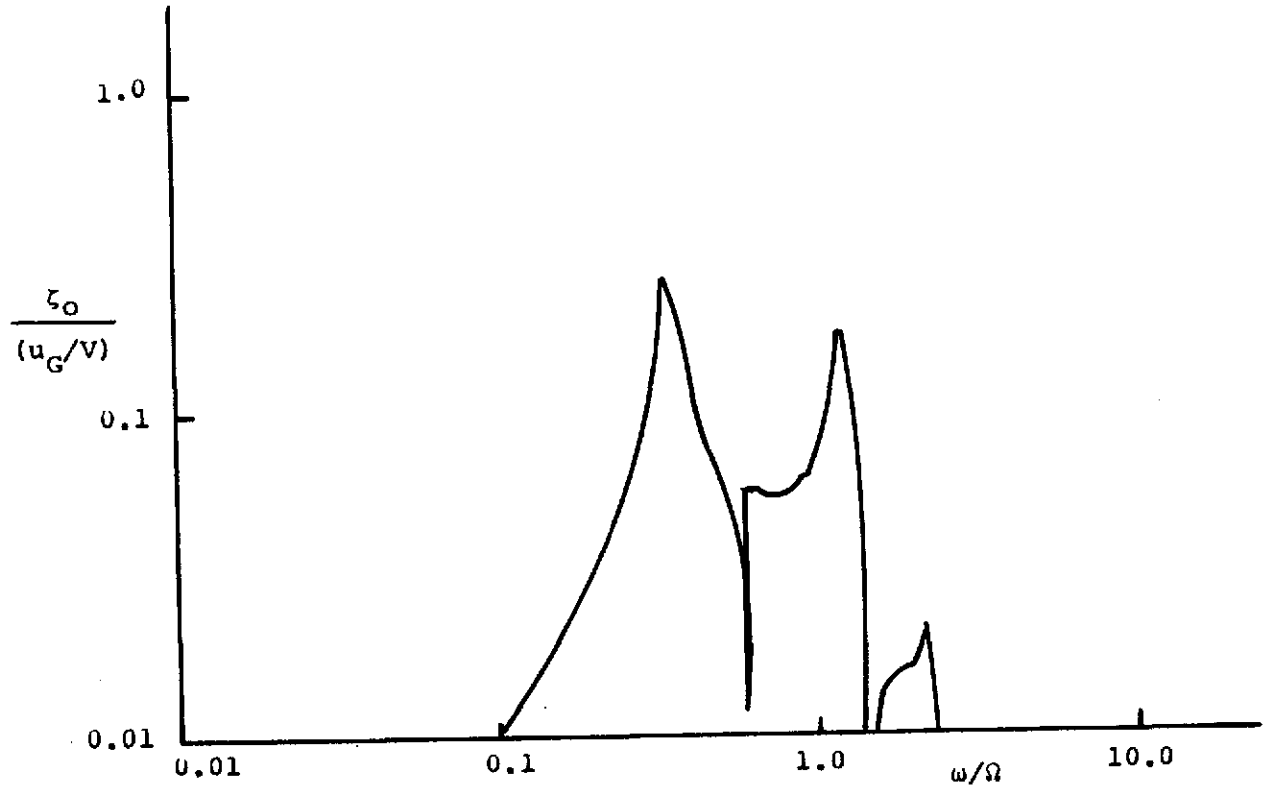

(d) Collective Lagging Motion ζ_o Response

FIG. 25 CONTINUED

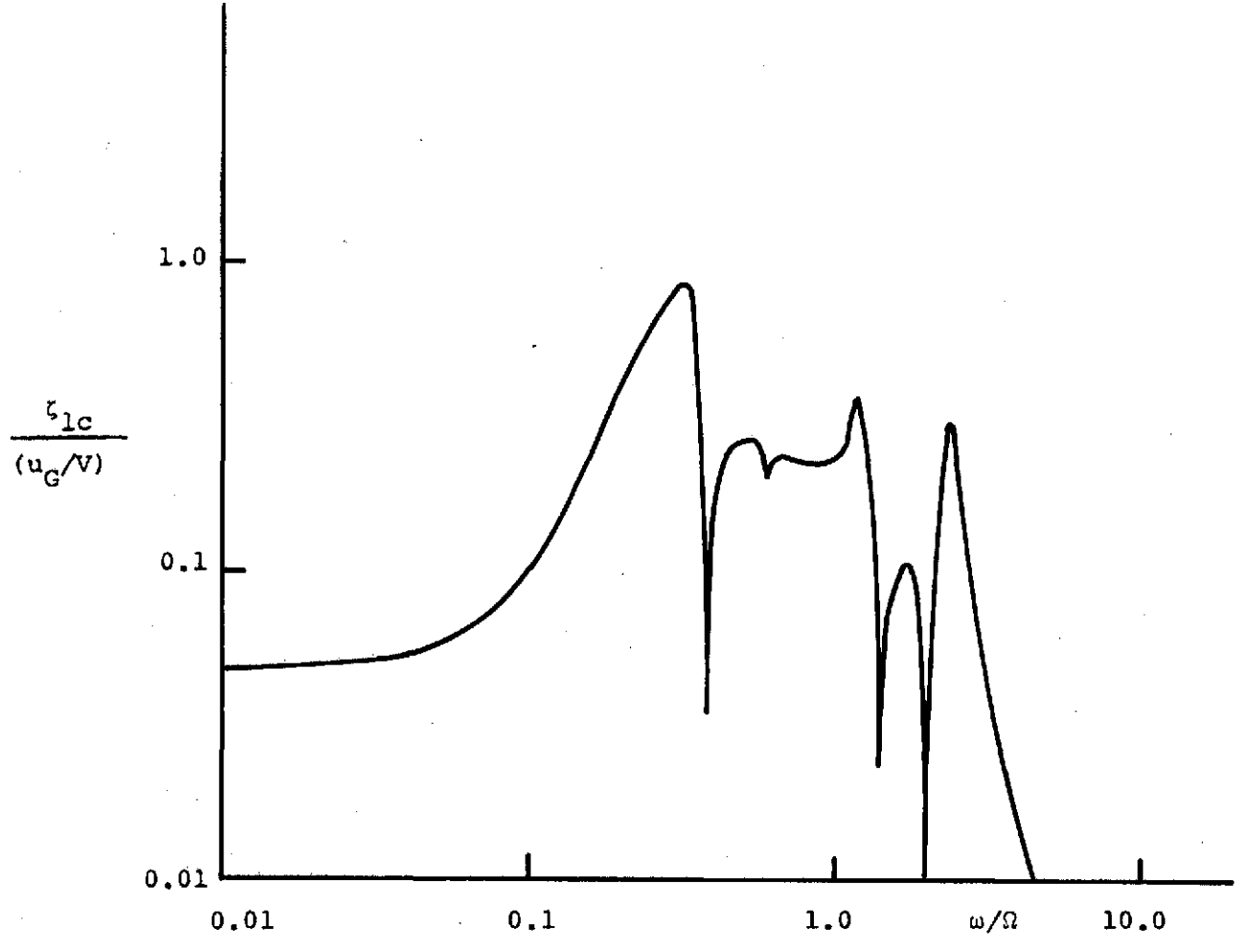

(e) Cyclic Lagging Motion ζ_{1c} Response to u_G

FIG. 25 CONTINUED

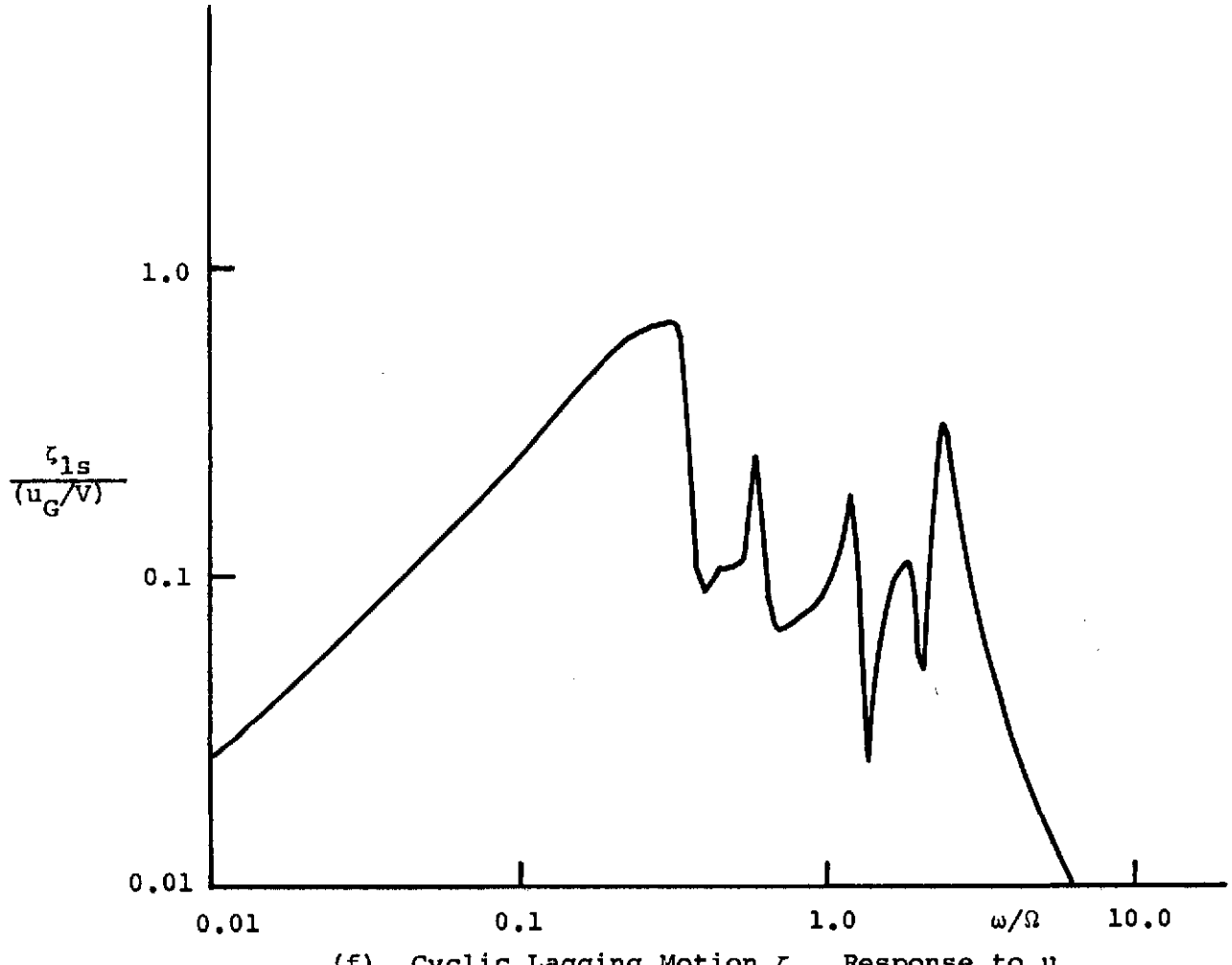

(f) Cyclic Lagging Motion ζ_{1s} Response to u_G

FIG. 25 CONTINUED

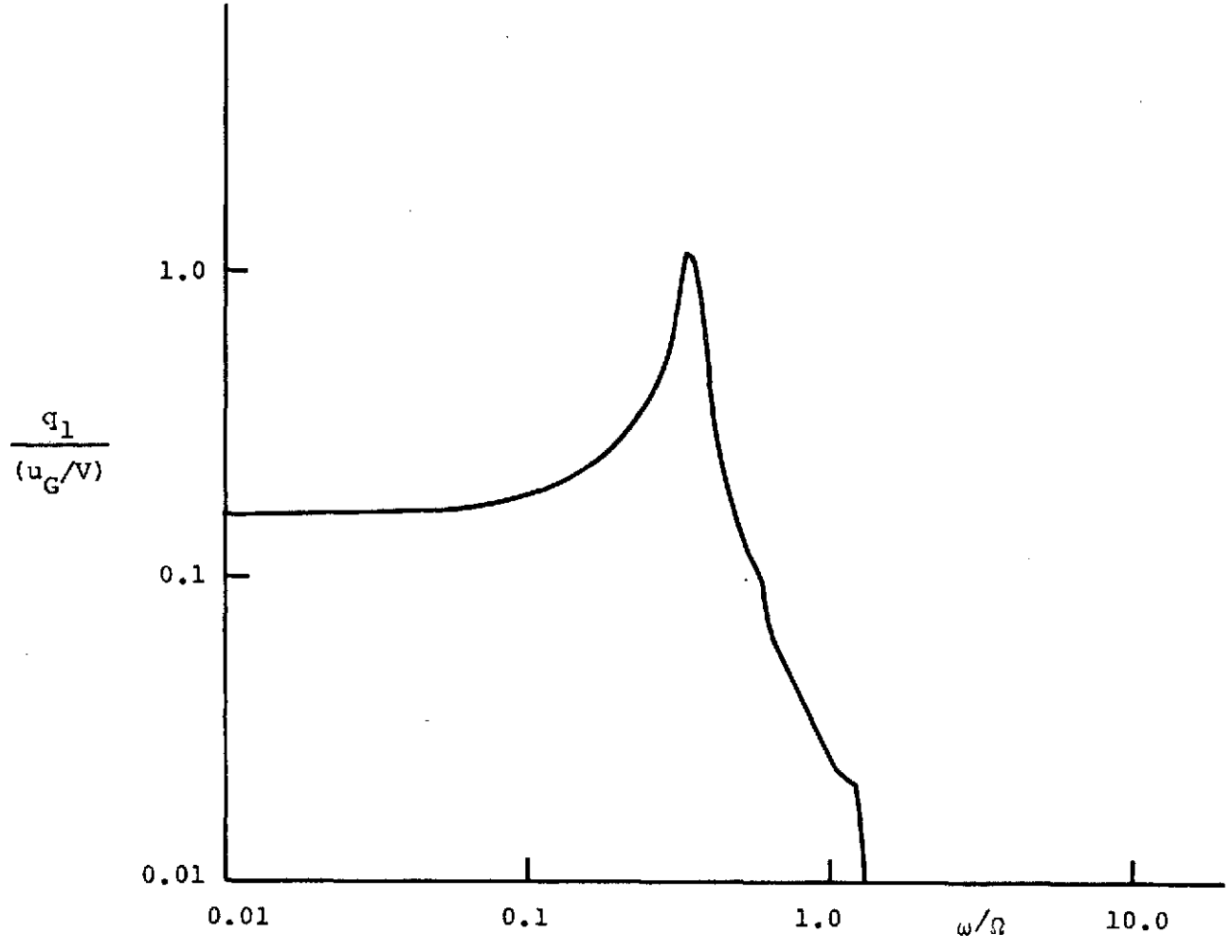

(g) Wing Vertical Bending q_1 Response to u_G

FIG. 25 CONTINUED

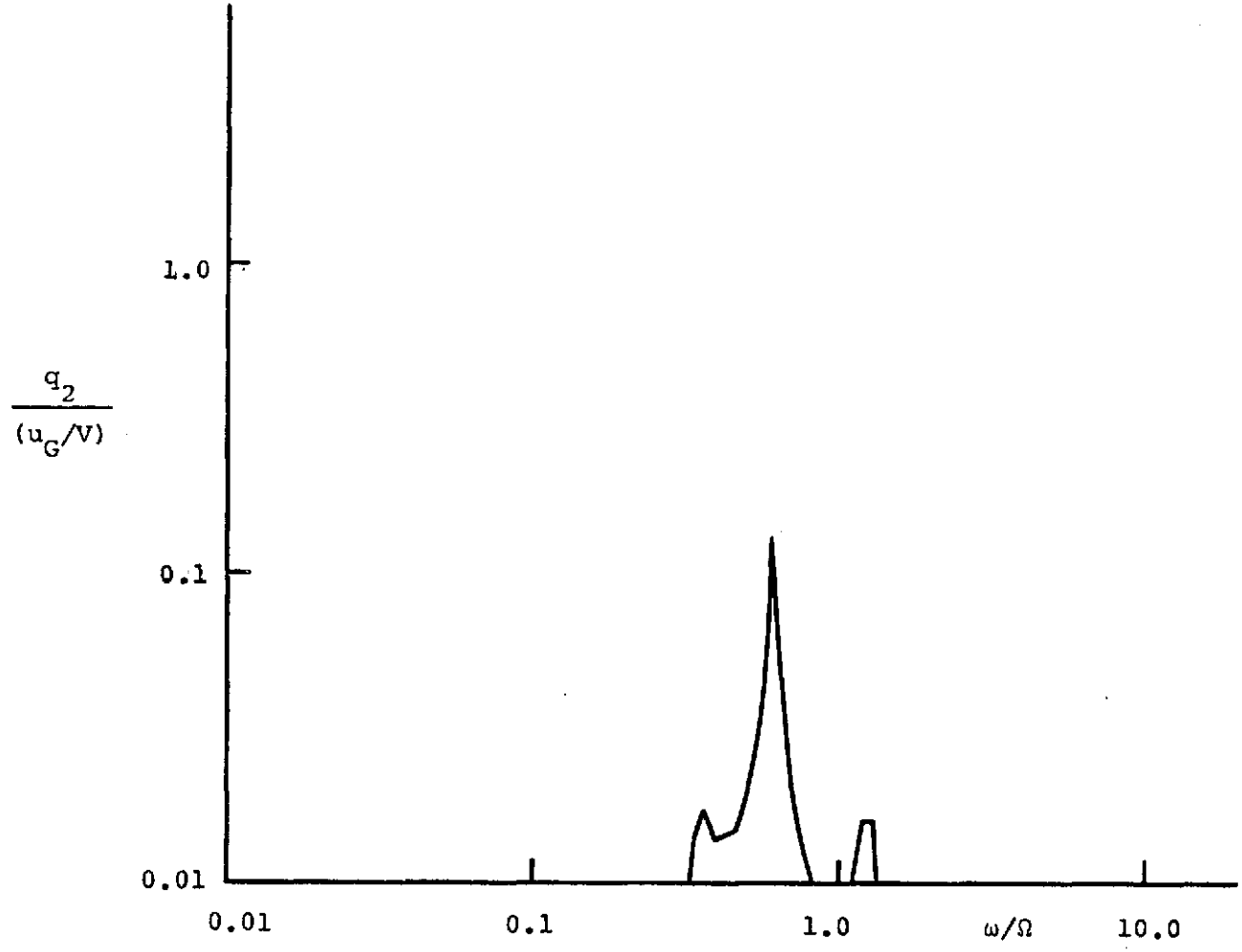

(h) Wing Chordwise Bending q_2 Response to u_G

FIG. 25 CONTINUED

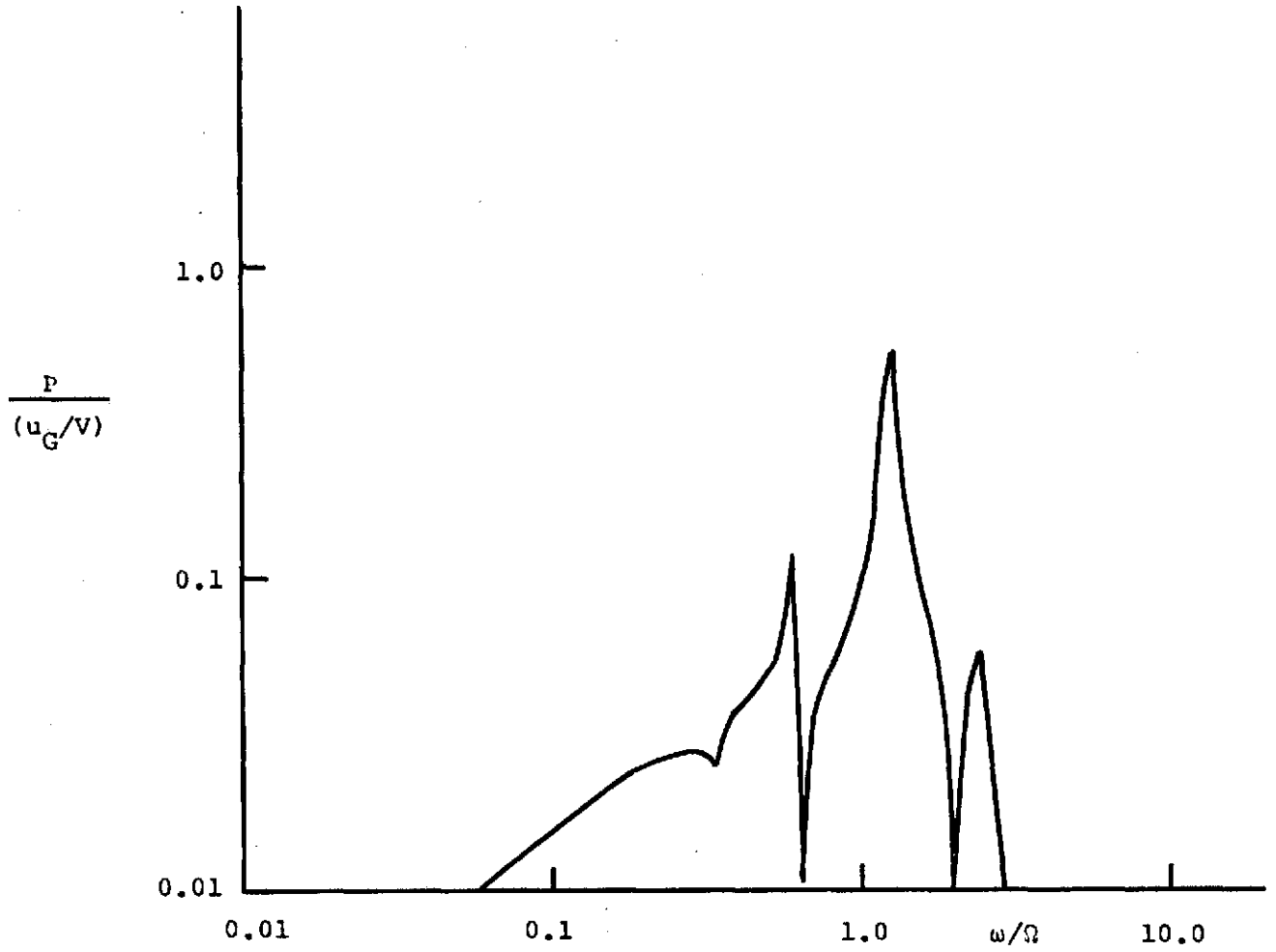

(i) Wing Torsion p Response to u_G

FIG. 25 CONCLUDED

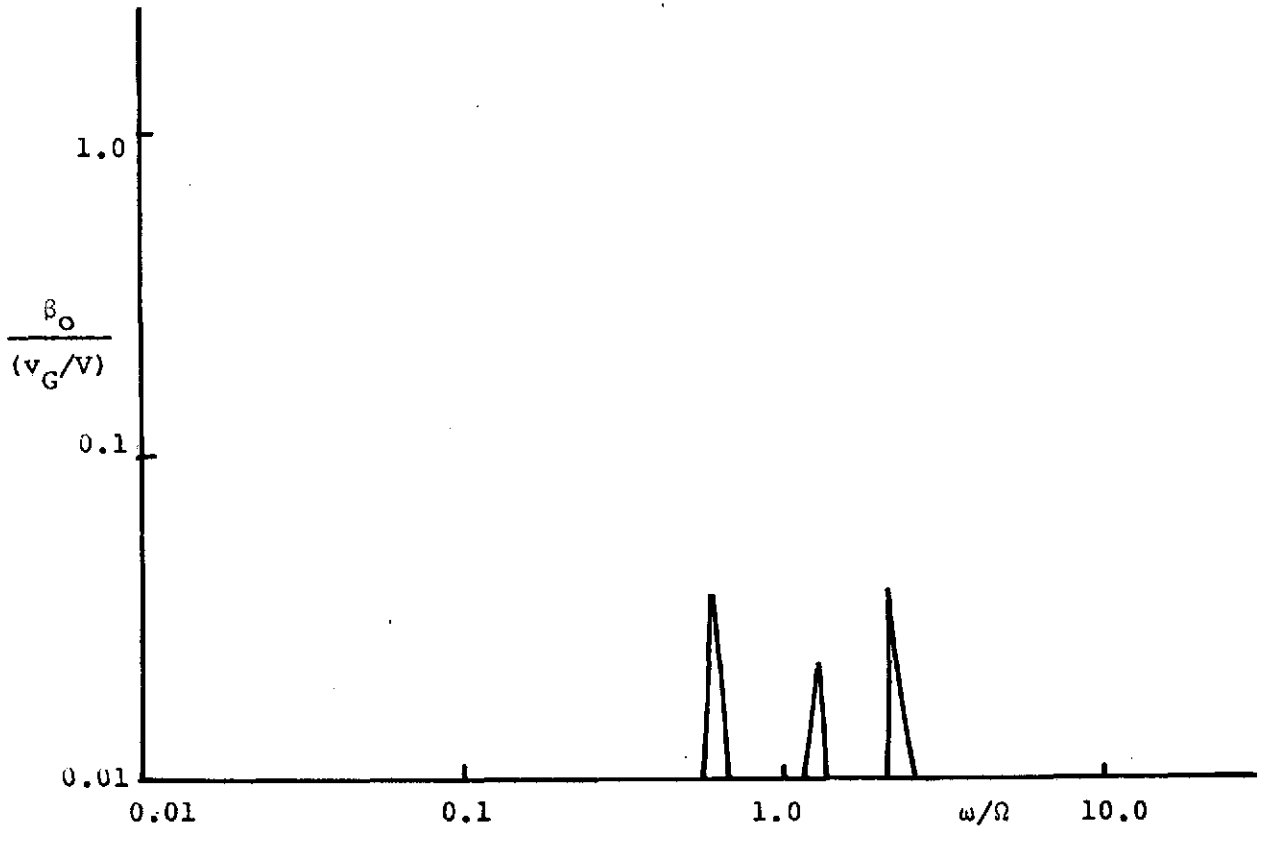

(a) Collective Flapping Motion β_o Response to v_G

FIG. 26 FREQUENCY RESPONSE OF BELL ROTOR TO LATERAL GUST v_G INPUT AT FREQUENCY ω

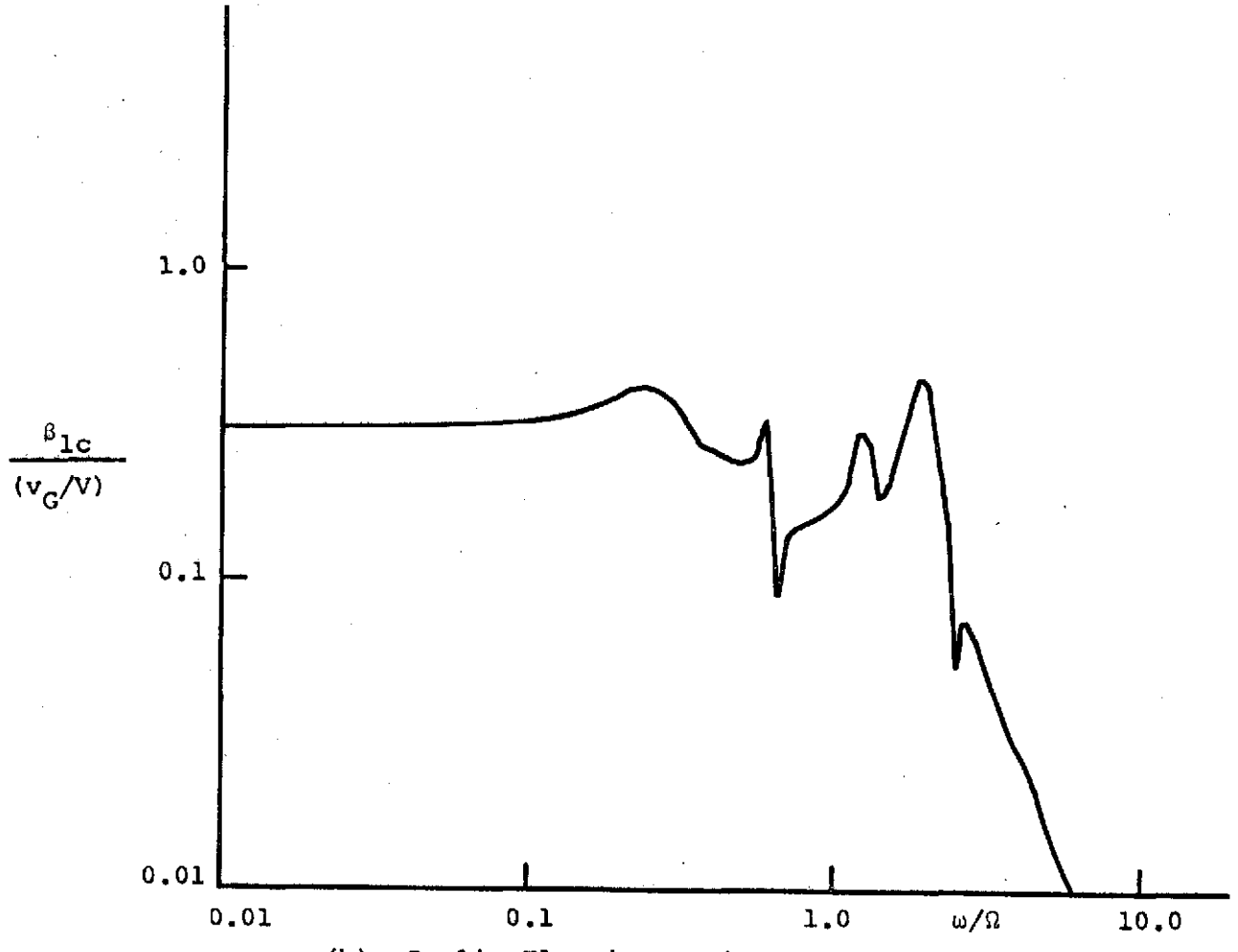

(b) Cyclic Flapping Motion β_{1c} Response to v_G

FIG. 26 CONTINUED

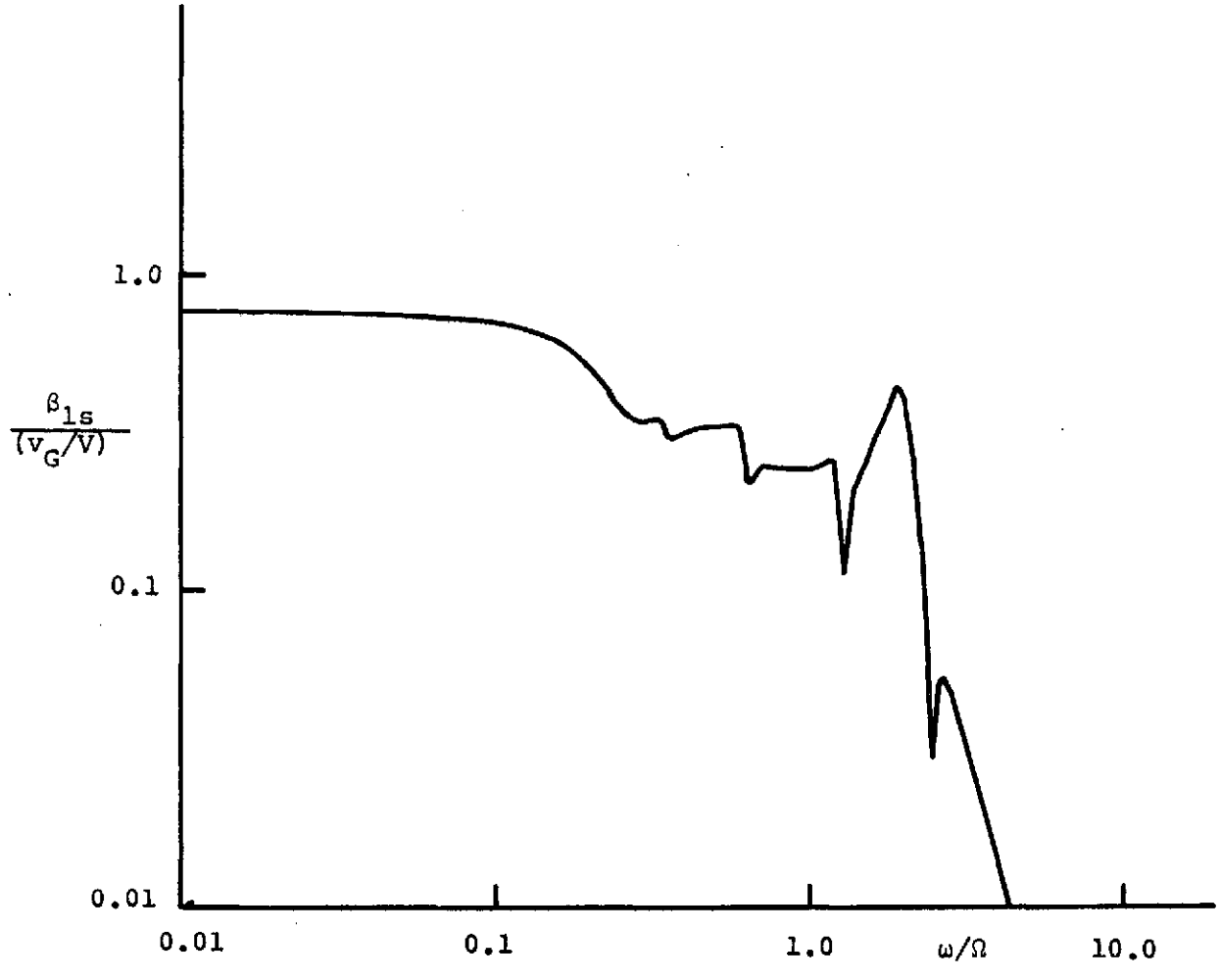

(c) Cyclic Flapping Motion β_{1s} Response to v_G

FIG. 26 CONTINUED

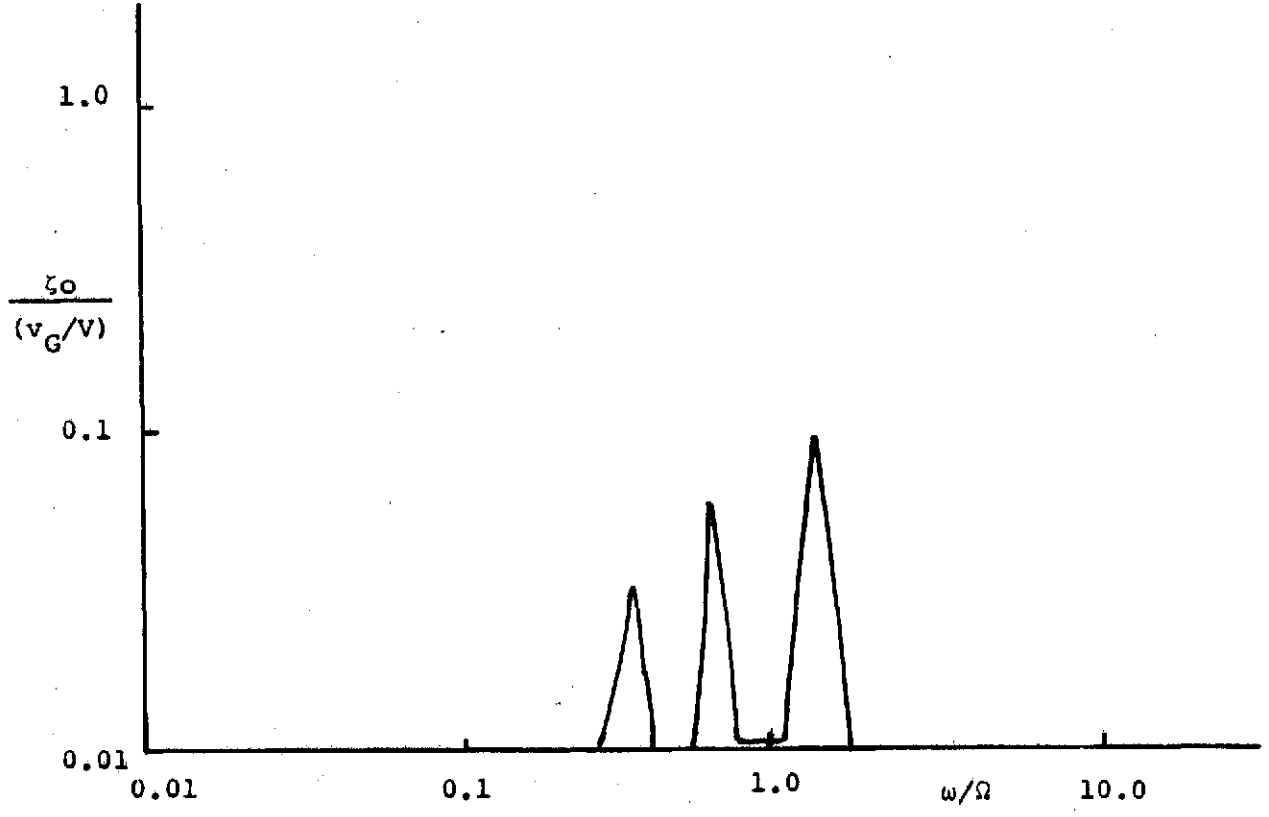

(d) Collective Lagging Motion ζ_o Response to v_G

FIG. 26 CONTINUED

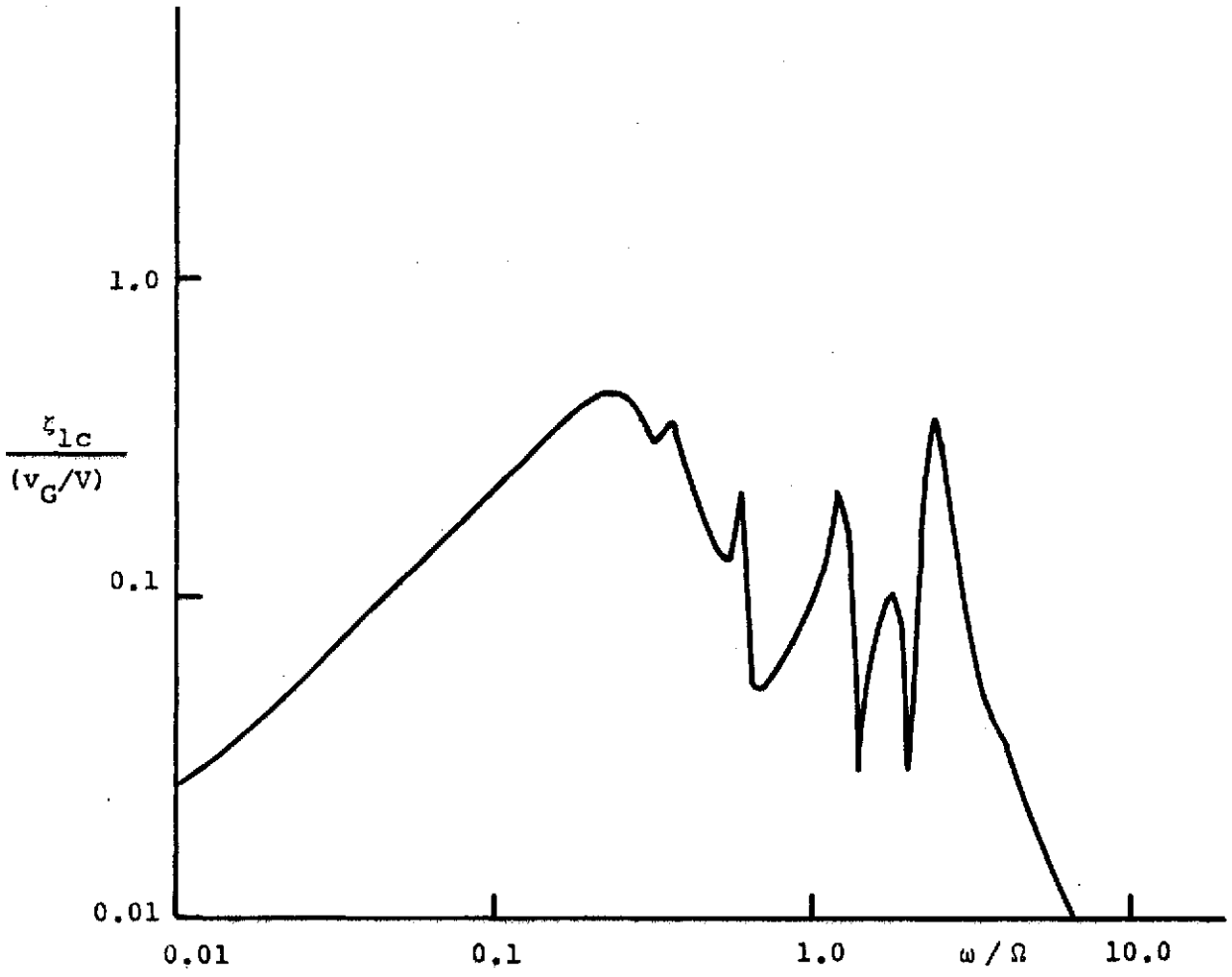

(e) Cyclic Lagging Motion ζ_{1c} Response to v_G

FIG. 26 CONTINUED

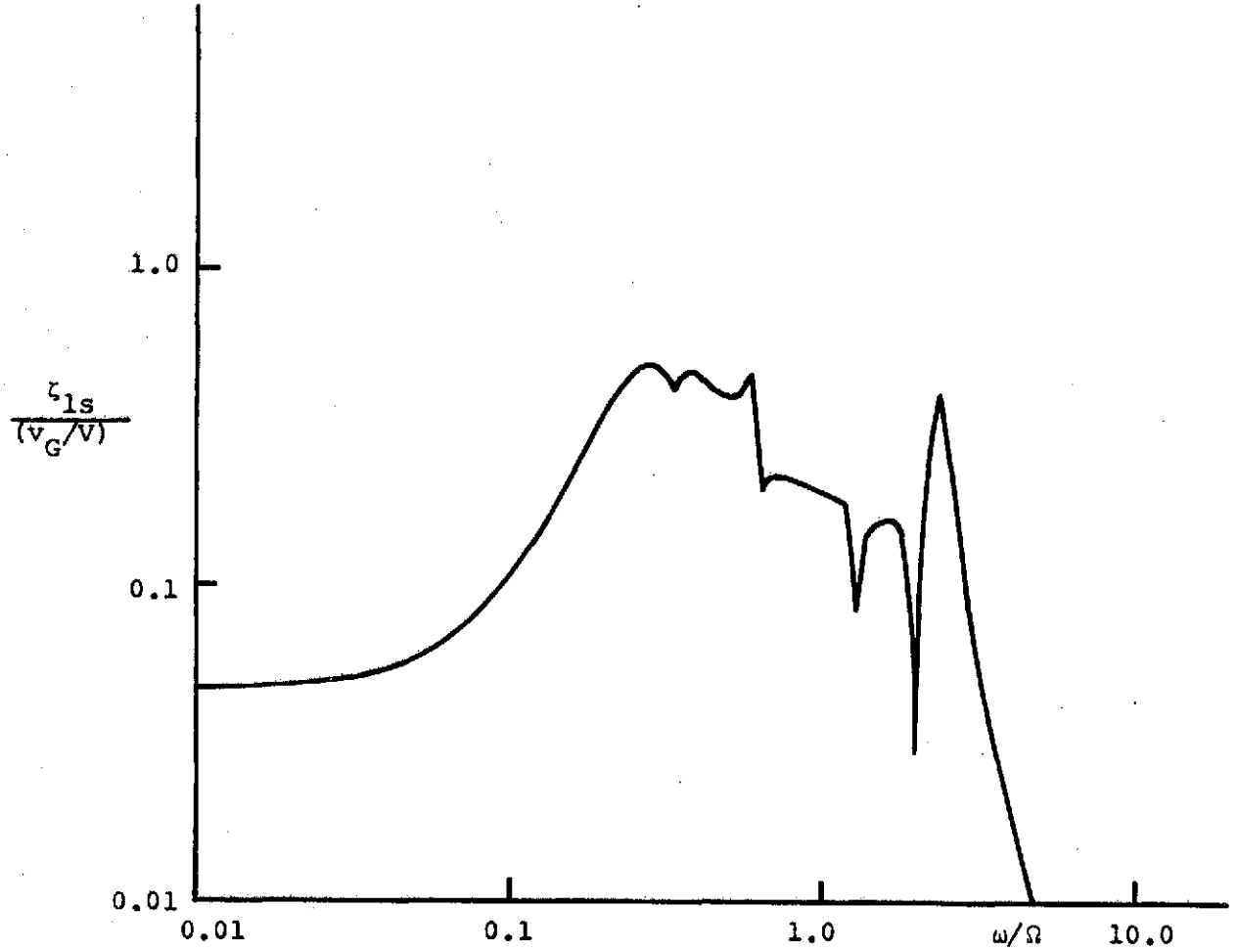

(f) Cyclic Lagging Motion ζ_{1s} Response to v_G

FIG. 26 CONTINUED

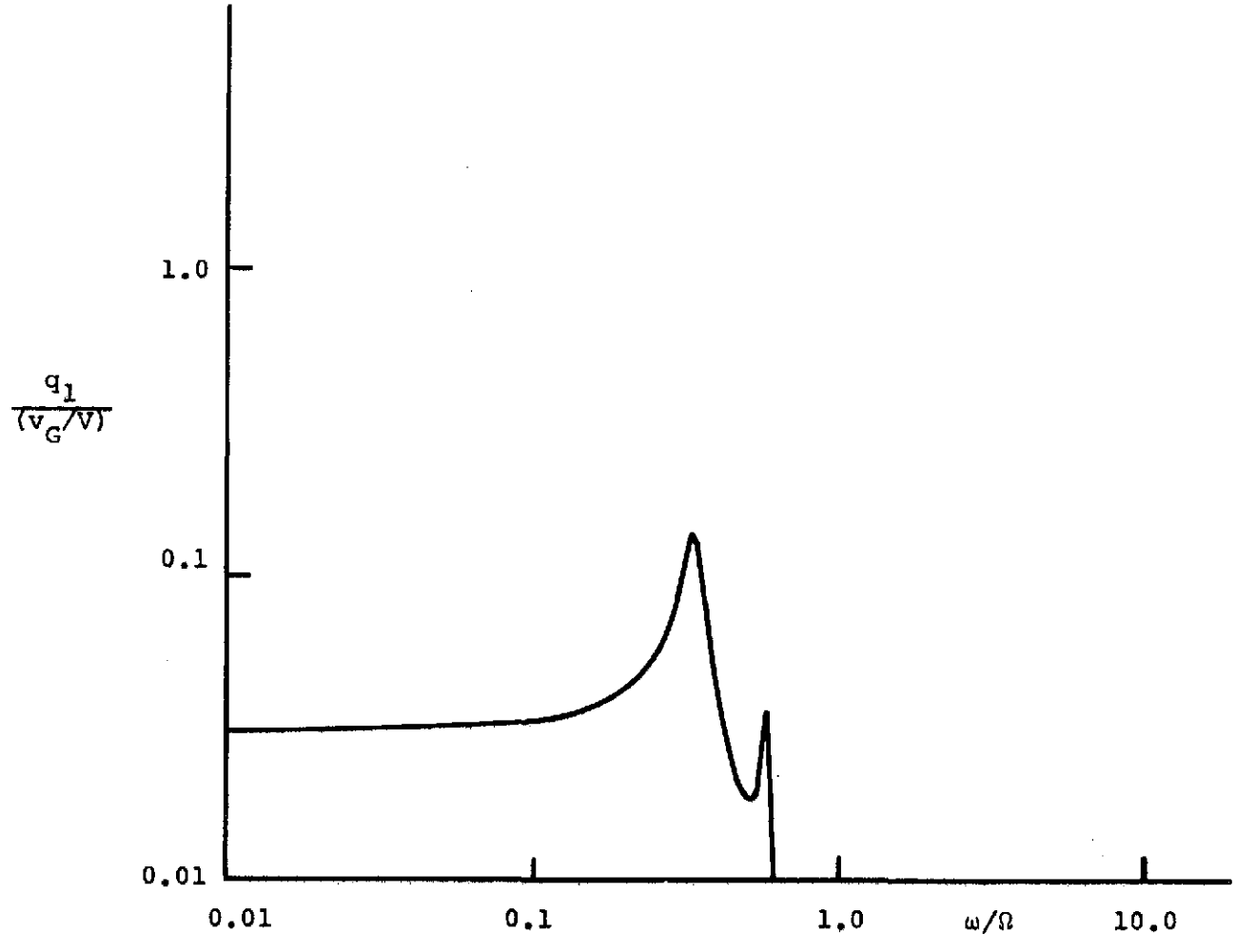

(g) Wing Vertical Bending q_1 Response to v_G

FIG. 26 CONTINUED

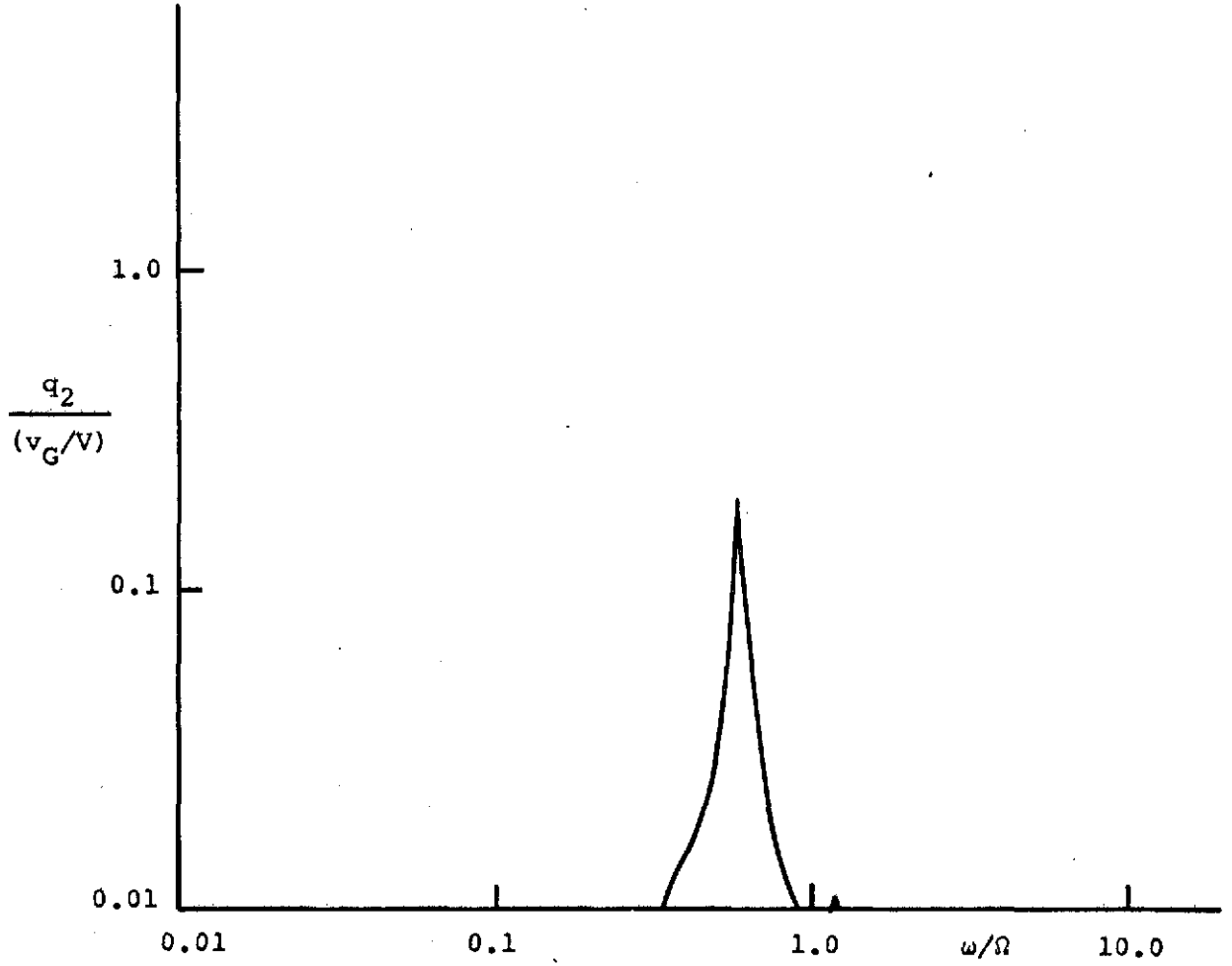

(h) Wing Chordwise Bending q_2 Response to v_G

FIG. 26 CONTINUED

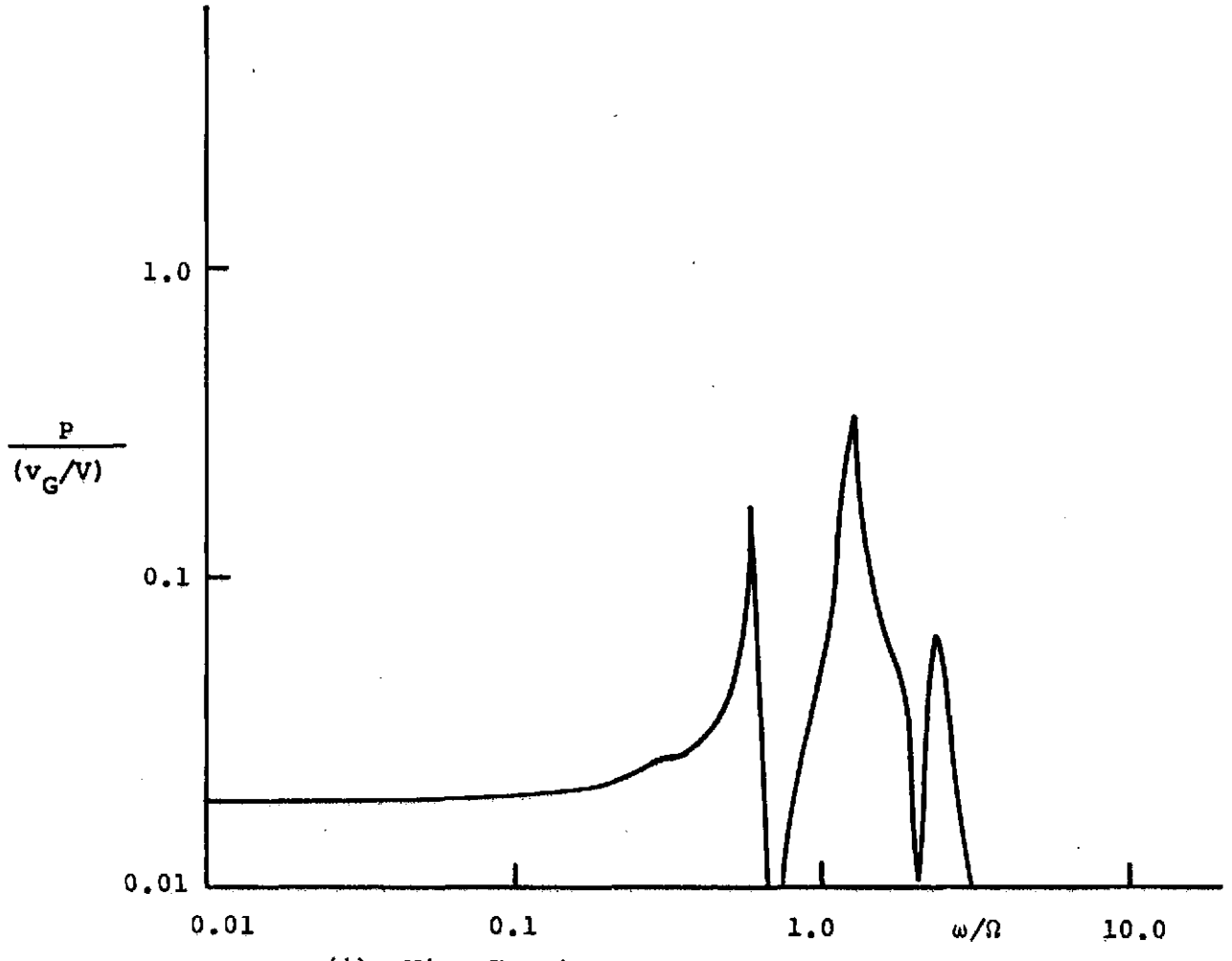

(i) Wing Torsion p Response to v_G

FIG. 26 CONCLUDED

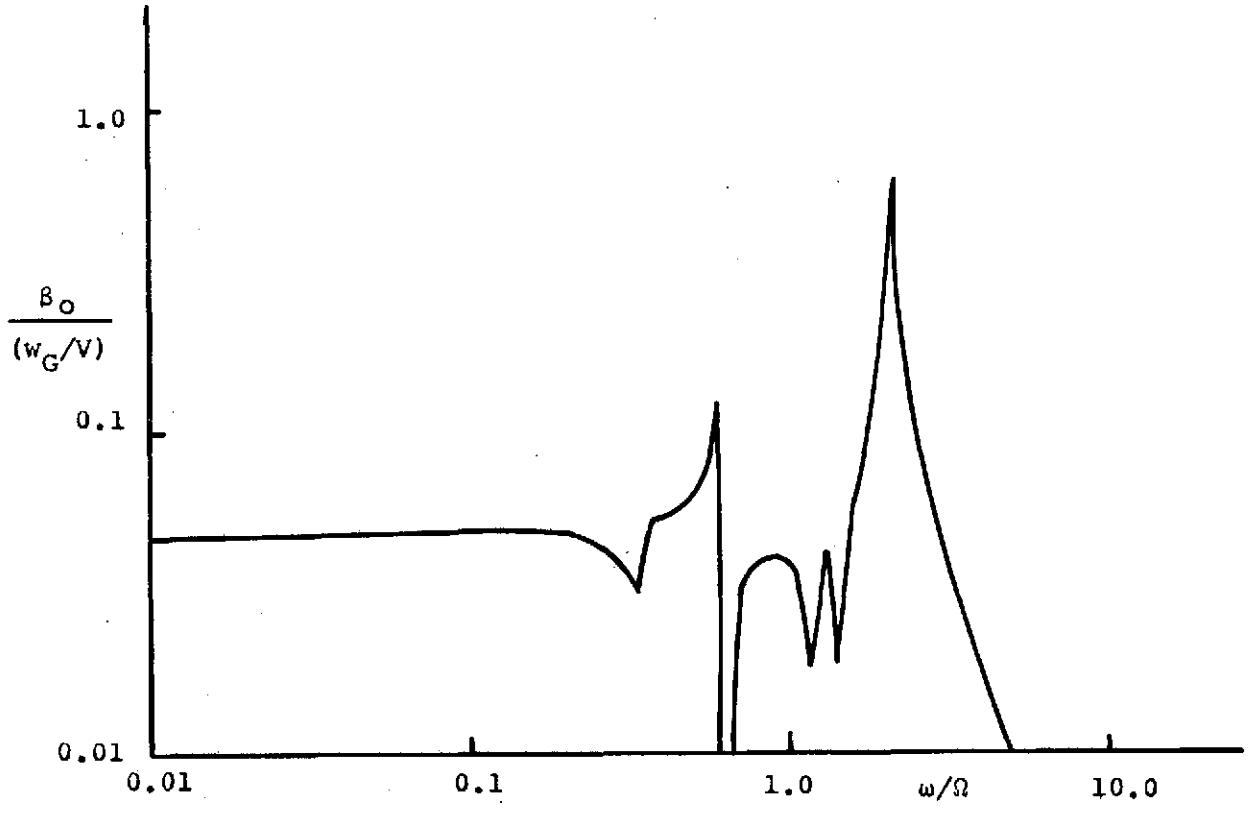

(a) Collective Flapping Motion β_o Response to w_G

FIG. 27 FREQUENCY RESPONSE OF BELL ROTOR TO LONGITUDINAL GUST w_G INPUT AT FREQUENCY ω

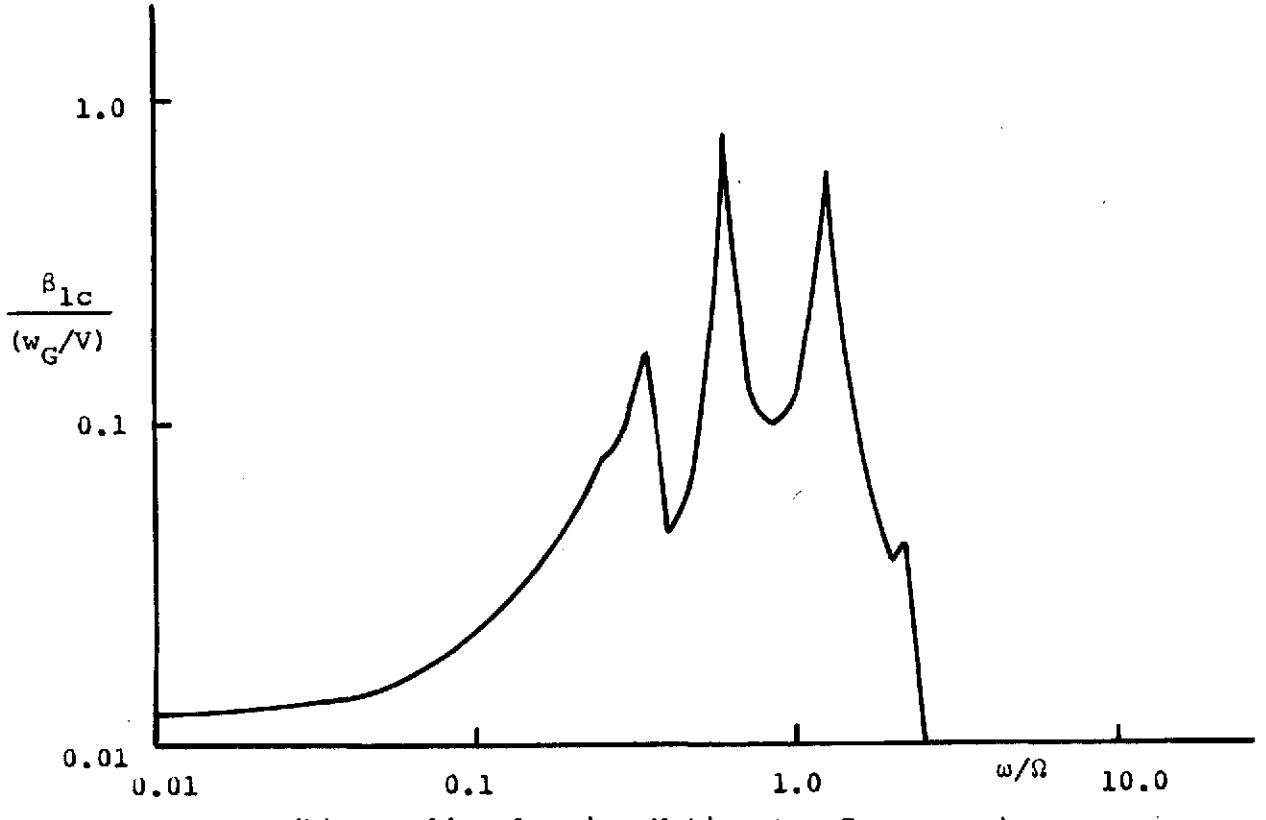

(b) Cyclic Flapping Motion β_{1c} Response to w_G

FIG. 27 CONTINUED

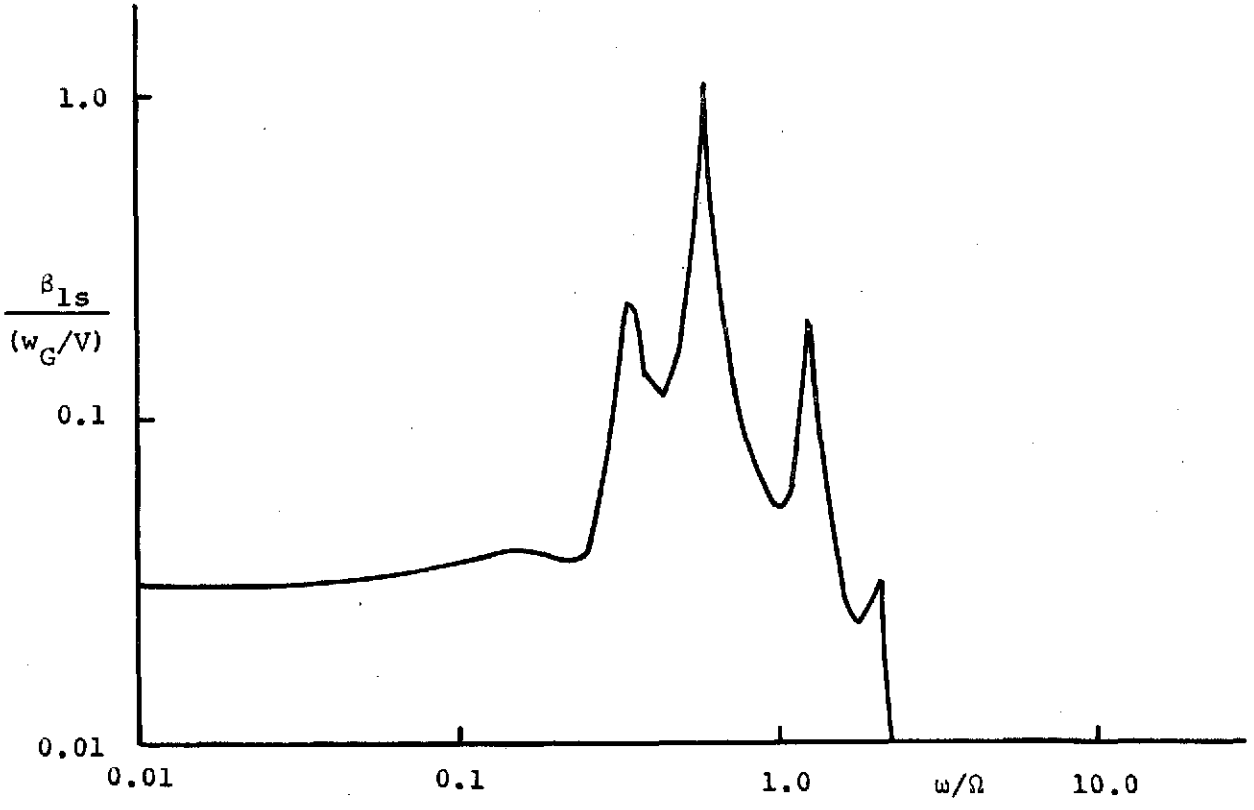

(c) Cyclic Flapping Motion β_{1s} Response to w_G

FIG. 27 CONTINUED

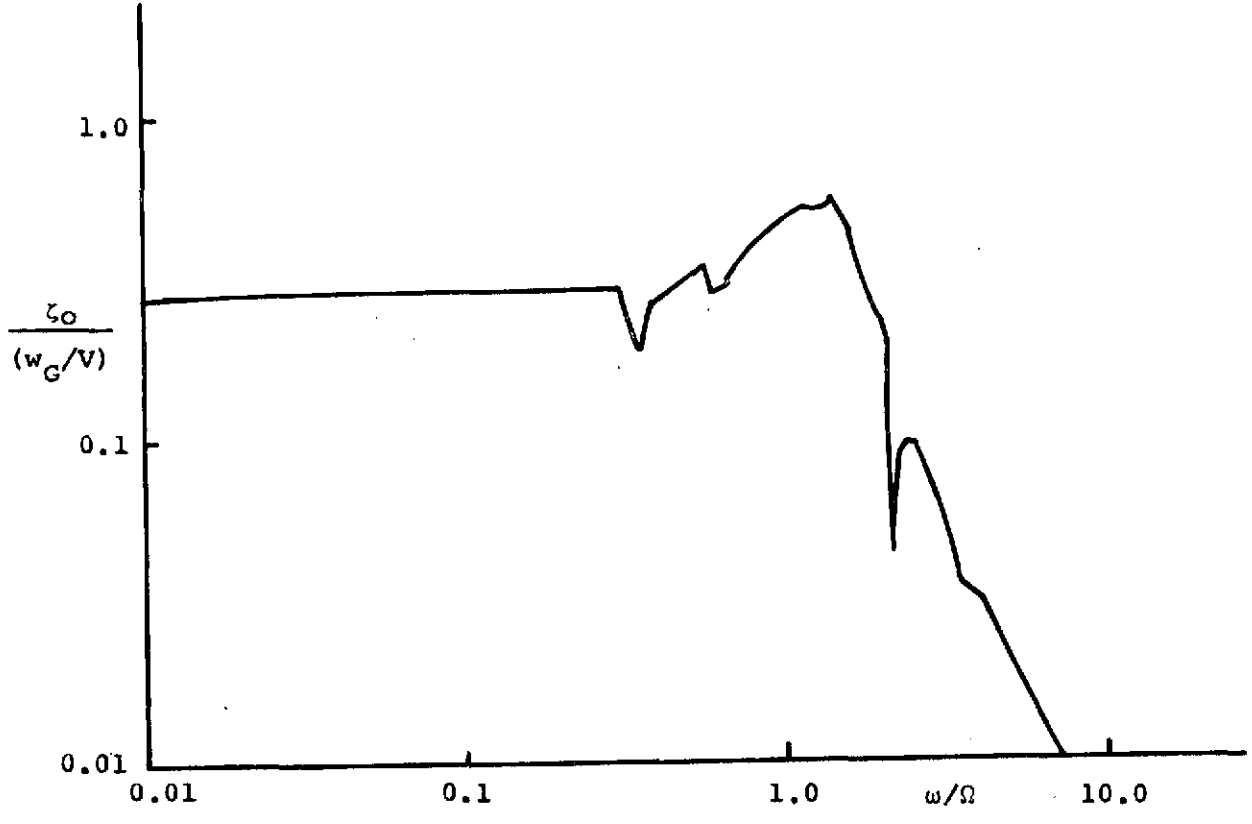

(d) Collective Lagging Motion ζ_o Response to w_G

FIG. 27 CONTINUED

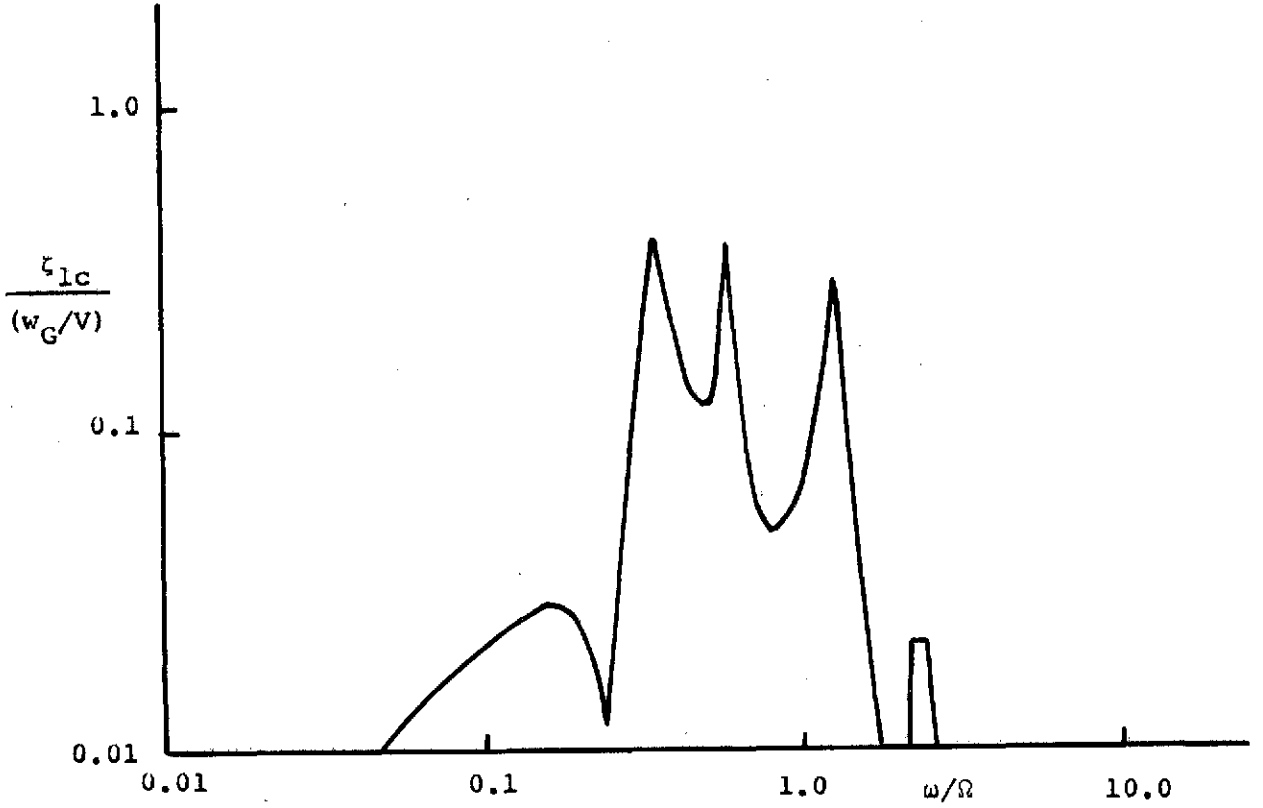

(e) Cyclic Lagging Motion ζ_{1c} Response to w_G

FIG. 27 CONTINUED

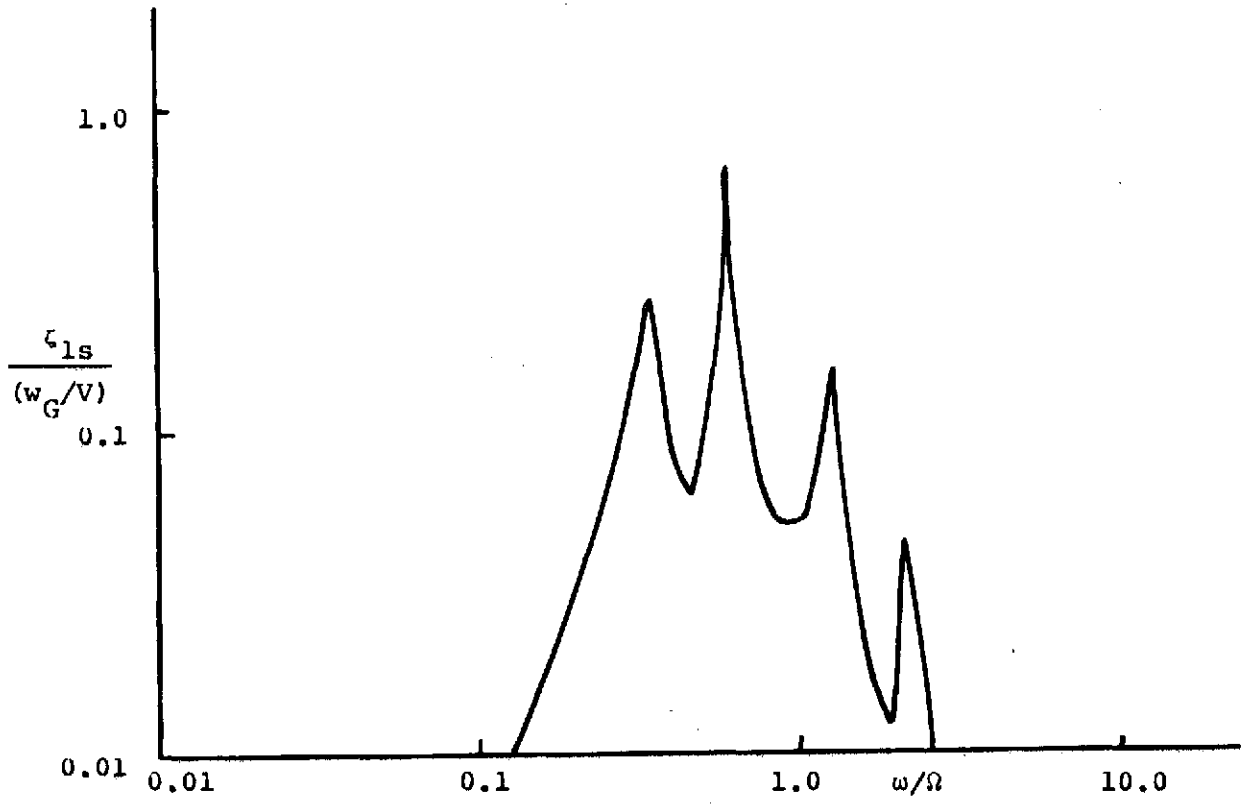

(f) Cyclic Lagging Motion ζ_{1s} Response to w_G

FIG. 27 CONTINUED

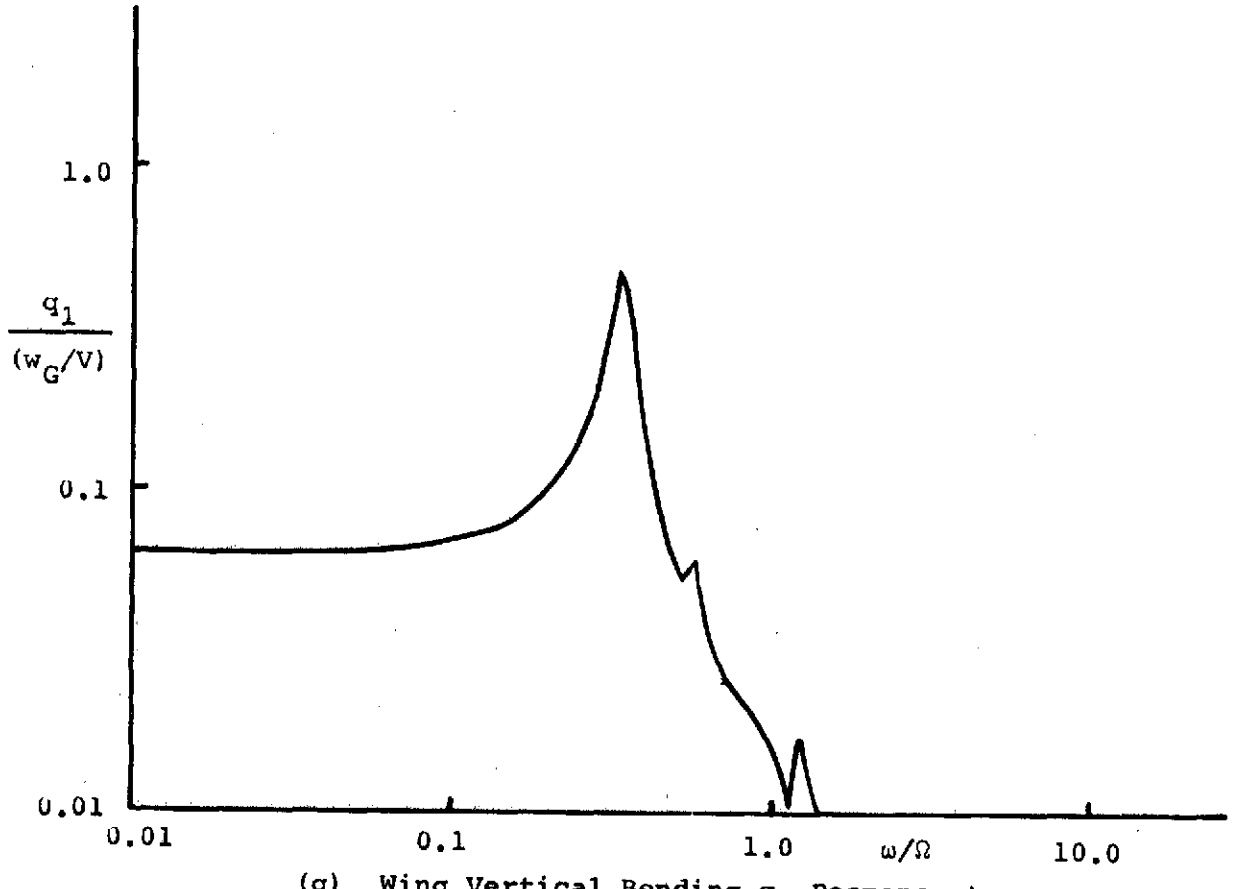

(g) Wing Vertical Bending q_1 Response to w_G

FIG. 27 CONTINUED

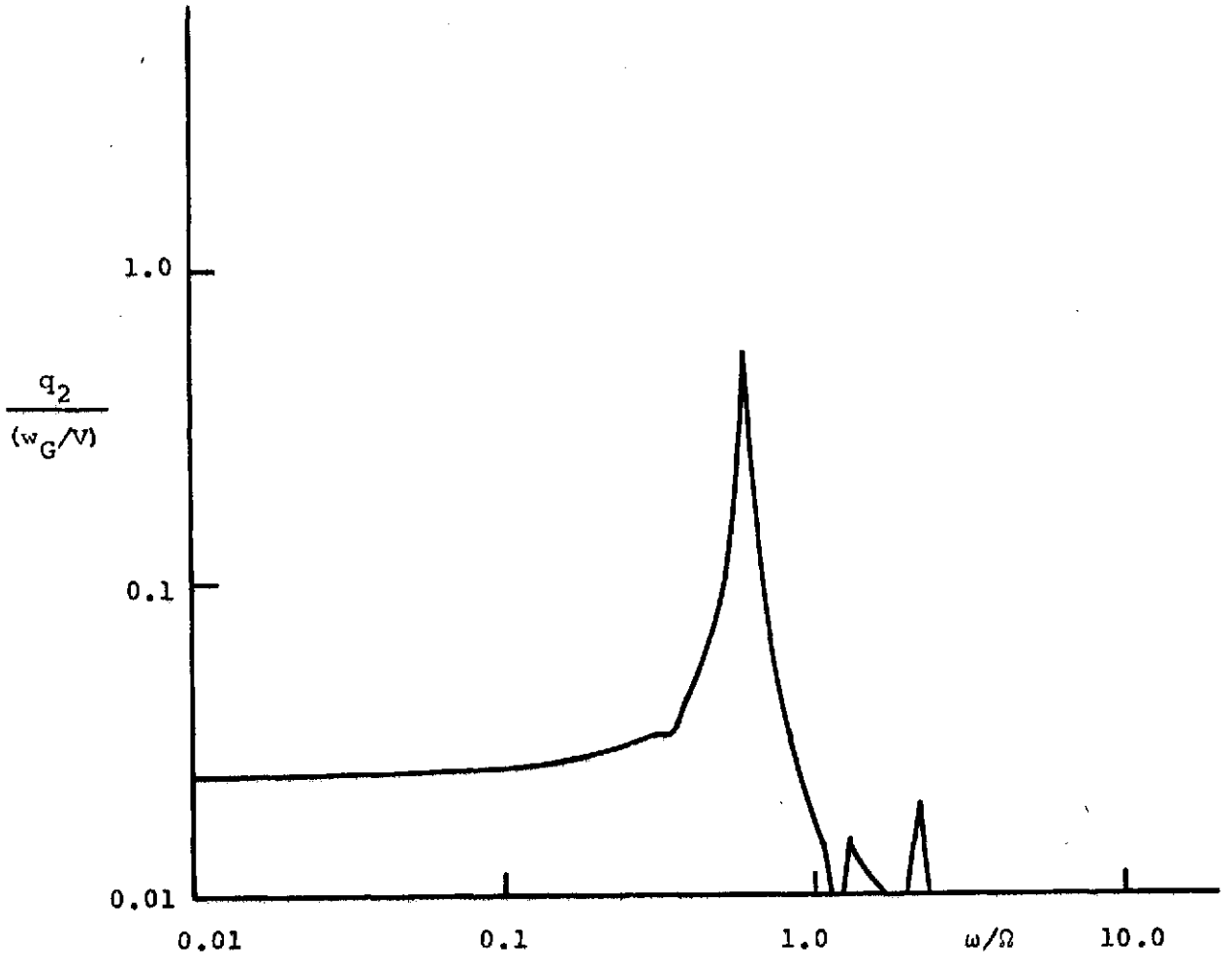

(h) Wing Chordwise Bending q_2 Response to w_G

FIG. 27 CONTINUED

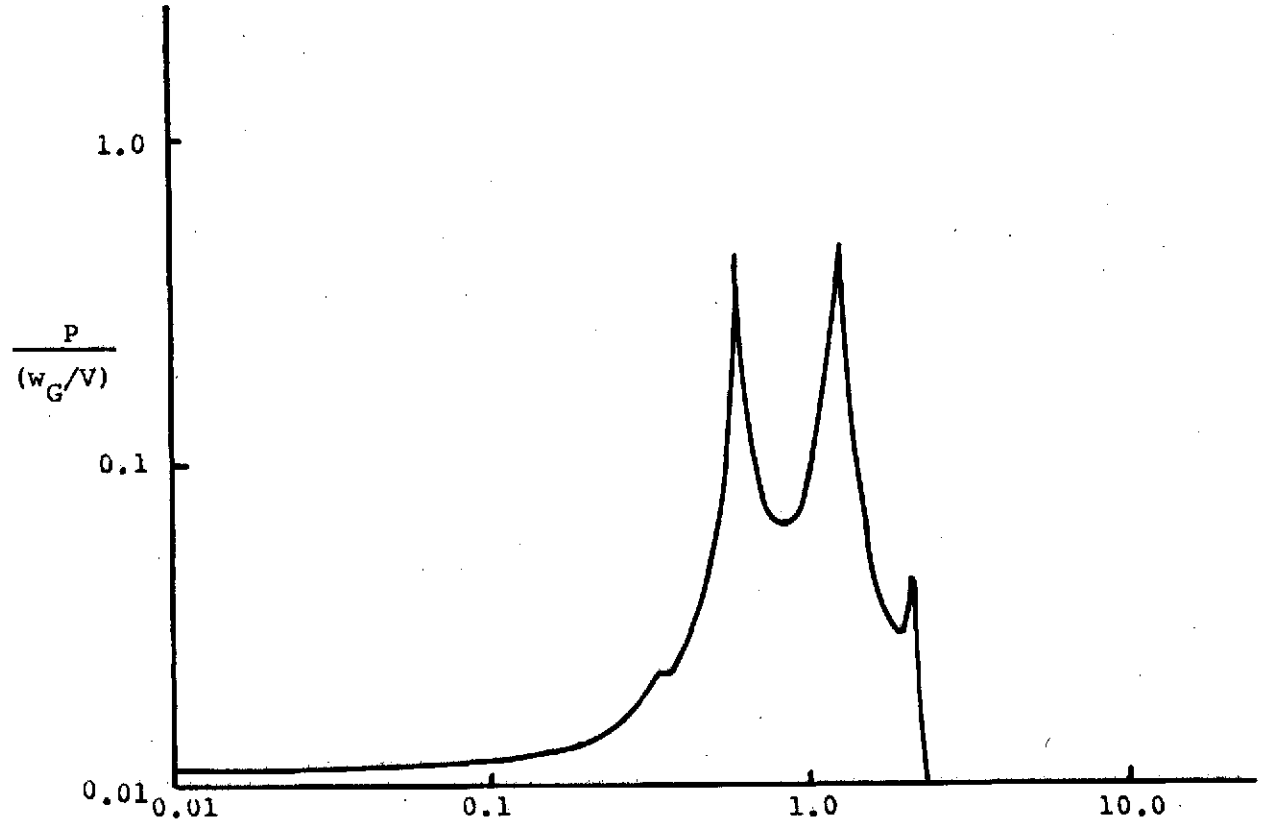

(i) Wing Torsion p Response to w_G

FIG. 27 CONCLUDED

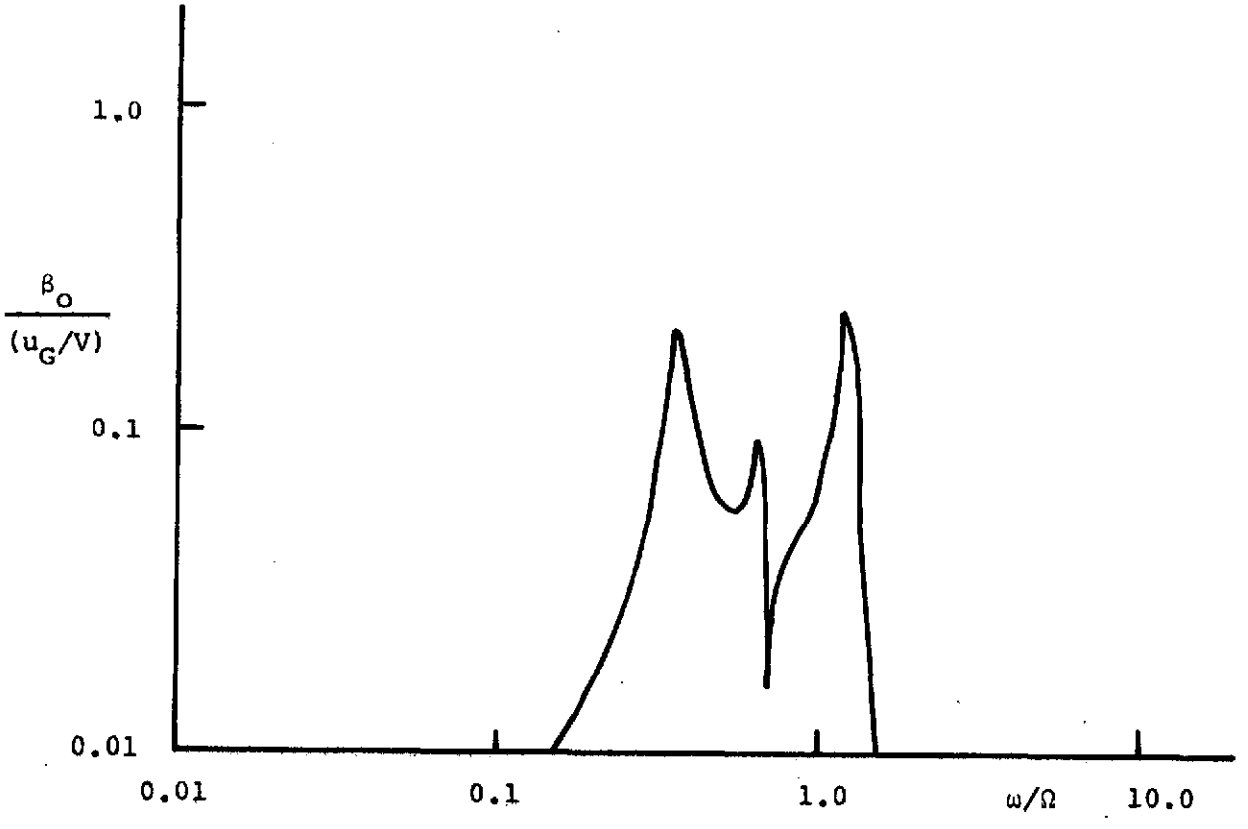

(a) Collective Flapping Motion β_o Response

FIG. 28 FREQUENCY RESPONSE OF BOEING ROTOR TO VERTICAL GUST u_G INPUT AT FREQUENCY ω

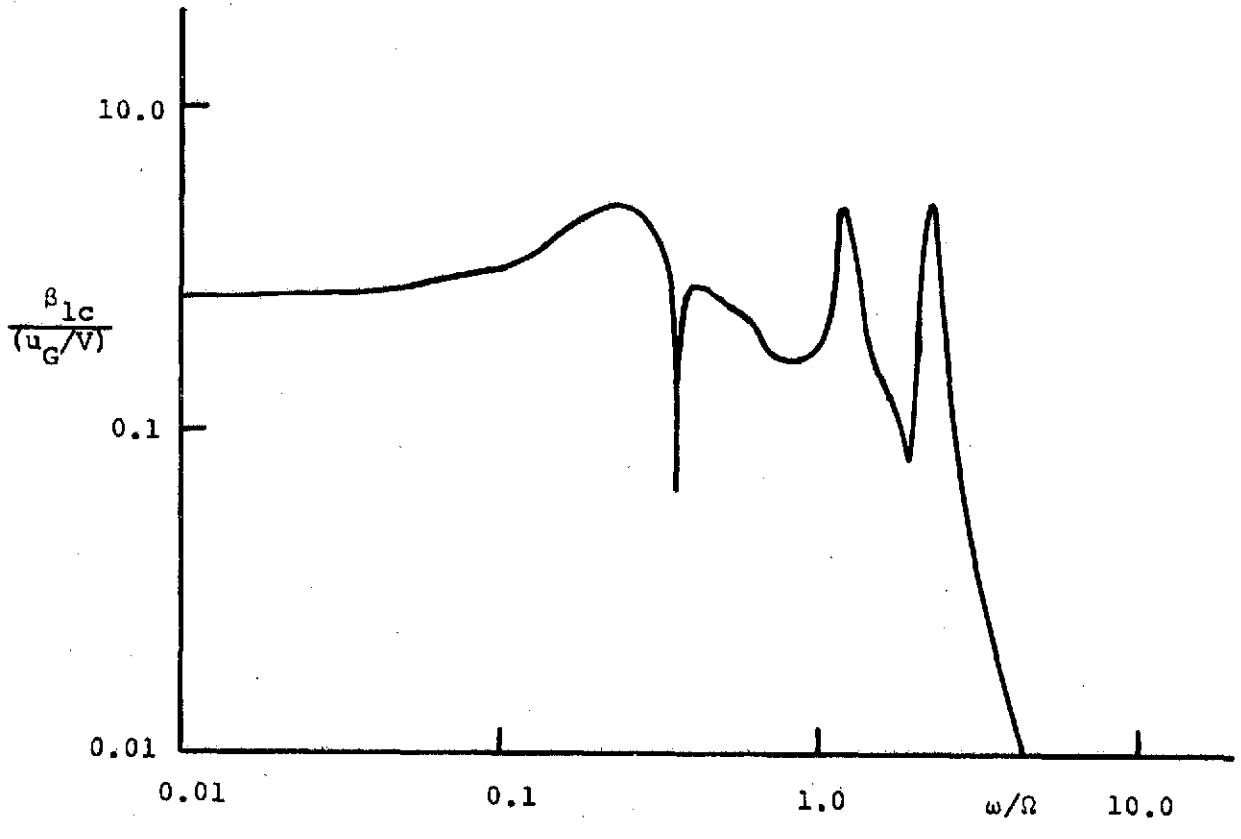

(b) Cyclic Flapping Motion β_{1c} Response to u_G

FIG. 28 CONTINUED

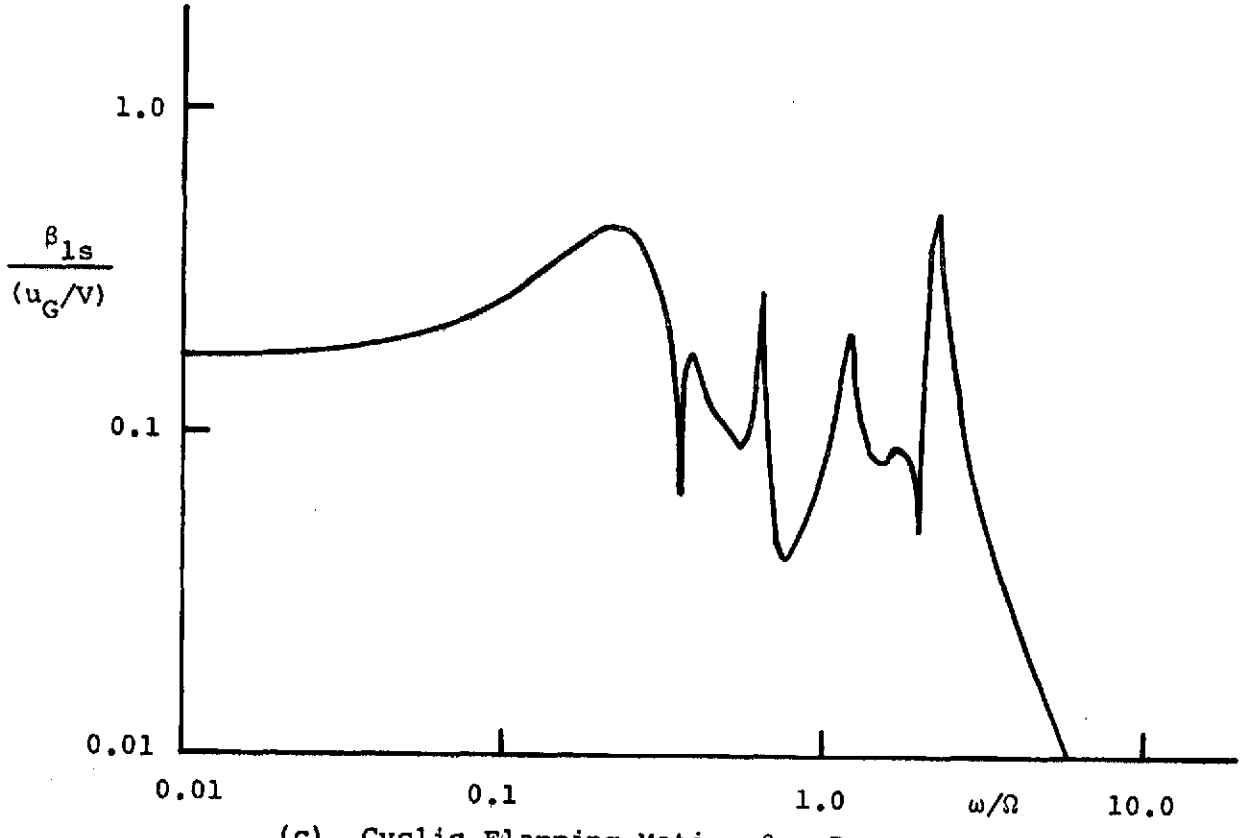

(c) Cyclic Flapping Motion β_{1s} Response to u_G

FIG. 28 CONTINUED

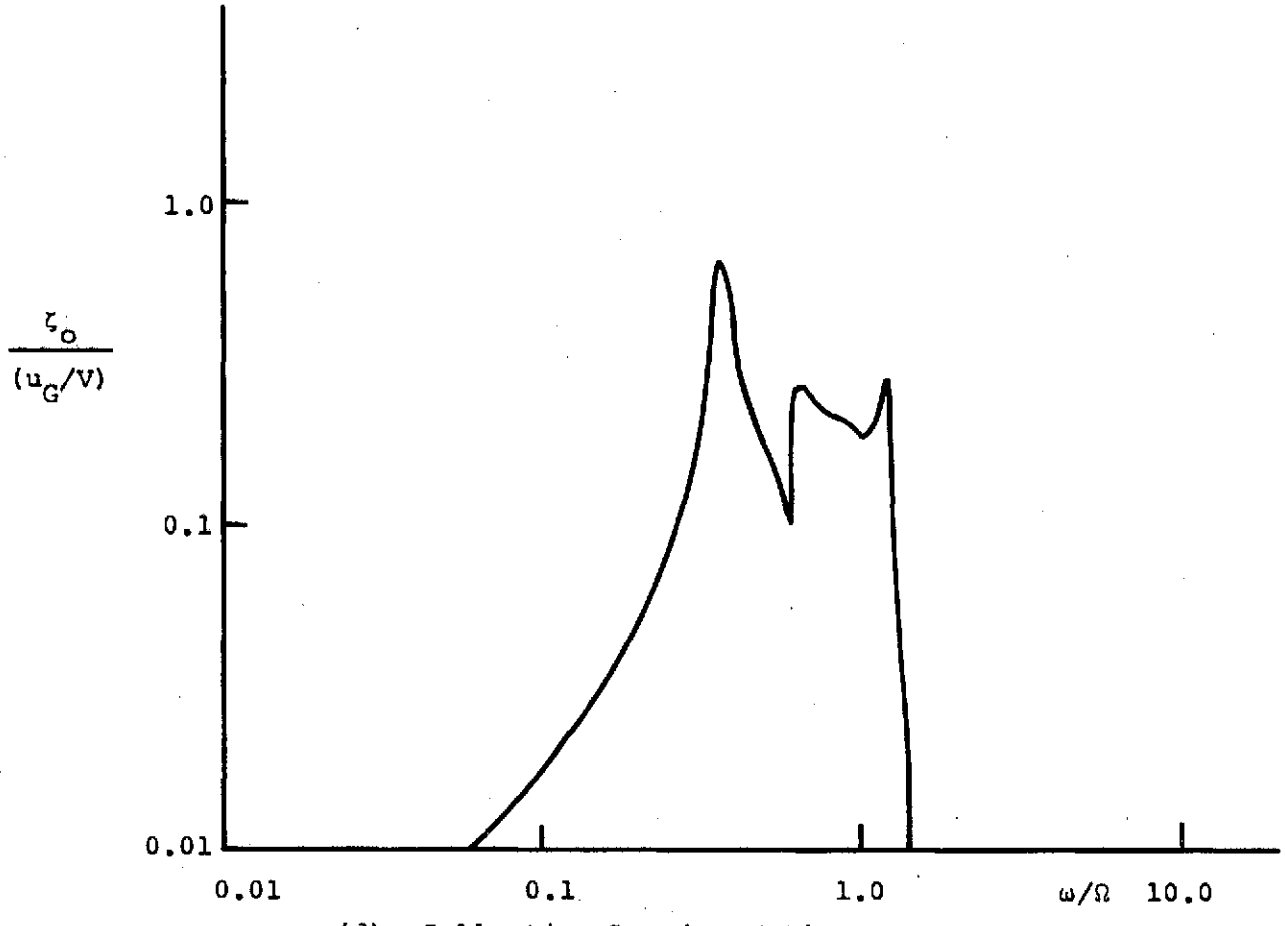

(d) Collective Lagging Motion ζ_o Response

FIG. 28 CONTINUED

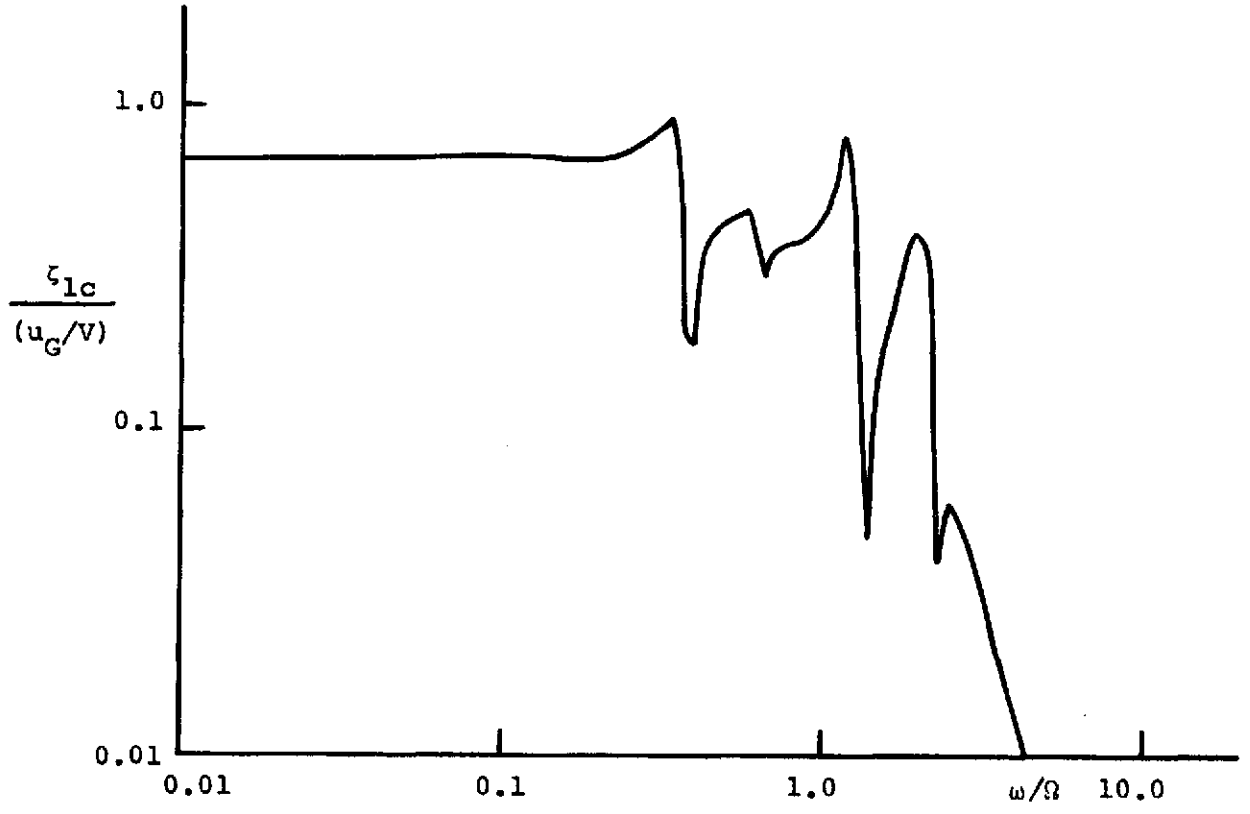

(e) Cyclic Lagging Motion ζ_{1c} Response to u_G

FIG. 28 CONTINUED

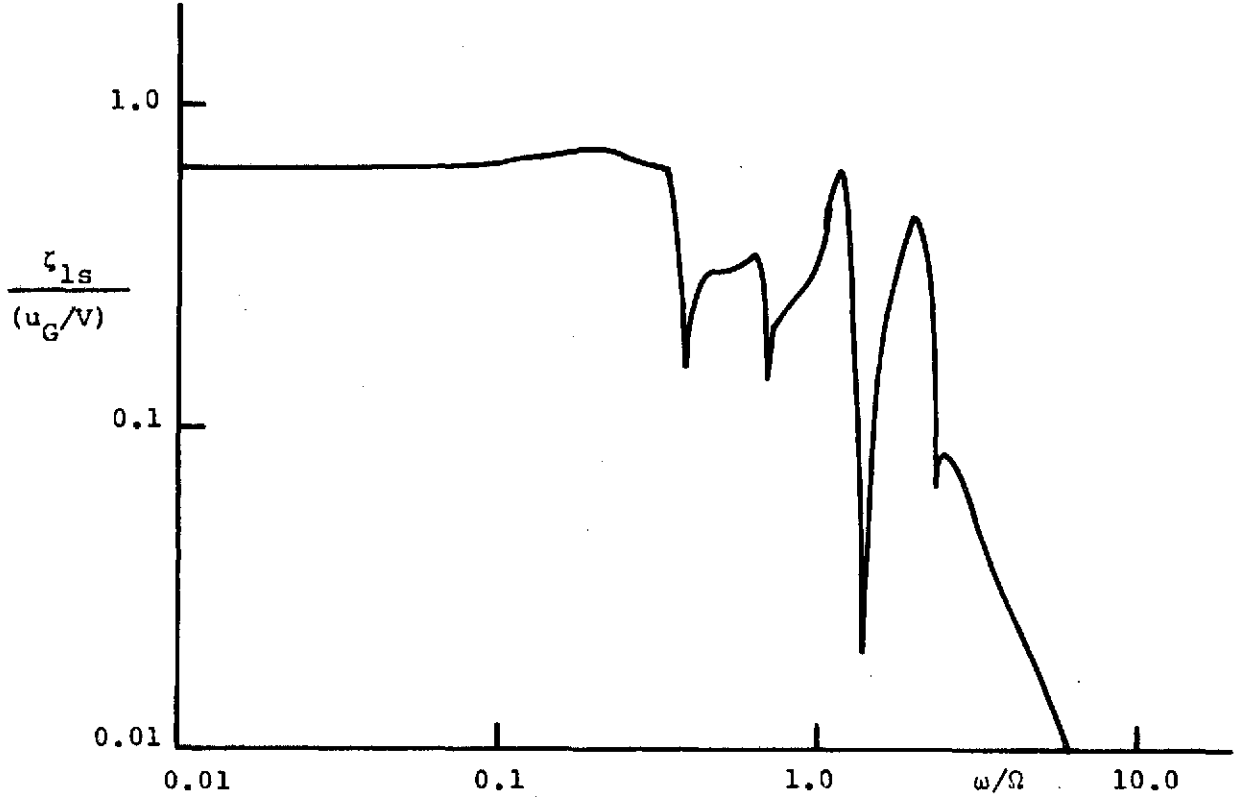

(f) Cyclic Lagging Motion ζ_{1s} Response to u_G

FIG. 28 CONTINUED

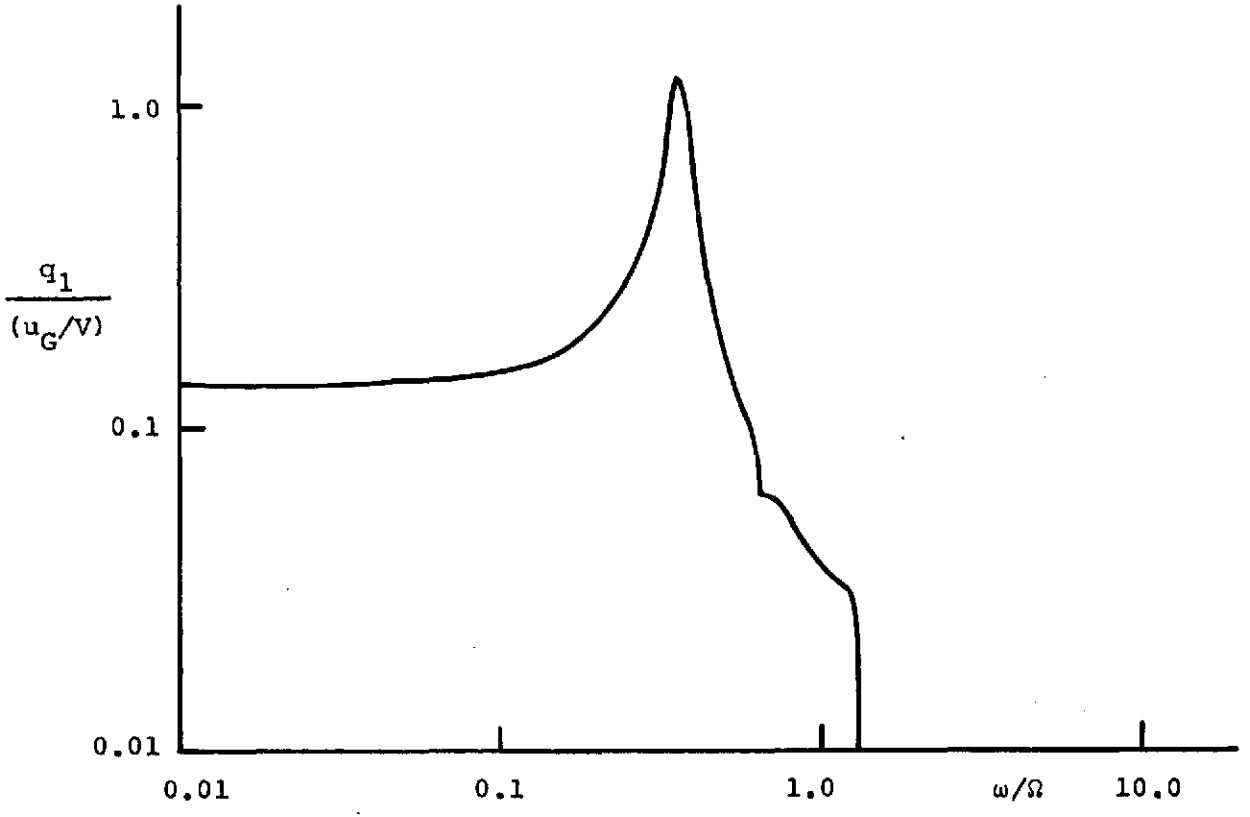

(g) Wing Vertical Bending q_1 Response to u_G

FIG. 28 CONTINUED

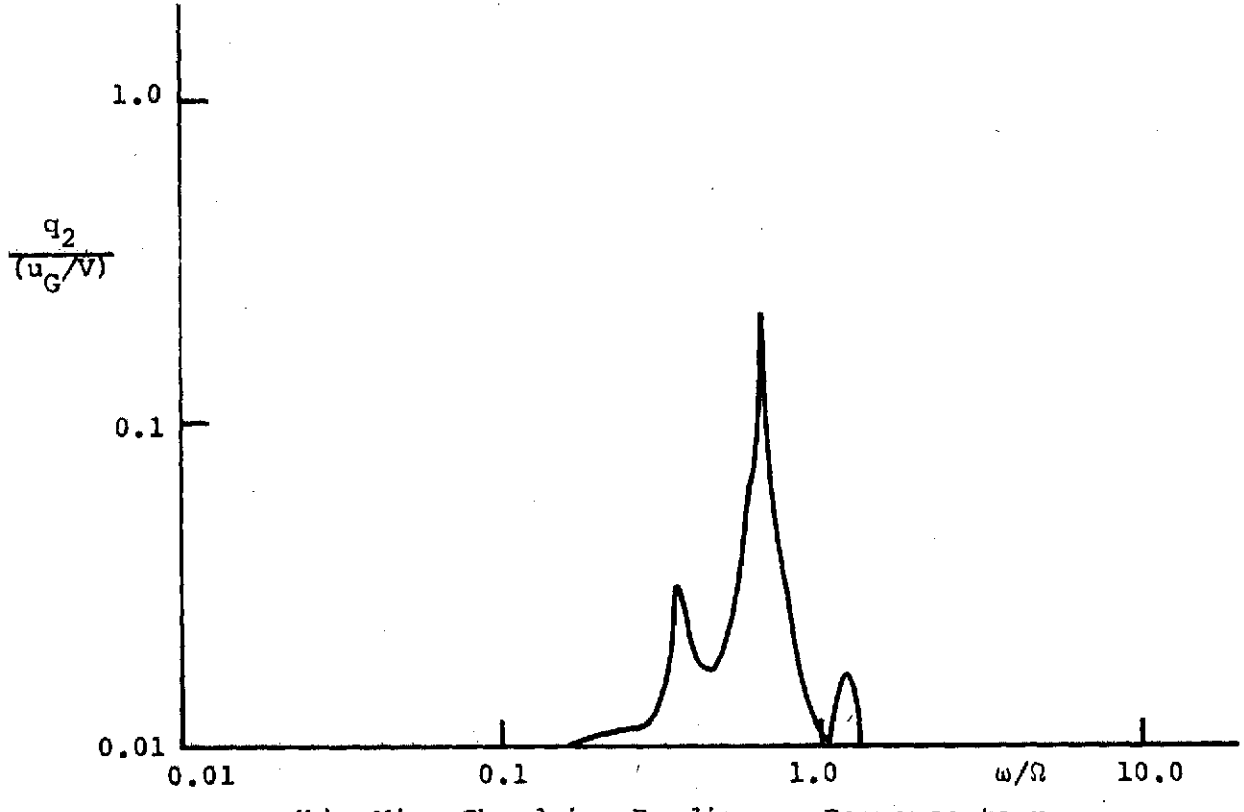

(h) Wing Chordwise Bending q_2 Response to u_G

FIG. 28 CONTINUED

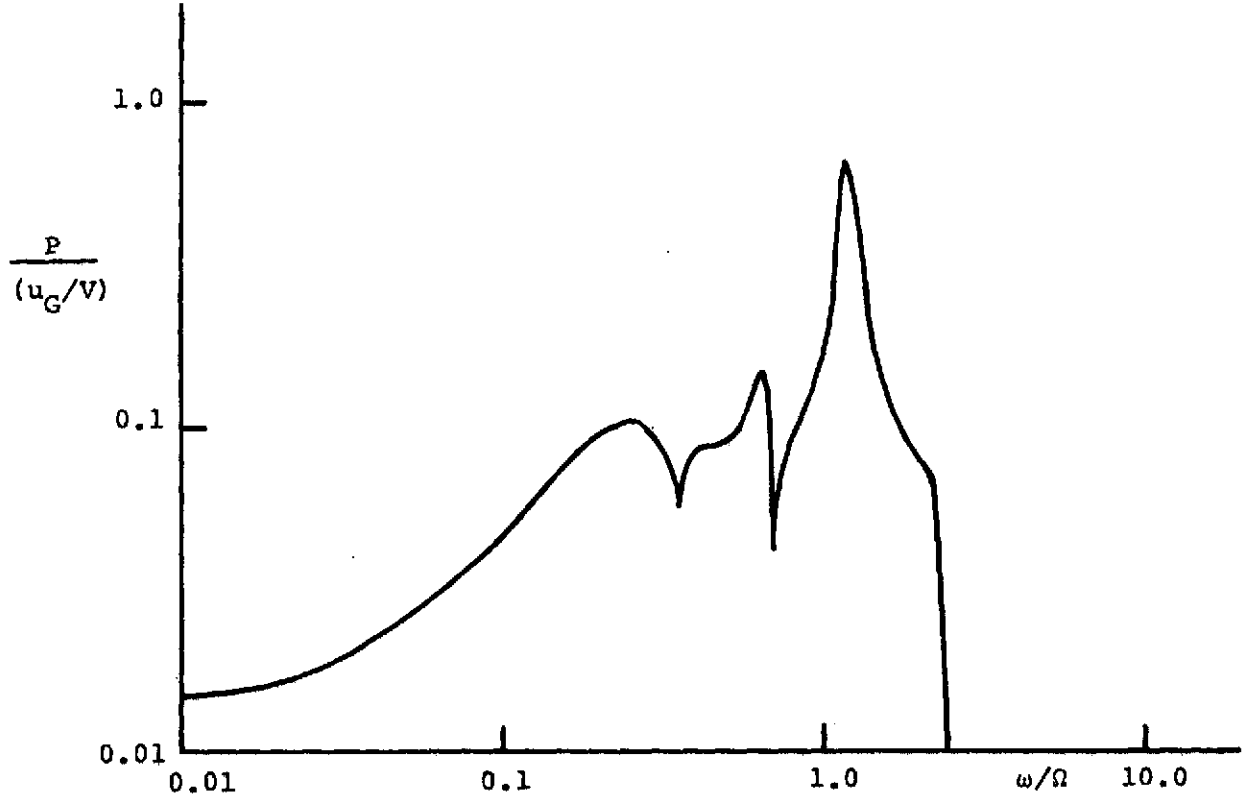

(i) Wing Torsion p Response to u_G

FIG. 28 CONCLUDED

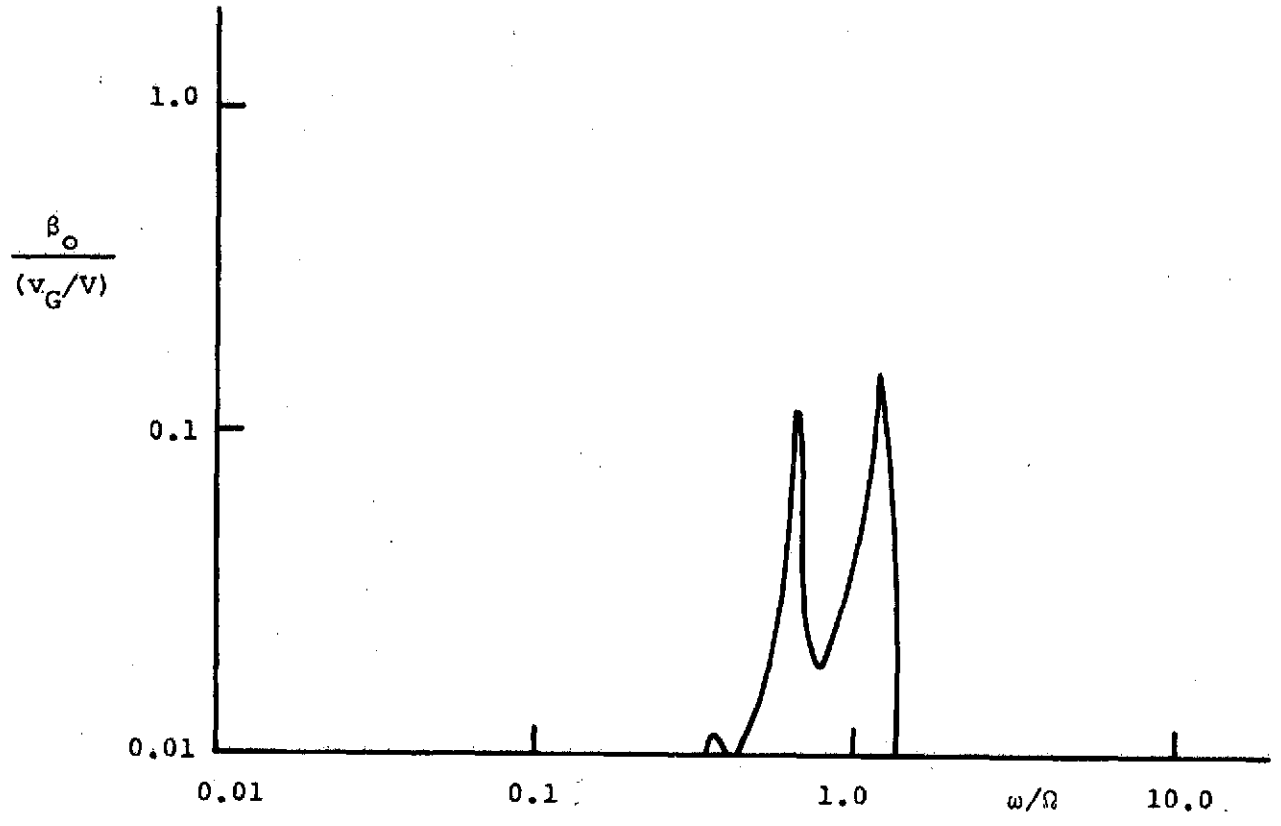

(a) Collective Flapping Motion β_o Response

FIG. 29 FREQUENCY RESPONSE OF BOEING ROTOR TO LATERAL GUST v_G INPUT AT FREQUENCY ω

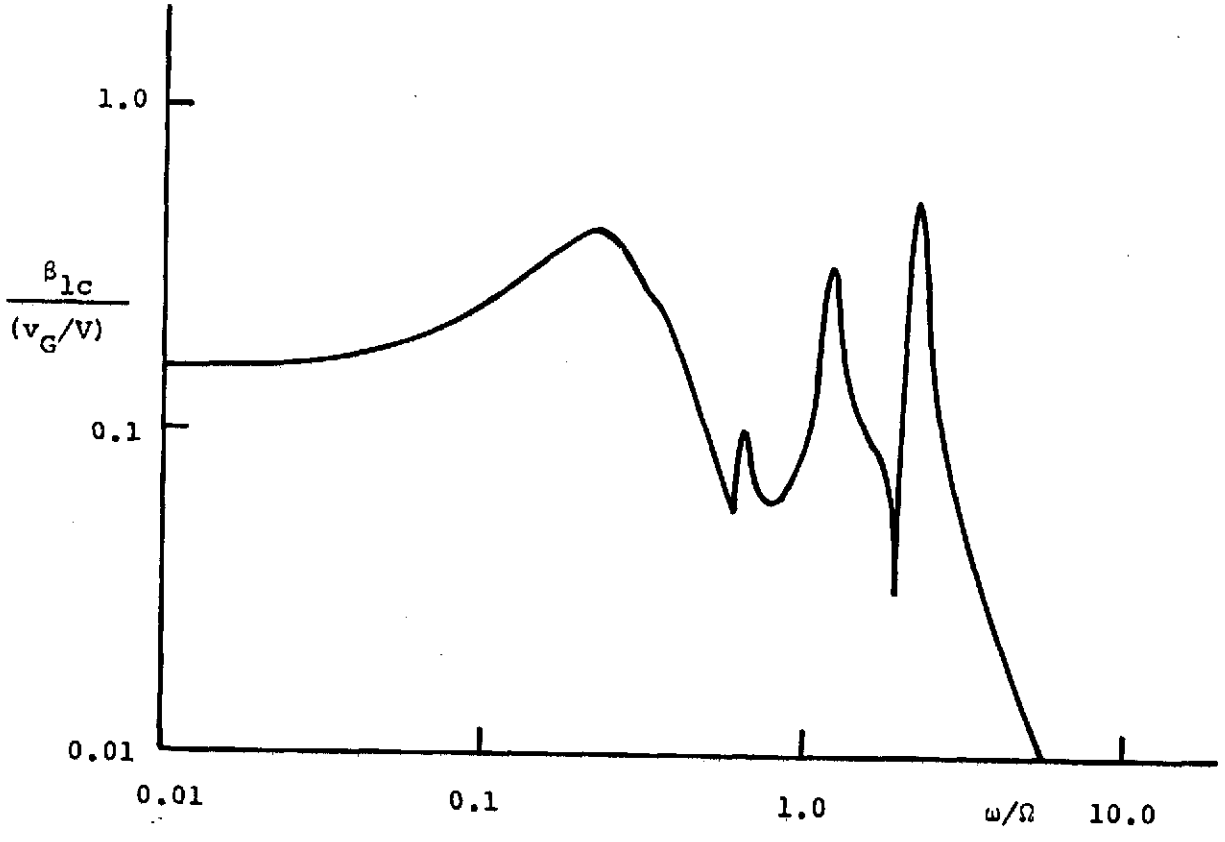

(b) Cyclic Flapping Motion β_{1c} Response to v_G

FIG. 29 CONTINUED

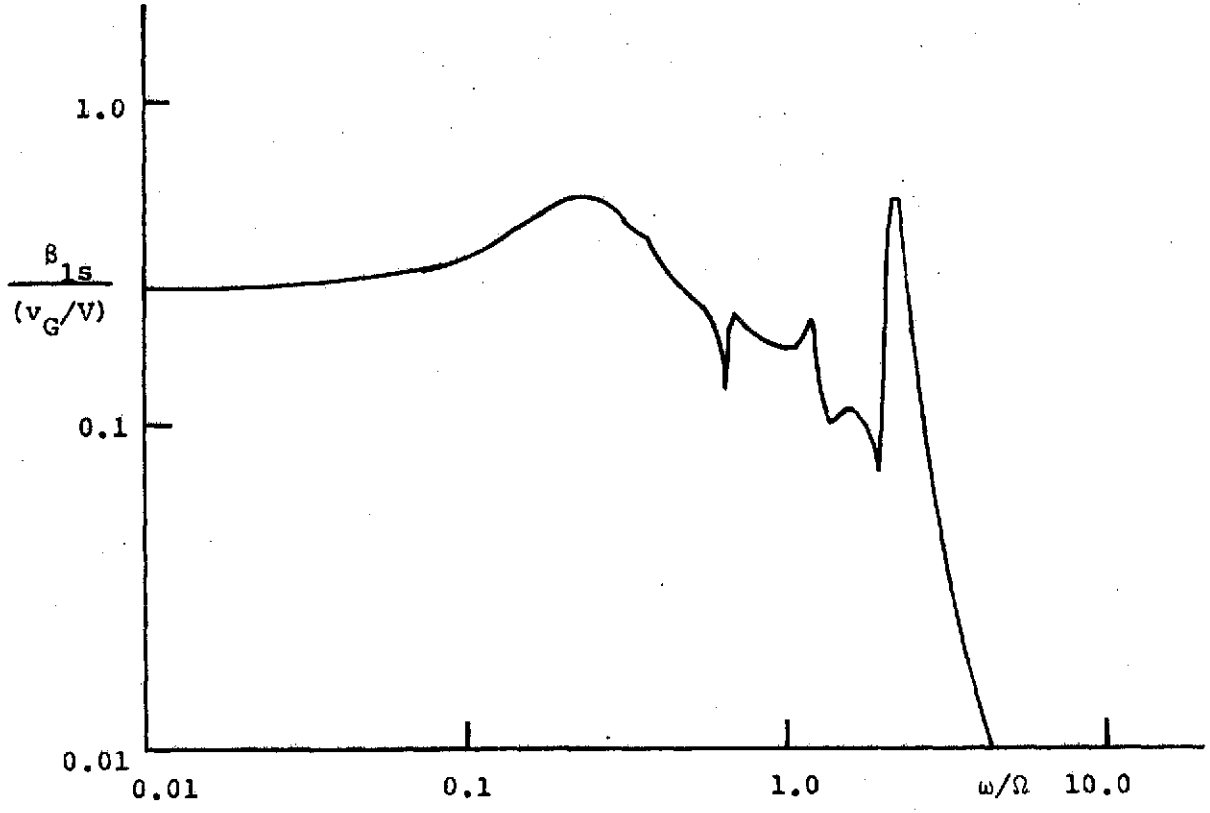

(c) Cyclic Flapping Motion β_{1s} Response to v_G

FIG. 29 CONTINUED

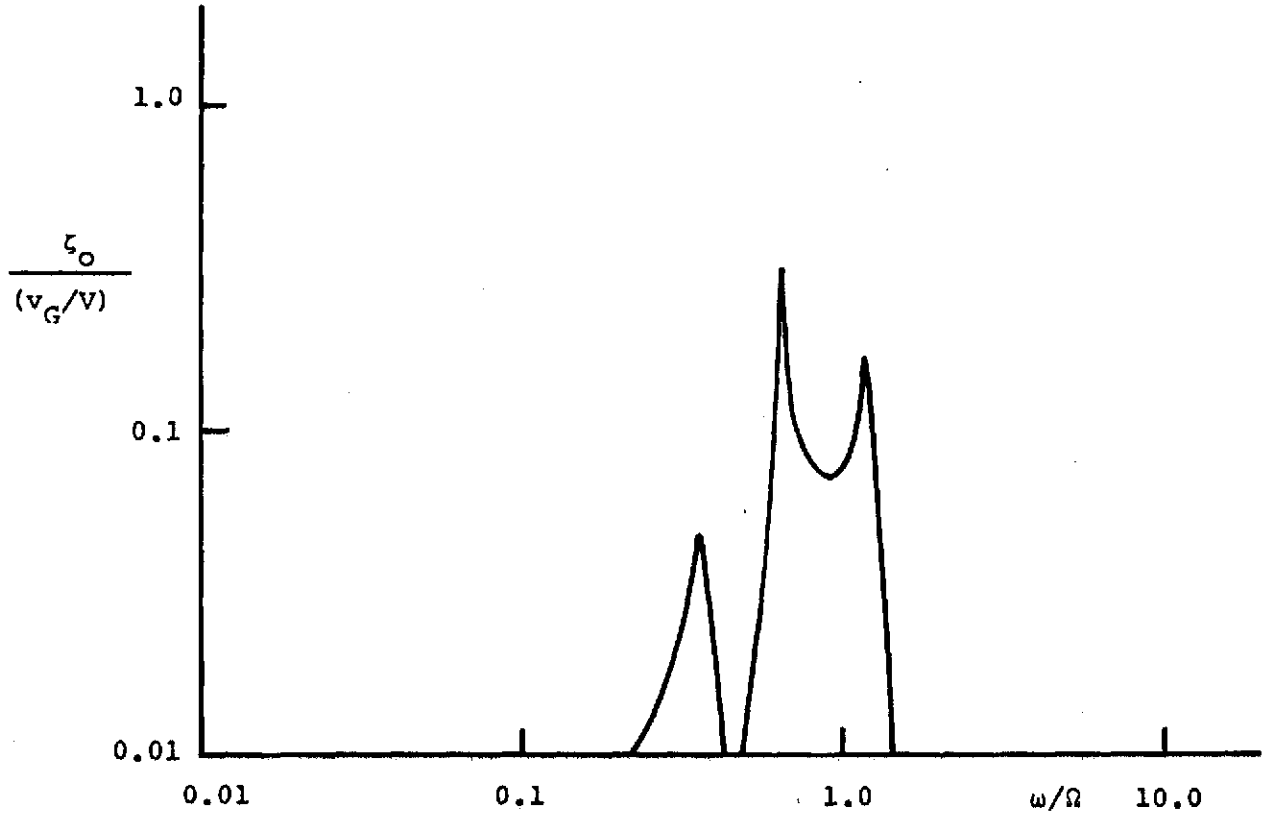

(d) Collective Lagging Motion ζ_o Response to v_G

FIG. 29 CONTINUED

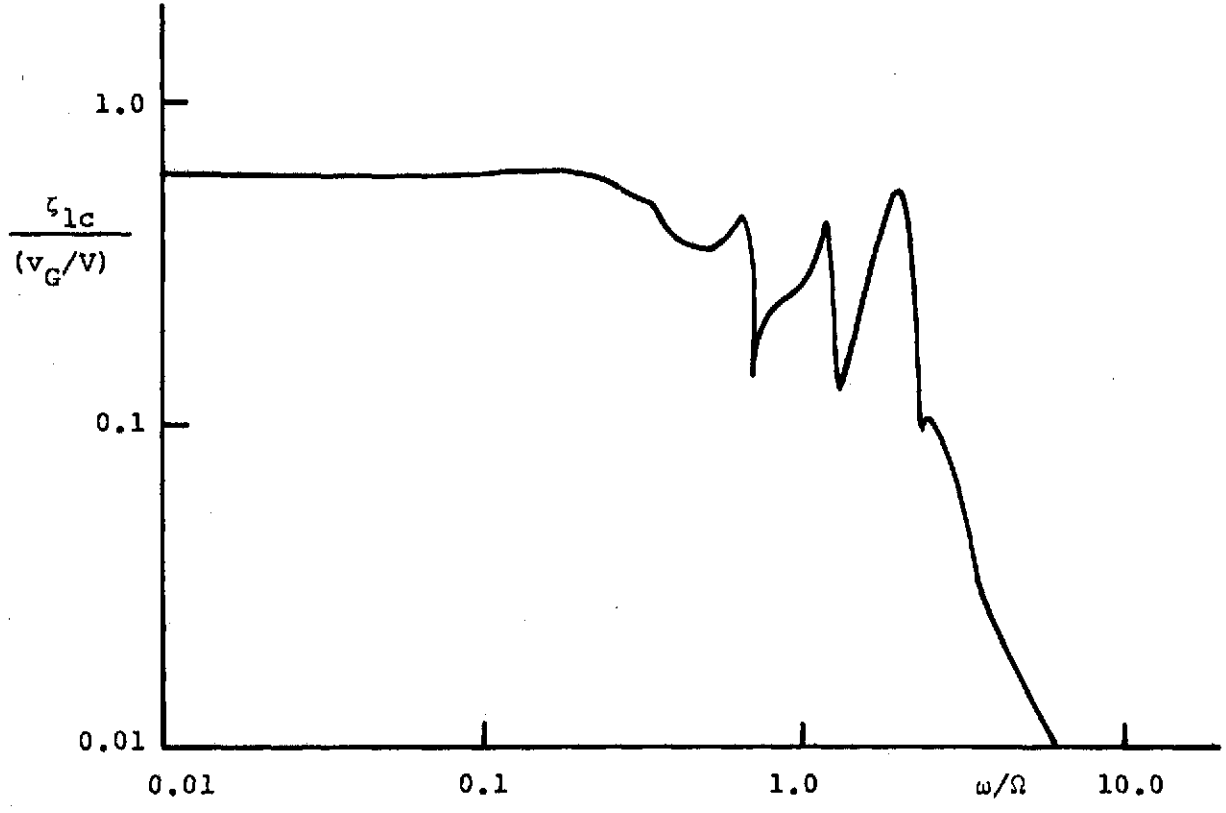

(e) Cyclic Lagging Motion ζ_{1c} Response to v_G

FIG. 29 CONTINUED

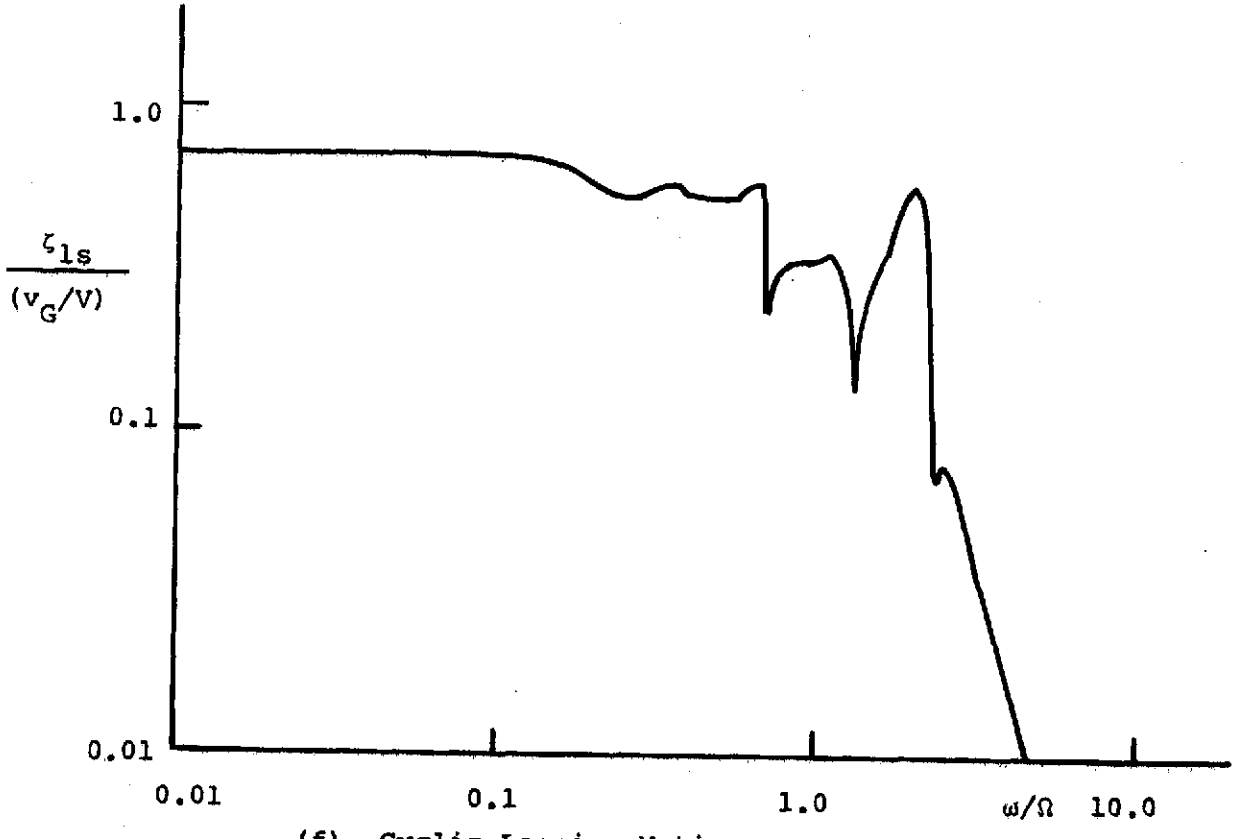

(f) Cyclic Lagging Motion ζ_{1s} Response to v_G

FIG. 29 CONTINUED

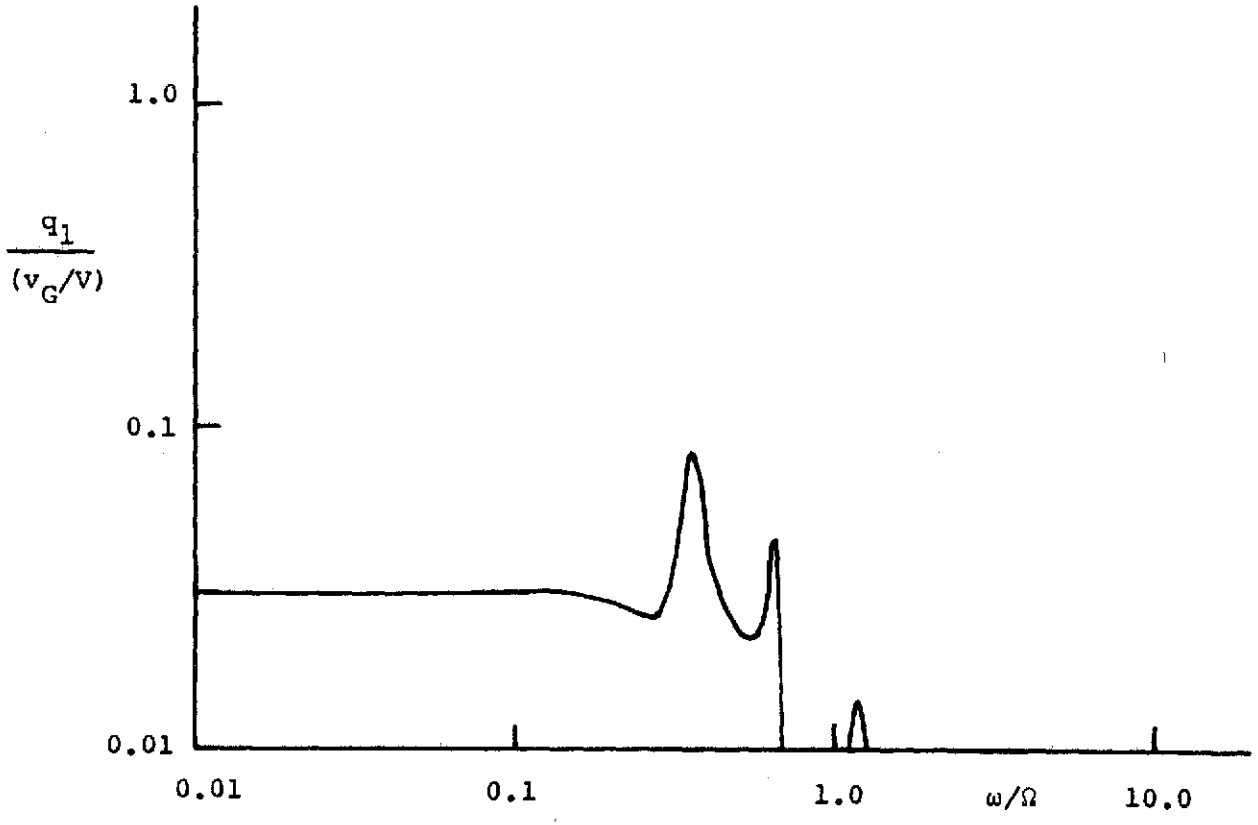

(g) Wing Vertical Bending q_1 Response to v_G

FIG. 29 CONTINUED

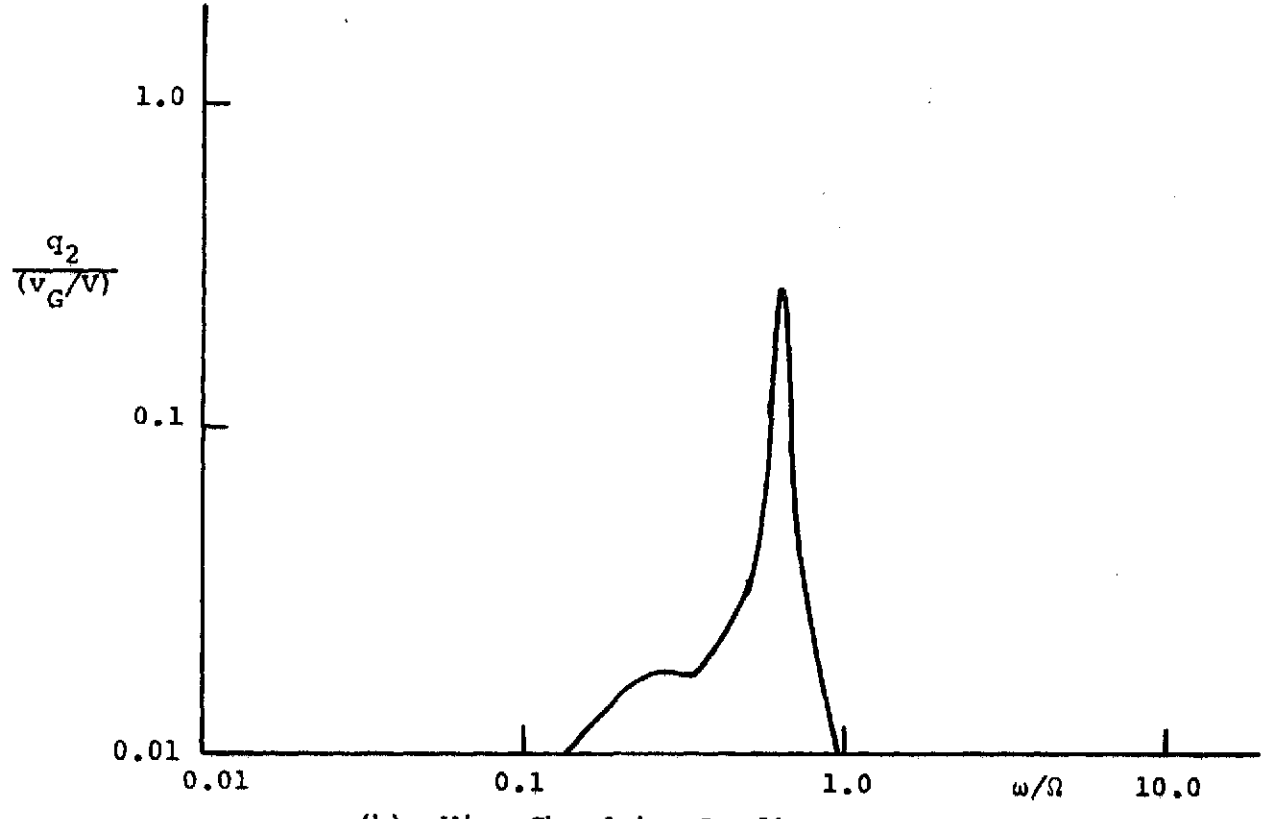

(h) Wing Chordwise Bending q_2 Response to v_G

FIG. 29 CONTINUED

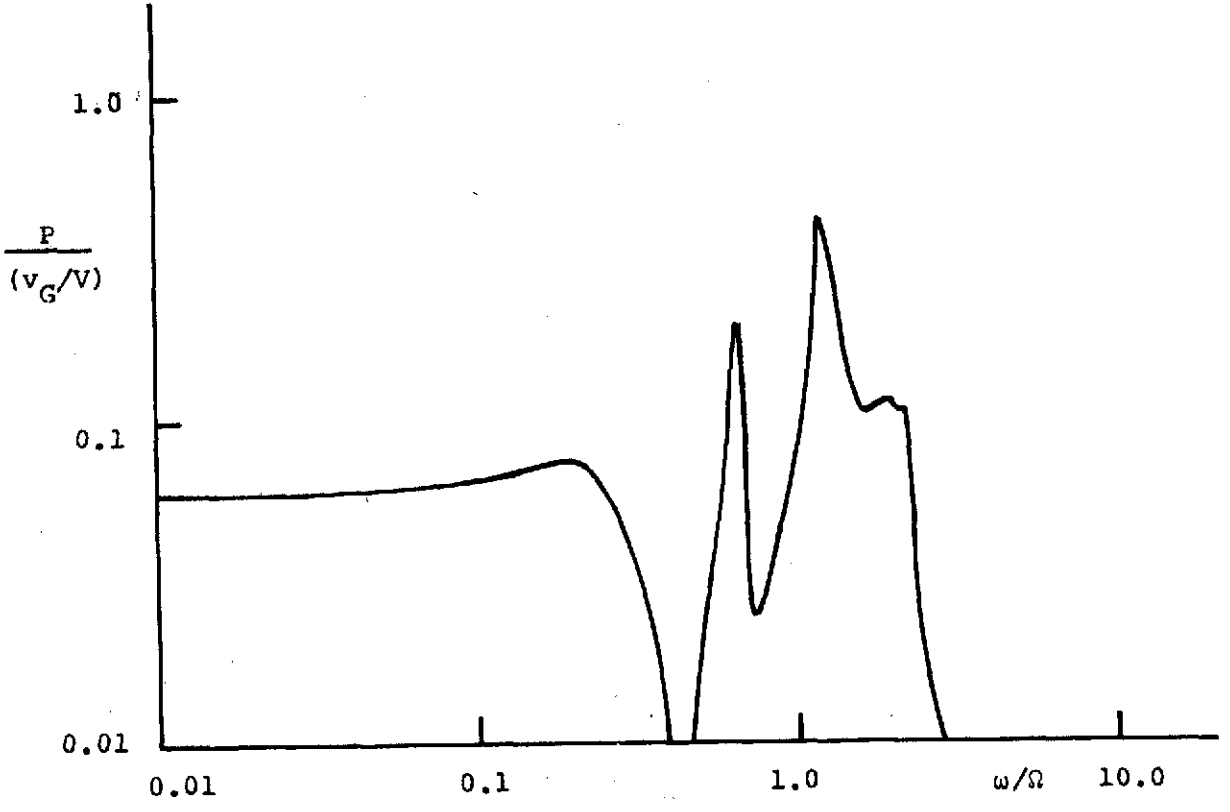

(i) Wing Torsion p Response to v_G

FIG. 29 CONCLUDED

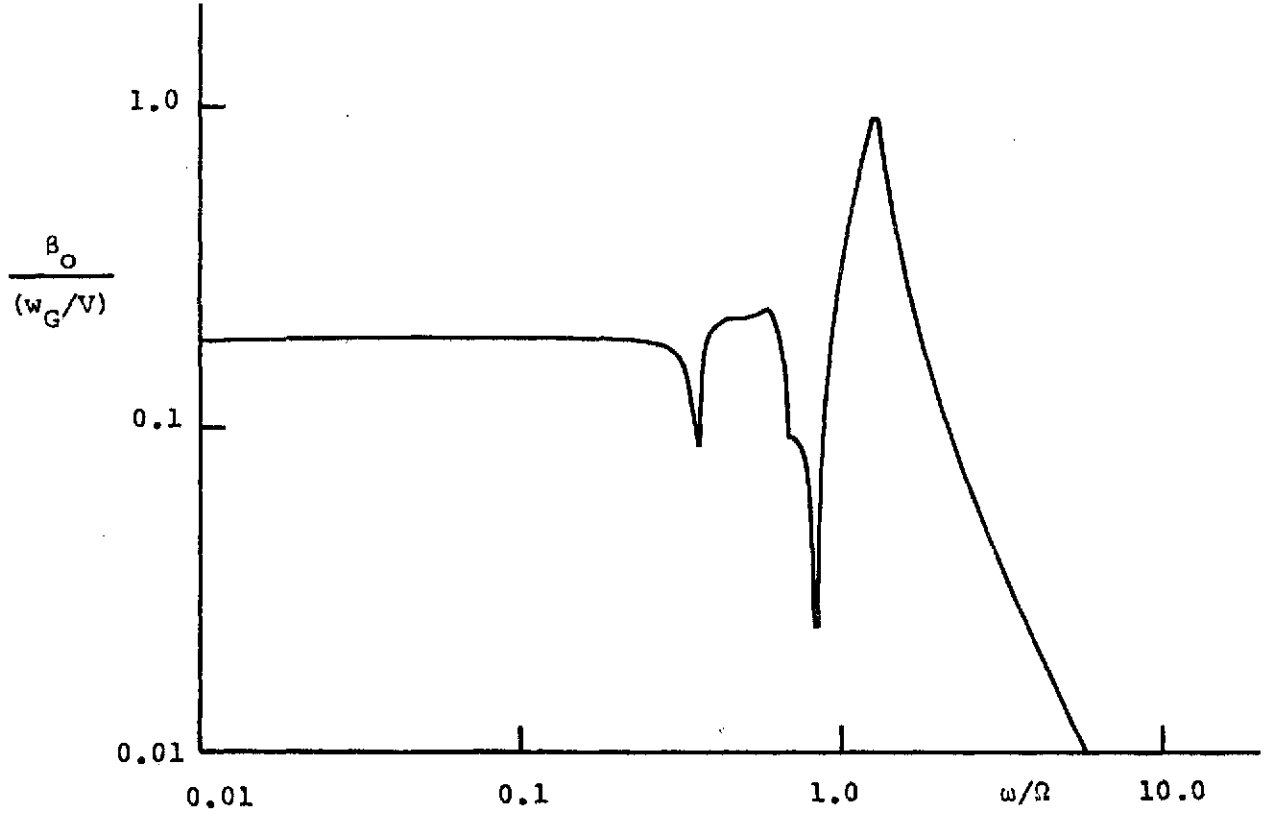

(a) Collective Flapping Motion β_o Response

FIG. 30 FREQUENCY RESPONSE OF BOEING ROTOR TO LONGITUDINAL GUST w_G INPUT AT FREQUENCY ω

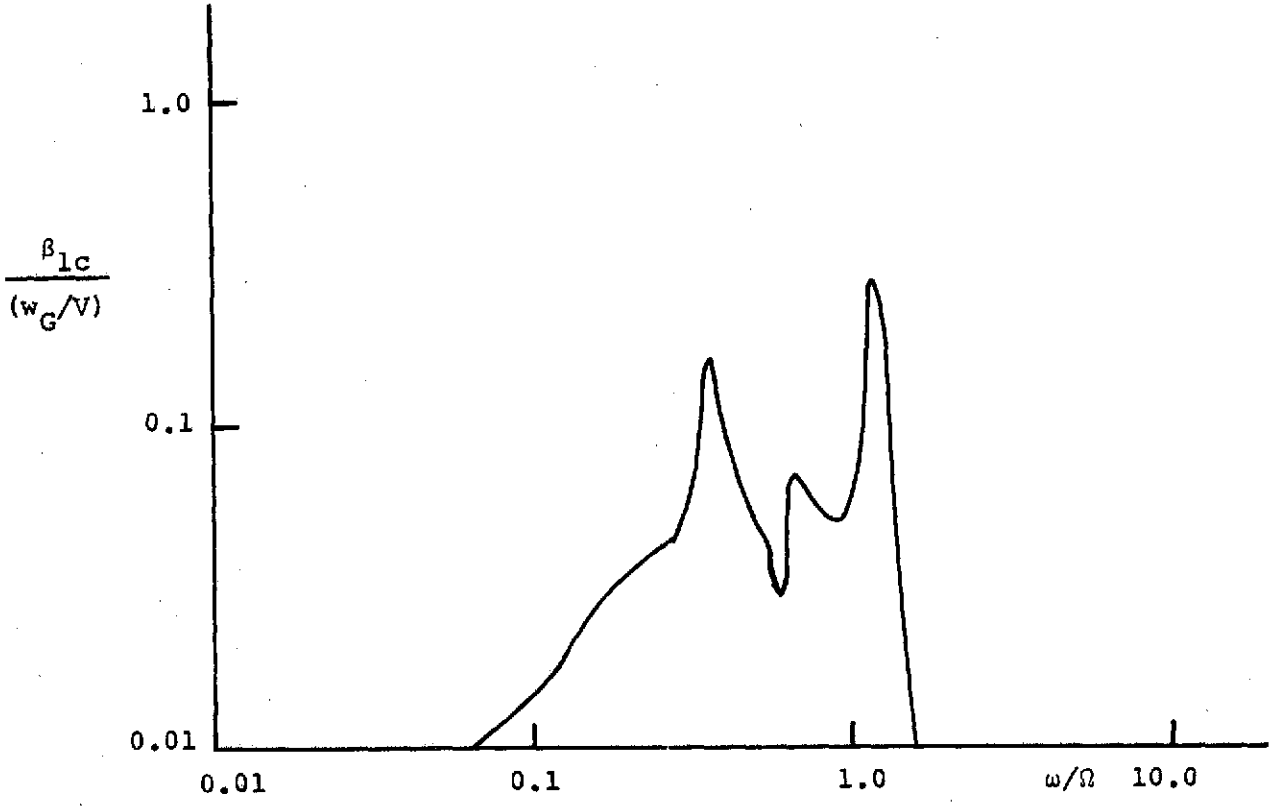

(b) Cyclic Flapping Motion β_{1c} Response to w_G

FIG. 30 CONTINUED

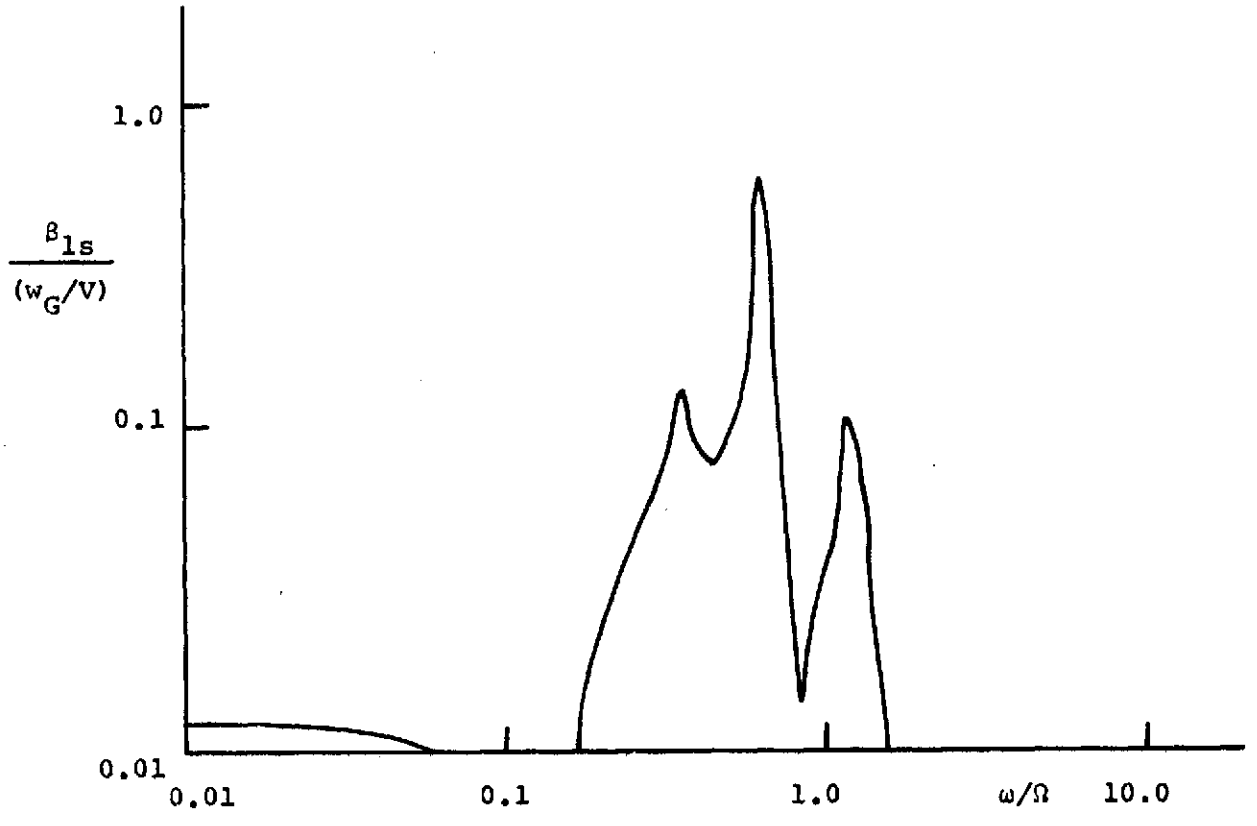

(c) Cyclic Flapping Motion β_{1s} Response to w_G

FIG. 30 CONTINUED

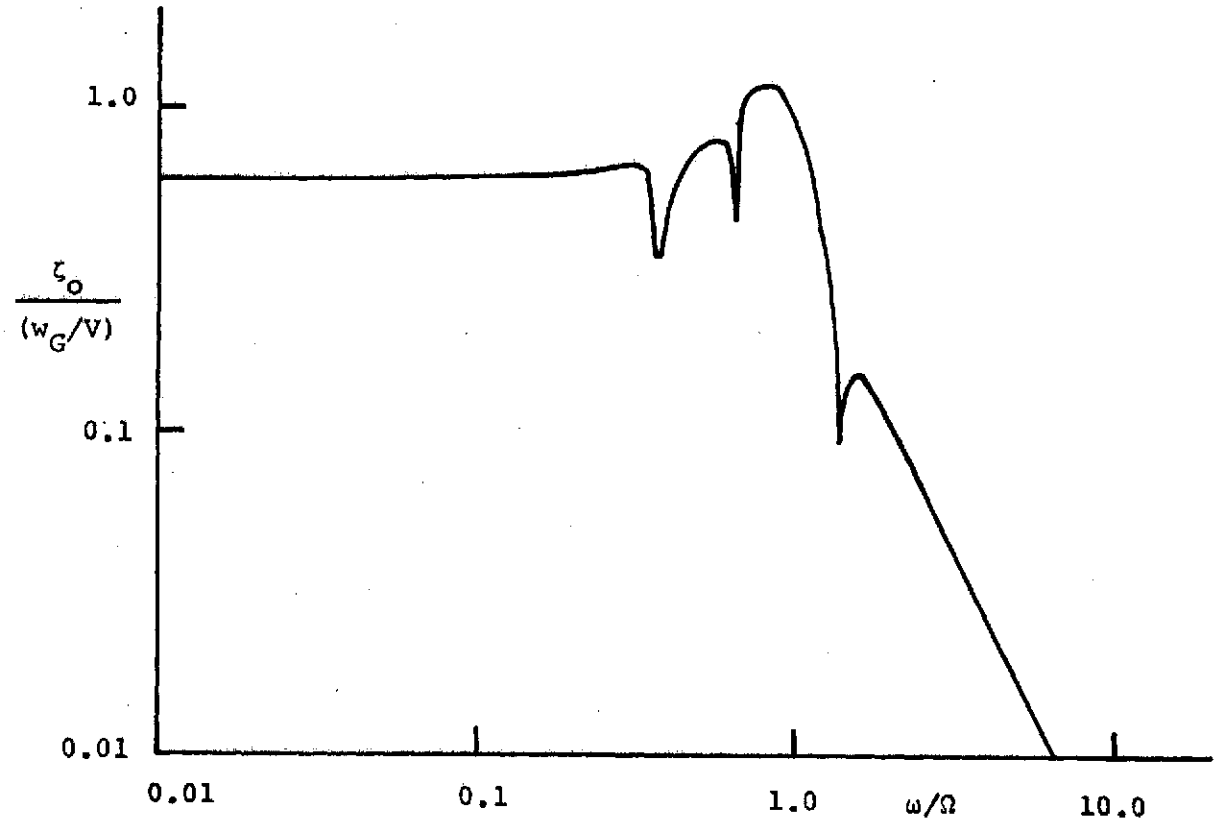

(d) Collective Lagging Motion ζ_o Response to w_G

FIG. 30 CONTINUED

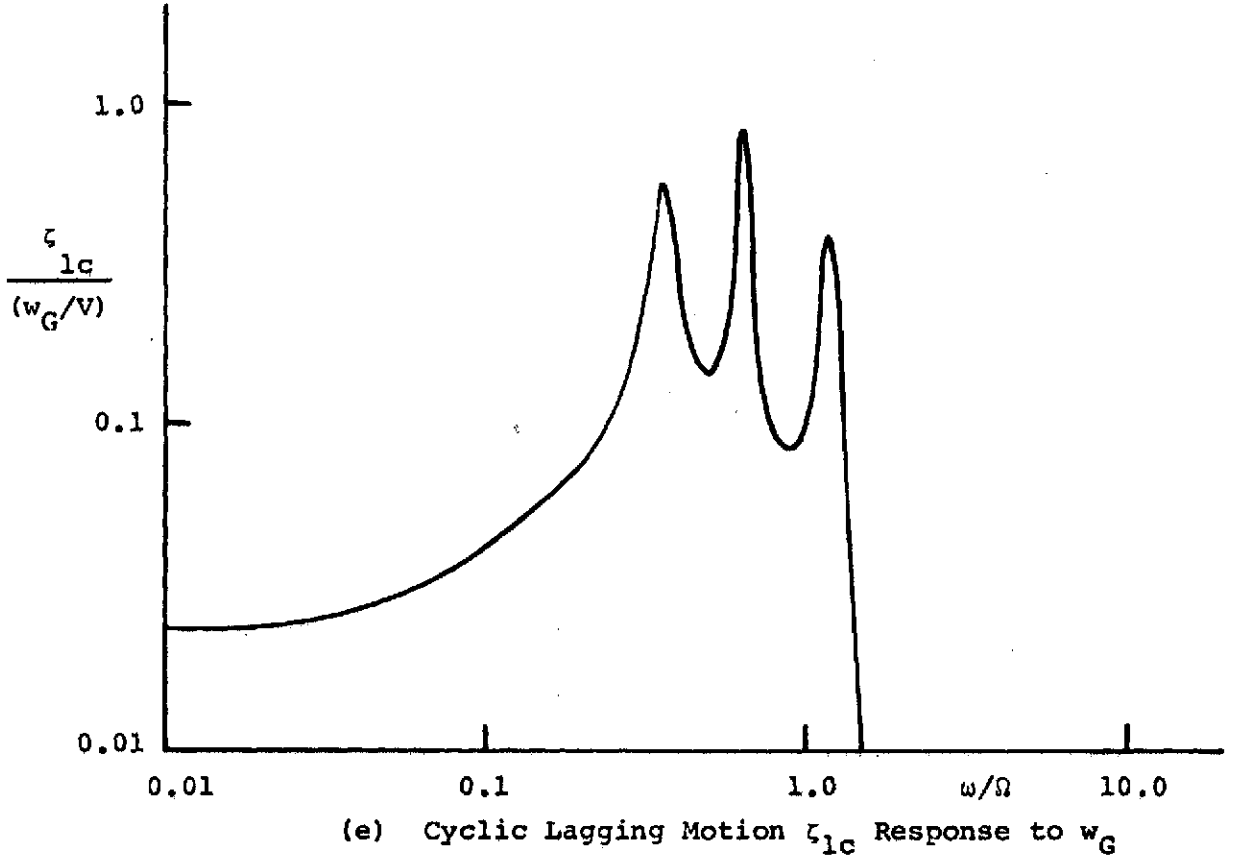

(e) Cyclic Lagging Motion ζ_{1c} Response to w_G

FIG. 30 CONTINUED

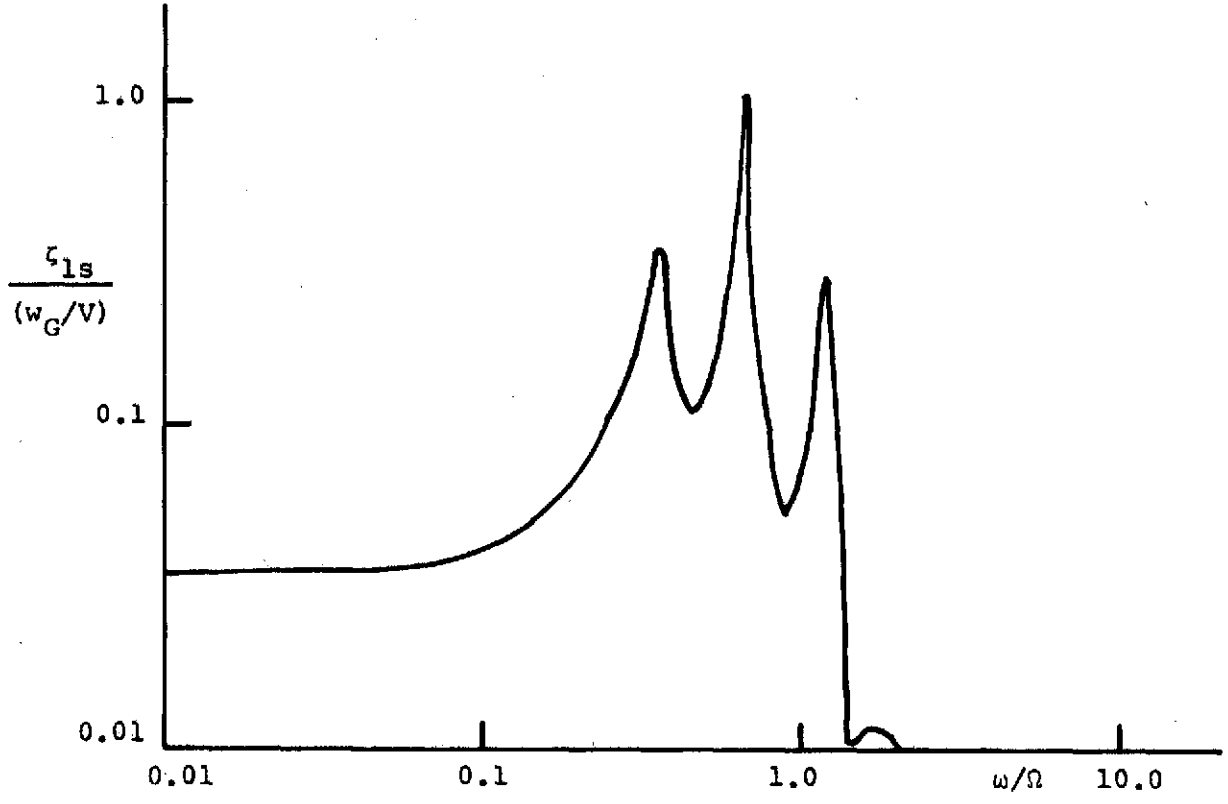

(f) Cyclic Lagging Motion ζ_{1s} Response to w_G

FIG. 30 CONTINUED

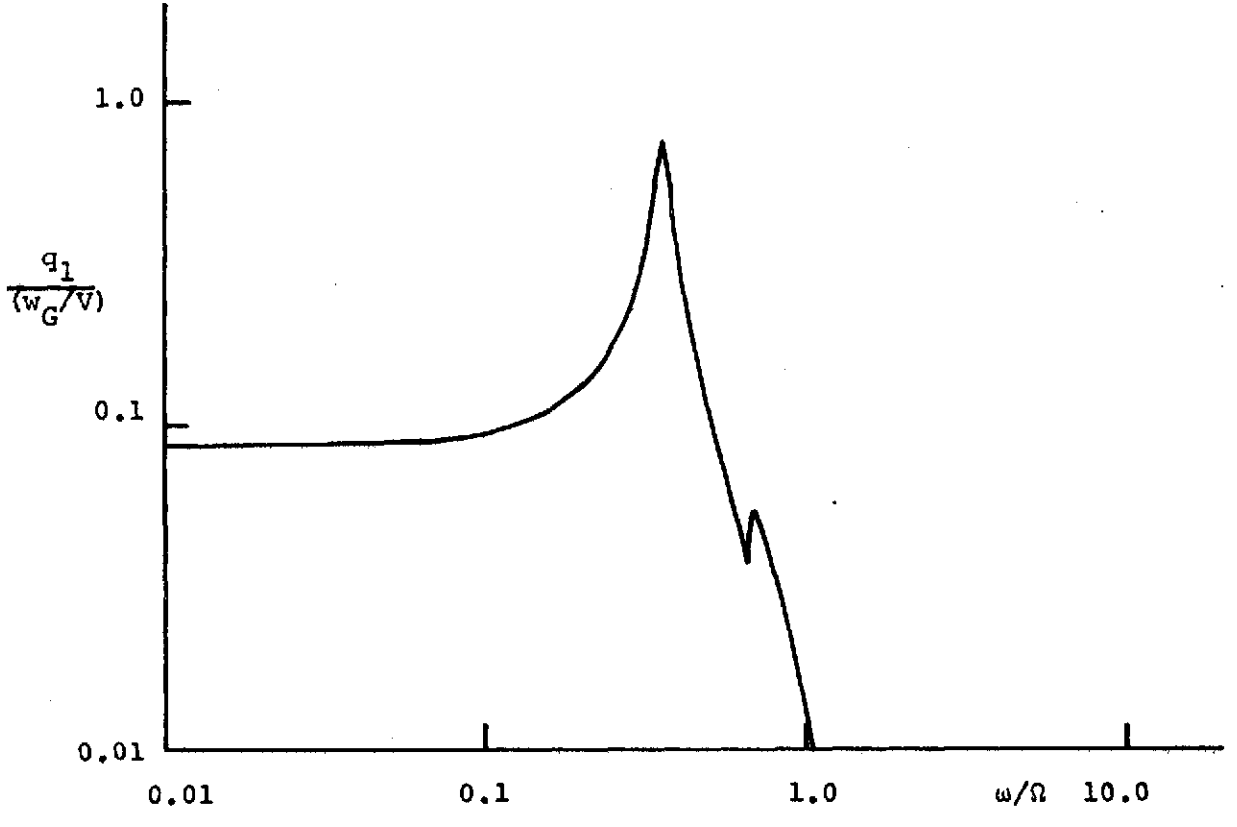

(g) Wing Vertical Bending q_1 Response to w_G

FIG. 30 CONTINUED

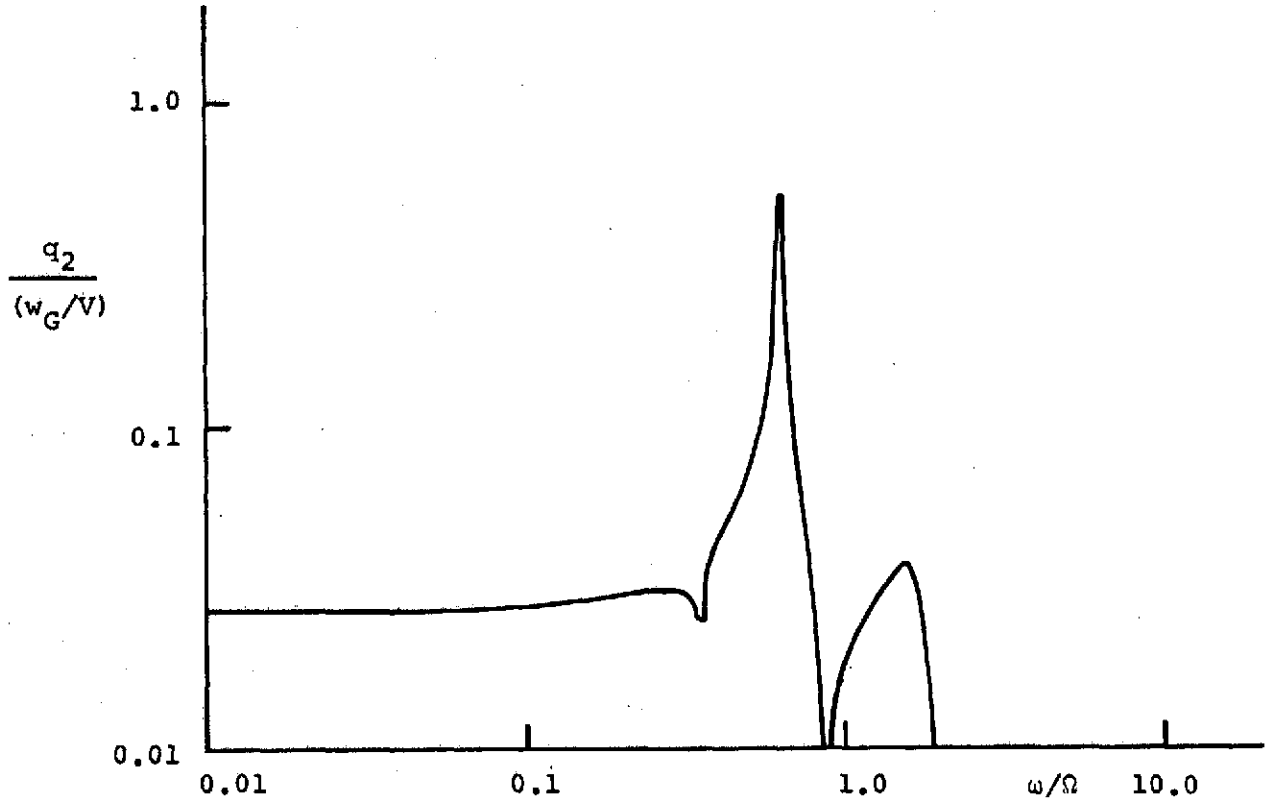

(h) Wing Chordwise Bending q_2 Response to w_G

FIG. 30 CONTINUED

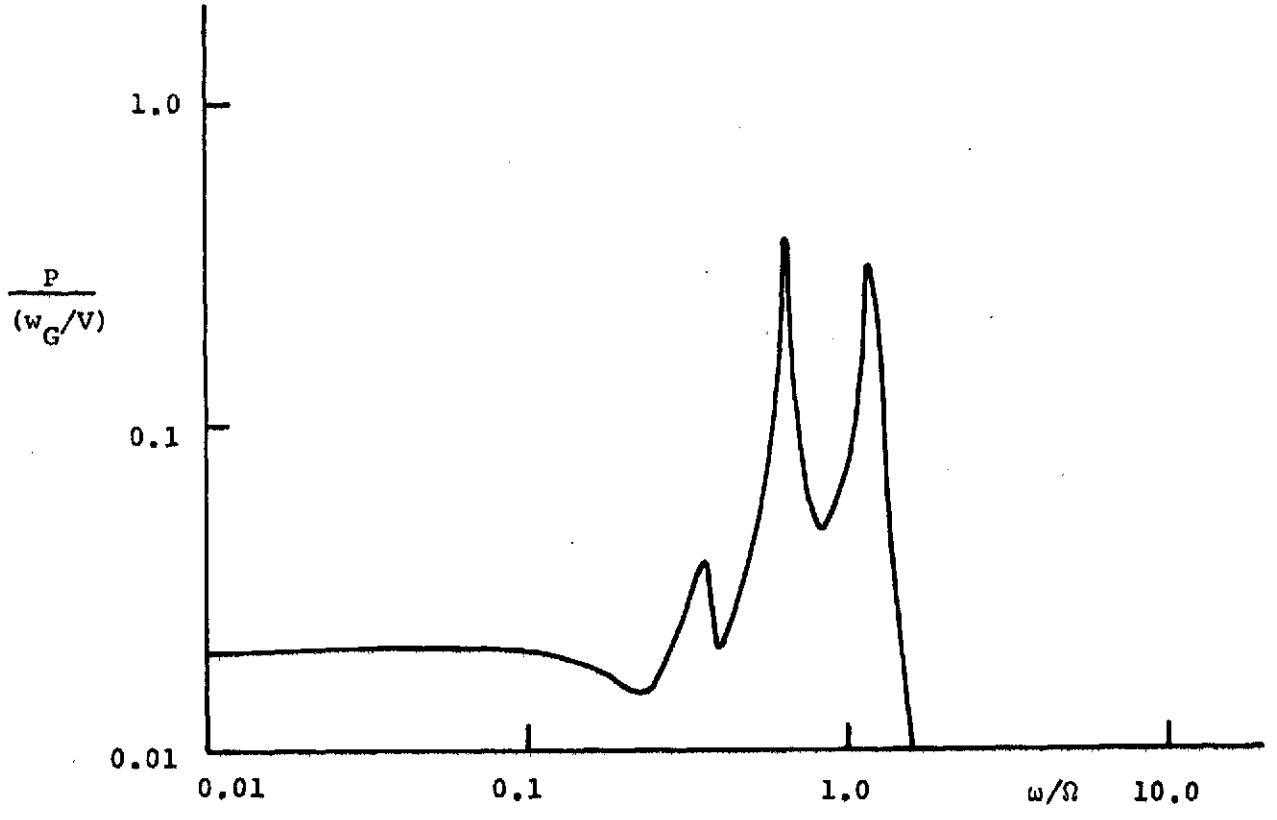

(i) Wing Torsion p Response to w_G

FIG. 30 CONCLUDED

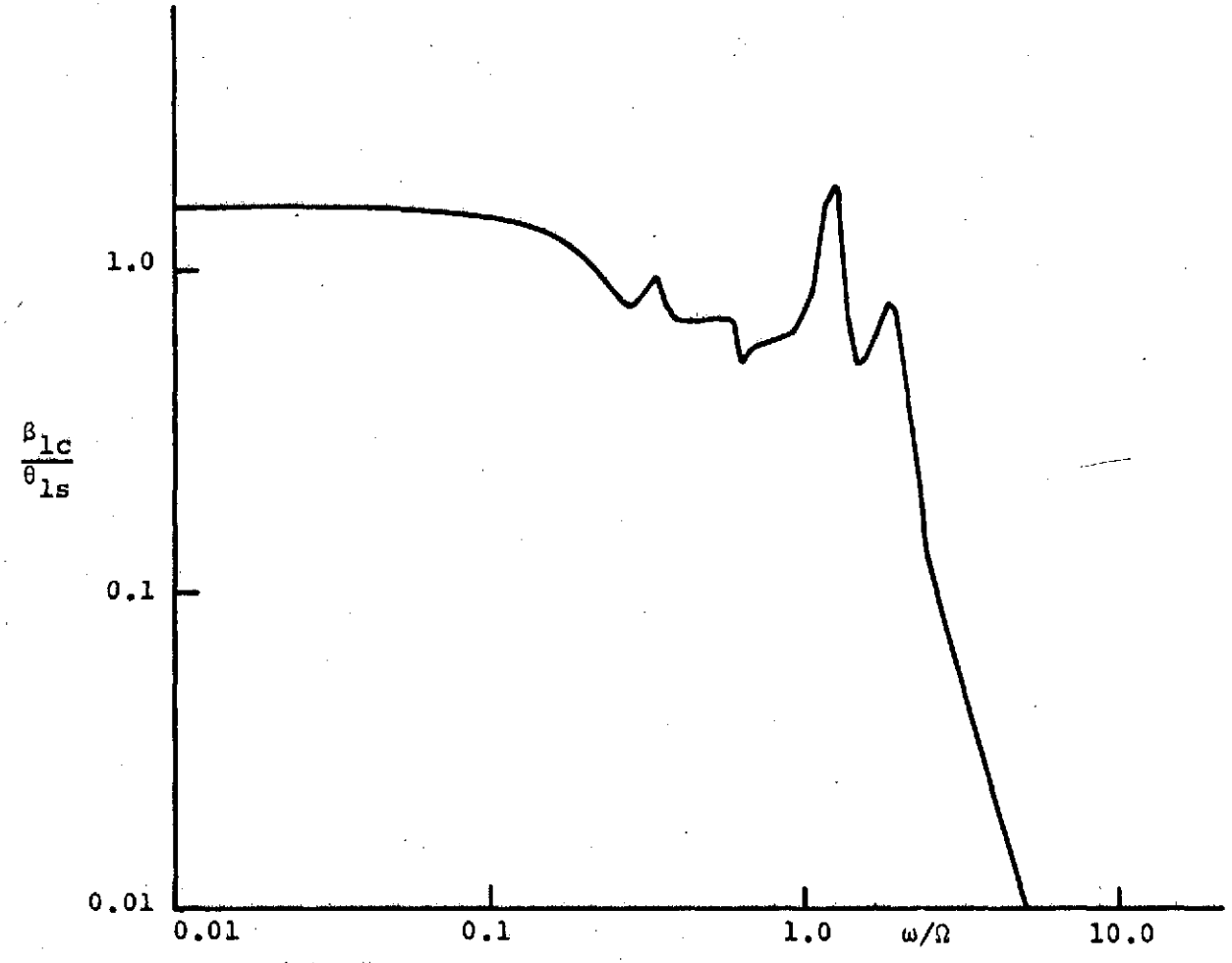

(a) Cyclic Flapping Motion β_{1c} Response to θ_{1s}

FIG. 31 FREQUENCY RESPONSE OF BELL ROTOR TO LONGITUDINAL CYCLIC PITCH θ_{1s} INPUT AT FREQUENCY ω

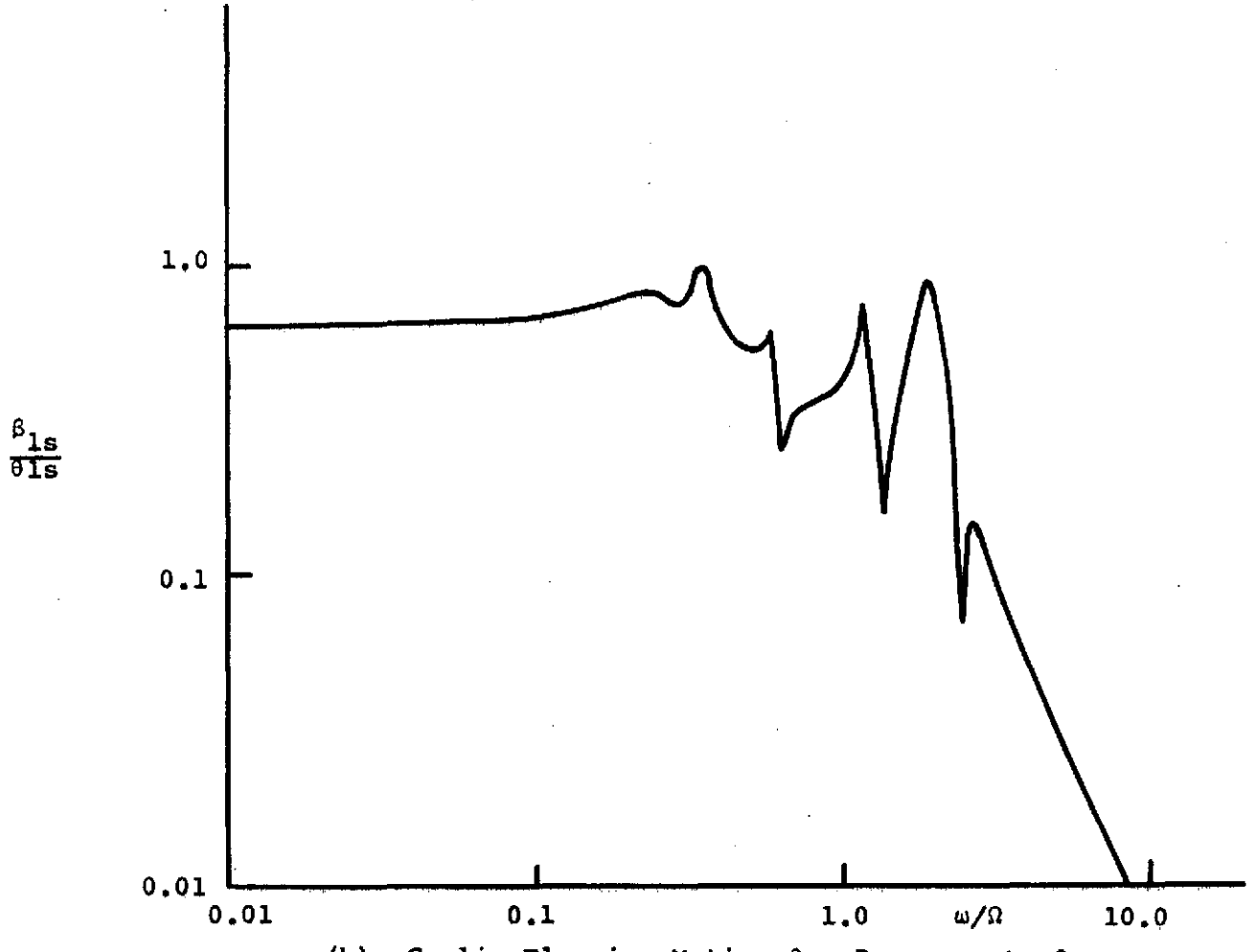

(b) Cyclic Flapping Motion β_{1s} Response to θ_{1s}

FIG. 31 CONCLUDED

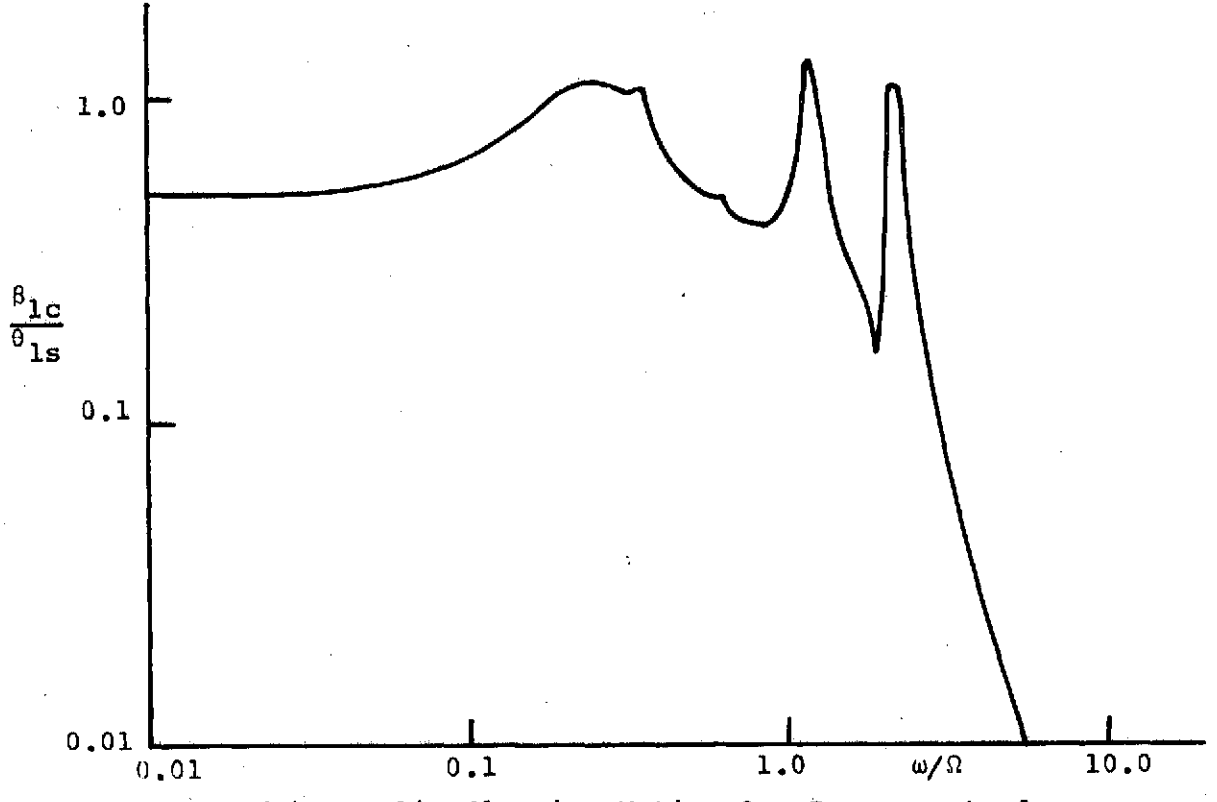

(a) Cyclic Flapping Motion β_{1c} Response to θ_{1s}

FIG. 32 FREQUENCY RESPONSE OF BOEING ROTOR TO LONGITUDINAL CYCLIC PITCH θ_{1s} INPUT AT FREQUENCY ω

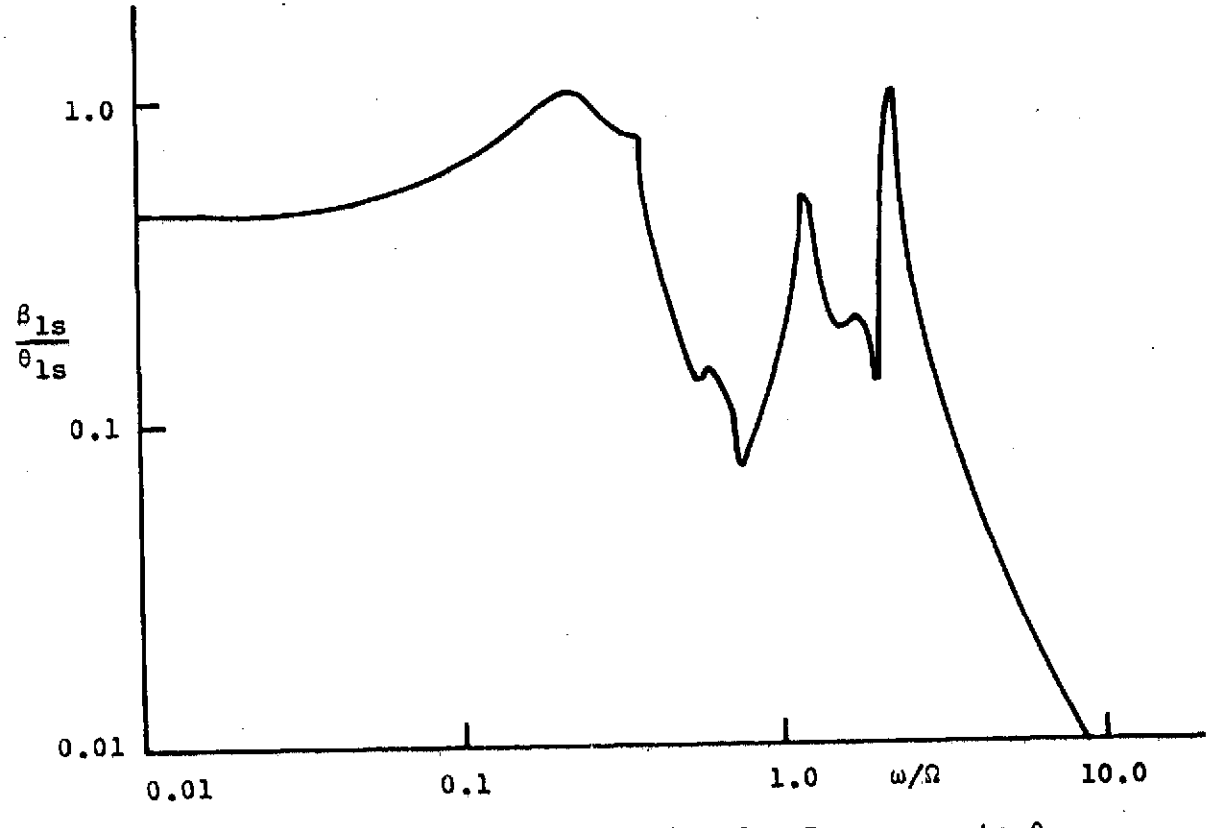

(b) Cyclic Flapping Motion β_{1s} Response to θ_{1s}

FIG. 32 CONCLUDED

APPENDIX A

DETAILED DERIVATION OF THE EQUATIONS OF MOTION

A.1 Blade Motion

The blade coordinate system is described in Section 2, and in Figs. 2 and 3. The position vector $\vec{r}_n$ defining an arbitrary point on the r-axis of the nth blade with respect to the inertial x-y-z system becomes

$$\vec{r}_n = \vec{r}_o + \ell \begin{Bmatrix} \nu_p \\ -\nu_y \\ 1 \end{Bmatrix} + \begin{bmatrix} 1 & 0 & 0 \\ 0 & \cos\nu_y & -\sin\nu_y \\ 0 & \sin\nu_y & \cos\nu_y \end{bmatrix} \begin{bmatrix} \cos\nu_p & 0 & \sin\nu_p \\ 0 & 1 & 0 \\ -\sin\nu_p & 0 & \cos\nu_p \end{bmatrix} \begin{Bmatrix} r\cos\Psi_n - v_n\sin\psi_n \\ r\sin\Psi_n + v_n\cos\psi_n \\ w_n \end{Bmatrix} \tag{A.1}$$

where $\vec{r}_o$ is the position vector which expresses translation at the wing tip as

$$\vec{r}_o = \begin{Bmatrix} r_x \\ L \\ r_z \end{Bmatrix} \tag{A.2}$$

The square of the velocity at an arbitrary point on the r-axis is expressed as

$$\begin{aligned} \dot{\vec{r}}_n \cdot \dot{\vec{r}}_n = {} & (r\Omega)^2 + \dot{w}_n^2 + \dot{v}_n^2 + (\Omega\dot{v}_n)^2 + \dot{r}_x^2 \\ & + \dot{r}_z^2 + r^2\dot{\nu}_r^2 + (\ell^2 + r^2\cos^2\psi_n)\dot{\nu}_p^2 \\ & + (\ell^2 + r^2\sin^2\psi_n)\dot{\nu}_y^2 + 2r\Omega\dot{v}_n \\ & - 2r\Omega\dot{r}_x\sin\psi_n - 2\ell r\Omega\dot{\nu}_p\sin\psi_n \end{aligned}$$

$$
\begin{aligned}
&+ 2r^2\Omega\,\dot{\nu}_r^2 - 2r^2\Omega\,\nu_y\,\dot{\nu}_p - 2r\Omega\,\dot{\nu}_p\,w_n \sin\psi_n \\
&- 2\Omega\,\dot{\upsilon}_n\,\dot{r}_z \cos\psi_n - 2h\,\Omega\,\upsilon_n\,\dot{\nu}_p \cos\psi_n \\
&- 2\dot{r}_z\,\dot{\upsilon}_n \sin\psi_n - 2h\,\dot{\upsilon}_n\,\dot{\nu}_p \sin\psi_n + 2r\,\dot{\upsilon}_n\,\dot{\nu}_r \\
&+ 2h\,\dot{r}_z\,\dot{\nu}_p - 2r\,\dot{r}_z\,\dot{\nu}_r \sin\psi_n \\
&- 2r\Omega\,\nu_r\,\dot{r}_z \cos\psi_n - 2hr\,\dot{\nu}_r\,\dot{\nu}_p \sin\psi_n \\
&- 4r^2\Omega\,\nu_r\,\dot{\nu}_r \sin\psi_n \cos\psi_n \\
&- 2r^2\Omega\,\nu_p\,\dot{\nu}_p \sin\psi_n \cos\psi_n - 2hr\Omega\,\nu_r\,\dot{\nu}_p \cos\psi_n \\
&- 2hr\Omega\,\dot{\nu}_y \cos\psi_n - 2r\Omega\,w_n\,\dot{\nu}_y \cos\psi_n \\
&- 2hr\,\dot{\nu}_r\,\dot{\nu}_y \cos\psi_n + 2hr\Omega\,\nu_r\,\dot{\nu}_y \sin\psi_n \\
&- 2h\,\dot{\nu}_y\,\dot{\upsilon}_n \cos\psi_n + 2h\,\Omega\,\upsilon_n\,\dot{\nu}_y \sin\psi_n \\
&- 2r^2\Omega\,\nu_y\,\dot{\nu}_y \sin\psi_n \cos\psi_n + 2\,\dot{w}_n\,\dot{r}_z \\
&- 2r\,\dot{w}_n\,\dot{\nu}_p \cos\psi_n + 2r\,\dot{w}_n\,\dot{\nu}_y \sin\psi_n \\
&- 2r\,\dot{r}_z\,\dot{\nu}_p \cos\psi_n + 2r\Omega\,\nu_p\,\dot{r}_z \sin\psi_n \\
&+ 2r\,\dot{r}_z\,\dot{\nu}_y \sin\psi_n + 2r\Omega\,\nu_y\,\dot{r}_z \sin\psi_n \\
&- 2r^2\Omega\,\nu_p\,\dot{\nu}_p \sin\psi_n \cos\psi_n \\
&- 2r^2\,\dot{\nu}_y\,\dot{\nu}_p \sin\psi_n \cos\psi_n \\
&+ 2r^2\Omega\,\nu_y\,\dot{\nu}_p \sin\psi_n \cos\psi_n
\end{aligned}
\qquad \text{(A.3)}
$$

The total kinetic energy T_E for N blades is expressed as

$$
T_E = \frac{1}{2} \sum_{n=1}^{N} \int_0^R m\,\dot{\vec{r}}_n \cdot \dot{\vec{r}}_n\,dr \qquad \text{(A.4)}
$$

where m is the blade mass per unit length.

The potential energy U_E of N blades is

$$U_E = \frac{1}{2}\sum_{n=1}^{N}\int_0^R \Big\{ [(EI)_B \cos^2\theta_B + (EI)_C \sin^2\theta_B]\left(\frac{\partial^2 w_n}{\partial r^2}\right)^2 + [(EI)_B \sin^2\theta_B + (EI)_C \cos^2\theta_B]\left(\frac{\partial^2 v_n}{\partial r^2}\right)^2 + [(EI)_C - (EI)_B]\sin\theta_B\cos\theta_B \frac{\partial^2 w_n}{\partial r^2}\frac{\partial^2 v_n}{\partial r^2}\Big\} dr \quad (A.5)$$

The virtual work done by the centrifugal forces δW_{CF} is described as

$$\delta W_{CF} = \sum_{n=1}^{N}\int_0^R \left[\frac{\partial}{\partial r}\left(T\frac{\partial w_n}{\partial r}\right)\delta w_n + \frac{\partial}{\partial r}\left(T\frac{\partial v_n}{\partial r}\right)\delta v_n\right] dr \quad (A.6)$$

A.2 The Work Done by Blade Aerodynamic Forces

Aerodynamic forces acting on the nth blade $(\vec{F})_n$ are derived in the z-y-z coordinate system from the P_Z and P_θ components as

$$(\vec{F})_n = \begin{bmatrix} 1 & -\nu_r & \nu_p \\ \nu_r & 1 & -\nu_y \\ -\nu_p & \nu_y & 1 \end{bmatrix} \begin{bmatrix} -P_\theta \sin\psi_n \\ P_\theta \cos\psi_n \\ P_Z \end{bmatrix} \quad (A.7)$$

Then the virtual work done by the aerodynamic forces of all blades δW_{AF} is described as

$$\delta W_{AF} = \sum_{n=1}^{N}\int_0^R \delta\vec{r}_n \cdot (\vec{F})_n \, dr \quad (A.8)$$

A.3 Lagrange's Equations

In addition to the above, the kinetic energy and potential energy of the wing derived from the simple beam theory are appended.

Then, Lagrange's equations are given by

$$\frac{d}{dt}\left(\frac{\partial T}{\partial \dot{q}_i}\right) - \frac{\partial T}{\partial q_i} + \frac{\partial U}{\partial q_i} = Q_i \qquad \text{(A.9)}$$

where T, U and Q_i are respectively, the total kinetic energy, potential energy and generalized forces of the system, and

$$q_i = w_n, u_n, r_x, r_z, v_y, v_p, v_r, u_w, w_w \qquad \text{(A.10)}$$
$$\text{or } p_w$$

Finally, the above represents the derivation of Eqs. 2.4, 2.5, 2.6, 2.7, 2.8, 2.10, 2.11, 2.12, 2.13, and 2.14.

APPENDIX B

STRESS ANALYSIS OF THE ROTOR BLADE AND THE WING

In this appendix, the method of deriving the stresses in the rotor blades and in the wing due to the gust are briefly stated. If the deformation of an elastic structure has been determined, it is a straightforward procedure to determine the stresses corresponding to this deformation. The mode acceleration method discussed in Ref. 15 is very suitable because the stresses can be determined accurately and directly when the deformation has been computed in terms of displacements of normal modes.

Equation 4.57 is written here again in matrix form as

$$[A]\{\ddot{x}\} + [B]\{\dot{x}\} + [C]\{x\} = [D]\{e\} + \{F\} \tag{B.1}$$

where [A], [B] and [C] are square matrices to define the coefficients of equations derived from mass, stiffness and aerodynamic forces, and the [D] matrix is the excitation. The generalized coordinates {x} and excitation input {e} are

$$\{x\} = \begin{Bmatrix} Q_{10} \\ Q_{1c} \\ Q_{1s} \\ Q_{20} \\ \vdots \\ a_1 \\ a_2 \\ a_3 \\ \vdots \end{Bmatrix}, \quad \{e\} = \begin{Bmatrix} u_g \\ v_g \\ w_g \\ \theta_0 \\ \theta_{1c} \\ \theta_{1s} \end{Bmatrix} \tag{B.2}$$

The static force {F} from the lift or drag of the wing and rotor in steady flight may be included if the total stresses are required. When only the additional stress due to the gust or control input varying with time is required, the {F} matrix may be dropped.

In general, the stress at a particular point p in the rotor wing structure is expressed by

$$\{\sigma_p\} = [A_p]\{x\} \tag{B.3}$$

where the $[A_p]$ matrix is a constant matrix that represents the stress at the point p due to a unit displacement in the normal mode.

The static mode displacements are given by setting $\{\ddot{x}\} = 0$ and $\{\dot{x}\} = 0$ in Eq. B.1.

$$\{x\}_{static} = [C]^{-1}[D]\{e\} + [C]^{-1}\{F\} \tag{B.4}$$

Therefore, the static stress becomes

$$\{\sigma_p\}_{static} = [A_p]\{x\}_{static} \tag{B.5}$$

When the rotor and wing are vibrating, the total displacements of the rotor or wing can be expressed as

$$\{x\} = [C]^{-1}[D]\{e\} + [C]^{-1}\{F\} - [C]^{-1}[A]\{\ddot{x}\} - [C]^{-1}[B]\{\dot{x}\} \tag{B.6}$$

Substituting Eqs.B.5 and B.6 into Eq. B.3, the total stress becomes

$$\{\sigma_p\} = \{\sigma_p\}_{static} - [A_p][C]^{-1}[A]\{\ddot{x}\} - [A_p][C]^{-1}[B]\{\dot{x}\} \tag{B.7}$$

This result gives the stress in the rotor or wing at any instant in terms of the static stress and an additional stress due to the vibration.